Department of Chemical and Environmental Engineering

The University of Nottingham

UNITED KINGDOM · CHINA · MALAYSIA

Treatment of Produced Water by Simultaneous Removal of Heavy Metals and Dissolved Polycyclic Aromatic Hydrocarbons in a Photoelectrochemical Cell

By

Ebenezer Temitope Igunnu

BSc (Hons), MSc, MRSC

Thesis submitted to the University of Nottingham

for the degree of Doctor of Philosophy

January 2014

Abstract

Early produced water treatment technologies were developed before carbon dioxide emissions and hazardous waste discharge were recognised as operational priority. These technologies are deficient in the removal of dissolved hydrocarbons and dissolved heavy metal ions which have been identified as major contributors to the high environmental impact factor of produced water. The simultaneous removal of heavy metals and polycyclic aromatic hydrocarbon (PAH) from produced water via photoelectrochemical process was identified in this work as a produced water treatment alternative with the potential to virtually eliminate the cost for chemical reagents and high energy input.

Several grades of simulated produced water were synthesised and used to understand different parameters necessary for developing a successful photoelectrochemical treatment. The process demonstrated in this work followed a simple two–electrode photoelectrochemical cell where heavy metals were recovered on a platinum electrode with simultaneous degradation of PAH (phenanthrene) on a photoanode, with the aid of sunlight (simulated) and an applied cell voltage of 1.0 V. Multiwall CNT-TiO_2 synthesised via a modified sol-gel method served as the photoanode after it was immobilised at a loading of 2.5 mg/cm^2 on a titanium plate. The results obtained from the photoelectrochemical treatment showed a recovery of 1.6 g/cm^2 of lead, 0.2 g/cm^2 of copper and 0.1 g/cm^2 of nickel from produced water on a 0.1 cm diameter platinum electrode after 24 hours of irradiation with simulated sunlight at 1.0 V cell voltage and a simultaneous degradation of up to 16 % phenanthrene on the photoanode, which gives a potential of scaling up the process to a commercial throughput.

List of Publications

Peer-Reviewed Publication

- G. Kim, E.T Igunnu and G.Z. Chen (2014). "A sunlight assisted dual purpose photoelectrochemical cell for low voltage removal of heavy metals and organic pollutants in wastewater." Chemical Engineering Journal **244**(0): 411-421.

- E. T. Igunnu, and G. Z. Chen (2012). "Produced water treatment technologies." International Journal of Low-Carbon Technologies **1**(0): 1 -21.

Conference Presentations

- E.T. Igunnu, G. Kim and G.Z. Chen (2013). "Case studies of a dual purpose photoelectrochemical cell for heavy metal recovery and decomposition of organic pollutants." Midlands Electrochemistry Group meeting, University of Nottingham, April 17, 2013.

- E.T. Igunnu, Z. Li and G.Z. Chen (2013). "Removal of dissolved hydrocarbons from produced water by photo-electro-catalysis o n a CNT-TiO$_2$ hybrid anode." Young Environmental Scientist conference, Krakow, Poland, Feb.11-13, 2013.

- E.T. Igunnu and G.Z. Chen (2012). "Photoelectrochemical Treatment of produced water." Midlands Electrochemistry Group meeting, University of Birmingham, June 27, 2012.

- E.T. Igunnu and G.Z. Chen (2011). "Electrochemical probe of Pb deposition from produced water." Midlands Electrochemistry Group meeting, University of Warwick, May 5, 2011.

    E.T. Igunnu and G.Z. Chen (2010). "Electrochemical mining of oilfield produced water for valuable metals." Midlands Electrochemistry Group meeting, University of Leicester April 19, 2010.

Acknowledgements

Table of Contents

List of Abbreviations

Abbreviation	Meaning
1 gallon	US gallon (3.785 Litres)
a.u.	Arbitrary unit
BAF	Biological aerated filter
bbl	US barrel (159 Litres)
BET	Brunauer-Emmett-Teller
BJH	Barrett-Joyner-Halenda
BOD	Biological oxygen demand
BOD_5	Biological oxygen demand day 5
Bq	Becquerel
BTEX	Benzene, toluene, ethylene and xylene
CA	Chronoamperometry
CBM	Coal bed methane
CNT	Carbon nanotubes
COD	Chemical oxygen demand
CV	Cyclic voltammetry/voltammogram
CVD	Chemical vapour deposition
EIF	Environmental impact factor
FTE	Freeze thaw evaporation
gpd	gallons per day
gpm	gallons per month
Kwh	Kilowatt-hour
MED	Multi effect distillation
MF	Microfiltration
MPPE	Macro porous polymer extraction technology
MSF	Mutli stage flash
MWCNT	Multiwalled carbon nanotubes

NaDDBS	Sodium dodecylbenzenesulfonate
NF	Nanofiltration
NHE	Normal hydrogen electrode
NORM	Naturally occurring radioactive materials
OIW	Oil in water
PAH	Polycyclic aromatic hydrocarbon
PEC	Photoelectrochemical
PW	Produced water
RO	Reverse osmosis
SCE	Standard calomel electrode
SWCNT	Single-walled carbon nanotubes
TEM	Transmission electron microscopy
TGA	Thermogravimetric analysis
TOC	Total organic carbon
TSS	Total soluble solids
TDS	Total dissolved solids
UF	Ultrafiltration
UV-vis	Ultraviolet – visible
VCD	Vapour compression distillation
WFD	Water framework directive
wt.	Weight
XRD	X-ray diffraction

Chapter 1: Introduction

1.1. Produced water: definition and key project aim

Produced water is a complex mixture of reservoir formation water, injected water, hydrocarbons and other impurities generated alongside oil and gas during petroleum exploration. Collecting and compiling accurate volumes of produced water generated worldwide is a challenging task; therefore international estimates are taken as approximations. An estimated global average of over 200 million barrels of produced water is generated daily from both oil and gas fields (Khatib and Verbeek, 2003), thereby making produced water the largest volume of liquid waste produced, and about 100 million barrels are discharged into the environment daily (Fakhru'l-Razi et al., 2009).

There are generally three types of produced water based on their source: oilfield produced water, gas field produced water and coal bed methane (CBM) produced water. Their composition is widely varied due to geological formation, lifetime of the reservoir and the type of hydrocarbon produced (Chan et al., 2002, Igunnu and Chen, 2012). It is a fact that produced water, irrespective of its source, is a toxic waste which is dangerous to the environment if discharged in its raw form. Although its composition may vary, dissolved minerals, especially heavy metals and polycyclic aromatic hydrocarbons (PAHs), are the main concerns when produced is discharged into the environment (Fakhru'l-Razi et al., 2009, Meijer and Madin, 2010).

Stringent environmental legislations have driven petroleum exploration companies to treat produced water before discharge, which are also largely responsible for research into produced water treatment in the academia. Research into treatment technologies of produced water started about three decades ago when green technology was not high on the environmental agenda. Therefore most treatment technologies require the use of chemical reagents which may result in the generation of secondary

wastes and usually demand huge energy use. Over the years several technologies have been developed to treat produced water both onshore and offshore where many of its constituent pollutants are considerably reduced before discharge into the environment. However, current treatment technologies are still not able to remove small-suspended oil particles and dissolved elements from produced water (Fakhru'l-Razi et al., 2009). Water legislations such as the US Clean Water Act of 1977, EU Water Framework Directive (WFD) of 2000, Canadian Arctic Water Pollution Prevention Act (AWPPA) of 1985 and other major environmental legislations call for "zero harmful discharge" of pollutants into the environment is another major limitation of these technologies. This implies that by 2030 most current produced water treatment technologies may become obsolete because they are not designed to meet the demands of new legislations. For example current treatment technologies are usually designed to reduce oil and grease up to 30 mg/L, however a "zero harmful discharge" policy would advocate for reduction of primary pollutants below their detection limits.

The key aim of this research was therefore the development of an environmentally friendly and sustainable photoelectrochemical process for the removal of heavy metals and PAHs from produced water via a dual purpose photoelectrochemical (PEC) reactor. The simultaneous removal of heavy metals and PAHs from produced water through the combination of photocatalysis and electrolysis into one system was first conceived and finally chosen, because it has the potential to set the foundation of a novel commercially-viable produced water treatment process.

The PEC treatment process developed in this research is in line with the concept of waste exchange within the limits of the wider petroleum industry. It has exploited the relatively high conductivity of produced water as a suitable electrolyte for metal recovery via electrodeposition and

recently reported carbon nanotubes supported photocatalysts for photoelectrochemical oxidation of polycyclic aromatic hydrocarbons. To assist discussion and understanding of the findings from this research, the petroleum industry, its use of resources, generation of produced water, current produced water treatment technologies/or disposal policies are outlined in this chapter as they indicate whether the processes developed in this research are realistically tailored to the petroleum industry. The technology developed in this research is able to combine with existing produced water technology to keep them relevant in meeting future environmental demands arising from new legislations.

1.2. Nature and production of produced water

Produced water is not a single commodity. It's physical and chemical properties vary significantly depending on the geological formation from where the water was produced, the type of hydrocarbon product being produced and the location of the field (Stephenson, 1992).

For example produced water from petroleum exploration consist mainly of oil and grease (various organic compounds associated with hydrocarbons in the formation), salt (expressed as salinity, or total dissolved solids (TDS) or conductivity), inorganic and organic compounds (introduced as chemical additives to improve drilling and production operations), and naturally occurring radioactive material (NORM) (Woodall et al., 2001, Fakhru'l-Razi et al., 2009, Igunnu and Chen, 2012). Additional water used to maintain sufficient pressure during oil production may contain additional solids and microorganisms which are also constituents of some produced waters (Dowd et al., 2000, Chapelle, 2001).

Produced water from sites where waterflooding is conducted may vary dramatically from that at sites where there is no injection of additional

water into reservoir formation to increase hydrocarbon production. In addition to formation water, gas field produced water contains condensed water, which is the water vapour in the reservoir which condenses into a liquid in the gas production separation system. CBM produced water differs from oil and gas because it contains very little quantity or no oil and grease (All, 2003).

At the initial stages of petroleum production in a well, produced water represents a small percentage of produced fluids, however as the well ages the quantity of produced water increases while hydrocarbons decreases. A world average estimate of 3 barrels (bbl) of produced water for each barrel of oil is reported to be generated in ageing oil wells (Khatib and Verbeek, 2003). In countries with typical further production lifetime than the global average, an average of more than 9.5 bbl of water for each barrel of oil has been reported (Veil et al., 2004). On the contrary in a typical CBM well large volumes of produced water are initially generated, which declines over time. Methane production is initially low, but later increases to a peak, and then decreases. When the cost of managing produced water exceeds the profit of selling crude oil, production is stopped and the well is closed.

1.3. Brief overview of produced water management

Produced water is an unavoidable fact of life for petroleum production and offers both opportunities and challenges for sustainable recovery of hydrocarbon resources. In order to cope with these challenges, a three-tiered water hierarchy strategy is currently adopted for produced water management as shown in Figure 1.1.
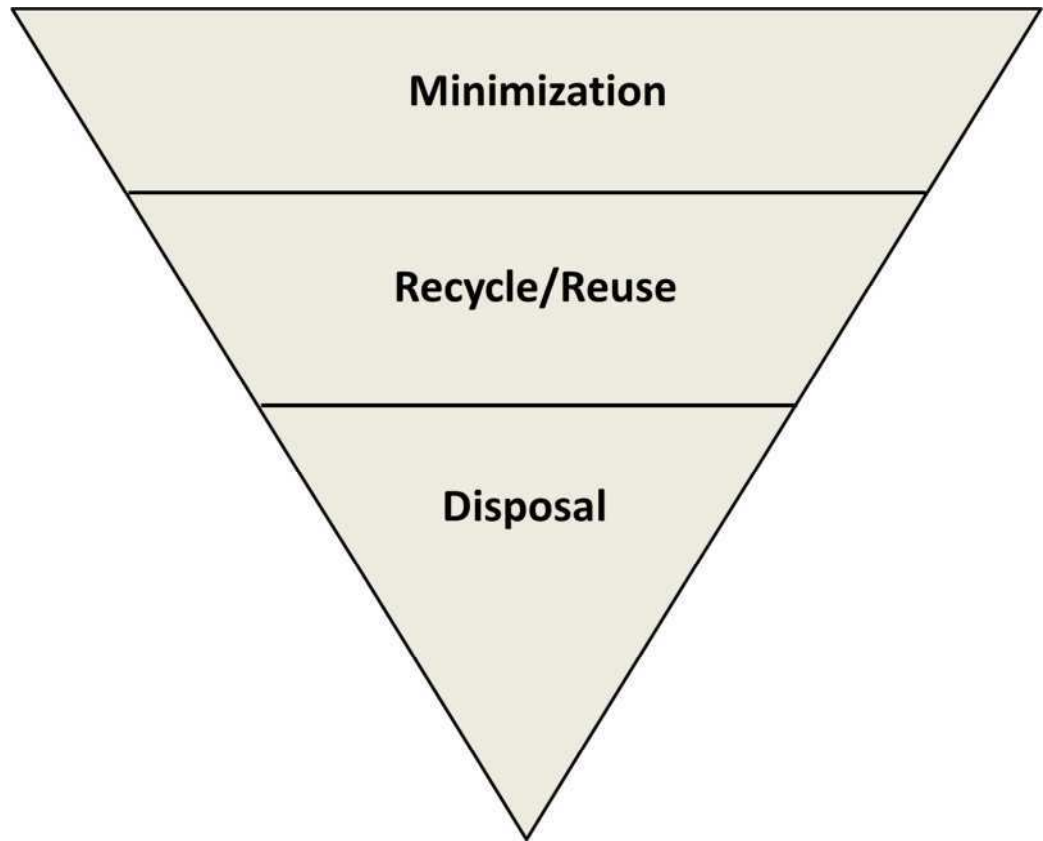
Figure 1.1: Produced water management Hierarchy

1.3.1.   Minimization

Since generation of produced water is unavoidable, minimization can be achieved by modification of processes and adaptation of advanced technologies so that less water is generated (Wells, 2011). The volume of water entering the wells can be blocked with mechanical devices such as packers, plugs and cement jobs. Polymer gels can also be used on platforms to prevent water from entering the well. Water generated on rigs using fracturing technology can be reduced by substituting water with other materials such as CO_2 or nitrogen as the main frac fluid ingredient or by using gelled frac fluids instead of slickwater fluids. Minimization can also be achieved by adopting remote separation of water at the sea floor (setting up separation modules on the sea floor), and using dual completion wells (downhole water sink) to reduce the volume of water managed at the surface of the oil rig (Fenton et al., 2005, Wells, 2011).

Although produced water minimization is achievable theoretically it has largely not been practically feasible. Only two sea floor separation modules were ever installed and the costs are significantly high (Wells, 2011). Produced water minimization is an emerging or future technology that will lead to greater environmental protection when practically feasible (in terms of application and cost).

1.3.2. Recycle/Re-use

Produced water that cannot be managed by water minimization approach can be moved to the next hierarchy, where they are reused or recycle. Reuse /recycling of produced water usually involve the following options

> ➢ Re-injection for enhanced oil recovery
>
> ➢ Injection for future water use
>
> ➢ Injection for hydrological purposes
>
> ➢ Agricultural use
>
> ➢ Industrial use
>
> ➢ Use of flowback water for future frac fluids
>
> ➢ Treatment to drinking water quality

Re-injection of produced water into producing formation for enhanced oil recovery is the most common way to re-use produced water because it is usually inexpensive, especially for onshore wells. Aquifer storage of produced water is a great option if possible but the danger of leakage is very high, hence only one example of this type of storage (in Wellington, Canada) actually exists today (Dusseault, 2008, Wells, 2011). Beneficial uses in agriculture (irrigation, livestock, wildlife, watering etc.), industry (as cooling water systems, substitute for fresh water in making drilling fluids) and drinking water sometimes involve significant treatment. Water is a scarce commodity in many parts of the world, and a substantial effort

is put into developing an economical treatment method for produced water in order to put it into new use. This is discussed in details in chapter 2.

1.3.3. Disposal

Produced water that cannot be managed through minimization, re-use, or recycling is disposed of. However prior to disposal produced water may need to be treated depending on their final disposition and the environmental legislation applicable to their disposal. Permits must normally be obtained from appropriate government agency before produced water disposal. The following options are available for produced water disposal:

> - Discharge
> - Underground injection
> - Evaporation
> - Offsite commercial disposal

Most produced water generated is disposed into the environment. Produced water generated offshore is usually treated and discharged directly into the ocean while that generated onshore is managed in several ways. The greatest concern at this stage is related to salt content, organic content and dissolved elements (heavy metals, dissolved hydrocarbons etc.). Salinity is not an issue for produced water discharged into the sea or ocean however it must be removed to acceptable limits for onshore discharges. Organic content has been reasonably removed by available treatment technologies but removal of dissolved elements from produced water is still a major setback to current treatment technologies (Fakhru'l-Razi et al., 2009). Underground injection other than for enhanced recovery is a common onshore practice. It is relatively cheap, widely used and an effective method for disposing produced water. In arid regions, natural disposal of produced water is achieved by evaporation using sun, wind and

humidity. Offshore commercial disposal services are available to oil and gas operators at a fee. It may remove the burden of produced water management from operators but it adds to the operational cost.

1.4. Environmental impact of produced water disposal

The major pollutants of environmental concern in produced water are toxic heavy metals, radioactive materials and petroleum hydrocarbons (especially PAHs). These pollutants are mutagenic and carcinogenic (DeLaune et al., 1999) when they exist at elevated concentrations (St. Pe, 1990), which can lead to contamination of streams, wetlands, and sediments. Migration of these compounds into aquifers from underground pits and tanks where produced water is disposed is also a big environmental concern. Their impact can range from mild to very severe depending on the source of the produced water, pre-disposal treatment and where they are discharged.

Discharge accounts for a significant quantity of produced water disposed into the environment. More than 40% of produced water is discharged into the ocean and it is often stated that its impact on the marine environment are negligible due to the dilution factors (Neff, 1993, UKOOA, 1999). However, contrary to popular opinion that produced water may not have significant effects when discharged into the environment (Owens, 1994, UKOOA, 1999), the full extent of produced water impact on the environment may not yet be understood (Law and Hudson, 1986, Wills, 2000). The actual oil content of produced water may have even been underestimated by half as a result of dissolved organics (Wills, 2000). In fact the presence of dissolved polycyclic aromatic hydrocarbons in produced water may make it more toxic than petroleum itself.

Research increasingly shows significant environmental effects of produced water discharges. It has been reported that planktonic larvae can be

adversely affected by produced water, even in high energy open coastal environment (Raimondi and Schmitt, 1992). Another report noted that zooplankton organisms are vulnerable at the embryonic and larva stages of development when in contact with produced water despite the impressive high dilution factor often claimed by oil operators (Patin, 1999). Also heavy metals discharged into the environment enter the food chain through plants causing severe health problems ranging from skin irritation to central nervous system damage (Naseem and Tahir, 2001, Khezami and Capart, 2005).

To understand the long term effect of produced water on the environment, oil operators and the Norwegian government have developed a model called the Environmental Impact Factor (EIF) which tracks the fate of all components present in produced water discharged into the environment (Meijer and Madin, 2010). This is done in order to comply with "zero" discharge of pollutants into the environment. In a study carried out by Statoil hydro, dissolved hydrocarbons especially PAHs showed significantly higher environmental impact factors than other pollutants in produced water (Buller et al., 2003). PAH as low as 0. 2 ppm was found to have a higher environmental effect than 300 ppm of benzene (Meijer and Madin, 2010). Hence it is important to develop an environmentally friendly system that can either stand alone or combine with existing technology to remove PAHs from produced water before its end use.

1.5. Research aim, thesis outline and summary

The main aim of this research is to develop a novel photo-electro-catalytic process for simultaneous removal of heavy metals and PAHs from produced water in a photoelectrochemical (PEC) cell. It should be noted that until now solar cells have only been used for a single purpose, either to remove heavy metals or organic pollutants. It has never been reported in the

literature that a single PEC cell was used for a dual purpose of heavy metals and organic pollutants removal. As a matter of fact such innovation has only been described as a future technology (Barakat, 2011). To achieve this research aim, several objectives are set:

➢ Synthetic produced water will be used as a natural electrolyte because of its high conductivity, forming the basis for electrolytic treatment.

➢ The understanding of the cathodic process will be carried out at different pH values and heavy metal concentrations, on platinum, glassy carbon and titanium electrodes.

➢ Multi-walled carbon nanotubes-based titania nanohybrid will be synthesised, characterised and used to make photoanodes for studying the photoanodic processes.

➢ A PEC cell will be built and used to demonstrate that both heavy metals and PAH can be co-removed from synthetic produced water.

➢ Detailed investigation of the influences of experimental conditions will be carried out to provide a framework for further process optimization.

➢ Future applications of the PEC process will also be investigated and discussed.

Chapter 1 presents the motivation for this research. It introduces the sources of produced water, reviews the aim and objectives of this work and outlines the details of the thesis structure. An in-depth review of past and current produced water treatment technologies and an overview of CNTs and CNT-semiconductor composite and their applications in photoanodic oxidation are presented in Chapter 2, and chapter 3 outlines the experimental routes that have been taken and the scientific theories behind them. Chapter 4 presents results of the studies of the cathodic processes of the dual purpose PEC cell. It examines the effects of pH,

concentration and the presence of multiple heavy metals on electrodeposition from synthetic produced water. In Chapter 5, results of MWCNT dispersion by anionic surfactant; synthesises, characterization and the performance of MCNT-TiO$_2$ hybrid for the removal of PAH are discussed. In Chapter 6 the principles, design and demonstration of simultaneous removal of heavy metals and PAHs from produced water in a PEC cell carried out on a laboratory scale is presented. The conclusions that have been drawn from this research and recommendations for future research are presented in Chapter 7.

Chapter 2: Literature review

2.1. Introduction

This chapter presents a series of reviews organised into 6 sections, which summarise the composition of produced water, legislations governing produced water discharge, the existing produced water treatment technologies, the potential application of electrochemistry in produced water treatment and the knowledge gaps that have prevented the development of a cost-effective and environmentally friendly treatment process for the removal of dissolved elements (heavy metals and hydrocarbons) from produced water. Section 2.2 gives a detailed overview of the definition, origin, and composition of produced water. It also examines the impact of heavy metals and PAHs present in produced water on the environment. Section 2.3 examines the legislations governing produced water discharge. A detailed description of current produced water treatment technologies are discussed in section 2.4. Section 2.5 gives a review of the application of electrochemistry for produced water treatment. It examines the principles of electrolysis and photoelectrochemistry for metal deposition and oxidation of organics in water. The properties of platinum, titanium and glassy carbon as cathode materials for electrodeposition are also discussed. The suitability of carbon nanotubes (CNT) and titania semiconductor properties as photoanodes are also examined. Section 2.6 summarises the main conclusions drawn from the review of produced water treatment technologies, the knowledge gaps and process limitations that have been identified, and the research objectives that have been drawn to develop a treatment process that is able to overcome these limitations.

2.2. Origin and composition of produced water

Petroleum is a major source of energy and revenue for many countries today and its production is one of the most important industrial activities of

the 21st century (Oliveira et al., 2005). Since the late 1850s when the first oil well was drilled, demand for petroleum has continued to rise. It was estimated that world daily petroleum consumption would increase from 85 million barrels in 2006 to 106.6 million barrels by 2030 (EIA, 2009). This rise in consumption will automatically translate to generation of produced water as discussed in Chapter 1. Petroleum production is accompanied with large volumes of waste, and produced water accounts for more than 80% of its liquid waste, which can be as high as 95% in aging oilfields (Fakhru'l-Razi et al., 2009, Kaur et al., 2009) as shown in Figure 2.1.
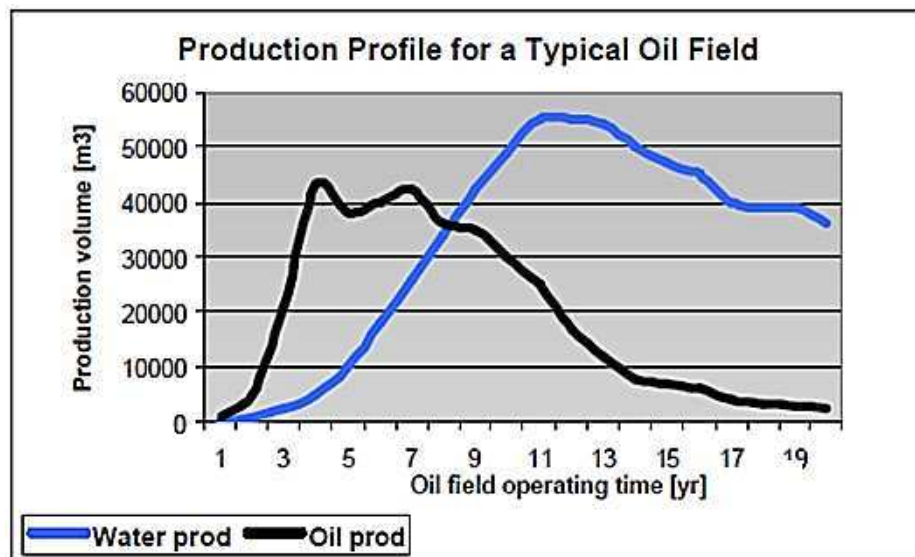
Figure 2.1: Typical production profile of an oilfield (Azetsu-Scott et al., 2007)

Natural water or formation water is always found together with petroleum in reservoirs. It is slightly acidic and sits below the hydrocarbons in porous reservoir media (Figure 2.2). Extraction of oil and gas often leads to reduction in reservoir pressure, and additional water is usually injected into the reservoir water layer to maintain hydraulic pressure and enhance oil recovery. In addition to injected water, there can be water breakthrough from outside the reservoir area (Strømgren et al., 1995, Azetsu-Scott et

al., 2007), and as oil and gas production continues, the time comes when formation water reaches production well, and production of water begins alongside the hydrocarbons. This water is also known as produced water or oil field brine (Chan et al., 2002, Reynolds, 2003).
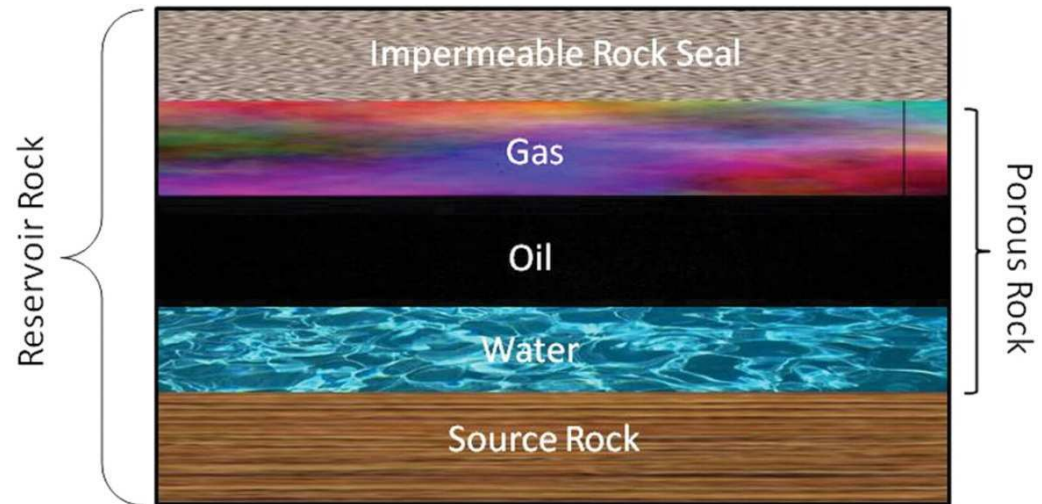
Figure 2.2: Sketch of a typical reservoir

Produced water has a varying and complex composition which is broadly classified into organic and inorganic compounds (Hayes, 2004). Organic compounds in produced water include oils, grease, phenol, carboxylic acids and glycols. Inorganic constituents are either soluble or insoluble; these include scales, precipitates, inorganic colloids and salts. There is a wide variation in the level of the organic and inorganic composition due to several factors (Ray and Engelhardt, 1992, Stephenson, 1992, Hayes, 2004, Sirivedhin et al., 2004, Azetsu-Scott et al., 2007).

2.2.1.   Oil content

The term "oil" is a generic term covering a wide spectrum of compounds with different properties. Oil is mainly hydrocarbons and is present in produced water as dispersed droplets or as dissolved oil (Hayes, 2004, Veil et al., 2004, Khosravi and Alamdari, 2009). BTEX, phenols, aliphatic

hydrocarbons, carboxylic acid and other low molecular weight aromatic compounds fall under dissolved oil while less soluble PAHs and heavy alkyl phenols are classified as dispersed oil in produced water (Igunnu and Chen, 2012). As a general rule, any form of hydrocarbon compound dissolved in produced water can be classified as dissolved oil/hydrocarbon while insoluble hydrocarbon compounds are classified as dispersed oil. Dissolved and dispersed oils are dangerous to the environment and their concentrations can range from very low to very high depending on the oilfields (Hayes, 2004, Hansen and Davies, 1994, NTG, 2005, Hudgins and Petrotech, 1994). The quantity of oil present in produced water is governed by a number of complex but interrelated factors (Stephenson, 1992, Hansen and Davies, 1994, Hayes, 2004). Therefore it is difficult to use a single method to measure the oil content of produced water. Sampling method, preservation and extraction are important factors considered in determining a suitable method for oil content measurement. The most frequently used methods to determine the oil content of produced water are based upon ultra violet (UV) spectroscopy, infra-red (IR) spectroscopy, gas chromatography and gravimetry (OGP, 2005).

2.2.2. Dissolved minerals

Dissolved inorganic species (ions, compounds or minerals) are usually high in concentration, and classified as cations, anions, naturally occurring radioactive materials (NORM) and heavy metals. Cations and anions play a significant role in the chemistry of produced water. Na^+ and Cl^- are responsible for salinity, ranging from a few mg/L to about 300,000 mg/L (Roach et al., 1992). Ions such as Cl^-, $[SO_4]^{2-}$, $[CO_3]^{2-}$, $[HCO_3]^-$, Na^+, K^+, Ca^{2+}, Ba^{2+}, Mg^{2+}, Fe^{2+}, and Sr^{2+} affect conductivity and scale formation potential. Typical oilfield produced water contains heavy metals in various concentrations, depending on the formation geology and the age of oil well

(Azetsu-Scott et al., 2007, Igunnu and Chen, 2012). Heavy metal concentrations in produced water are usually higher than those of injected or receiving water (for enhanced oil recovery) and those found in sea water (Roach et al., 1992).

Radioactivity of produced water results primarily from radium that is derived from the radioactive decay of uranium and thorium associated with certain rocks and clays in the reservoir Reid (1983), (Kraemer and Reid, 1984, Michel, 1990, OGP, 2005). The most abundant naturally occurring radioactive elements present in produced water are the ^{226}Ra and ^{228}Ra isotopes (Utvik, 2003) and are usually co-precipitated with barium sulphate (scale) or other types of scales. The concentration of barium ions in produced water could therefore give a strong indication of radium isotopes present in it (Jerez Vegueria et al., 2002). In some oilfields up to 21 Bq/L of ^{228}Ra have been detected in produced water samples (Fakhru'l-Razi et al., 2009). Other naturally occurring radionuclides have been identified in produced water including ^{212}Pb, ^{214}Pb, ^{228}Ac and ^{212}Bi (Van Hattum et al., 1992, Roe, 1998, OGP, 2005). Tables 2.1 and 2.2 list typical composition and properties of oil and gas fields produced water, respectively.

Table 2.1: Composition of oil field produced water (Igunnu and Chen, 2012)

Parameter	Minimum value (mg/L)	Maximum value (mg/L)	Metals	Minimum value (mg/L)	Maximum value (mg/L)
Density*	1,014	1,140	Calcium	13	25,800
Conductivity**	4,200	58,600	Sodium	132	97,000
Surface tension***	43	78	Potassium	24	4300
pH****	4.3	10	Magnesium	8	6,000
TOC (mg/L)	0	1,500	Iron	< 0.1	100
TSS (mg/L)	1.2	1,000	Aluminium	310	410
Total oil (IR)	2	565	Boron	5	95
Volatile (BTX)	0.39	35	Barium	1.3	650
Base/neutrals	-	< 140	Cadmium	< 0.005	0.2
Chloride	80	200,000	Copper	< 0.02	1.5
Bicarbonate	77	3,990	Chromium	0.02	1.1
Sulphate	< 2	1,650	Lithium	3	50
Ammoniacal nitrogen	10	300	Manganese	< 0.004	175
Sulphite	-	10	Lead	0.002	8.8
Total polar	9.7	600	Strontium	0.02	1,000
Higher acids	< 1	63	Titanium	< 0.01	0.7
Phenol	0.009	23	Zinc	0.01	35
Volatile fatty acids	2	4,900	Arsenic	< 0.005	0.3
			Mercury	< 0.005	0.3
			Silver	< 0.001	0.15
			Beryllium	< 0.001	0.004

* Unit is Kg/m^3 *** Unit is dynes/cm   ** Unit is μS/cm   **** no unit

Table 2.2: Composition of gas field produced water (Fakhru'l-Razi et al., 2009)

Parameter	Minimum Value (mg/L)	Maximum Value (mg/L)	Parameter	Minimum value (mg/L)	Maximum value (mg/L)
pH*	3.1	7	Iron	ND	1,100
Conductivity**	4200	586000	Lead	< 0.20	10.2
Alkalinity	0	285	Lithium	18.6	235
TDS	2600	360000	Magnesium	0.9	4,300
TSS	8	5484	Manganese	0.9	4,300
BOD5	75	2870	Nickel	ND	9.2
COD	2600	120000	Potassium	149	3,870
Aluminium	ND	83	Silver	0.05	7
Arsenic	< 0.005	151	Sodium	520	120,000
Barium	ND	1740	Strontium	-	6,200
Boron	ND	56	Sulfate	ND	47
Bromide	150	1149	Tin	ND	1.1
Cadmium	ND	1.21	Zinc	ND	0.022
Calcium	ND	51,300	TOC	67	38,000
Chloride	1400	190,000	Surfactants	0.08	1,200
Chromium	ND	0.03	Benzene	< 0.01	18
Copper	ND	5	Oil/grease	2.3	60

* no unit   ** Unit is µS/cm   ND = non-detectable

2.2.3. Production chemicals

Production chemicals (Table 2.3) can be pure compounds or compounds containing active ingredients dissolved in a solvent or a co-solvent which is used during exploration for inhibition of corrosion, hydrate formation, scale deposition, foam production, wax deposition, bacterial growth, gas dehydration and emulsion breaking in order to improve the separation of oil from water (Stephenson, 1992). These chemicals enter produced water in traces but sometimes in significant amounts (Hudgins and Petrotech, 1994) and vary from platform to platform. Active ingredients partition themselves into all phases present depending on their relative solubility in oil, gas or water. The fate of these chemicals is difficult to determine because some active ingredients are consumed in the process (Hudgins and Petrotech, 1994).

Table 2.3: Production chemicals in oil & gas fields produced water

(Stephenson, 1992)

Chemical	Concentration – Oil Field		Concentration – Gas field	
	Typical, mg/L	Range, mg/L	Typical, mg/L	Range, mg/L
Corrosion inhibitor[a]	4	2 – 10	4	2 – 10
Scale inhibitor[b]	10	4 – 30	-	-
Demulsifier[c]	1	1 – 2	-	-
Polyelectrolyte[d]	2	0 – 10	-	-
Methanol			2000	1000 - 15000
Glycol (DEG)			1000	500 – 2000

[a] typically containing amide/imidazoline compounds

[b] typically containing phosphate ester/phosphate compounds

[c] typically containing oxylated resins/polyglycol ester/alkyl aryl sulphonates

[d] e.g. polyamine compounds

2.2.4. Produced solids

Produced solids include clays, waxes, precipitated solids, bacteria, carbonates, sand and silt, corrosion and scale products, proppant, formation solids and other suspended solids (Fakhru'l-Razi et al., 2009, Igunnu and Chen, 2012). Their concentrations vary from one platform to another and could cause serious problems during oil production. For example common scales and bacterial can clog flow lines, form oily sludge and emulsions which must be removed (Cline, 1998).

2.2.5. Dissolved Gases

The major dissolved gases in produced water are carbon dioxide, oxygen and hydrogen sulfide. They are formed naturally by the activities of bacterial or by chemical reactions in the water.

2.2.6. Heavy metals in Produced Water

Heavy metals are defined as elements with specific gravity greater than 5.0 and atomic weight between 63.5 and 200.6 (Srivastava and Majumder, 2008). They are toxic or carcinogenic even at low concentrations, including mercury (Hg), lead (Pb), cadmium (Cd), chromium (Cr) and silver (Ag), and their concentrations in produced water range from non-detectable to ~510 mg/L as shown in Tables 2.1 and 2.2. Their origins in produced water are either as a result of leaching and dissolution from source rocks or as lattice bound constituents in solid particles entrained in fluids flowing from the reservoir (OGP, 2005). Although their concentrations in produced water are in trace amount compared with other compounds present, a relatively high amount of heavy metals is discharged into the environment annually. For example more than 19 tonnes of heavy metals worth over $ 100,000 are discharged into the North Sea annually from offshore petroleum platforms as shown in Figure 2.4. Heavy metal pollution of water bodies

and soils is a major environmental and human health problem. Therefore the amount of heavy metals in produced water is of particular interest to environmental regulators, because they are non-biodegradable and are likely to accumulate in living organisms (Fu and Wang, 2001).

Heavy metals in trace amounts are normal constituents of marine organisms and some are essential for normal growth and development. However additional quantities of heavy metals to the marine or estuarine environment at sufficiently high concentrations are toxic to living organisms (Bryan, 1971). Their discharge into the sea will undergo dilution, precipitation, adsorption or absorption by marine organisms.

Table 2.1: Estimates of annual metal inputs (tonnes) from oil and gas platforms in the North Sea

Metal	Input from produced water (tonne)[*]	Value based on 2013 price[**] ($)
Zinc	5.5	11,034.11
Lead	1.2	2,460.36
Copper	0.7	4,660.58
Cadmium	1.2	2,380.00
Chromium	3.8	1,463.00
Nickel	5.2	85,292.16
Arsenic	4.0	7,672.09

* Data obtained form (OGP, 2005)
** Prices obtained from www.metalprices.com

Apart from marine organisms, all plants have the ability to accumulate heavy metals which are essential for their growth and development from soil and water; however they also have the ability to accumulate heavy metals which have no known biological function. Excessive accumulation of these metals can be toxic to most plants and subsequently animals feeding on them (Salt et al., 1995). There are several problems encountered when studying the toxicity of heavy metals. One is that heavy metal pollution is never due to one single metal, it varies from mainly two to almost all possible metals. This makes conclusions regarding relative toxicity between metals hard to draw (Baath, 1989).

However studies have shown that heavy metals mainly reach humans via the food chain and each metal is responsible for specific health issues. For example Pb is responsible for central nervous system damage in humans. It accumulates in the skeleton and is only slowly released from the body. According to the World Health Organisation, Pb has a half-life of about one month in blood and 20 – 30 years in skeleton (WHO, 1995). In produced water it may react with organic compounds under certain conditions to become organic Pb, which is more dangerous than ordinary Pb metal. Studies have also shown that organic lead compounds can penetrate body and cell membranes, crossing the blood-brain barrier in adults, which results in encephalopathy (Jarup, 2003). Ni is a known human carcinogen that can cause gastrointestinal distress, skin dermatitis, pulmonary fibrosis and other serious lung and kidney infections when it exceeds critical level in humans (Fu and Wang, 2001, Borba et al., 2006). Excess Fe in humans is deposited in body organs particularly in liver, endocrine glands and heart leading to organ damage (Aessopos et al., 2008). Fe gets into the human digestive systems faster through consumption of animal products than plant products.

United States Environmental Protection Agency (USEPA) lists several heavy metals including copper, lead and nickel as priority chemical pollutants (USEPA, 2011) whose discharge into the environment must be carefully controlled. Therefore the reduction of heavy metal concentration of produced water discharged into the environment is a priority for both oil operators and legislators in order to maintain a safe environment.

2.2.7. Polycyclic Aromatic Hydrocarbons in produced water

Polycyclic aromatic hydrocarbons (PAHs) are among the most toxic and persistent environmental pollutants. They are a large group of organic compounds with two or more fused aromatic rings known to affect a

variety of biological processes (Karacik et al., 2009). PAHs are natural constituents of crude oil and are present in produced water as dissolved or dispersed oil. They are cosmopolitan in the environment (Wilcke, 2007) and the commonly found ones include anthracene, benz(a)anthracene, benzo(a)pyrene, fluorene, naphthalene and phenanthrene (Burritt, 2008). PAHs are present in produced water in a varying degree of toxicity and their acute and chronic toxicity have been determined (Neff et al., 2006). The European Union (EU), EU Scientific Committee for Food (SCF) and the US Environmental Protection Agency (EPA) list several PAHs as priority pollutants as shown in Table 2.5.

Table 2.5: Frequently monitored PAHs (Lerda, 2010)

List	Common Name	Structure	List	Common Name	Structure
EPA, SCF, EU	Benzo[a] pyrene		EPA, SCF, EU	Dibenzo[a,h] anthracene	
EPA	Acenaphthene		EU+SCF	Dibenzo [a,e]pyrene	
EPA	Acenaphthylene		EU+SCF	Dibenzo [a,h]pyrene	
EPA	Anthracene		EU+SCF	Dibenzo [a,i]pyrene	
EPA, SCF, EU	Benzo[a] anthracene		EU+SCF	Dibenzo [a,l]pyrene	
EPA, SCF, EU	Benzo[b] fluoranthene		EPA	Fluoranthene	
SCF, EU	Benzo[j] fluoranthene		EPA	Fluorene	
EPA, SCF, EU	Benzo[k] fluoranthene		EPA, SCF, EU	Indeno[1,2,3-cd]pyrene	
EU	Benzo[c]fluorene		EU+SCF	5-Methyl chrysene	
EPA, SCF, EU	Benzo[ghi] perylene		EPA	Naphthalene	
EPA, SCF, EU	Chrysene		EPA	Phenanthrene	
SCF, EU	Cyclopenta [cd]pyrene		EPA	Pyrene	

PAHs are highly persistent in the soil where they may cause changes in the community composition of soil by decreasing the total soil microbial biomass and microbial activities (Johnsen et al., 2002, Shi et al., 2002, Mellendorf et al., 2010, Anders R. Johnsen, 2002, Shi W., 2002). They have deleterious influences on microbial activities necessary for the early stage development of some plants (Maliszewska-Kordybach and Smreczak, 2003). Terrestrial plants can take up PAHs but bioavailability may be limited because they bind tightly to soil particles (Kuhn et al., 2004).

Two and three ring PAHs are known to be biodegradable in soil to non-toxic and non-carcinogenic levels, but phenanthrene is a dangerous exception because phenanthrene-degrading species are not the predominant organisms in the natural soils (Mellendorf et al., 2010).

PAHs may reach humans through ingestion of particles, dermal contacts or bioaccumulation in the food chain (Mellendorf et al., 2010). They generally have a low degree of acute toxicity to humans at low concentrations but may lead to cancer after chronic exposure. Most PAHs are only slightly mutagenic or even non mutagenic in vitro but their metabolites can be potent mutagens (Rubin, 2001). However several studies have shown that exposure to PAHs can affect animals significantly. Reproductive, neurologic and developmental effects have been observed in animals exposed to PAHs, and the immune systems of some animals have equally been affected (Blanton et al., 1986, Blanton et al., 1988, Dasgupta and Lahiri, 1992, Hahon and Booth, 1986, Malmgren et al., 1952, Zhao, 1990).

PAHs are considered a greater threat in the aquatic environments affecting both plants and animals. Some researchers and several oil and gas operators claim that the impact of PAHs on aquatic life is of no significant concern because of the high dilution factor of PAHs in sea or ocean (UNEP, 1997, Rice, 1999, OGP, 2005). On the contrary, studies on marine and freshwater ecosystems have shown that PAHs have major impacts on

aquatic plants and animals including the population of subsurface organisms. It has been reported that the development of fish embryo was significantly stunted when in contact with PAHs at very low ppb levels. Fish that survive embryonic exposure to PAH concentrations of < 5.2 ppb have a low chance of survival to maturity (Heintz et al., 2000, Carls et al., 1999). Another study showed that fish populations exposed to PAHs even at low ppb levels would experience increased mortality, reduced survival and reduced output at maturity (Heintz et al., 2000). It is therefore important to remove PAHs from produced water before discharge.

2.3. Produced water Legislation

The general practice in use for produced water treatment is gravity based separation and discharge into the environment (Fakhru'l-Razi et al., 2009). For a long time only non-polar oil in water (OIW) was regulated by government while little attention was given to dissolved organics in produced water (Hansen and Davies, 1994). Current researches are paying more attention to the consequences of dissolved organic components, heavy metals and production chemicals on living organisms since their long term effects on the environment are not fully documented and understood.

A general legislation for discharging produced water into sea has been 40 mg/L OIW, but the increase in environmental concerns has led to many countries implementing more stringent regulatory standards. The Oslo Paris Convention (OSPAR) agreed that the maximum discharge be reduced to 30 mg/L OIW and the overall oil discharges in produced water be reduced by 15% from what they were in 1999 (Hansen and Davies, 1994, Igunnu and Chen, 2012). United States Environmental Protection Agency (USEPA) sets a daily maximum for oil and grease in produced water at 42 mg/L. In Australia permitted offshore discharge of oil and grease in produced water is 30 mg/L and the People's Republic of China sets the

monthly average limits of oil and grease and chemical oxygen demand (COD) at 10 mg/L and 100 mg/L, respectively (Igunnu and Chen, 2012). The Convention for the Protection of the Marine Environment of the North – East Atlantic sets the annual average limit for discharge into the sea at 40 mg/L (NTG, 2005).

The EU Water Framework Directive (WFD) adopted in 2000 is committed to "zero discharge" in response to the need for a more protective system to tackle aquatic pollution (OSPAR, 2008). In 2005, oil operators in Norway agreed to implement a zero environmental harmful discharge. To achieve this, the Norwegian Oil Industries Associations developed the Environmental Impact Factor (EIF), which examines the environmental impact of all contaminants in produced water (Igunnu and Chen, 2012). Similarly OSPAR commission has agreed on zero discharge of pollutants into the sea (OSPAR, 2008). Most oil and gas companies around the world are now working towards implementation of "zero-discharge" of contaminants (Pollestad, 2005). In the near future produced water discharged into the environment will be required to contain "zero pollutants". Therefore it is necessary to develop a process that can deal with pollutants that are not currently covered in the already established conventional treatment technologies.

2.4. Produced water treatment technologies

For several decades oil operators have treated produced water for the removal of suspended particles, sand, soluble organics, gases, NORM, de-oiling (removal of dispersed oil and grease), desalination, softening (to remove excess water hardness) and disinfection (Arthur et al., 2005). To meet these objectives operators have applied many stand-alone and combined physical, biological and chemical treatment processes for produced water management. Some of these technologies are reviewed in

this section with particular emphasis on their merits and demerits.

2.4.1. Membrane Filtration Technology

Membranes are films with specific pore or permeability ratings, which selectively separate a fluid from its solid or liquid particulate, molecular and even ionic components. Microfiltration (MF), Ultrafiltration (UF), Reverse Osmosis (RO) and Nanofiltration (NF) are the four established membrane separation processes (Madaeni, 1999). RO is employed for the removal of dissolved and ionic components, MF for suspended particles, UF for macromolecules and NF for selective multivalent ions (Judd et al., 2003, CSM, 2009). MF and UF can be used as a stand-alone technology for treating industrial wastewater, whereas RO and NF are usually employed in water desalination.
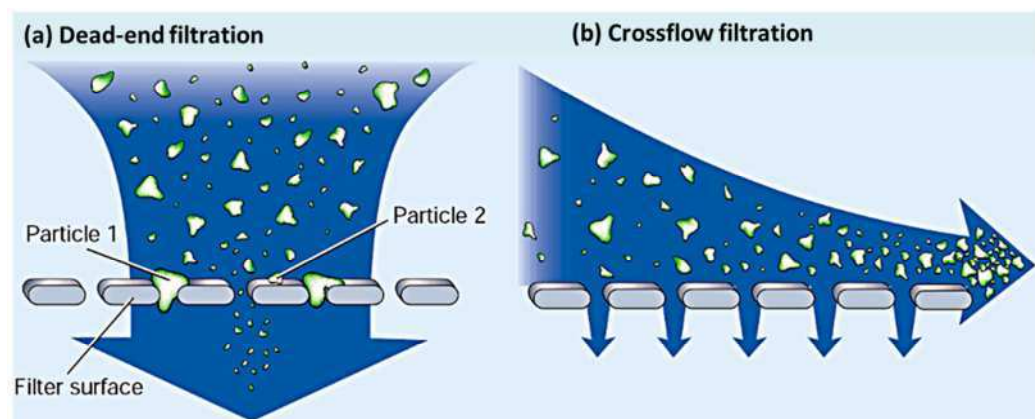
Figure 2.1: Comparison of dead–end filtration and cross-flow filtration (Brainerd, 2001)

Membrane filtration technology operates in either cross-flow or dead-end mode as illustrated in Figure 2.3, which may be a pressure or vacuum driven system (He and Jiang, 2008). In dead end filtration the feed is passed through a membrane, the solids are trapped in the filter and the filtrate is released at the other end, whereas in cross flow filtration the feed flow travels tangentially across the surface of the filter.

2.4.1.1. Microfiltration/Ultrafiltration

MF is typically used for turbidity reduction and removal of suspended solids in produced water treatment while UF is employed in the removal of colour, odour, viruses and colloidal organic matters (CSM, 2009, Han et al., 2010). UF is the most effective method for de-oiling produced water compared to traditional separation methods (He and Jiang, 2008) and it is more efficient than MF in the removal of hydrocarbons, suspended solids and dissolved constituents from produced water (Bilstad and Espedal, 1996). Both MF and UF operate at low trans-membrane pressure (1 – 30 psi) and can serve as a pre-treatment to desalination but cannot be used to remove salt from water (CSM, 2009).

2.4.1.2. Polymeric/Ceramic Membranes

Polymeric and ceramic membranes are used for UF/MF treatment of water. Polymeric MF/UF membranes are made from polyacrylonitrile and polyvinylidene while ceramic membranes are made from clays of nitrides, carbides and oxides of metals (Khemakhem et al., 2009). Ceramic UF/MF membranes can operate in both cross-flow filtration and dead-end filtration modes and usually have a lifespan greater than 10 years. They are efficient membrane technologies for produced water treatment (CSM, 2009). Product water from these treatments is free of suspended solids and nearly all non-dissolved organic carbon (Faibish and Cohen, 2001a, Konieczny et al., 2006, Faibish and Cohen, 2001b, Lobo et al., 2006, Gutierrez et al., 2008). Also chemicals are not used for this process except during periodic cleaning of membranes and pre-coagulation.

2.4.1.3. Reverse Osmosis (RO) and Nanofiltration (NF)

RO and NF are pressure driven membrane processes. Osmotic pressure of the feed solution is suppressed by applying hydraulic pressure which forces permeate (clean water) to diffuse through a non-porous but water

permeable membrane (Spiegler and Kedem, 1966). Seawater RO can remove contaminants as small as 0.0001 µm but its major disadvantage is membrane fouling and scaling (Mark, 2007, CSM, 2009). Early studies on using RO to treat produced water failed due to insufficient process integration and poor treatment results (Doran et al., 1998, Lawrence et al., 1995, Allen, 2008, Nicolaisen and Lien, 2003). However, a successful pilot system was reported for RO treatment of oilfield produced water in Bakersfield, California which operated for over 1,700 hours in six months and produced 20 gpm of clean water (Nicolaisen and Lien, 2003). Other bench scale studies have also shown the ability of brackish water RO membranes to successfully treat oil and gas produced water. Experiments carried out indicated that the RO membrane technology would be excellent for produced water treatment with appropriate pre-treatment technology (Xu and Drewes, 2006, Mondal and Wickramasinghe, 2008). The capital costs of RO membrane systems vary depending on the size of rejection required, materials of construction and site location. They generally have a life expectancy of 3 – 7 years and their operating costs depend on energy price and the level of total dissolved solids (TDS) in the feed water (CSM, 2009).

Nanofiltration is a robust technology for water softening and metals removal and is designed to remove contaminants as small as 0.001 µm. It is similar to RO and applicable for treating water containing TDS in the range of 500 to 25,000 mg/L (CSM, 2009). NF membranes have been employed for produced water treatment on both bench and pilot scales (Nicolaisen and Lien, 2003, Xu and Drewes, 2006). However the effectiveness of NF membranes for the treatment of oilfield produced water is only minimally better than the brackish water RO treatment of the same feed water (Mondal and Wickramasinghe, 2008). A summary of various membrane treatment technologies is presented in table 2.6.

Table 2.6: Summary of membrane treatment technologies (Igunnu and Chen, 2012)

Technology	Ceramic MF/UF membrane	Polymeric MF/UF membrane	NF	RO
Feasibility	Ceramic membranes have been used to treat oilfield produced water and extensively used in other industrial water treatments. They are applicable to all types of produced water irrespective of their TDS and salt concentrations, but produced water with high concentrations may be problematic.	Applicable to water with high TDS and salt concentrations and also has the potential to treat produced water but is extensively used in the municipal water treatment.	This technology is used for water softening and removal of metals from wastewater. It is specifically efficient for feed water containing TDS ranging from 500 to 25 000 mg/L. NF is a poor technology for produced water treatment and is inappropriate as a standalone technology.	This is a robust technology for seawater desalination and has been employed in produced water treatment. For this technology to be effective in produced water treatment, extensive pre-treatment of feed water is necessary. Several pilot studies failed due to poor pre-treatment and insufficient system integration.
Energy Consumption	Not available	Not available	It uses electrical energy and its energy requirement is less than what is required in RO systems. Approximately NF system requires 0.08 Kwh/bbl to power its high-pressure pumps.	RO use electrical energy for its operation. SWRO requires 0.46 − 0.67 KWh/bbl if energy recovery device is integrated. BWRO require less energy than equivalent SWRO system. BWRO requires 0.02 − 0.13 KWh/bbl of energy to power the system's pumps.
Chemical Use	Ferric chloride, polyaluminium chloride and aluminium sulphate are common coagulants used for pre-coagulation. Acids, bases and surfactants are used in cleaning process.	Ferric chloride, polyaluminium chloride and aluminium sulphate are common coagulants. Aluminium sulphate are common used for pre-coagulation. Acids, bases and surfactants are used in cleaning process.	Caustic and scale inhibitors are required to prevent fouling. $NaOH$, H_2O_2, Na_2SO_4, HCl, or Na_4EDTA are required for cleaning the system.	Caustic and scale inhibitors are required to prevent fouling. $NaOH$, H_2O_2, Na_2SO_4, H_3PO_4, HCl, or Na_4EDTA are required for cleaning the system.
Pre/Post treatment	Cartridge filtration and coagulation are usually used as a pre-treatment. Post-treatment may be required for polishing depending on the product water.	Cartridge filtration and coagulation are usually used as a pre-treatment. Post-treatment may be required for polishing depending on the product water.	Extensive pre-treatment is required to prevent fouling of membrane. Product water may require remineralisation to restore SAR values.	Extensive pre-treatment is required to prevent fouling of membrane. Product water may require remineralisation or pH stabilization to restore SAR values.
Overall cost	Not available	Capital costs depend on feed water quality and size of the polymeric membrane system. Approximate capital cost is $0.02 −0.05/bpd while approximate Operation and Maintenance costs $ 0.02 −$ 0.05/bpd.	Capital cost range from $ 35 to $ 170/bpd. Operating cost is $ 0.03/bbl.	Capital costs of BWRO vary from $ 35 to $ 170/bpd and operating costs are $ 0.03/bbl. Capital costs of SWRO vary from $ 125 to $ 295/bpd and operating costs are $ 0.08/bbl.
Life cycle	10 years	7 years or more	3−7 years	3 −7 years
Advantages	(1)Product water is totally free of suspended solids. (2)It can be operated in cross-flow or dead-end filtration mode. (3)Product water recovery range from 90 % to 100 %. (4)Ceramic membranes have a longer lifespan than polymeric membranes.	(1)Product water is free of suspended solids. (2) Product water recovery range from 85 to 100 %.	(1)It has high pH tolerance. (2)System can be operated automatically leading to less demand of skilled workers. (3)Energy costs can be reduced by implementing energy recovery subsystems. (4)Does not require solid waste disposal. (5)Water recovery between 75 % and 90 %.	(1)It has high pH tolerance. (2)System can be operated automatically leading to less demand of skilled workers. (3)Energy costs can be reduced by implementing energy recovery subsystems. (4)It performs excellently in produced water treatment with appropriate pre-treatment. (5)It does not require concentrate treatment as brine generated is usually disposed into sea. (6)Product water recovery in SWRO is between 30 % and 60 % and between 60 and 85 % in BWRO.
Disadvantages	(1)Irreversible membrane fouling can occur with significant amount of iron concentration is in feed water. (2)Membrane requires periodic cleaning. (3)Waste generated during backwash and cleaning processes require disposal/ recycling or further treatment.	(1)Membrane requires periodic cleaning. (2)Waste generated during backwash and cleaning processes require disposal/recycling or further treatment.	(1)It is highly sensitive to organic and inorganic constituents in the feed water. (2)Membranes cannot withstand feed temperatures in excess of 458 ^{o}C. (3)Requires several backwashing cycles.	(1)It is highly sensitive to organic and inorganic constituents in the feed water. (2)Membranes cannot withstand feed temperatures in excess of 458 ^{o}C.

2.4.2. Thermal Technologies

The thermal treatment technology was the choice for water desalination before the development of the membrane technology and it is employed in

regions where the cost of energy is relatively cheap. Multistage flash distillation (MSF), vapour compression distillation (VCD) and multi effect distillation (MED) are the major thermal desalination technologies however hybrid thermal desalination plants, such as MED – VCD, have been used to achieve higher efficiency (Ettouney et al., 2002, GWI, 2006). Although membrane technologies are typically preferred to thermal technologies, recent innovations in engineering make thermal processes more attractive and competitive in treating highly contaminated water (Darwish et al., 2003, Han et al., 2010).

2.4.2.1. Multi Stage Flash

Multi stage flash (MSF) distillation process is a mature and robust technology for brackish and sea water desalination. Its operation is based on evaporation of water by reducing the pressure instead of raising the temperature. The feed water is preheated and flows into a chamber with lower pressure where it immediately flashes into steam (GWI, 2006). Water recovery from the MSF treatment is about 20 % and its energy requirement is between 3.35 and 4.70 kWh/bbl (Darwish et al., 2003). A major setback in operating MSF is scale formation on heat transfer surfaces, which often requires the use of scale inhibitors and acids. Its overall cost varies depending on size, site location and materials of construction (Ettouney et al., 2002). Its market share has also significantly decreased globally due to competition with membrane technologies but it is a relatively cost effective method with plant life expectancy of more than 20 years, and can be employed for produced water treatment (GWI, 2006).

2.4.2.2. Multi Effect Distillation (MED)

A MED process involves application of sufficient energy that converts saline water to steam which is then recovered as pure water via condensation. Multiple effects are employed in order to improve efficiency and minimize

energy consumption as shown in Figure 2.4. The energy efficiency gained through the combination of several evaporator systems is a major advantage of this process.
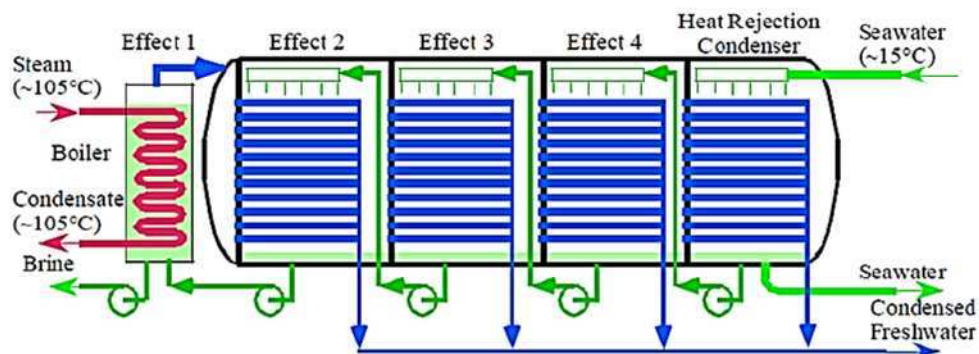
Figure 2.2: Schematic diagram of a conventional Multi effect distillation system (Peterson and Zhao, 2006)

Water recovery from MED systems are in the range of 20 - 67 % depending on the type of evaporator design employed (Watson et al., 2003). Despite the high water recovery from MED systems, it has not been extensively used for water production like MSF because of scaling problems associated with old designs. Falling film evaporators have been introduced recently to improve heat transfer rates and reduce the rate of scale formation (Igunnu and Chen, 2012).

MED can be applied to a wide range of feed water quality (including produced water). Their power energy consumption is in the range of 1.3 – 1.9 KWh/bbl and they usually have a life cycle of 20 years (Darwish et al., 2003, CSM, 2009). Scale inhibitors and acids may be required to prevent scaling and pH control is essential to prevent corrosion. Their cost of power and operation is approximately $0.11/bbl, while their total unit cost is $0.16/bbl on average (Ettouney et al., 2002).

2.4.2.3. Vapour Compression Distillation (VCD)

In VCD, vapour is generated in the evaporation chamber and then compressed thermally or mechanically, which raises the temperature and

pressure of the vapour. The heat of condensation is returned to the evaporator and utilized as a heat source (Figure 2.5). This is a reliable and efficient desalination process and can operate at temperatures below 70 ºC, which reduces scale formation problems (Khawaji et al., 2008). It is an established desalination technology for treating seawater and reverse osmosis concentrate (CSM, 2009).
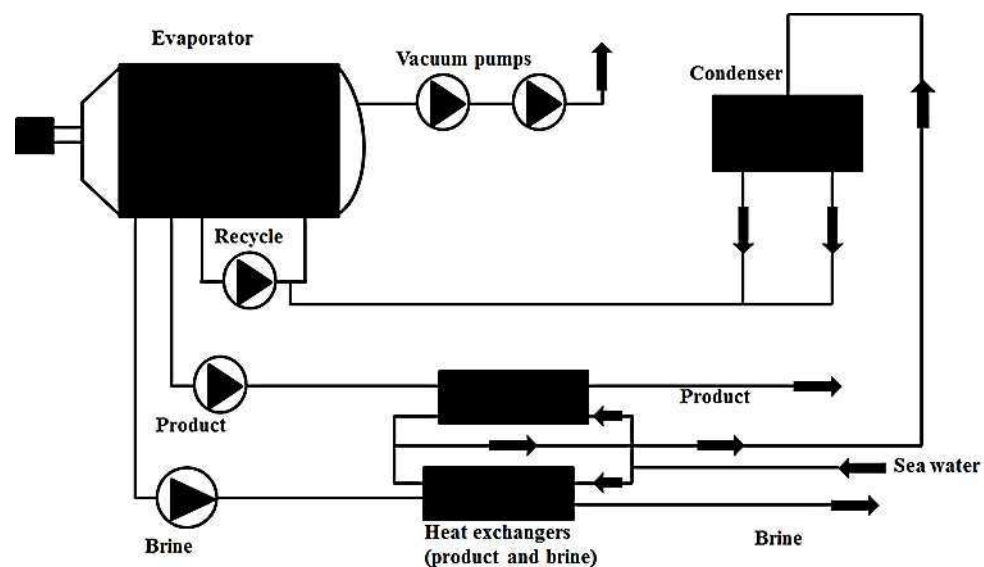
Figure 2.3: Flow diagram of a vapour compression process (Veza, 1995)

The energy consumption of a VCD plant is significantly lower than that of MED and MSF and this depends on various factors. However cogeneration of low pressure steam has been identified as a major factor in significantly reducing the overall cost (Igunnu and Chen, 2012). Although this technology is mainly associated with sea water desalination, various enhanced vapour compression technologies have been employed for produced water treatment (CSM, 2009).

2.4.2.4. Multi Effect Distillation – Vapour compression Hybrid

A hybrid of MED and VCD has been developed which increases production and improves energy efficiency. It is believed that this new technology

46

would replace the older MSF plants. GE has recently developed produced water evaporators with a life expectancy of 30 years which use mechanical vapour compression (CSM, 2009). These evaporators exhibit a number of advantages over conventional produced water treatment methods including reduction in chemical use, overall cost and fouling severity. Other advantages include softer sludge, better handling and storage (Heins, 2005). More than 16 produced water evaporators have been installed in Canada, and more are expected to be installed in other regions of the world (Heins and McNeill, 2007). However the huge generation of carbon dioxide and high energy cost associated with all thermal technologies are still a major disadvantage of this technology.

Table 2.7: Summary of thermal treatment technologies (Igunnu and Chen, 2012)

Technology	Multi Stage Flash (MSF)	Multi Effect Distillation (MED)	Vapour Comparison Distillation (VCD) Technology	Multi Effect Distillation- Vapour Compression Hybrid	Freeze thaw evaporation
Feasibility	This is a mature and robust desalination technology that can be employed for produced water treatment. MSF is applicable to all types of water with high TDS range up to 40,000 mg/L	This is a mature and robust desalination technology that can be employed for produced water treatment. MED is applicable to all types of water and a wide range of TDS	This is a mature and robust seawater desalination technology. It is applicable to all types of waste water with TDS level greater than 40,000 mg/L. Various enhanced VCD have been applied in produced water treatment	A mature desalination technology that has been employed in produced water treatment. It is usually employed for treating water with high TDS. In future product, water quality may be increased. For example, product water recovery of 75% was achieved by GE using brine concentrator and analyser	This is a mature and robust technology for produced water treatment. It does not require infrastructure. This process requires favourable soil conditions, a significant amount of land and a substantial number of days with temperatures below freezing
Energy consumption	Electrical energy required ranges from 0.45 kWh/bbl to 0.9 kWh/bbl. Thermal energy required is estimated at 3.35 kWh/bbl. Overall energy required for MSF ranges from 3.35 to 4.70 kWh/bbl	MED requires both thermal and electrical energy types. Electrical energy consumed is approximately 0.48 kWh/h/bbl and power consumption is 1.3 –1.9 kWh/bbl	VCD requires both thermal and electrical energy. For desalination, power energy consumption is 1.3 kWh/bbl. Electricity consumption is 1.1 kWh/bbl for mechanical vapour compression (MVC) and to achieve zero-liquid discharge energy demand is 4.2 –10.5 kWh/bbl	It uses both thermal and electrical energy. Power consumption for desalination is 0.32 kWh/bbl. To achieve zero-liquid discharge energy consumption is around 4.2 –10.5 kWh/bbl	It uses electrical energy, but data are not available
Chemical use	EDTA, acids and other antiscaling chemicals are used to prevent scaling. pH control is also necessary to prevent corrosion	Scale inhibitors are required to prevent scaling. Acid, EDTA and other antiscaling chemicals are required for cleaning and process control	Scale inhibitors and acids are required to prevent scaling. EDTA and other antiscaling chemicals are required for cleaning and process control. Corrosion is prevented by pH control	Scale inhibitors are required to prevent scaling. Acids, EDTA and other antiscaling chemicals are required for cleaning and process control. Corrosion is prevented by pH control	None
Pre/Post treatment	Pre-treatment is done to remove large suspended solids. This requires screens and rough filtration. Product water stabilization is required because of its low TDS	Pre-treatment is done to remove large suspended solids similar to MSF. This requires screens and rough filtration. Product water stabilization is required because of its low TDS	Pre-treatment and post-treatments are required in order to avoid fouling and because of low TDS level in product water, respectively	It requires a less rigorous pre-treatment compared with membrane technologies. Lime bed contact post-treatment is required because of low TDS of product water	It requires minimal pre- and post-treatment depending on product water quality and discharge standards
Overall Cost	Capital costs vary between $250 and $360 per bpd. Operating costs are $0.12/bbl and total unit costs are $0.19/bbl	Overall cost is lesser than in MSF. Capital costs ranges from $ 250 to $330 per bpd. Operating costs are 0.11/bbl and total unit costs are $ 0.16/bbl	Capital costs of vapour compression for sea water desalination ranges from $140 to 250 per bpd depending on various factors. Operating costs are 0.075/bbl and total unit costs are $0.08/bbl for seawater desalination	Capital cost is $250 per bbl per day. Operation costs depend on the amount of energy consumed	It depends on location
Life cycle	Typically 20 years but most plants operate for more than 30 years	Typically 20 years	Typically 20 years but may operate for more years	Typically 20 years but may be longer if made of materials with high corrosion resistance	Expected lifespan is 20 years
Advantages	(1)It requires less rigorous pre-treatment and feed condition compared with membrane technologies (2)It has a significantly long lifespan (3)MSF system can withstand harsh conditions (4)It can easily be adapted to highly varying water quality (5)Cost of labour is cheaper than using membrane technology (6)Good for high TDS produced water treatment (7)Product water quality is high with TDS levels between 2 mg/L and 10 mg/L	(1)It requires less rigorous pre-treatment and feed condition compared with membrane technologies (2)It has a long lifespan (3)Energy requirement is cheaper than using MSF (4)It can easily be adapted to highly varying water quality (5)Cost of labour is cheaper than using MSF or membrane technology (6)Good for high TDS produced water treatment (7)Product water quality is high (8)It does not require special concentrate treatment (9)Product water recovery of up to 67% can be achieved using stacked vertical tube design	(1)Applicable to all types of water and water with high TDS 40,000 mg/L (2)It is a smaller unit compared with MSF and MED (3)It has high ability to withstand harsh conditions (4)It does not require special concentrate treatment (5)Pre -treatment is less rigorous compared with membrane treatment	(1)It has high product water quality (2)Excellent treatment technology for produced water with high TDS and zero liquid discharge (3)System can withstand harsh condition	(1) Excellent for zero liquid discharge (2) It requires low skilled labour, monitoring and control (3) It is highly reliable and can be easily adapted to varying water quality and quantity
Disadvantages	(1)Low product water recovery usually between 10 and 20% (2)It is not flexible for varying water flow rates (3)Scaling and corrosion can be a problem	(1)Typically low product water recovery usually between 20% and 35% (2)It is not flexible for varying water flow rates (3)Scaling and corrosion can be a problem (4)High level of skilled labour required	(1)Typically low product water recovery is usually around40% (2)It is not flexible for varying water flow rates (3)Scaling and corrosion can be a problem (4)High level of skills are required to operate system	(1)Not applicable to produced water wells point source (2)Being a hybrid design, it requires very highly skilled labour	(1)Cannot treat produced water with high methanol concentration (2)Moderate product water quality containing 1000 mg/L TDS (3)Can only work in winter time and in places with below freezing temperatures (4)A significant amount of land is required (5)It generates secondary waste streams

2.4.3. Biological Aerated Filters

Biological Aerated Filters (BAFs) are a class of biological technologies which consist of permeable media that use aerobic conditions to facilitate biochemical oxidation and removal of organic constituents in polluted water. The media are usually not more than 4 inches in diameter to prevent clogging of pore spaces when sloughing occurs (CSM, 2009). BAFs are most effective for produced water with chloride levels below 6,600 mg/L and can remove oil, ammonia, suspended solids, nitrogen, chemical oxygen demand (COD), biological oxygen demand (BOD), heavy metals (iron in particular), soluble organics, trace organics and hydrogen sulfide from produced water (Su et al., 2007). This process consumes 1 – 4 kWh/day, and requires upstream and downstream sedimentation to allow the usage of the filter's full bed. Water recovery from this process is nearly 100 % since waste generated is removed in solid form, and removal efficiencies of up to 70 % nitrogen, 80 % oil, 60 % COD, 95 % BOD and 85 % suspended solids have been achieved with the BAF treatment (Su et al., 2007).

BAFs usually have a long lifespan and do not require any chemicals or cleaning during normal operations. However solids disposal may be required for accumulated sludge in the sedimentation basins, which can account for up to 40 % of the total cost of this technology (Schmidt et al., 1980), but capital accounts for the main cost of this technology.

2.4.4. Hydrocyclones

Hydrocyclones use a physical method to separate solids from liquids based on the density of the solids to be separated. They can remove particles in the range of 5 – 15 µm and have been widely used for the treatment of produced water (CSM, 2009). Nearly 8 million barrels of produced water are treated with hydrocyclones daily (Svarovsky, 1992). Hydrocyclones are

usually made from metals, plastics, or ceramics and they usually have a cylindrical top and a conical base with no moving parts (Figure 2.6). Their performance is determined by the angle of the conical section (CSM, 2009).
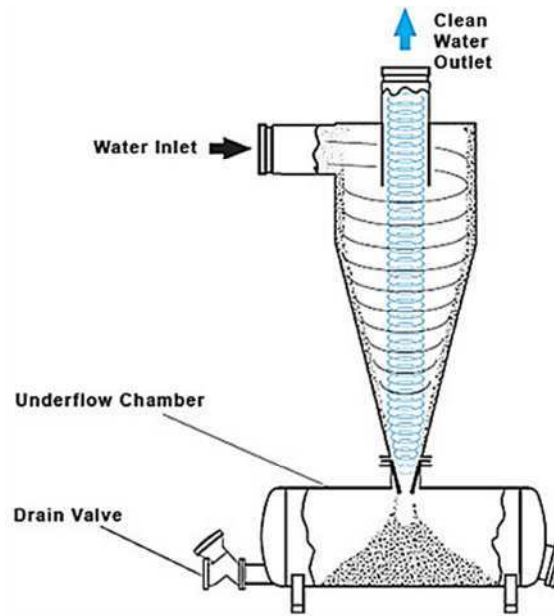
Figure 2.6: Hydrocyclone flow scheme and mode of operation (Igunnu and Chen, 2012)

They have a long lifespan and can be used in combination with other technologies as a pre-treatment process. Also they do not require use of chemicals or pre-treatment of feed water, but a major challenge of this technology is dealing with the large amount of slurry of concentrated solid waste generated during operation.

2.4.5.   Gas Flotation

The flotation technology uses fine gas bubbles to separate suspended particles that are not easily separated by sedimentation. It is widely used for the treatment of conventional oilfield produced water with an estimated cost of \$0.60/m^3 (Çakmakce et al., 2008). When the gas is injected into the produced water, suspended particulates and oil droplets are attached

to the air bubbles as it rises. This results in the formation of foam on the surface of the water which is skimmed off as froth (Cassidy, 1993).

There are two types of gas flotation technology (dissolved gas flotation and induced gas flotation) based on the method of gas bubble generation and resultant bubble sizes. In dissolved gas floatation units, the gas is introduced into the flotation chamber by a vacuum or by creating a pressure drop however mechanical shear or propellers are used to create bubbles in induced gas flotation units (Çakmakce et al., 2008). Gas floatation can remove particles as small as 25 µm and can even remove contaminants down to 3 µm in size if coagulation is added as pre-treatment, but it cannot remove soluble oil constituents from water (CSM, 2009). Flotation is most effective when the gas bubble size is less than the oil droplet size and it is expected to work best at low temperature since it involves dissolving gas into water stream.

This technology can be used to remove grease, oil, natural organic matter, volatile organics and small particles from produced water (Cassidy, 1993, Hayes, 2004, Çakmakce et al., 2008, CSM, 2009). Gas flotation does not require chemical use except when coagulants are added to enhance removal of target contaminants; however solid disposal will be necessary for the sludge generated from this process.

2.4.6.   Evaporation Pond

An evaporation pond is an artificial pond designed to efficiently evaporate water by solar energy. It requires a relatively large space of land and has been employed for the treatment of produced water onsite and offsite (Velmurugan and Srithar, 2008). It is designed to either prevent subsurface infiltration of water or the downward migration of water depending on produced water quality (ALL, 2003). It is a favourable technology for warm and dry climates because of its ability to achieve and

maintain high evaporation rates. Evaporation ponds are typically economical and usually covered with nettings to prevent potential problems to migratory waterfowl caused by contaminants in the produced water (CSM, 2009). All water is lost to the environment when using this technology which is a major setback when water recovery is an objective for water treatment.

2.4.7. Adsorption

Adsorption is generally utilized as a polishing step in water treatment process rather than as a stand-alone technology since adsorbents can be easily overloaded with organics. It requires a vessel to contain the adsorption media and pumps to implement backwashes which happen periodically to remove particulates trapped in the media voids. It is reported that it can be used to remove manganese, iron, TOC, BTEX, oil and more than 80 % of heavy metals present in produced water (CSM, 2009). Common adsorbents used in this technology include activated carbon, organoclays, activated alumina and zeolites (Spellman, 2003). The adsorption process is applicable to water treatment irrespective of salinity, although replacement or regeneration of the adsorption media may be required depending on feed water quality and media type. The rate of media usage is one of the main operational costs of adsorption technology (Spellman, 2003). The use of chemicals to regenerate the adsorption media when all active sites are blocked also often results in liquid waste disposal and media replacement results in extra solid waste management.

2.4.8. Media Filtration

The filtration treatment technology uses various types of media such as sand, gravel, anthracite, walnut shell for the removal of oil, grease and TOC from produced water (CSM, 2009, Igunnu and Chen, 2012). This process is not affected by water salinity and is applicable to any type of

produced water. The media filtration technology is highly efficient for the removal of oil and grease. It is reported that more than 90 % of oil and grease has been removed from produced water by this technology (CSM, 2009). The efficiency of media filtration can be enhanced if coagulants are added to the feed water prior to filtration. The setbacks of this technology are media regeneration and solid waste disposal, which adds extra cost to water treatment.

2.4.9.   Ion Exchange Technology

Ion exchange is a widely applied technology in industrial operations for various purposes including utilization for the treatment of coal bed methane produced water. It is especially useful in the removal of monovalent and divalent ions via resins from produced water (Clifford, 1999). It was suggested that ion exchange had the potential to remove boron from reverse osmosis permeate of produced water (Nadav, 1999). Ion exchange often requires the use of chemicals for resin regeneration and disinfection, and has a lifespan of about 8 years. It will require pre-treatment options for solids removal and its operating cost accounts for more than 70 % of its overall cost (CSM, 2009).

2.4.10.   Chemical Oxidation

The chemical oxidation treatment is based on oxidation and reduction reactions occurring together in produced water. Since free electrons cannot exist in solution, the oxidant mixes with contaminants and causes them to break down (ALL, 2003). Oxidants commonly used include ozone, peroxide, permanganate, oxygen and chlorine. This is an established and reliable technology for the removal of colour, odour, COD, BOD, organics and some inorganic compounds from produced water (Barratt et al., 1997). The oxidation rate of this technology depends on the chemical dose; type of oxidant used, raw water quality and contact time between oxidants and

water. This potentially makes the chemical cost during this process relatively high. Energy consumption accounts for about 18 % of the total operations and maintenance (Barratt et al., 1997). Chemical oxidation requires minimal equipment and has a life expectancy of 10 years or longer. Post- treatment may be required to remove oxidized particles (CSM, 2009).

2.4.11. Electrodialysis and Electrodialysis Reversal

Electrodialysis (ED) and electrodialysis reversal (EDR) are mature electrochemically driven desalination technologies used for the separation of dissolved ions in water via ion exchange membranes.
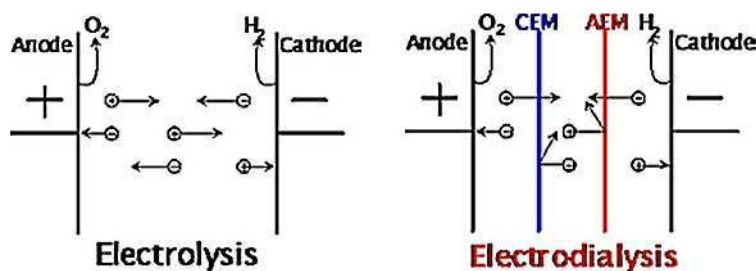
Figure 2.7: Comparison of electrolysis and Electrodialysis (CEM = cation exchange membrane, AEM = anion exchange membrane) (Jurag Separation, 2013)

They use a series of ion exchange membranes containing electrically charged functional sites arranged in an alternating mode between anode and cathode to remove charged substances from feed water (Figure 2.7). If the membrane is positively charged, only anions are allowed to pass through it. Similarly, negatively charged membranes allow only cations to pass through them. EDR uses periodic reversal of polarity to optimize this operation (CSM, 2009).

ED is an excellent produced water treatment technology that will work best for treating relatively low saline produced water (Sirivedhin et al., 2004).

However EDR and ED technologies have only been tested on the laboratory scale for the treatment of produced water (Igunnu and Chen, 2012). The lifespan of ED/EDR membranes is between 4 and 5 years. Regular membrane fouling and high treatment cost are the major limitations of this technology (CSM, 2009).

2.4.12. Freeze Thaw Evaporation

Developed in 1992 by Energy & Environmental Research Centre (EERC) and B.C Technologies Ltd. (BCT), freeze thaw evaporation (FTE$^®$) is a mature and robust technology for produced water treatment and disposal (Igunnu and Chen, 2012). The FTE$^®$ process employs freezing, thawing and conventional evaporation for wastewater management. Natural salts and other dissolved constituents in produced water cause the freezing point to be lowered below 32 $^°$F. Therefore when produced water is cooled below 32 $^°$F, but not below its freezing point, relatively pure ice crystals and an unfrozen solution are formed. The unfrozen solution contains high concentration of dissolved constituents in the produced water and it is drained from the ice. The ice can then be collected and melted to obtain clean water. About 50 % of water can be recovered from this process during winter but at other seasons no water is recovered because FTE$^®$ works as a conventional evaporation pond. FTE$^®$ can remove over 90 % of heavy metals, total dissolved solids, volatile and semi volatile organics, total suspended solids, and total recoverable petroleum hydrocarbons in produced water (Boysen et al., 1999, Boysen, 2007). This process does not require chemicals, complicated infrastructure or expensive supplies. FTE$^®$ is easy to operate and monitor, and has a life expectancy of about 20 years (CSM, 2009). However it can only work in a climate that has substantial number of days with temperatures below freezing and usually requires a significant area of land. This technology generates significant amounts of

concentrated brine and oil, and therefore waste disposal is essential for produced water treatment.

2.4.13. Dewvaporation – AltelaRain[SM] Process

Dewvaporation is a prototype system based on a dewvaporation process (AltelaRain[SM]) which was developed by Altela Inc. It is a desalination technology which is already applied in full scale commercial treatment of produced water.
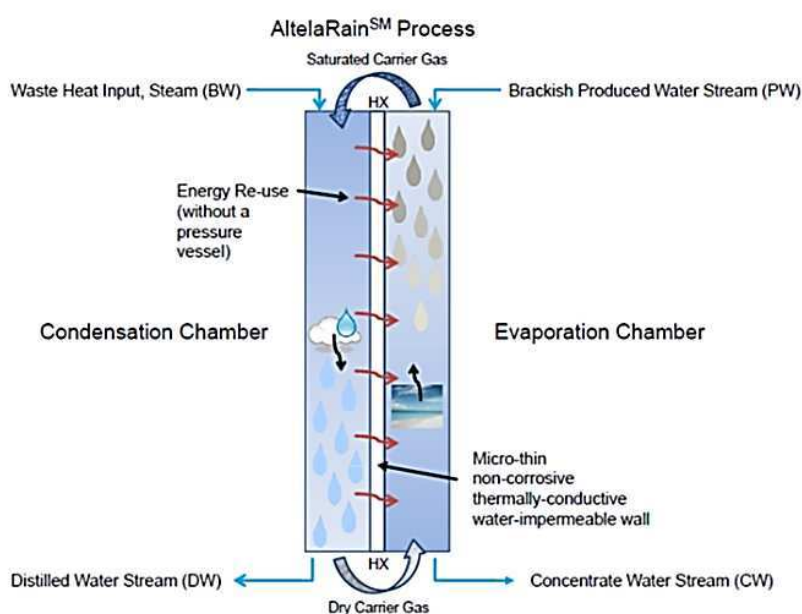
Figure 2.8: Schematic diagram of AltelaRainSM Process (AltelaRainTM System, 2007)

Its principle of operation is based on counter current heat exchange to produce distilled water (AltelaRain[TM] System, 2007). Feed water is evaporated in one chamber and condenses as distilled water on the opposite chamber of a heat transfer wall as shown in Figure. 2.8. Approximately 100 bbl/day of produced water with the salt concentration in excess of 60,000 mg/L TDS can be processed by this system (Godshall, 2006). High removal rates of heavy metals, organics and radionuclides from produced water have also been reported for this technology.

It was reported that in one plant, chloride concentration was reduced from 25,300 mg/L to 59 mg/L, TDS was reduced from 41,700 mg/L to 106 mg/L and benzene concentration was reduced from 450 µg/L to non-detectable after treatment with AlterRain[SM] (Godshall, 2006).The energy requirement of this system is low because it operates at ambient pressures and low temperatures. This makes it a viable alternative water treatment at remote oil wells where there is no high power grid (Godshall, 2006). Nonetheless, there is no information on the overall cost of the system which may be its major disadvantage.

2.4.14. Macro Porous Polymer Extraction Technology

Macro porous polymer extraction technology (MPPE) is one of the best available technologies for produced water management on offshore oil and gas platforms in terms of best environmental practice (Igunnu and Chen, 2012). It is a liquid-liquid extraction technology where the extraction liquid is immobilized in the macro porous polymer particles. These particles have a diameter of 1000 µm, pore sizes of 0.1 – 10 µm and porosity of 60 - 70 %. Polymers were initially designed for absorbing oil from water but were later applied to produced water treatment (Meijer and Madin, 2010). Later the first commercial MPPE units were successfully installed on platforms in the Dutch part of the North Sea. It has been reported that MPPE can be used for the removal of dissolved and dispersed hydrocarbons with performance of > 99 % removal of BTEX, PAHs and aliphatic hydrocarbons at 300 – 800 mg/L influent concentrations. It is also reported that removal efficiency of 95 – 99% for aliphatics below C_{20} and total aliphatic removal efficiency of 91 – 95 % is possible (Pars and Meijer, 1998).
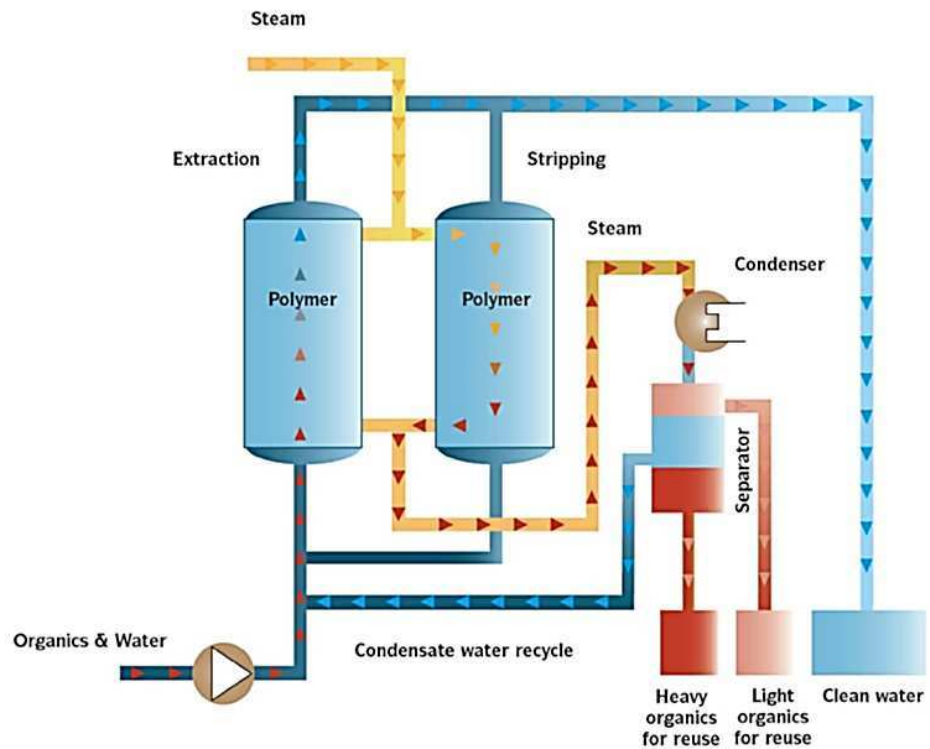
Figure 2.9: A schematic diagram of MPPE process (Meijer and Madin, 2010)

In the MPPE unit, produced water is passed through a column packed with MPPE particles containing a specific extraction liquid. The immobilized extraction liquid removes hydrocarbons from the produced water as shown in Figure 2.9. The two columns allow for continuous operation with simultaneous extraction and regeneration (Akzo Nobel MPP Systems, 2004). Almost all hydrocarbons present in produced water can be recovered from this process which can in turn be disposed or recycled. Stripped hydrocarbons can be condensed and separated from feed water by gravity and product water is either discharged or reused.

MPPE is essentially used to reduce the toxic content of produced water and can withstand the contained salt, methanol, glycols, corrosion inhibitors, scale inhibitors, H_2S scavengers, demulsifiers, defoamers, and dissolved heavy metals. Pretreatment through hydrocyclones or flotation is necessary before letting oilfield produced water flow into the MPPE unit. However for gas field produced water pretreatment is not required and MPPE can

remove the whole spectrum of aliphatics, as well as BTEX and PAHs (Meijer et al., 2004)

MPPE is considered a major player in produced water treatment in meeting international legislations of "zero discharge" of contaminants into the environment. A study comparing the effect of different treatment technologies of oilfield produced water on EIF found that the MPPE technology had the highest EIF reduction of about 84% (Grini et al., 2002, Buller et al., 2003b, Buller et al., 2003a), but high cost of unit is a major disadvantage of this technology.

A summary of produced water treatment technologies discussed in this section are presented in Tables 2.6, 2.7, 2.8a and 2.8b.

Table 2.8a: Summary of Produced Water Treatment Technologies (Igunnu and Chen, 2012)

Technology	Biological Aerated Filters (BAF)	Media Filtration	Gas Flotation	Evaporation pond	Macro Porous Polymer Extraction (MPPE) Technology
Feasibility	This is a well-established technology that has been used for produced water treatment. It is mostly effective for feed water with chloride levels below 6600 mg/L	This technology has been extensively used for produced water treatment. It is applicable for all TDS and independent of salt concentration	This technology is widely used in the petroleum industry, primarily used for conventional oil and gas produced water treatment. It is applicable for produced water with high TO and particulate, 7% solids	This technology is often employed for produced water at full scale. It is applicable to any kind of produced water and its efficiency depends on system design	It is a robust technology applicable for treating both oil and gas produced water. MPPE unit are easy to operate, reliable, fully automated and idea
Energy Consumption	1 –4 KWh	Minimal energy required. Energy is required for backwashing filters	Energy required to dissolve gas in the feed stream	None, except pumping is required to get water to/from the pond	Low energy consumption
Chemical Use	None	Chemicals required for media regeneration. Coagulants may also be required	Coagulants may be required to remove target contaminants	No chemicals required	None
Pre/Post treatment	Sedimentation may be required as a pre-treatment process. Typically, post-treatment is not required	None required	No post-treatment required, but coagulation may be required as a pre-treatment process	Typically no pre- or post-treatment is required. But post-treatment may be required depending on product water quality	Pre-treatment is required for oilfield produced water but not necessary for gas field produced water
Overall Cost	Not available but capital accounts for majority of overall cost	Not available	No information available	Not available	Not available
Life cycle	Long lifetime expected	It depends on media type	No information available	Long lifespan	Long
Advantages	1)Water recovery is almost 100% 2)Easy to adapt to wide range of water quality and quantity 3)Little need for maintenance 4)Does not require post-treatment 5)Some BAF does not require any equipment	(1)90% oil and grease removal efficiency (2)Can achieve nearly 100% water recovery	(1)Product water recovery is almost 100% (2)No post-treatment required	(1)It is very cheap (2)Does not require the use of chemicals and energy	1)No sludge formation 2)No emission to air 3)Separated hydrocarbons can be reused 4)It is flexible and ideal for process integrated applications and can be used offshore 5)Hydrocarbon removal efficiency is about 99% 6)Fully automated and can be remotely controlled 7)No biological fouling because of periodic in situ regeneration steam
Disadvantages	Solid disposal required for sludge that accumulates in the sedimentation basin can cost up to 40% of the overall cost	Waste disposal system required for spent media or waste produced during media regeneration	(1)Not ideal for high-temperature feed water (2)Solid disposal is required for sludge generated	(1)Water volume may be lost due to evaporation (2)Waste disposal is required for materials that settle out of feed water	(1)High cost of unit (2)Energy consumption is relatively high compared with other technologies (3)Pre-treatment of oilfield produced water increases the cost of processing

Table 2.8b: Summary of Produced Water Treatment Technologies (Igunnu and Chen, 2012)

Technology	Adsorption	Hydrocyclone	Ion Exchange process	Chemical Oxidation	Electodialysis/Electrodialysis Reversal
Feasibility	This technology is commonly used for produced water treatment. Applicable to all types of produced water irrespective of TDS and salt concentrations. It can significantly reduce heavy metals, TOC, BTEX and oil concentrations. It is best used as a polishing step rather than a major treatment process in order to avoid rapid consumption of adsorbent material	It is applicable for the treatment to all types of produced water irrespective of TDS, organic and salt concentrations. It can reduce oil and grease concentration to 10 ppm	This is a large industrial operation applicable to produced water treatment. It is applicable to produced water with TDS range of 500 – 7000 mg/L. Efficiency of this technology depends on the quality of feed water and IX resin	This is a well-established and reliable technology for the removal of COD, BOD, organic and some inorganic compounds present in produced water. It is applicable to all types of produced water irrespective of TDS and salt concentration	This technology is robust for seawater desalination and waste water reclamation. Although it is excellent for produced water application it has only been tested for produced water treatment on laboratory scale
Energy Consumption	Minimal	Does not require energy except to pump water to/from the hydrocyclone	Uses electrical energy. Energy requirements only include pumping costs. Typically 0.07 KWh/bbl assuming a 200 gpm flow rate, 5m pumping head	Energy consumption accounts for 18% of the total operation and maintenance of the oxidation process	Energy type: electricity. 0.14 – 0.20 KWh/lb NaCl equivalent removed
Chemical Use	Chemicals required for media regeneration	None	Regenerant solution may be H_2SO_4, NaOH, HCl, NaCl or Na_2CO_3. H_2O_2 or NaOCl cleaning solutions may be used to limit fouling	Chemicals such as chlorine, chlorine dioxide, permanganate, oxygen and ozone are required as oxidants	Scale inhibitor required to prevent scaling. Acid, caustic, disinfectant, EDTA and other antiscaling chemicals are required for cleaning and process control
Pre/Post treatment	Not relevant because adsorption is usually a polishing stage in produced water treatment	Pre-treatment is not required. Post-treatment may be required to remove other contaminants from feed water	Pre-treatment is essential to remove suspended solids, scaling mineral and oxidized metals. Product water may require remineralization of pH stabilization	No pre- or post-treatment is required	Filtration of fouling and scaling substances in addition to solid particles is a necessary pre-treatment process. Remineralization of product water is also necessary for SAR adjustment and disinfection
Overall Cost	Not available	Not available	Cost for IX resin varies between $0.08 and $0.11/bbl at 5bbl per minute and $0.04 – $0.07/bbl at 21bbl per minute. Operating costs account for 70% of the total cost at lower flow rate. At 21 bbl per minute, operating costs increase to 80%	Capital cost is about $0.01/gpd. Operation and maintenance cost is about $0.01/bbl.	Total costs depend on feed water TDS and site location. 8000 bbl/day treatment train of CBM produced water is estimated to cost 15 cents per barrel
Life cycle	It depends on media type	Long lifespan	Average lifecycle of anion resins is 4 – 8 years. Average lifecycle of cation resins is 10–15 years	Expected life of chemical metering is 10 years	ED membrane lifetime is estimated to be 4 –5 years
Advantages	(1)80% removal of heavy metals (2)Can achieve nearly 100% water recover	(1)Does not require the use of chemicals and energy (2)High product water recovery (3)Can reduce oil and grease concentrations to 10 ppm (4)Can be used for treating any produced water	(1)It requires minimal supervisory oversight (2)May operate continuously for 10 –20h (3)Energy requirements are minimal	(1)It requires minimal equipment (2)No waste is generated from this process (3)It does not require pre- and post-treatment (4)It has 100% water recovery rate	(1)It does not require special infrastructure (2)Modest to withstand harsh conditions (3)Excellent for produced water application
Disadvantages	Waste disposal system required for spent media or waste produced during media regeneration	(1)Solids can block inlet and scales formation can lead to extra cost in cleaning (2)Disposal is required for secondary waste generated	(1)High operating and chemical costs (2)High sensitive to fouling	(1)Chemical cost may be high (2)Periodic calibration and maintenance of chemical pump is required (3)Chemical metering equipment is critical for this process	(1)This technology has only been tested on a laboratory scale for produced water treatment (2)Fairly flexible to varying water quality (3)Operation requires highly skilled labour (4)Process requires periodic maintenance and chemical cleaning (5)Concentrate disposal is required

2.5. Electrochemistry and produced water treatment

Electrochemistry is rarely employed in produced water treatment even though it has been widely used in the treatment of other wastewaters (Panizza et al., 2000, Rajkumar and Palanivelu, 2004, Lin et al., 1998). So far only ED and EDR are known electrochemical technologies for produced water treatment and they are mainly useful when removing salts from produced water. Progress in electrochemistry suggests that it could enable future produced water treatment technologies even though current treatment technologies have been able to achieve desalination, de-oiling, removal of suspended solids, and NORM (in some cases). High treatment cost and energy requirements, production and discharge of secondary wastes, and the use of chemicals are common problems facing these known or existing technologies. Electrochemistry on the other hand can help in the development of relatively cheap and green technologies. Such a technology in principle does not generate secondary waste nor involve the use of additional chemicals, and offers improved beneficial uses of produced water. It can be used to produce clean water, remove organics, and recover valuable materials from produced water with little or no negative impact on the environment via electrolysis, electrocrystallization, photoelectrochemistry, and other electrochemical processes (Igunnu and Chen, 2012).

Recent investigations of electrochemical technologies for produced water treatment have focused on the removal of organics. A catalytic electrochemical pilot-scale plant set up for the removal of organics from oilfield produced water, using double anodes with active metal and graphite, and iron as cathode and a noble metal containing catalyst with big surface (Figure 2.10) was reported to have reduced COD and BOD by over 90 % in 6 minutes, suspended solids by 99 %, the Ca^{2+} content by

22%, corrosion rate by 98 % and bacteria (sulphate reducing bacteria and iron bacteria) by 99 % in 3 min under conditions of 15V/120A (Ma and Wang, 2006).
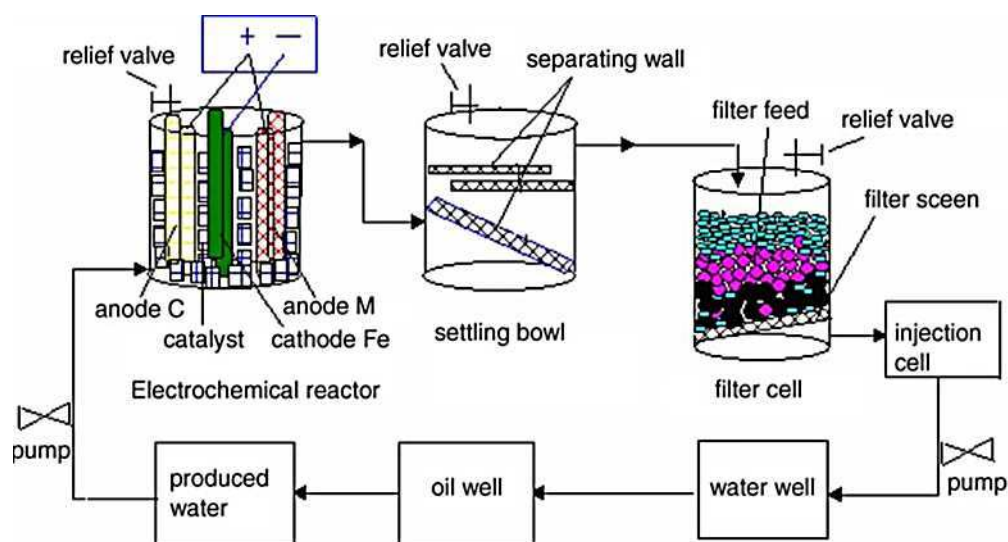
Figure 2.10: Flow diagram of electrochemical pilot-scale plant (Ma and Wang, 2006)

Since the photocatalytic decomposition of water on TiO_2 electrodes was first reported (Fujishima and Honda, 1972), photoelectrolysis has played significant roles in the removal of organics from wastewater including produced water (Pelizzetti et al., 1990, Tien and Chen, 1992, Leng et al., 2006, Gaya and Abdullah, 2008, Lindquist et al., 2009, Yang et al., 2010). In some cases, photodegradation of organics has been enhanced by the addition of oxidants such as hydrogen peroxide, peroxymonosulphate (oxone) and peroxydisulphate. However some of these oxidants introduce other problems to the system. For example, hydrogen peroxide has been reported to have also induced corrosion processes in the reactor, which is a major setback for this method (Malato et al., 1998, Bessa et al., 2001). Semiconductor photocatalysis has also been reported to effectively reduce organics in wastewaters by 90 % (Adams et al., 2008), but photoelectrocatalysis is considered to be the most efficient process for the

removal of organics from wastewaters. Furthermore, powder semiconductor photocatalysts, nano photocatalysts, photoanodes, several metal oxides, fuel cell and other electrochemical techniques are being investigated for waste removal and energy generation from water (Ashokkumar, 1998, Tryk et al., 2000).

However the simultaneous removal of organics and heavy metals from produced water is a desirable electrochemical process but has not been studied or reported in literature. This can be achieved by the amalgamation of electrocrystallization and photoelectrochemistry in a dual purpose photo-electrochemical (PEC) reactor.

2.5.1. Electrocrystallization

Electrocrystallization is a term coined by Fischer in the 1940s to describe a crystallization process where mass transfer is accompanied by charge transfer (Walsh and Herron, 1991). Although some scientists believe there is not a true "theory of electrocrystallization", it is generally considered as the science and technique of obtaining solid metal at the cathode of an electrolytic cell (Winand, 1992). Fundamental aspects of electrocyrstallization of metals are directly related to nucleation and crystal growth. Early development of electrocrystallization theories and fundamentals were based on the work of Volmer, Kossel, Stranski, Stranski and Kaischew, Becker and Doring amongst others using statistical and molecular-kinetic approaches (Budevski et al., 2000). In this section a brief overview of electrocrystallization theory and fundamentals, mechanism of electrodeposition, electrode materials, nucleation and growth, and factors affecting electrocrystallization are presented.

2.5.1.1. Theory and Fundamentals

Electrocrystallization may be broadly defined as the result of a direct or indirect electrochemical influence on crystallization (Walsh and Herron,

1991). A direct electrochemical influence may apply if the value of electrode potential determines predominantly the type of nucleation and growth kinetics for electrodeposition of a metal, while an indirect electrochemical influence may alter the local reaction environment (for example pH), hence the nature of the reaction product. In many cases, both of these processes are experienced to some extent. For example hydrogen evolution as a side reaction at the cathode may result in the co-deposition of metal oxides/hydroxides in the metal deposit (Walsh and Herron, 1991).
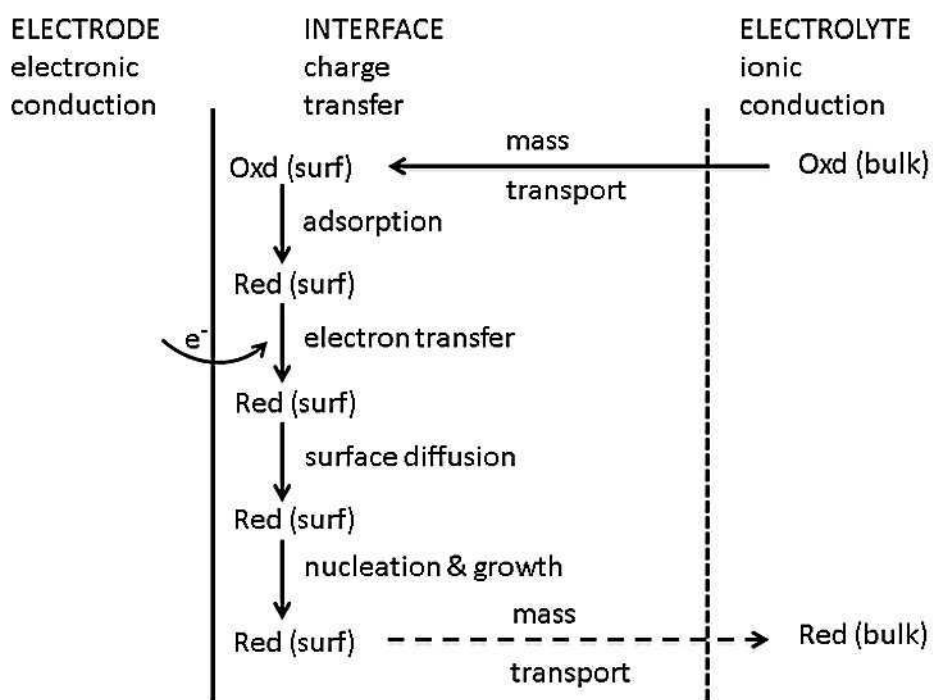
Figure 2.11: Steps involved in electrocrystallization process (Walsh and Herron, 1991)

A simple heterogeneous charge transfer cathodic reduction may be considered as illustrated equation 2.1.

$$O + n\,e^- \rightarrow R \qquad\qquad 2.1$$

This reaction takes place at an electronic conductor (or semiconductor)/ionic interface as shown in Figure 2.11. For example,

copper deposition will follow equations 2.2 and 2.3 (Walsh and Herron, 1991)

$$Cu^{2+}_{(bulk)} \rightarrow Cu^{2+}_{(surf)} \qquad\qquad 2.2$$

$$Cu^{2+}_{(surf)} + 2e^- \rightarrow Cu_{(surf)} \qquad\qquad 2.3$$

The reactants are first transported via convection and diffusion to the interface (this step may be sensitive to the relative rates between the reactions on electrode and the transport in electrolyte) (Walsh and Herron, 1991). This will result in a concentration profile for each of the electrolyte species near the electrode surface due to the build-up or depletion of species. Electron transfer then occurs after surface adsorption of the ions. This in turn is followed by surface diffusion of the metal atoms which nucleate and grow to form a surface deposit. The reaction product remains on the electrode surface in this case. It should be noted that electrode potential may exert influences over any of these steps.

2.5.1.2. Electrodeposition of metals

Electrodeposition of metals is a field of elctrocrystallization that has been studied extensively, contributing greatly to the understanding of adsorption, nucleation and growth processes. The mass of metal deposited per unit area, m, is given by Faraday's laws (equations 2.4 - 2.5).

$$m = q/nF \qquad\qquad 2.4$$

$$m = \int idt/nF \qquad\qquad 2.5$$

where q is the charge density at the electrode surface (C/m^2), n the number of electrons, F the Faraday's constant (J), I the current density (A/m^2), and t the time (s). The driving force of electrocrystallization is known as the overpotential, η, defined as:

$$\eta = E - E_e \qquad\qquad 2.6$$

where E is the electrode potential and E_e is the electrode potential at equilibrium or reversible electrode potential (Walsh and Herron, 1991).

The overpotential is directly related to the change of the chemical potential, μ, or the change in Gibbs free energy as expressed in equations 2.7 and 2.8 (A is the unit electrode area).

$$\eta = \Delta\mu/nF \qquad\qquad\qquad 2.7$$

$$\eta = \Delta G/mnFA \qquad\qquad\qquad 2.8$$

A new phase may be formed in direct crystallization by perturbing the equilibrium via the application of a potential field or by alteration of the temperature or composition of the electrolyte for indirect electrocrystallization (Walsh and Herron, 1991). Figure 2.12 illustrates an idealised growth process that occurs during electrodeposition of metal onto a substrate.
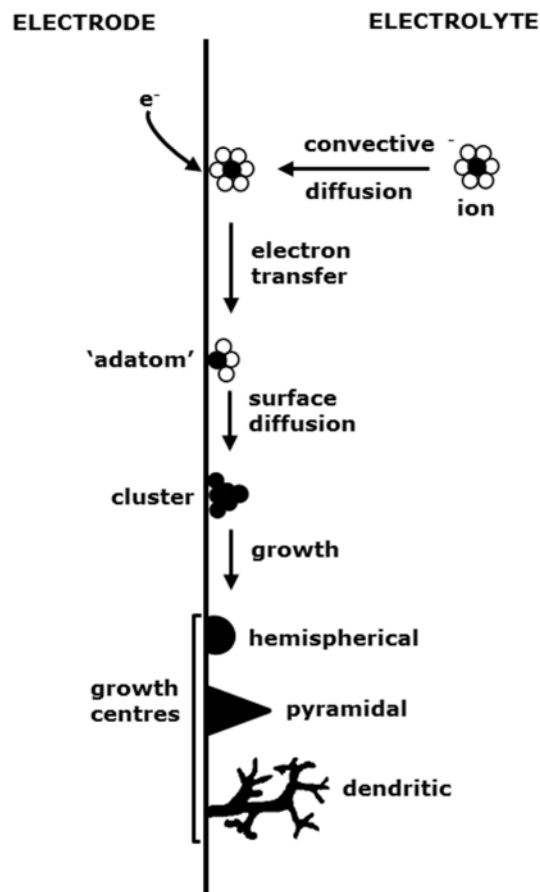
Figure 2.12: Mechanism of metal electrodeposition on electrode surface (Walsh and Herron, 1991)

In practice, several complications may occur during electrocrystallization. Several competitive electrochemical reactions and time-dependent effects may be experienced. Electrolyte decomposition or chemical changes which modify the electrolyte composition may occur. The reaction environment is extremely important for electrodeposition and this includes the electrolyte composition, the nature and state of the electrode, flow effects and temperature (Pletcher and Walsh, 1990).

The solid phase may be an alloy, a metal/metal oxide composite or combined crystallographic phases. Chemical steps may lead to an increase in electrolyte pH, consequently leading to formation of oxide/hydroxide. Chemical steps may also lead to precipitation where the solubility limit is exceeded. In some cases deposition of metallic monolayers may occur at potentials more positive than the equilibrium potential. This phenomenon, also known as underpotential deposition, results in controlled formation of two-dimensional array of adsorbed metal atoms, with a surface coverage almost equal to a monolayer of adatoms.

Electrode precipitation is another factor affecting electrocrystallization in practice. This results in corrosion with the formation of intermetallics or other metal compounds. Electrode surface and composition may significantly affect the nature of adsorption and nucleation processes. Rough surfaces may give rise to increased surface area, electrocatalysis or improved mass transfer effects (Walsh and Herron, 1991). Electrode potential may also change the morphology, chemical composition or phase of the products. In order to minimise these effects inert platinum, glassy carbon and titanium electrodes are used as cathodes in this research.

2.5.2. Photoelectrochemistry

Photoelectrochemistry is a multidisciplinary field involving photocatalysis, photoelectrolysis, surface chemistry, optics, solid state physics, and electrochemistry (Mills and Le Hunte, 1997, Strandwitz et al., 2011). The definition of each discipline in photoelectrochemistry can be controversial. Photoelectrolysis has been defined as a chemical process of breaking down molecules into smaller units by light under the influence of electrochemical conditions (Lindquist et al., 2009). However the idea of a photocatalysed reaction is considered fundamentally incorrect because it suggests that light is acting as a catalyst when in reality it acts as a reactant that is being consumed in the chemical process (Suppan, 1994). Photocatalysis may therefore be defined as the acceleration of a photoinduced or photoactivated reactions by the presence of a catalyst (Mills and Le Hunte, 1997). Since the report that this process is enhanced by TiO_2 photocatalysts (Fujishima and Honda, 1972), other semiconductors have been employed (Kim et al., 2010, Chen et al., 2012, Huang et al., 2013) but TiO_2 still remains the most widely used photocatalyst in environmental applications for the remediation of hazardous wastes, contaminated waters, and the control of toxic air contaminants (Hoffmann et al., 1995, Nakata and Fujishima, 2012).

2.5.2.1. Titanium Dioxide

Titanium dioxide (also known as titania or titanium (IV) oxide) is an n-type semiconductor that exists in three crystalline structures, namely anatase, rutile and brookite.

Anatase polycrystals exhibit higher photoactivity than the other two and have been the main type of TiO_2 employed in photodecomposition of organics (Linsebigler et al., 1995). Its higher photoactivity is attributed to its good capacity of adsorbing reactants and photons to create photo-

induced electrical charges (Sclafani, 1996, Sclafani and Herrmann, 1998). The differences in distortions and lattice arrangement in anatase and rutile structures (Figure 2.13) have also been attributed to their photocatalytic performance (Linsebigler et al., 1995). Although anatase shows better photocatalytic activity, both have been employed as photocatalyst in the treatment of wastewater.
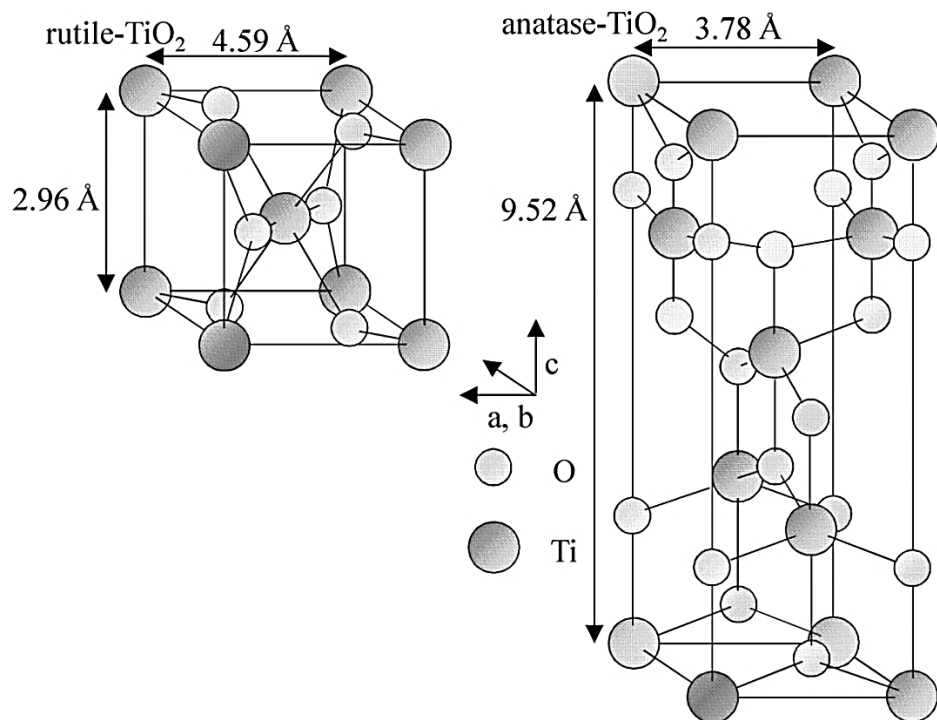
Figure 2.13: A schematic representation of the molecular structures of rutile-TiO$_2$ and anatase –TiO$_2$ (Li et al., 2001)

2.5.2.2.   Mechanism of Photocatalysis in semiconductors

A semiconductor material has a valence band (VB) which is mostly filled with electrons and a conduction band (CB) which is nearly empty. The electrons in the valence band become excited when illuminated by light. The excess energy of the excited electron promotes it to the conduction band thereby creating a negative electron (e^-) and a highly-active positive hole (h^+) pair as shown in Figure 2.14. The energy difference between the valence band and the conduction band is known as the "band gap".

Therefore the minimum excess energy needed to initiate a charge transport from the VB to CB must be greater than the band gap energy. The holes may be quickly separated from the VB and transferred to the surface of the semiconductor to react with the substances (e.g. H_2O, OH^-, pollutants/organic) adsorbed on it, oxidising them
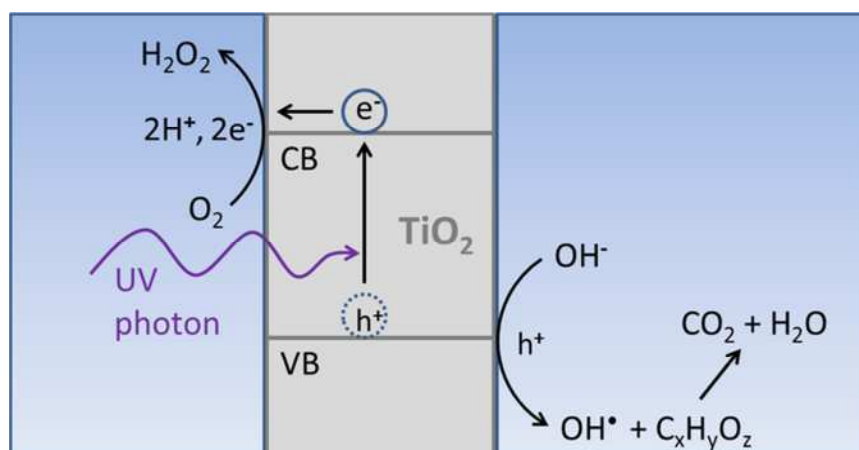
Figure 2.14: Principle of photocatalysis on TiO_2 in an aqueous solution containing hydrocarbons

The energy difference between the valence band and the conduction band is known as the "band gap". Therefore the minimum excess energy needed to initiate a charge transport from the VB to CB must be greater than the band gap energy. The holes may be quickly separated from the VB and transferred to the surface of the semiconductor to react with the substances (e.g. H_2O, OH^-, pollutants/organic) adsorbed on it, oxidising them. On the other hand, the electrons and holes generated may recombine again, releasing heat within or on the surface of the semiconductor. This recombination may occur within a fraction of a nanosecond (Linsebigler et al., 1995) which makes photogenerated electron-hole pairs extremely unstable. This problem can be overcome by introducing electron acceptors which allows the highly active holes to scavenge electrons from other particles or solvent molecules, adsorbed

onto the semiconductor surface. This invariably allows the photo-oxidation of species which are normally inert to irradiation.

The key objective of a typical photocatalytic reaction is to prevent recombination of electrons and holes and make them react with electron receptors and donors respectively. Therefore photocatalytic enhancement is considered a necessity to facilitate either or both of these processes. This may include impregnation with impurities, use of specific solvents, modification of semiconductor surface, or the use of hybrid semiconductor such as CNT-TiO_2. The presence of embedded CNTs in TiO_2 hybrid matrix has been reported to improve the mechanical strength and increase the surface area of TiO_2, and invariably the photocatalysis process by acting as carrier acceptor for charge carriers (Krishna et al., 2005, Lee et al., 2005, Feng et al., 2005, Chao et al., 2013, Gao et al., 2009b). This is why it is preferred as a photoanode in this research.

2.5.2.3. Carbon Nanotubes

Carbon nanotubes (CNTs) are hollow cylinders of graphene sheets which can be single-walled or multiwall in form (Iijima, 1991, Reich et al., 2004) as shown in Figure 2.15.
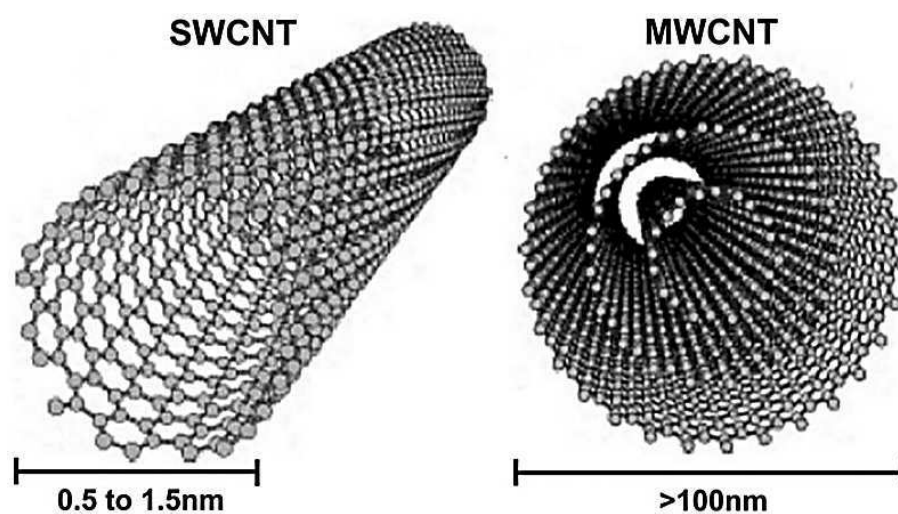
Figure 2.15: Schematic representation of single-walled carbon nanotubes (SWCNT) and multi-walled carbon nanotubes (MWCNT) (Martins-Junior et al., 2013)

Single walled carbon nanotubes (SWCNT) are individually made of a single layer of graphene with the ends either open or closed. Its internal diameter is 0.4 nm at minimum, but can be larger, and its length can vary from a few microns to several millimetres (Terrones, 2003, Merkoçi, 2006). A multiwall carbon nanotube (MWCNT) is a tube consisting of a stack (from two to a few tens) of concentric cylinders of graphene sheets with 0.34 nm spacing between the layers and a typical diameter from 2 nm to 100 nm (Ajayan, 1999).
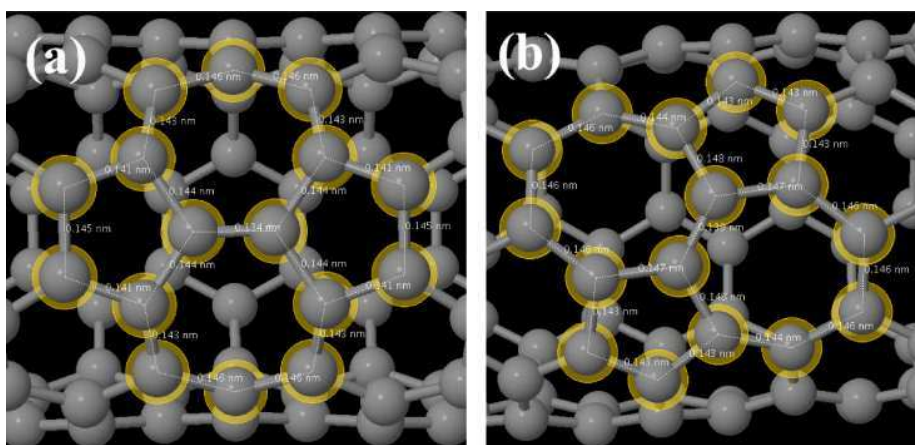
Figure 2.16: A section in a modelling derived SWNT showing two stone-wales defects in different orientations (a) longitudinal defect (b) circumferential defect (Partovi-Azar and Namiranian, 2012)

The carbons in a CNT can be broadly divided into two kinds, those at the sidewall and those at the tube end of the nanotubes, and both groups behave differently in electrochemistry. The former resembles the basal plane of highly orientated pryolytic graphite (HOPG) and shows slow electron transfer, while the latter behaves like the edge plane of HOPG and possess favourable electrochemical properties (Gong et al., 2005). A third situation is the defected sites along the sidewall of CNTs, which are well exemplified by the Stone–Wales defects illustrated in Figure 2.16 (Partovi-

Azar and Namiranian, 2012). These defects can enrich the chemistry and electrochemistry of CNTs, for example the incorporation of oxygen containing surface groups that help dispersion of CNTs in water.

A wide range of complex pores which can be divided into primary inner cavities and secondary cavities are observed throughout the CNT structures. The primary pores may aid the performance of CNTs in photocatalysis, however the secondary pores such as cracks between individual carbon nanotubes, aggregated interspaces among CNT bundles and separation zones in large diameter MWCNT, may lead to structural and crystallinity defects which can weaken tube elasticity of CNT and affect its absorption performance negatively (Dai, 2006, Gao, 2008).

Despite these defects, CNTs have found impressive applications in many fields such as energy conversion and storage, electrochemical actuators, chemical sensing, construction of aviation materials and surpercapacitors (Chen, 2013, Gong et al., 2005, Chae and Chen, 2012).

2.5.2.3.1.   Properties of CNT

CNTs have been attractive materials of research interest in various fields of science and engineering over the last 20 years because of their unique properties. Their nano dimensions together with their near perfect alignment in tubular lattice give them unique structural, electronic and mechanical properties. High surface area, good stiffness and strength, chemical specificity, inertness and high conductivity are amongst their most desirable properties.

The Young's modulus of commercial carbon fibre is $\sim$ 800 GPa while that of individual MWCNT and SWCNT are $\sim$ 1.8 TPa $\sim$ 50 GPa respectively. This very high mechanical strength is attributed to their strong carbon-carbon covalent bonds, hollow structure and close topology (Gao, 2008). Also CNTs may demonstrate a metallic, semi metallic or semiconducting

behaviour depending on the carbon atom arrangement along the tube and the tube diameter (Mills and Le Hunte, 1997, Gao, 2008). They are intrinsically electrochemically inert over a wide potential range, but can have defects as mentioned above that allow modification of their surface to achieve desirable electrochemical properties. The thermal conductivity of CNTs is another property of interest for both research and industrial applications. Experimental investigations have shown that the thermal conductivity of CNTs are higher than that of graphite which makes CNTs suitable filler materials in functional hybrid materials (Kim et al., 2001).

2.5.2.3.2.   Electrochemistry of CNTs

Defect-free CNTs are electrochemically inert and do not exhibit voltammetric response in the potential window commonly used. They exhibit a special sidewall curvature which possess a framework structure with sp^2 carbon and a π-conjugative structure with a highly hydrophobic surface. However, defected CNTs can be rationally functionalised. Surface modification can be achieved through covalent or noncovalent chemistry (Gong et al., 2005). Impurities such as amorphous carbon and nanoparticles are generally introduced into CNT samples via their synthesis methods, therefore raw CNTs are usually purified before they are put to use. Purification methods include acidic oxidation treatment, thermal treatment, chemical oxidation and liquid phase oxidation (Hou et al., 2008). These treatments on the other hand introduce additional atoms to the defects along the sidewall (which dramatically modify the electronic and structural properties of the CNTs), resulting in the partial oxidation of CNTs to produce functional oxygenated groups, which are said to be electroactive (Chou et al., 2005). However some researchers have questioned the electroactivity of purified CNTs, claiming that this is only true for SWCNT because purification cuts the SWCNTs but not MWCNT. It

was demonstrated that oxygenated MWCNT led to slower electron-transfer for $[Fe(CN)_6]^{3-/4-}$ (Pumera, 2007b). It was also reported that oxygenated MWCNT actually slowed the rate of heterogeneous electron transfer (Banks et al., 2006) and (Ji et al., 2006). It is believed that the increase in the rate of heterogeneous electron transfer in the case of purified SWCNT might arise from a higher amount of edge-like tips of SWCNT available after their cutting, whereas enhanced heterogeneous electron transfer in a MWCNT is due to defects introduced into its structure via electrochemical oxidation (Pumera et al., 2008, Pumera, 2009).

It is true that CNTs possess inherent electrocatalytic properties; however there is no agreement on why this is the case. While some researchers attribute this wholly to the structure of CNTs, others argue that the metallic impurities in carbon nanotubes dominate their electro-photochemistry. It has been suggested that the metal catalyst particles used during the synthesis of CNT via chemical vapour deposition (CVD) process are incorporated in the grown CNT and are responsible for the electrocatalytic behaviour of CNTs, even after purification at high temperatures (Harris, 2007, Hofmann et al., 2007, Pumera, 2007a, Batchelor-McAuley et al., 2008, Kruusma et al., 2007). Whatever the case, it is evident that CNTs enhance electrocatalysis and will be useful either as a catalyst or a catalyst support (in hybrid CNT-TiO$_2$) for wastewater treatment.

2.5.2.4. CNT-TiO$_2$ Nanohybrid

A typical application of CNT-based hybrid materials is the CNT-TiO$_2$ hybrid. It has attracted attention from material and chemical scientists because of its novel properties. Various synthesis methods of CNT-TiO$_2$ are reported in literature (Yao et al., 2008, Jiang et al., 2013, Woan et al., 2009, Gao et al., 2009a). However for the purpose of this research, a modified sol gel method is used as presented in Chapter 3. Since CNTs can conduct

electricity at room temperature with essentially no resistance, a phenomenon known as ballistic transport can be observed where electrons are considered to be moving freely through the CNT structure without any defects (Li et al., 2001, Charlier, 2002). The high surface area of CNTs is a unique property that makes them particularly useful as catalyst support. This is essential to disperse catalyst particles and to maintain their catalytic activity. The high surface area of CNT-TiO_2 electrode would therefore help to improve mass transport and amperomeric response during photocatalysis.

There are two main mechanisms used to explain the photocatalytic properties of CNT-TiO_2 as presented in Figure 2.17. In the first mechanism, it is explained that when high-energy photon excites an electron from the VB to the CB, photogenerated electrons formed in the space-charge regions are transferred into the CNTs, and holes remain on the TiO_2 to take part in the redox reactions (Hoffmann et al., 1995). The second mechanism however assumes that CNTs act as sensitizers and transfer electrons to the TiO_2, causing the formation of superoxide radicals by adsorbed molecular oxygen. The positively charged CNTs then remove an electron from the VB of the TiO_2, thus leaving a hole. The now positively charged (h^+) TiO_2 then reacts with adsorbed water to form hydroxyl radicals (Wang et al., 2005).

Recently the contributions of the carbon-oxygen-titanium bond and the electronic configuration of the CNTs to the mechanism of CNT-TiO_2 have also been examined. It was reported that light absorption was extended to lower wavelengths by Ti-O-C bond, potentially leading to the improvement of CNT-TiO_2 photocatalytic activity (Pyrgiotakis et al., 2005). Although the electrons generated from irradiation migrate to the surface of TiO_2, it is also easy for these electrons to be transported in CNTs bound to TiO_2.
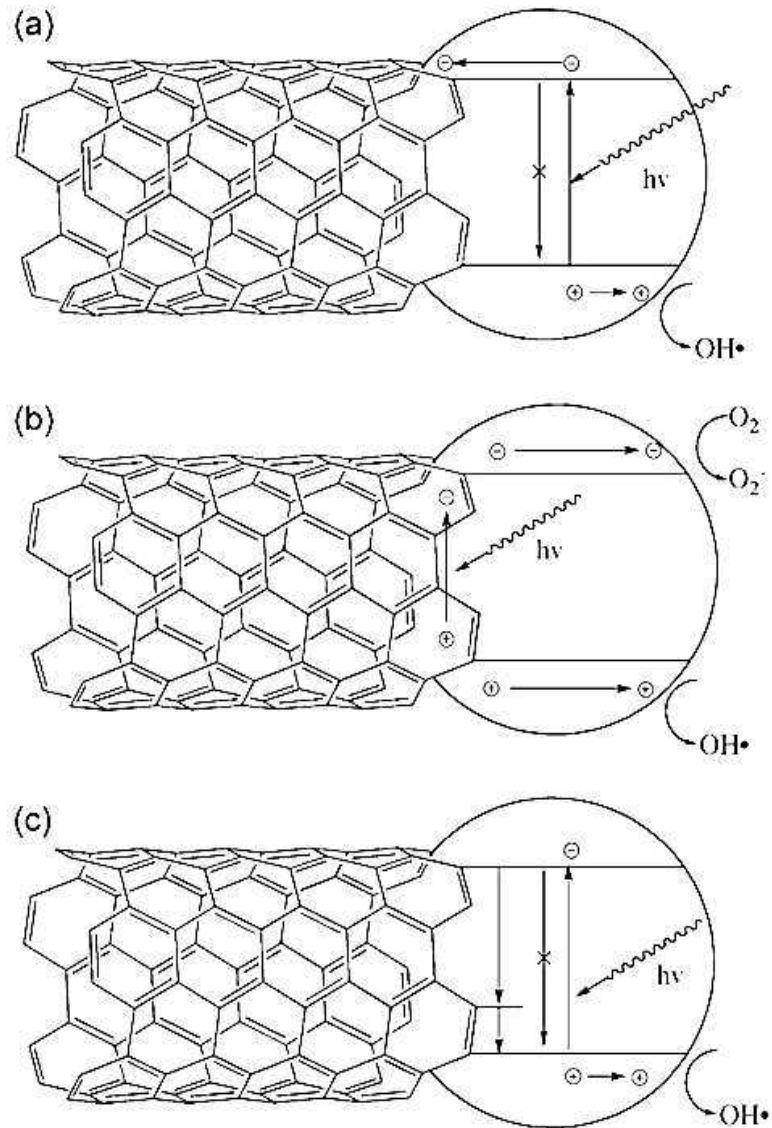
Figure 2.17: Mechanisms for the CNT-TiO2 enhancement of photocatalysis (a) CNT acts as an electron sinks, and scavenge away the electrons preventing recombination. (b) Photons generate an electron-hole pair in the CNT. An electron (or hole) is injected in the titania generating O_2^- or a OH^- species based on the positions of the band (Wang et al., 2005). (c) CNTs can act as impurity through the Ti-O-C bonds (Woan et al., 2009).

Therefore the quantum yield of the TiO_2 process can be increased because the rate of e^-/h^+ recombination is now reduced. The strong interaction between CNT and TiO_2 also supports the fact that electrons are transported in the CNT-TiO_2 hybrid. In another study, it was observed that arc-

discharge grown CNTs via sol gel process have a degradation rate ten-fold higher than CVD-grown CNTs via the same process. The difference in activity is therefore attributed to the electronic nature of the CNTs (Pyrgiotakis et al., 2005). Therefore the electronic band structure of the CNT is a more important factor than the chemical bond between the CNT and TiO_2 (Woan et al., 2009).

$CNT-TiO_2$ is a complex system, and its final mechanism may not yet be known. Although CNTs may enhance the photocatalytic activities of TiO_2, excess CNTs have been reported to shield TiO_2 from absorbing UV light. It is therefore important to determine the optimum CNT/TiO_2 ratio needed for efficient photocatalysis. It is also important to note that some degree of CNT oxidation is expected during photocatalytic degradation. Although this is not well documented literature, in the long run complete degradation of CNTs may be possible which would significantly diminish the photocatalytic ability of $CNT-TiO_2$.

2.5.3.   Degradation of PAH by CNT-TiO_2 Nanohybrid

The degradation of PAH on hybrid $CNT-TiO_2$ may follow two different mechanisms. The first mechanism involves degradation by radicals and hydroxyl ions and the second involves direct oxidation by trapped holes (Lawless et al., 1991, Turchi and Ollis, 1990, Pramauro et al., 1998). It should be noted that oxygen and water are essential components in photocatalytic processes.

In the first mechanism $^{\bullet}OH$ radicals, hydroxyl ions and other species, such as hydroperoxide radical ($HO_2^{\bullet}$) are formed through oxidation of water by the photogenerated electron–hole pair under irradiation with light energy higher than the semiconductor band gap (wavelength <380nm) as shown in equation 2.9 -2.15 (Turchi and Ollis, 1990). These ions and radicals are highly oxidizing species capable of attacking the PAH.

$$TiO_2 \longrightarrow e^- + h^+ \qquad\qquad 2.9$$

$$h^+ + H_2O \longrightarrow H^+ + OH^{\bullet} \qquad\qquad 2.10$$

$$2h^+ + 2H_2O \longrightarrow 2H^+ + H_2O_2 \qquad\qquad 2.11$$

$$H_2O_2 \longrightarrow OH^{\bullet} + OH^{\bullet} \qquad\qquad 2.12$$

$$e^- + O_2 \longrightarrow O_2{}^{\bullet} \qquad\qquad 2.13$$

$$O_2{}^{\bullet} + HO_2{}^{\bullet} \longrightarrow H_2O_2 + O_2 \qquad\qquad 2.14$$

$$H_2O_2 \longrightarrow OH^{\bullet} + OH^{\bullet} \qquad\qquad 2.15$$
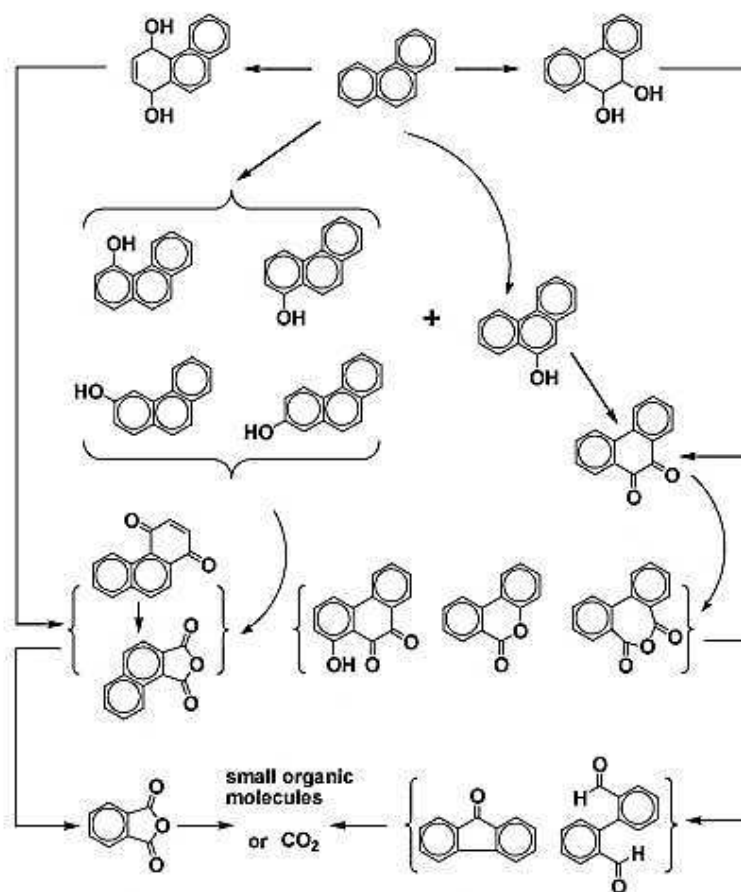
Figure 2.44: A proposed pathway for phenanthrene degradation by direct oxidation or by photogenerated holes (Kou et al., 2010)

The second mechanism involves the direct oxidation of PAH by trapped holes. Photo-induced holes and active H^+ are initially produced, followed by

80

the reaction of holes with PAHs to produce PAHs$^{+\bullet}$ as presented in equation 2.16 (Kou et al., 2010).

$$h^+ + PAHs \rightarrow PAHs^{+\bullet} \qquad\qquad 2.16$$

PAHs$^{+\bullet}$ are active enough to react with oxygen and active H species to form hydroxyl compounds or hydrogenated hydroxyl intermediates. These intermediates are further oxidised to ketones or quinones, and further oxidation of these intermediates results in production of CO_2 or small molecules as illustrated in Figure 2.18. During the photocatalytic degradation of PAH both mechanisms may be involved. It is also possible that only one of these mechanisms will be involved.

The degradation of aromatic compounds is also reported to be enhanced by CNT-TiO$_2$. This enhancement may be due to the good adsorption between these compounds and CNT surface. Since the CNT-TiO$_2$ nanohybrid is porous, the hydrophobic and π-staking interactions between CNT and aromatic compounds are stronger than those with other carbon based materials (which are flat graphene sheets). This strong adsorption of aromatic compounds to CNT surfaces can be attributed to the charge-transfer and hydrophobic interactions between the organic compounds and CNTs, in which the CNTs serve as electron donor and the aromatic compounds as electron acceptor (Zhang et al., 2003, Gong et al., 2005). The excess photoelectrons generated during this process are expected to flow to the cathode where they will assist in metal deposition. A detailed mechanism of the dual purpose cell under different conditions is explained in Chapter 6. This knowledge has informed the use of CNT–TiO$_2$ as a photoanode in the dual purpose PEC cell used for produced water treatment in this research.

2.6. Summary, Knowledge gaps and research objectives

A review of the environmental implications of produced water together with the technologies developed for its treatment has been carried out. The key issues that are preventing the development of a cost effective environmentally sustainable treatment process have also been identified.

Although produced water can be a valuable source of materials, there is currently no technology aimed at recovery of metals from it in the form of products that can be re-used. Thermal treatment technologies typically involve evaporation and condensation of clean water from produced water which leaves residues that do not comply with disposal standards. MPPE and membrane technologies have been shown to perform well in the removal of metals and hydrocarbons as worthless wastes; however their high operation cost, use of chemicals and generation of secondary waste attract extra environmental penalties.

Despite the robust technologies available for produced water treatment, the problem of dissolved elements (metals) and dissolved oil (hydrocarbons) remains a major challenge not fully addressed by any current technology. The amalgamation of electrocrystallization and photocatalysis into a dual purpose photoelectrochemical cell has been identified as the alternative with the most promising and potential to be developed into a low-carbon process where heavy metals can be recovered and reused while simultaneously breaking down PAH into small non-toxic molecules or CO_2 and water. This treatment method is energy efficient, environmentally friendly and cost effective because it does not generate secondary wastes, uses sunlight as energy source, and metals recovered from this process can be sold.

2.6.1.   Knowledge gaps

There is a series of knowledge and technology gaps in the photoelectrochemical treatment of produced water

- ➢ Experimental research has not been correlated with the wealth of stability constant and solubility data available for metal-chloride complexation equilibria. Mathematical modelling and validation of the ionic equilibria of synthetic produced water would help identify the oxidation states of metal species in produced water and how this can be manipulated to selectively recover heavy metals via electrodeposition

- ➢ The optimum CNT to surfactant concentration ratio to obtain a well dispersed CNT in a heavily concentrated CNT suspension has not been reported. It is not clear from literature whether the same CNT-surfactant ratio will be ideal at different concentrations of CNT suspensions. This knowledge will be necessary to achieve a good quality of CNT-TiO$_2$ nanohybrid composite on an industrial scale. Also it is not clear whether CNT-TiO$_2$ nanohybrid made into a photoanode for the treatment of produced water will have a similar performance as CNT-TiO$_2$ nanohydrid employed in the treatment of other wastewaters reported in literature. Moreover the degradation of dissolved PAH in produced water via photocatalysis has not been investigated. This work is needed to base a decision on whether to design and build a dual purpose PEC pilot cell.

- ➢ An environmentally sustainable photoelectrochemical process has not been used to date for the treatment of produced water. This is the key factor preventing the removal of dissolved elements in produced water. Produced water has been identified as a suitable electrolyte but the feasibility of a simultaneous recovery of metals

and oxidation of organics in a PEC cell has not been investigated to date

2.6.2.   Project aim and objectives

The aim of this project was to investigate the produced water treatment associated with the development of a dual purpose photoelectrochemical process for the recovery of heavy metals and oxidation of PAH that meets the concept of environmental sustainability.

2.6.3.   Objectives

The main objectives of this study were as follows

- ➢ To understand the metal-chloride complexation equilibria associated with produced water using a mathematical model
- ➢ To assess the feasibility of multiple metal recovery from produced water via electrodeposition on inert electrodes
- ➢ To study the photoanodic process of oxidation of PAH on MWCNT-TiO_2 photoanode synthesised via a modified sol gel method
- ➢ To devise a photoelectrochemical process for a laboratory–scale demonstration of the simultaneous removal of metals and PAH from produced water.

The experiments carried out to achieve these objectives are presented in Appendix A and Chapters 3, 4, and 6.

Chapter 3: Methodology

3.1. Introduction

A theoretical and experimental research design was formed based on the knowledge acquired from the study of available literature (already mentioned in chapter 2). The theoretical research included: possible cathode and anode reactions, thermodynamic analysis of electrochemical/potential windows, and properties of CNTs and CNT-TiO$_2$ as relevant to the overall objective of this research. The experimental aspects include cell and electrode design, electrochemical analysis for the reduction and oxidation processes, and synthesis and characterisation of CNT-TiO$_2$. The differences and similarities of this research methodology in comparison with those in literature are described in this chapter. A pre-experimental thermodynamic modelling was carried out to understand the chemistry of produced water using MEDUSA software. The experimental work undertaken in this research is divided into three main themes: electrodeposition of heavy metal metals, photoanodic oxidation of polycyclic aromatic hydrocarbons (PAHs) and simultaneous removal of heavy metals and PAH from produced water in a photoelectrochemical (PEC) cell. In this chapter, materials/chemicals, experimental procedures and theory of analytical techniques employed in this research are discussed. In section 3.2 a full list of chemicals, electrodes and other materials used in this research, and their importance in the overall experimental set up is described. Section 3.3 provides detailed descriptions of experimental procedures, including synthetic oilfield produced water, synthesis of CNT-TiO$_2$ hybrids, characterisation of the hybrids and fabrication of photoanode. This section also describes the electrodeposition of heavy metals on the cathode (titanium, platinum and glassy carbon) from synthetic produced water and the degradation of phenanthrene (PAH) in synthetic oilfield produced water on photoanodes. Section 3.4 gives brief

description of the electrochemical techniques, thermodynamic modelling of solution equilibra equations and characterization methods used in this research. Theories of cyclic voltammetry (CV), chronomaperometry (CA), X-ray diffraction (XRD), scanning electron microscopy (SEM), transmission electron microscopy (TEM), ultraviolet-visiblelight (UV-Vis) spectroscopy, thermogravimetric analysis (TGA) and others are presented.

3.2.   Chemicals and Materials

A detailed list of chemicals and materials used for this study are presented in Table 3.1 and 3.2.

Table 3.1: Details of major materials used for this research

Materials	Symbol	Manufacturer /Supplier	Grade/Model	Note
Multi-walled carbon nanotubes	MWCNT	Shenzhen nanotech Port Co., Ltd, China	Purity ≥ 95%, diameter: 10 ~30 nm, length: 5 ~ 15 μm	This was used as received or after acid treatment.
Platinum, disk	Pt	CH Instruments	diameter: 2mm	
Titanium sheet	Ti	Advent		Porous titanium obtained by molten salt oxidation of titanium surface was used as a support upon which CNT-TiO_2 nanohybrid was cast in photoanode fabrication because it had better adhesion property than ordinary titanium plate.
pH/TDS/Temperature meter		Hanna instruments		These were used to measure the pH of solutions.
universal pH indicator paper		Fisher		
Centrifuge		Hettieh Zentrifugen	Rotofix 32 A	
Furnace		Carbolite	CWF 1100	
Oven		LTE	OP 100	This was used for drying samples
Solar simulator		Oriel	96000 (150 W, AM 1.5 G)	This is a xenon lamp-based used to simulate full sun spectrum and served as the light source for photo catalytic experiments.
Potentiostat		Autolab	PGSTAT 100	This were used for electrochemical measurements such as CV and CA
		IVIUM Technologies	Ivium-n-Stat	
		CHI Instrument		
Scanning electron microscope	SEM	FEI	Quanta 600	
Thermogravimetric analyzer		TA instrument	SDT Q600	
Transmission electron microscope	TEM	JEOL	2000 Fx II	
UV-vis spectrophotometer		Thermo Scientific	Evolution 201	
X-ray diffractometer	XRD	Philips	EXPERT	

Table 3.2: Details of major chemicals used for this research

Chemicals	Formula/Symbol	Supplier	Grade	Note
Sodium chloride	NaCl	Fisher	Laboratory grade	
Anhydrous copper (II) chloride	$CuCl_2$	Acros organics		These were used as received for the preparation of synthetic oilfield produced water.
Anhydrous magnesium chloride	$MgCl_2$	Sigma-Aldrich	99%	
Iron (II) chloride tetrahydrate	$FeCl_2.4H_2O$	Sigma-Aldrich		
Lead (II) nitrate	$Pb(NO_3)_2$	Sigma-Aldrich		
Nickel (II) chloride hexahydrate	$NiCl_2.6H_2O$	Fisher	AR grade	
Phenanthrene	$C_{14}H_{10}$	Aldrich	AR grade, 98%	It serves as a model polycyclic aromatic hydrocarbon compound present in produced water used in photodegradation (photo-oxidation) experiments.
Dilute Hydrochloric acid	HCl	sigma Aldrich	37%	These were used to adjust the pH of electrolytes as appropriate.
Sodium hydroxide	NaOH	sigma-Aldrich	AR grade, 98%	
Concentrated sulphuric acid	H_2SO_4	Fisher	AR grade >95%, S.G. 1.83	These were used for the purification
Concentrated nitric acid	HNO_3	Fisher	AR grade 70%, S.G. 1.42	of multi-walled carbon nanotubes.
Titanium isopropoxide	TTIP	Fluka, purum		This was used as hydrolysation precursor in modified sol-gel method.
Sodium dodecylbenzesulphonate	NaDDBS	Aldrich	Technical grade	This was used in modified sol-gel method as the surfactant for the solubilisation of high weight fraction of MWCNTs in water.
Glacial acetic acid	CH_3CO_2H	Acros organics	99.80%	This was used for the dissolution of the precursor in ethanol.
Water	H_2O	Milipore Corporation	Milipore grade	This was used for the preparation of all solutions and unless otherwise stated
Ammonia	NH_3	Fisher	35%, S.G. 0.88	This was added to hydrolyse precursor residues left after MWCNT-TiO_2 synthesis.
Ethanol	CH_3CH_2OH	Fisher	35%, S.G. 0.88	This was used to hydrolyse precursor residues left after synthesis of MWCNT-TiO_2.

3.3. Experimental procedures

In this section the experimental procedures carried out and their related laboratory techniques are described. Millipore water was used for the preparation of all solutions unless otherwise stated and all experiments were carried out at 25 ^{0}C and 1 atm.

Electrochemical experiments to study the behaviour of heavy metals deposition from synthetic oilfield produced water at different pH values were carried out in a three-electrode cell configurations (Figure 3.1.) except otherwise stated. The reference electrode was Ag/AgCl (3M). The counter (auxiliary) electrode was graphite rod, and the working electrodes were platinum (0.02 cm^2), titanium (0.03 cm^2) or glassy carbon (0.07 cm^2) in disc configuration.
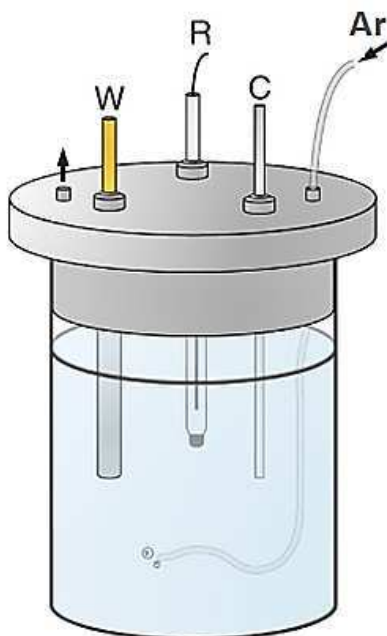
Figure 3.1: Schematic representation of a three-electrode cell where W is the working electrode, R the reference electrode, C the counter electrode and argon gas for purging the cell

The working electrodes were cleaned by polishing with 1 µm alumina paste, and rinsed with water and acetone prior to use. Analytical grade argon gas was used to purge oxygen from the electrolytes.

The photoelectrochemical (PEC) cell used for photoelectrocatalytic experiments was made from Teflon because of its strength, stability and amenability. Details are discussed in Chapter 6.

3.3.1. Synthetic produced water

Several types of synthetic produced water were prepared for this study based on the data available in literature (Fakhru'l-Razi et al., 2009, Igunnu and Chen, 2012). A typical oilfield produced water contain mainly sodium chloride, magnesium chloride, calcium chloride and potassium chloride salt solutions (which form the basic matrix for all synthetic produced water

types used in this research), and various level of pollutants including grease, oil, heavy metals, acid, BTEX, sand, etc. (cf. Table 2.1). Different grades of synthetic produced water were prepared to mimic real oilfield produced water. The synthetic produced water used in this study contains the main salt solutions in real oilfield produced water but excludes other pollutants except the heavy metals of interest (Iron, lead, Nickel and Copper) and phenanthrene (a typical PAH).

A pre-weighed gram of sodium chloride, calcium chloride dehydrate, anhydrous magnesium chloride, anhydrous copper (II) chloride, Lead (II) nitrate, nickel (II) chloride hexahydrate and iron (II) chloride tetrahydrate were dissolved in Millipore water to make the different types of produced water used. Table 3.3 shows the types of synthetic produced water and the concentration ranges of their composition used to study the electrodeposition process in the photoelectrochemical treatment of oilfield produced water.

Table 3.3: Composition of synthetic produced water used for cathodic process studies

Produced water	Composition
PW I	$NaCl$ (1 mol/L), $CaCl_2$ (1 mol/L), $MgCl_2$ (1 mol/L)
PW II	$NaCl$ (1 mol/L), $CaCl_2$ (1 mol/L), $MgCl_2$ (1 mol/L), $CuCl_2$ (0.1 – 1 mol/L Cu^{2+})
PW III	$NaCl$ (1 mol/L), $CaCl_2$ (1 mol/L), $MgCl_2$ (1 mol/L), $PbCl_2$ (0.1 – 1 mol/L Pb^{2+})
PW IV	$NaCl$ (1 mol/L), $CaCl_2$ (1 mol/L), $MgCl_2$ (1 mol/L), $NiCl_2$ (0.1 – 1 mol/L Ni^{2+})
PW V	$NaCl$ (1 mol/L), $CaCl_2$ (1 mol/L), $MgCl_2$ (1 mol/L), $FeCl_2$ (0.1 – 1 mol/L Fe^{2+})
PW VI	$NaCl$ (1 mol/L), $CaCl_2$ (1 mol/L), $MgCl_2$ (1 mol/L), $CuCl_2$ (0.1 – 1 mol/L Cu^{2+}), $PbCl_2$ (0.1 – 1 mol/L Pb^{2+}), $NiCl_2$ (0.1 – 1 mol/L Ni^{2+}), $FeCl_2$ (0.1 – 1 mol/L Fe^{2+})

These were spiked with different concentrations (mg/L) of phenanthrene to study photoanodic degradation process of PAH and for understanding the simultaneous removal of heavy metals and phenanthrene in a PEC cell.

The pH of synthetic produced water was adjusted with 1 mol/L concentrated hydrochloric acid or 1 mol/L sodium hydroxide according to different experimental requirement. Salt dissolution was aided by irradiation with ultrasonic waves in some instances.

3.3.2.   Thermodynamic prediction of synthetic produced water equilibria equations

MEDUSA (Make Equilibrium Diagrams Using Sophisticated Algorithms) software was developed by Ignasi Puigdomenech based on SOLGASWATER and HALTAFALL algorithms (Ingri et al., 1967, Ingri et al., 1968, Eriksson, 1979). It is a free algorithm program available at the KTH Royal Institute of Technology, Sweden (http://www.kemi.kth.se/medusa) for calculating the composition of aqueous multicomponent, multiphase equilibria and equilibrium mixtures. The basic parameters, including equilibrium constants that are necessary for the calculation of distribution diagrams are in the program database.

MEDUSA software was used in this research for the construction of distribution diagrams of different metal ion forms present in the electrolyte (synthetic produced water). Their solubility, concentration, effect of applied potential and potential deposition potentials on the cathode was predicted. Activity coefficients of each solution were determined by equations 3.1 – 3.2 (Tissue, 2000).

$$\mu = \frac{1}{2}\sum_i z_i^2 C_i \qquad\qquad\qquad 3.1$$

Where μ is ionic strength, Z is charge and C is concentration

$$\log \gamma_i = \frac{-0.509 z_i^2 \sqrt{\mu}}{1 + (3.29 \propto_i \sqrt{\mu}} \qquad\qquad 3.2$$

Table 3.4: Charge distribution of ions in aqueous solution (Kielland, 1937)

Ion	Charge	α (nm)
CO_3	-2	0.45
HCO_3	-1	0.45
$HCOO$	-1	0.30
C_2O_4	-2	0.45
CH_3COO	-1	0.45
C_6H_5COO	-1	0.60
Ca	2	0.60
Cl	-1	0.30
ClO_3	-1	0.35
ClO_4	-1	0.35
Cu	2	0.60
Fe	2	0.60
Fe	3	0.90
H	1	0.90
K	1	0.30
Li	1	0.60
Mg	2	0.80
Na	1	0.40
NH_4	1	0.25
Ni	2	0.60
NO_2	-1	0.30
NO_3	-1	0.30
OH	-1	0.35
Pb	2	0.45
S	-2	0.50
HS	-1	0.35
SCN	-1	0.35
SO_3	-2	0.45
HSO_3	-1	0.40
SO_4	-2	0.40

Where γ is the activity coefficient and α is the hydrated ion radius. α values used for this modelling are shown in Table 3.4.

This activity coefficient was used in the calculation of the pH (saturation pH) but it was also used to determine the minimum concentration of a

dissolved element required to be in equilibrium with its solid (salt) element. For example the minimum concentration of sodium that would be required in solution to be in equilibrium with the solid sodium chloride was determined as illustrated in equations 3.3 - 3.8.

$$NaCl = Na^+ + Cl^- \qquad\qquad 3.3$$

The equilibrium constant K_{sp} (solubility product constant) of this equilibrium was calculated using equations 3.4 – 3.5:

$$K_{sp} = \gamma_{Na^+}.[Na^+].\gamma_{Cl^-}.[Cl^-] \qquad\qquad 3.4$$

$$\gamma = \gamma_{Na^+} = \gamma_{Cl^-} \qquad\qquad 3.5$$

The minimum concentration of ions required in solution to be in equilibrium with their salt was calculated using equations 3.6 – 3.8.

$$C = [Na^+] = [Cl^-] \qquad\qquad 3.6$$

Therefore

$$K_{sp} = \gamma^2.C^2 \qquad\qquad 3.7$$

$$C = \frac{\sqrt{K_{sp}}}{\gamma} \qquad\qquad 3.8$$

The calculated ionic strength of PW I is 7 mol/L and the highest calculated ionic strength of PW II – PW V was 7.04 mol/L each while PW V was 7.16 mol/L as determined from Equation 3.2. This indicates that synthetic produced waters used for this research have relatively high conductivity since a linear relationship exist between ionic strength and conductivity (Russell, 1995, Shackelford et al., 1999, Abdul Ghafoor. et al., 2000). Therefore synthetic produced water is a natural electrolyte and needs no supporting electrolyte to carry out electrochemical measurements.

The electrodeposition potentials of metals predicted by MEDUSA program are calculated based on the standard redox potentials of the metal ions. The redox potentials are measured with reference to the reduction of hydrogen ions to hydrogen gas at standard state conditions (25 °C, 1 atmospheric pressure, and one unit activity for all species). The potential of the overall reaction at the standard state was calculated by equation 3.9.

$$E^0 = E^0_{ox} + E^0_{red} \qquad\qquad 3.9$$

Where E^0_{ox} and E^0_{red} are oxidation half reaction and reduction half reaction, respectively.

For nonstandard states, the redox potential (E) was related to standard potential by the Nernst equation as illustrated in equation 3.10 (Snoeyink and Jenkins, 1980):

$$E = E^0 - RT/nF \ln Q \qquad\qquad 3.10$$

Where R is the gas constant (J/(mol.K), T the absolute temperature (K), n the number of electrons involved in the reaction, F the Faraday constant (C/mol) and Q, the reaction quotient.

The redox potentials may also be related to the Gibbs free energy as illustrated by equations 3.11 and 3.12 (Snoeyink and Jenkins, 1980):

$$\Delta G^0 = -nFE^0 \qquad\qquad 3.11$$

$$\Delta G = -nFE \qquad\qquad 3.12$$

In the results generated from MEDUSA, I represents ionic strength, E_H represents redox potential, $[X]_{TOT}$ represents total concentration of X (where X can be any ion). E_{SHE} is the potential that a platinum electrode would ideally have in contact with the aqueous solution when measured against a standard hydrogen electrode (SHE). This is sometimes

represented as E_h instead of E_{SHE} in a galvanic cell. "e⁻" represents the activity of electrons which is defined as the relative tendency for a given dissolved oxidant to accept electrons, or for electrons to "leave" the electrode in a galvanic cell. Four phase states are recognised by MEDSA indicated at the end of the name as shown in Table 3.5.

**Table 3.5: Symbols used to represent phase state in MEDUSA**

Phase	Description
Solid	Ending in (c) for crystalline, (s) for solid, (am) for amorphous. For example $Fe_2O_{3(c)}$
Gas	Ending in (g) like $CO_{2(g)}$
Liquid	Ending in (l) e.g. $Hg_{(l)}$
Aqueous	Any name not ending in (c), (s), (am), (g) or (l). For example: Na^+, $Fe(OH)_3$

3.3.3. Deposition of heavy metal from synthetic produced water

Heavy metal deposition from synthetic oilfield produced water was done both via a 3 –electrode cell and a 2-electrode cell. In the three-electrode cell, metal electrodeposition mechanisms and kinetics were studied at various pH values (basic, acid and neutral) as reported in Chapters 4 and 5. Cyclic voltammetry (CV) was first carried out to determine the deposition potentials of each metal at a particular pH value after which the potential obtained from the CV was set for metal electrodeposition using chronomaperometry (CA) technique. The effect of time and pH on metal deposition from synthetic oilfield produced water was determined from the chronoamperograms obtained. For both CV and CA measurements the electrochemical cell set up was similar to what is shown in Figure 3.1. The structure and morphology of deposits on the surface of working electrodes

were viewed under scanning electron microscope (SEM) and their elemental composition was determined using energy-dispersive X-ray spectroscopy (EDX) as illustrated in Figure 3.2.
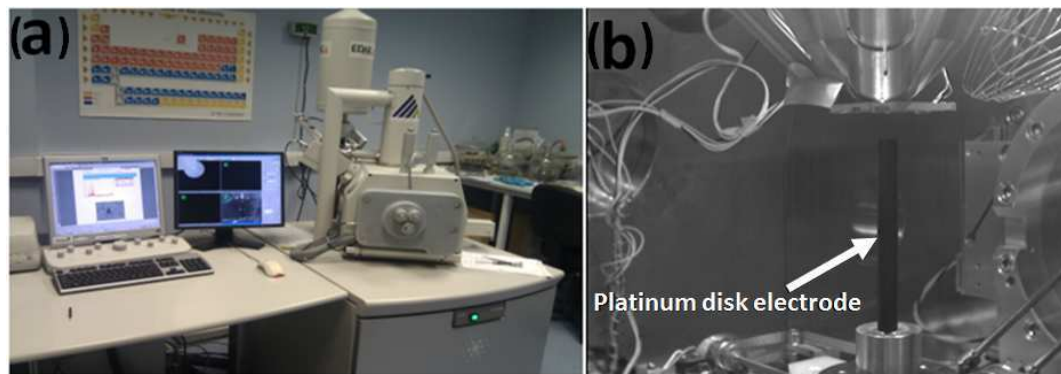
Figure 3.2: (a) Image of QUANTA 600 SEM machine and (b) image of QUANTA 600 chamber used for SEM-EDX Analysis

3.3.4.   Acid Treated CNT

Multi wall carbon nanotube (MWCNT) was purified by a nitric acid treatment method (Hou et al., 2008, Gao et al., 2009a). 1 gram of MWCNT was mixed with 30 mL of concentrated sulphuric acid and 10 mL of nitric acid in a round bottom flask. The CNT-acid mixture was irradiated with ultrasonic (> 20 kHz) waves in an ultrasonication bath for 15 minutes to disperse the carbon nanotubes in the mixture and improve the contact between the MWCNT surface and acid molecules. The mixture was then heated to 140 ºC under reflux for 20 minutes (and not longer to maintain the tubular structures of the CNTs). The mixture was allowed to cool naturally to room temperature and returned to the sonication bath where it was again irradiated with ultrasonic waves for another 20 minutes. Deionised water was added to the mixture and filtered in a Pyrex Gooch crucible with fritted disc (Grade 4) via an air pump which was used to generate negative pressure for the filtration. The residue (acid treated

MWCNT) was washed continuously until the pH of the filtrate reached between 6 and 7.

3.3.5. CNT –TiO$_2$ Synthesis by Surfactant Wrapping Sol –Gel Method

MWCNT-TiO$_2$ hybrid was synthesised via a sol-gel method with surfactant functionalization technique (Gao et al., 2009a). Raw/purified CNTs were dispersed in 0.5 wt% sodium dodecylbenezenesulfonate (NaDDBS) to make a suspension. The suspension was irradiated with ultrasonic waves for 10 hours in a sonication bath to form a uniform aqueous suspension (Islam, Rojas et al, 2003; Matarredona, Rhoads et al. 2003). Surfactant molecules assembled on the surface of individual nanotubes under this condition with the alkyl chain groups lying flat along the tube length as illustrated in Figure 3.3. Tube stabilization depends on surfactant molecules lying flat on the tube surface parallel to the cylindrical axis which is also responsible for better dispersion of nanotubes (Islam, Rojas et al., 2003). A known amount of the prepared CNT precursor solution was dispersed into 20 mL ethanol and mixed on a magnetic stirrer for 30 minutes to get a uniform solution (solution A). A known amount of titania precursor (titanium isopropoxide) according to the CNT to TiO$_2$ weight ratio required together with few drops of glacial acetic acid were added into 15 mL ethanol and the solution was stirred for 30 minutes until it became clear (solution B). The function of the glacial acetic acid was to aid the dissolution of the titanium precursors in ethanol. Solution B was transferred to a syringe and dropped by a syringe pump at 20 mL/h into solution A which was kept under vigorous stirring.

NaDDBS

$C_{12}H_{25}$—⬡—SO_3^- Na^+
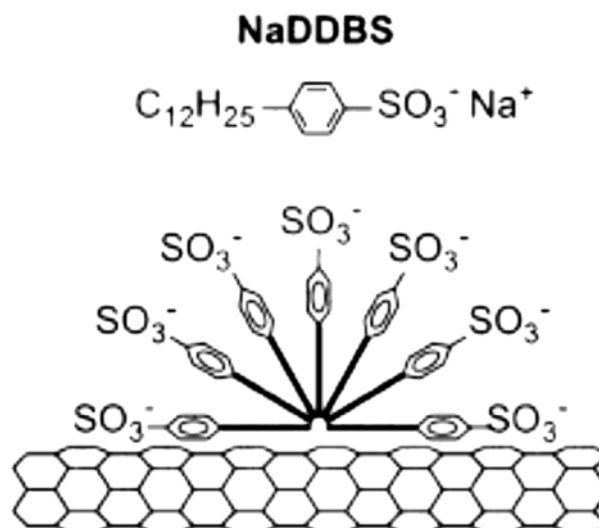
Figure 3.3: A schematic representation of surfactant adsorptions onto nanotube surface (Islam, Rojas et al., 2003)

The mixture was continually stirred for a further 2 hours to allow the titanium metal cations be captured by the negatively charged CNTs surface. A diluted ammonia solution (1 mL 35% ammonia solution in 17.1 mL Millipore water) was then added into the mixture to hydrolyse the precursor residues and stirring was maintained for another 30 minutes. The suspension was centrifuged and washed with ethanol in three consecutive cycles. The final precipitate was dried in an oven at 60 ^{0}C for 12 hours to obtain a powder product. The powder product (synthesised CNT-TiO2 nanohybrid) was later calcined at 500 ^{0}C for 30 minutes to crystallise the TiO$_2$.

In this research the effect of NaDDBS surfactant on CNT dispersion and the optimum CNT to surfactant ratio needed for maximum MWCNT dispersion in aqueous suspension was studied as discussed in Chapter 5.

3.3.6. Characterization of CNT-TiO$_2$

Several methods were used to characterise synthesised CNT-TiO$_2$ hybrid catalyst. Powder X-ray diffraction (XRD) was used to determine the crystallinity of TiO2 in the synthesised CNT-TiO$_2$. A Philips EXPERT θ - 2θ X-ray diffractometer were used to measure XRD patterns (diffraction intensity versus 2θ) of samples. In a typical XRD measurement, samples were ground and placed on a modified glass microscope slide and scanned at a step of 0.020 $^0sec^{-1}$ over a 2θ range of 10 - 80^0. The composition of the synthesised hybrid material was determined by comparing obtained XRD results with the Joint Committee on Powder Diffraction Standards (JCPDS) database. Crystallite size was calculated from the line where there is negligible CNT interference, anatase TiO$_2$ reflection plane (2θ = ca. 48.1^0). Thermogravimetric analysis (TGA) was performed using a TA Q600 SDT analyser operating at a heating rate of 20 ^{O}C/minute under air flowing at 100 mL/minute. Transmission electron microscopy (TEM) and Brunauer-Emmett-Teller - Barrett-Joyner-Halenda (BET-BJH) was used to determine the surface structures and morphology of the synthesised nanohybrids.

3.3.7. Preparation of CNT-TiO$_2$ photoanode

A typical CNT-TiO$_2$ photoanode was prepared by loading CNT-TiO$_2$ nanohybrid on a solid electrode. Graphite, titanium and porous titanium electrodes were examined as suitable solid support for the CNT-TiO$_2$ hybrid. A 2.5 mg/cm^2 paste of the CNTs-TiO$_2$ hybrid were loaded onto the solid supports and allowed to dry at room temperature. The adhesion between the CNT-TiO$_2$ catalyst and each solid support material was tested by dipping the electrode in Millipore water. The adhesion on porous titanium was better than that on graphite or titanium as shown in Figure 3.4. Therefore for this research, porous titanium electrode was used as the solid support.
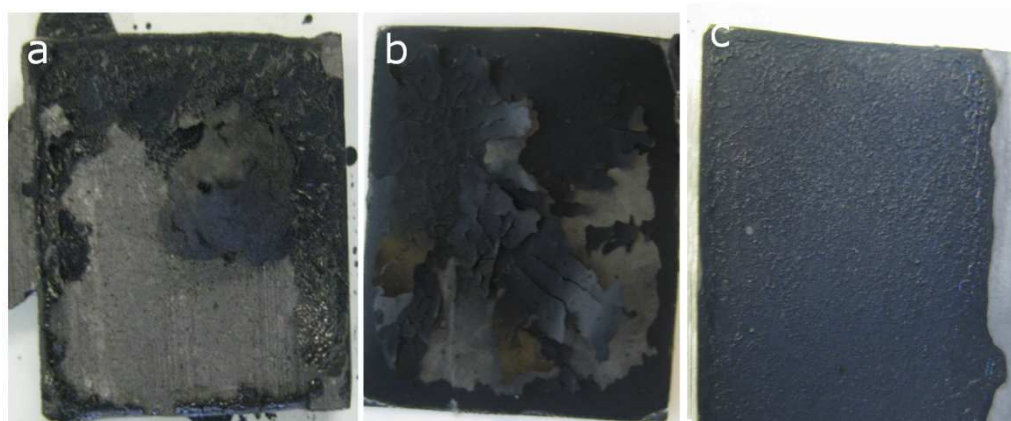
Figure 3.4: Images showing the adhesion of synthesized CNT-TiO$_2$ on (a) Graphite (b) Titanium and (c) porous titanium surfaces after drying at room temperature for 24 hours

3.3.7.1. Preparation of porous titanium plate

Titanium foils were treated in air under high temperature for 2 hours to form titanium oxide coating on their surface at different temperatures, including 750 °C, 800 °C, and 900 °C (Figure 3.5). However after 2 hours of high-temperature treatment at 900 °C, titanium foils became brittle and a relatively thick and white titanium oxide coating was observed as shown in Figure 3.5 (b). Titanium foils, which were treated at temperatures below 900 °C, i.e., 750 °C and 800 °C, remained flexible and their coating layers were not liable to crack or flake. Titanium foils treated at 800 ^{0}C were sandwiched in between molybdenum meshes by stainless steel wire (Figure 3.6) to maintain their stability in molten salt. The wrapped titanium foils were placed at the bottom of a graphite crucible (used as cathodic current collector for electro-deoxidation of high-temperature treated titanium foils) and dried CaCl$_2$ was poured inside the crucible. The whole crucible was employed as the cathode assembly, and a graphite rod (HK-3) was used as the anode to conduct the electro-deoxidation process (3.2 V, 900 °C and 5 hours).
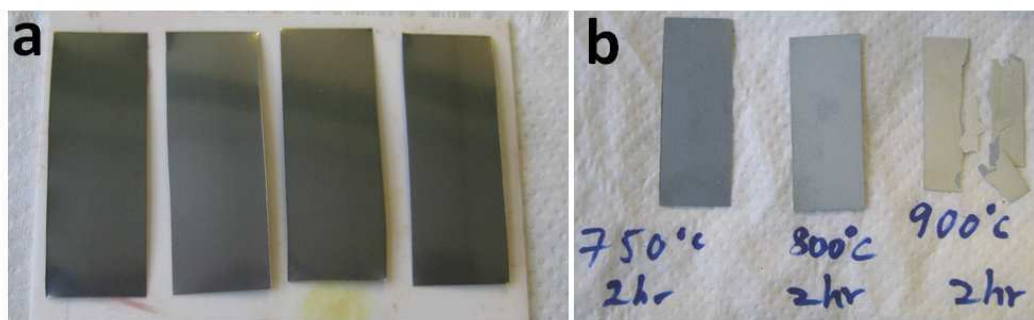
Figure 3.5: Images of (a) untreated Ti foils and (b) high-temperature treated titanium foils

Figure 3.6: An image of wrapped high-temperature treated titanium foil before electrolysis

Conventional experimental design was used, i.e., the cathode assembly was suspended into the melt contained in alumina crucible. The high-temperature treated titanium foil (treated for 2 hours, at 800 °C) was successfully electro-deoxidised after 5 hours of electrolysis (3.2 V, 900 °C). The cathode assembly was kept in the melt during the whole course of the electrolysis and cooling process to avoid re-oxidisation of the electro-deoxidised titanium foils. Therefore, both cathode assembly and anode were frozen in the solidified salt after the electro-deoxidisation process, as shown in Figure 3.7a.
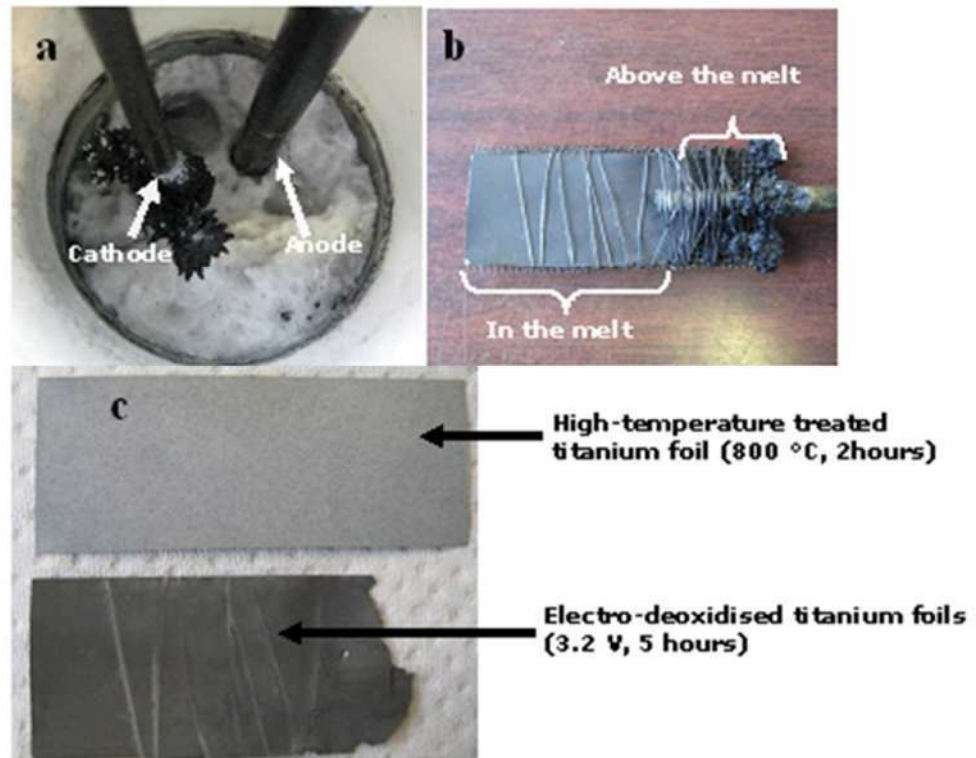
Figure 3.7: : Photos of (a) relative clean salt in an alumina crucible after 5 hours electrolysis, (b) obtained cathode assembly, and (c) a comparison of high-temperature treated Ti foil (800 °C, 2 hours) and electro-deoxidised Ti foil

The improved adhesion between CNTs and porous titanium is believed to be a result of the porosity of the titanium surface which allows CNTs to fill in the pores on the surface and hence give a better adhesion than what was obtainable when graphite or ordinary titanium electrodes were used.

3.3.8.   Photocatalytic activity of CNT-TiO$_2$ photoanode

Electrochemical experiments were carried out in both two and three-electrode cell configurations. The electrochemical properties of the MWCNT-TiO$_2$ photoanode were first tested in a conventional three electrode cell (photoanode, platinum disk electrode and 3M KCl Ag/AgCl reference

electrode) to identify the photocurrent response and the percentage degradation of phenanthrene in PW I by chronoamperometry. Afterwards, a two-electrode PEC cell (WE: MWCNT-TiO$_2$ photoanode and CE: Pt disk electrode) was built in order to investigate the electrochemical behaviour of metal deposition and the decomposition of phenanthrene by chronoamperometry and cyclic voltammetry. The potential of each electrode was simultaneously monitored by a multi-channel potentiostat (IviumnStat) while applying a cell voltage to the two electrode cell to identify the deposition potential of each metal ion in the synthetic produced water.

The experiments were conducted in both light and dark conditions to study the effect of photocatalysis on heavy metal deposition and phenanthrene oxidation. A xenon lamp-based Newport 66902 150W solar simulator (AM 1.5G) served as the light source for photo catalytic experiments. The cell was placed at a distance of 3 mm from the simulated sunlight. Samples were taken at regular intervals and analysed to monitor the concentration of phenanthrene with time using UV-Vis spectrophotometer. The results obtained from these experiments are discussed in Chapters 5 and 6.

3.4. Theory of Analytical Techniques

The theories of the analytical techniques employed in the experimental procedures are discussed in this section

3.4.1. Cyclic Voltammetry

Cyclic voltammetry (CV) is possibly the most versatile electroanalytical technique for the study of electroactive species. It is often the first experiment performed in an electrochemical study of a compound or an electrode surface. The effectiveness of CV comes from its ability to rapidly

observe the redox behaviour of the target compound over a wide potential range (Kissinger P.T, 1985).

CV measurement involves cycling the potential of an electrode immersed in an unstirred solution, and measuring the resulting current. The potential of the working electrode is controlled versus a reference electrode such as silver/silver chloride (Ag/AgCl) or saturated calomel electrode.
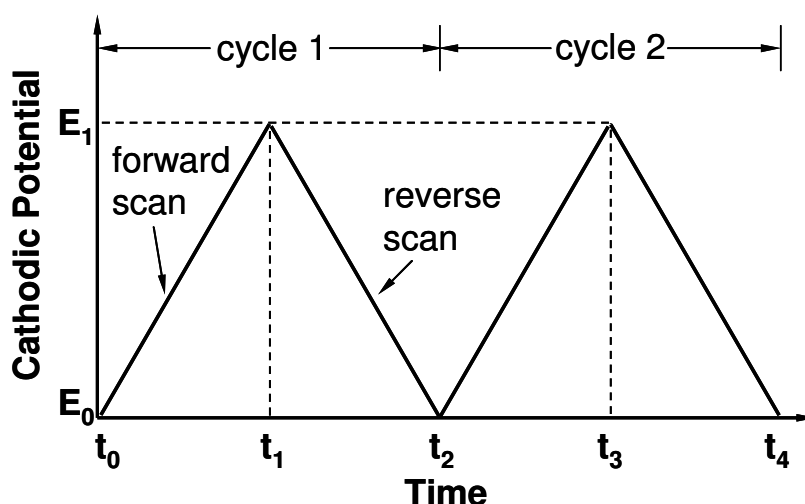

Figure 3.8: Typical waveform of cyclic voltammetry (Kissinger and Heineman, 1983)

In this research silver/silver chloride (Ag/AgCl) was employed for all CV measurements. The controlling potential which is applied across these two electrodes can be considered as an excitation signal. This excitation signal is a linear potential scan with a triangular waveform as shown in Figure 3.8.

The potential starts from an initial value (E_o) and changes linearly to a pre-set point (E_1), the potential then switches to a reverse direction to complete the second cycle which can be attributed to the name cyclic. The slope in figure 3.8 is equivalent to the scan rate (mV/s). Modern instruments now enable switching potentials and scan rates to be easily

varied. Autolab/IviumnStat potentiostats were used for this purpose in this research.
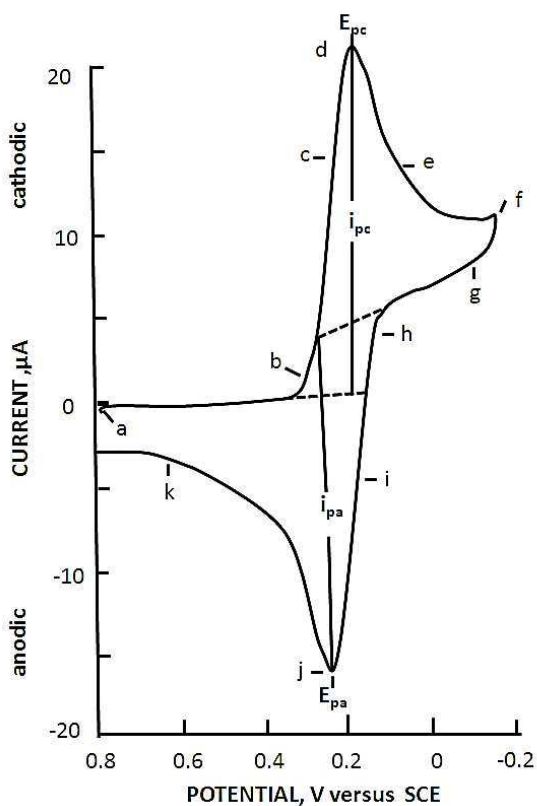
Figure 3.9: A typical cyclic voltammogram (Kissinger P.T, 1985)

A typical cyclic voltammogram is shown in figure 3.9 is obtained by measuring the current at the working electrode during the potential scan. The voltammogram is a display of current versus potential. It may also be thought of as current versus time graph because the potential varies linearly with time.

In figure 3.9 the potential is scanned negatively (forward scan) to reduce the electroactive X to Y as illustrated in equation 3.13. This process generates a cathodic current indicated at (b).

$$X + e^- \quad \rightarrow \quad Y \qquad\qquad 3.13$$

This makes the electrode a sufficiently strong reductant to reduce X. The cathodic current increase rapidly from (b – d) until the concentration of X at the electrode surface is significantly diminished causing the current to peak at (d). A current decay (d –g) occurs as the solution surrounding the electrode is depleted of Y. The scan direction is changed to positive at -0.15 V vs. SCE (f) for the reverse scan. Cathodic current continues because the potential is still negative enough to reduce X although it is scanning in the positive direction. When the electrode becomes sufficiently positive, Y which has accumulated around the electrode surface is then oxidised by the electrode process as illustrated in equation 3.14.

$$Y \quad \rightarrow \quad X + e^- \qquad\qquad 3.14$$

This causes anodic current (g –j), which rapidly increases until the surface concentration of Y is diminished, causing the current to peak at (j). The current then decays (j –K) as the solution surrounding the electrode is depleted of Y. The first cycle is completed as the potential reaches +0.8 V vs. SCE obtaining a cyclic voltammogram. A detailed understanding of CV can be gained by examining the Nernst equation (cf. equation 3.10) and concentration gradient in the solution adjacent the electrode during electrolysis. The important parameters of a CV are: the magnitudes of the anodic peak (i_{pa}), cathodic peak (i_{pc}), anodic peak potential (E_{pa}) and cathodic peak potential (E_{pc}) (Kissinger P.T, 1985).

The electrochemical reversibility of a reaction can be determined from a cyclic voltammogram if equation 3.15 is true

$$\frac{i_{pa}}{i_{pc}} = 1 \qquad\qquad 3.15$$

Likewise the formal reduction potential, (E^O), for a reversible couple can be determined from CV using equation 3.16.

$$E^0 = \frac{E_{pa} + E_{pc}}{2} \qquad\qquad 3.16$$

The number of electrons transferred in the electrode reaction (n) for a reversible couple can also be determined using the equation 3.17

$$\Delta E_p = E_{pa} - E_{pc} \cong \frac{0.059}{n} \qquad\qquad 3.17$$

The real electrode surface area involved in a reversible system can be determined from cyclic voltammogram using Randles – Sevick equation (equation 3.18) for the forward sweep of the first

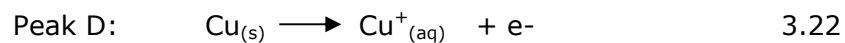$$i_p = (2{,}69 \times 10^5) n^{3/2} A D^{1/2} C v^{1/2} \qquad\qquad 3.18$$
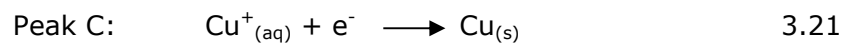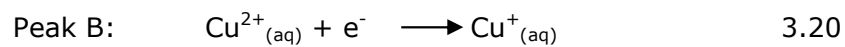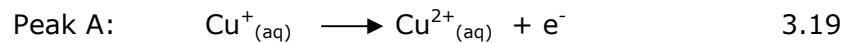
[Where i_p is the peak current (A), n the stoichiometry number of electrons, A the electrode area (cm^2), D the diffusion coefficient (cm^2/s), C the concentration (mol/cm^3) and v the scan rate (V/s)]

However the vast majority of electrochemical reactions involve an electron step where another species is generated during the redox process, called coupled chemical reactions. CV is very useful for the diagnosis of these homogenous chemical reactions that are coupled to the electrode surface reaction. For example the cyclic voltammogram for the reduction of $Cu^{2+}_{(aq)}$ to $Cu_{(s)}$ is illustrated in figure 3.10.

The reactions at the four peaks observed are illustrated in equations 3.19 – 3.22. In this research, CV was carried out to investigate metal deposition and phenanthrene oxidation in synthetic produced water on working electrode surfaces at different pH values. Details of this work are presented in Chapters 4, 5 and 6.
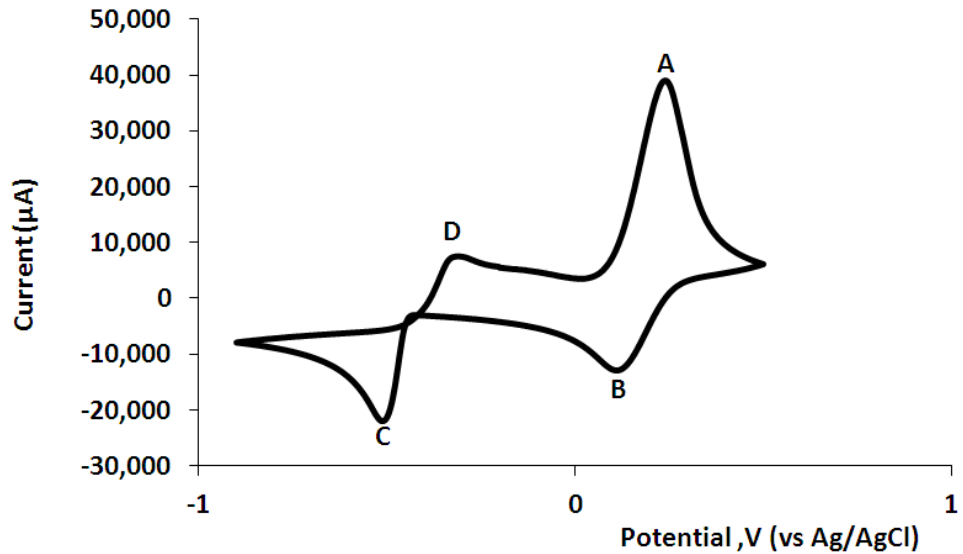
Figure 3.10: Cyclic voltammogram of $Cu^{2+}_{(aq)}/Cu_{(s)}$ in PW II on glassy carbon at scan rate 30 mV/s

Peak A: $Cu^{+}_{(aq)} \longrightarrow Cu^{2+}_{(aq)} + e^{-}$ 3.19

Peak B: $Cu^{2+}_{(aq)} + e^{-} \longrightarrow Cu^{+}_{(aq)}$ 3.20

Peak C: $Cu^{+}_{(aq)} + e^{-} \longrightarrow Cu_{(s)}$ 3.21

Peak D: $Cu_{(s)} \longrightarrow Cu^{+}_{(aq)} + e-$ 3.22

3.4.2.   Chronoamperometry

Chronoamperometry (CA) is an electrochemical technique where the potential of the working electrode is subjected to a voltage step change and the transient response from the cell current is recorded. The transient response is due to faradic processes caused by the potential difference between working and reference electrodes, and monitored as a function of time. It has one of the simplest potential wave forms as shown in Figure 3.11. In a single potential step experiment, the potential is changed instantaneously from the initial potential (E_o) to the first step potential (E_1) and it is held at this value for the first step time (t_1). The potential is

changed to the second step potential (E_2) after the first step time (t_1), in a double step experiment and it is held at this value for the second step time (t_2).
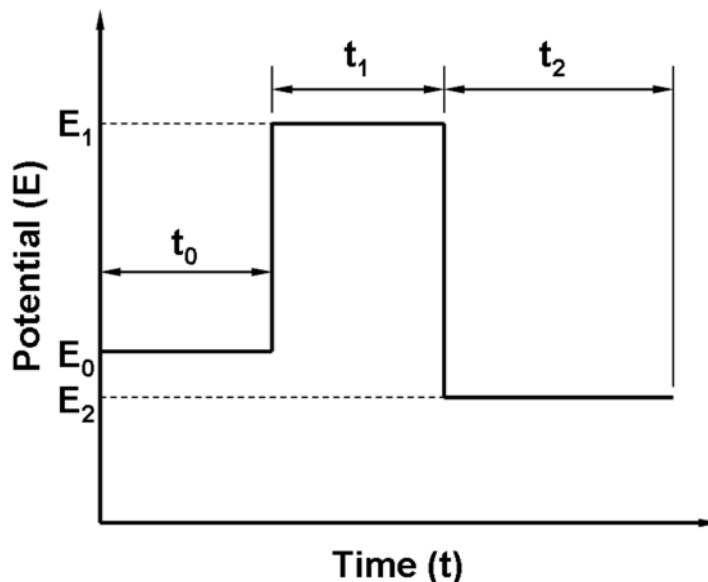
Figure 3.11: Potential wave form for Chronoamperometry (Bioanalytical Systems, 2000)

In CA, current is monitored as a function of time. In an electrochemical reaction ($R = O + e^-$) there is no net conversion of R to O in a single potential step at potentials well negative of the redox potential, whereas at potentials well positive of the redox potential, R species are electrolysed as soon as they arrive at the electrode surface (diffusion-controlled). In most potential step experiments, E_1 is well negative of the redox potential and E_2 is well positive of the redox potential in order to eliminate any effects of slow heterogeneous electron transfer kinetics.

For a diffusion-controlled current, the current-time (i-t) curve is described by the Cottrell equation (equation 3.23):

$$i = nFACD^{1/2}\pi^{-1/2}t^{-1/2} \hspace{2cm} 3.23$$

Where: F is the Faraday's constant (C/mol), A the electrode area (cm^2), D the diffusion coefficient (cm^2/s), n the number of electrons transferred/molecule and C the concentration (mol/cm^3).

In this research CA was carried out using Autolab and CHI instrument. It was used to monitor the current intensity at the working electrode versus the reaction time of metal decomposition from synthetic produced water. It was also used to monitor the current intensity at the working electrode versus the time of reaction of phenanthrene degradation, while a selected constant anodic potential is pre-programmed. CA results were useful for the prediction of possible mechanisms of some reactions.

3.4.3. Ultraviolet – visible (UV-vis) spectrophotometry

A spectrophotometer consists of a spectrometer (for producing light of any selected colour or wavelength) and a photometer (for measuring the intensity of light). The design of spectrophotometer is such that the cuvette (where the liquid sample is placed) is placed between the spectrophotometer beam and the photometer. The amount of light passing through the cuvette is measured by the photometer which then delivers a voltage signal to a display device. This signal changes as the amount of light absorbed by the liquid changes (Caprette, 2012).

A UV-visible spectrophotometer uses a beam of ultraviolet (200~400 nm) or visible light (400~800 nm) which is scattered or absorbed by the atom or molecules of the substance present in solution in the cuvette. The light source is usually a tungsten lamp for the visible region of spectrum, and either a hydrogen or deuterium lamp for ultraviolet wavelengths. Absorption spectra in the ultraviolet and visible regions are due to energy transitions of both bonding and nonbonding outer electrons of the molecule. Since the wavelength of UV –visible is between 200 nm and 800

nm it is not suitable for organic solvents which have a very strong absorption. Therefore water or ethanol is usually selected as a reference solution.

The concentration of a substance in solution can be measured by determining the extent of absorption of light at the appropriate wavelength. The Beer-Lambert law states that when monochromatic light of a specific wavelength passes through a solution there is usually a quantitative relationship between the solute concentration and the intensity of the transmitted light (Commoner and Lipkin, 1949) as illustrated in equations 3.24.

$$I = I_0 * 10^{-kcl} \qquad\qquad 3.24$$

Where I_0 (W/cm^2)is the intensity of transmitted light using a pure solvent, I (W/cm^2) the intensity of the transmitted light when a coloured compound is added, l (cm) the distance light travels through the solution (light path) and k a constant.

In a spectrophotometer the light path (l) is a constant, therefore Beer Lambert's law may be written as equation 3.25.

$$\frac{I}{I_0} = 10^{-kc} = T \qquad\qquad 3.25$$

Where T is the transmittance and k is a new constant.

Therefore a logarithmic relationship exist between transmittance and the concentration of the coloured compound as shown in equation 3.26

$$-\log T = \log\left(\frac{1}{T}\right) = kc = \text{Absorbance} \qquad\qquad 3.26$$

Since absorbance is directly proportional to the concentration, therefore the concentration of a solute in solution can be determined from

spectrophotometer from its absorbance as shown in equation 3.26. It is however important to note that this law may not be applicable to all solutions since solutions can ionise at higher concentrations, or precipitate to give a turbid suspension which may increase or decrease the apparent absorbance. The Beer-Lambert law is most accurate between absorbance values of 0.05 and 0.70. Measured absorbance above 0.70 tends to underestimate the real absorbance and any absorbance below 0.02 may not be accurate due to machine error.

In this study, UV-Vis analysis was used to measure the concentration of phenanthrene in synthetic produced water and its remaining concentration after photocatalytic oxidation.

3.4.4. Scanning Electron Microscopy / Energy-dispersive X-ray Spectroscopy

Scanning Electron Microscopy (SEM) is a technique that uses a beam of electrons to scan the surface of a sample in order to build a 3-dimensional image of the specimen. In a typical SEM, a fine beam of electrons are generated by heating a filament such as tungsten and accelerated towards the anode. The electron beam is then focused by the condenser lenses onto a very fine focal spot and deflected by the objective lens to scan the sample.

When the electron beam (primary electrons) hits the surface of the sample, a variety of signals are generated from the interaction of the beam and the atoms of the sample. These can include transmitted electrons (beams that pass through the sample), secondary electrons (electrons from the sample itself), backscattered electrons (electrons that bounce off nuclei of atoms in the sample), X-rays, light and heat as illustrated in figure 3.12. However

secondary electrons, backscattered electrons, and X-rays signals provide the most important information in SEM.
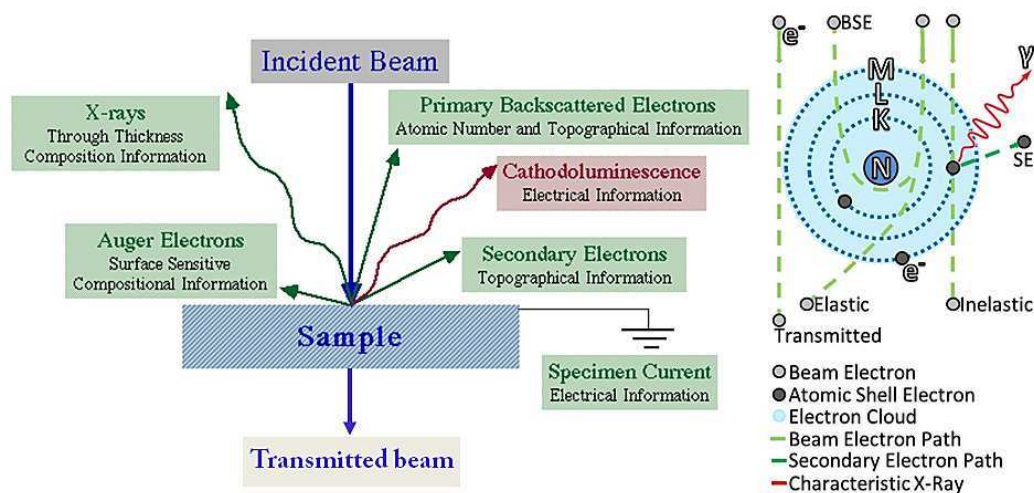
Figure 3.12: Typical specimen-beam interactions in SEM (Wright, 1999)

Secondary electrons are emitted from the atoms occupying the top surface of the sample, and are used to produce a high resolution readily interpretable image of the surface because of the smaller penetration diameter of the primary electron beam. Backscattered electrons (BSE) are primary beam electrons reflected from atoms in the sample. BSE images show the distribution of different chemical phases in the sample. However the image resolutions of BSE are of lower quality compared to secondary electrons because they (BSE) are emitted from a depth in the sample. X-rays are produced by the interaction of the primary electron beam with atoms in the sample. This causes shell transitions resulting in the emission of X-rays. The emitted X-ray has an energy characteristic of the parent element. The measurement and detection of this energy permits elemental diffraction analysis (EDX). EDX can provide qualitative and quantitative analysis of elemental composition of a sample with a sampling depth of 1-2

microns. It may also be used to measure the elemental distribution on a sample surface.

Since electron flow is continuously in contact with the specimen during SEM measurement, charge tends to accumulate on the sample surface without discharge. This often results in the reduction of image quality. Coating of the specimen with gold or carbon is usually used to overcome this problem. However the sample is usually unusable after the measurement and coating can lead to obscurity of some surface details of the sample due to possible electric field build up between the sample and the surface coating.

In this research, SEM was used to reveal the surface topography of electrodeposited metals and synthesised nanohybrid powders. EDX on the other hand was used to determine the elemental composition of all electrodeposited metals and synthesised CNT-TiO$_2$ nanohybrid.

3.4.5.   Transmission Electron Microscopy

Transmission Electron Microscopy (TEM) is an imaging technique similar to SEM, but with the electron beam being partially transmitted through the sample. Therefore, an appropriately thin specimen is required for the beam to penetrate in this measurement in an out-gassed ambience. While the image is formed, it reveals the actual spatial configuration of the sample particle in a two-dimensional plane. This approach is widely utilized in material sciences for characterization from a morphological and crystallographic point of view. By careful selection of sample orientation, it is possible to reveal not only the position of the structure fault but the type of deficiency.

TEM can generate either a bright field (or so-called light field) image or a dark field image. A bright field image is formed by filtering the deflected electrons away and allowing only the unscattered ones to pass through and

reveal the crystal structure of a specimen. The image formation depends on the mass-thickness and diffraction contrast of the sample, for example the thick areas appear with dark contrast. However, it should be mentioned that this technique is particularly sensitive to the lattice disorder associated with the crystal defects, resulting in local displacement of the details around the defect. The dark field image, on the other hand, is formed from the scattered electrons rather than from the direct beam by either changing the aperture position or tilting the direction of electron beam. This imaging method is useful to examine the lattice defects or grain boundaries. However it is difficult to utilize this approach for electron tomography since the contrast of dark field image is strongly affected by the direction of the incident electron beam. (Kimura et al., 2005)

Furthermore, High-Resolution TEM (HRTEM), known as phase contrast imaging, is also available for most of the TEM instruments, which can be formed by using phase differences of electron beams transmitted through a thin layer of the sample. It provides a direct observation of crystal structure without any dislocation of the positions between a defect and the contrast variation appeared in the image, which is still an advantage over other techniques. HRTEM is subject to some limitations, such as the difficulty to correlate the lattice image with specimen structure or composition without other supplementary techniques (Spence, 1988).

In this study, TEM and EDX measurements were conducted to identify the sample structure and element compositions, and thus, to confirm the formation of CNT-TiO_2 hybrid particles. It was as also used to determine the consistency of particle sizes obtained from XRD measurements.

3.4.6.   X-ray Diffraction

X-ray diffraction (XRD) is a non-destructive analytical technique used to identify crystalline phases and orientation, structural properties, thickness of thin films, multi-layers and atomic arrangement in a solid material. XRD analytical results are correlated with references and standards of the International Centre for Diffraction Data (ICDD) and Joint Committee on Powder Diffraction Standards (JCPDS).

When an X-ray beam hits an atom, the electrons around the atom start to oscillate with the same frequency as the incoming beam. If the rays are scattered in all directions and the combining waves are out of phase, it is called a destructive interference and there is no resultant energy leaving the sample. This is the case with amorphous materials. However since the atoms in a crystal are arranged in a regular pattern and in very few directions, constructive interference occurs when X-rays are incident on a crystalline solid (Figure 3.13).
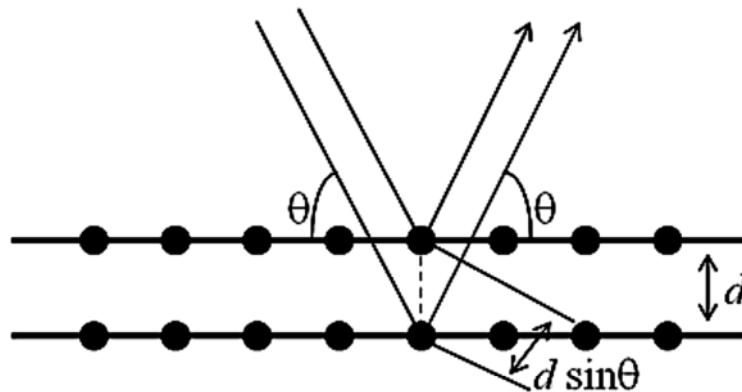
Figure 3.13: A schematic diagram of X-ray Diffraction on atomic crystal planes

The waves in phase result in well-defined diffracted X–ray beams leaving the sample at various directions. This diffracted beam is composed of a

large number of scattered rays mutually reinforcing one another. The angular positions and intensities of the resultant diffracted peaks of radiation produce a pattern which is characteristic of the sample.

$$n.\lambda = 2d.\sin\theta \qquad\qquad 3.27$$

This will only occur under certain conditions explained by Bragg's law. Bragg assumes that when a perfectly parallel monochromatic X-ray beam, of wavelength λ, is incident on a crystalline solid at angle θ, diffraction will occur if equation 3.27 is true.

Where d is the distance between atomic planes, n the integer (1, 2, 3…n), λ the wavelength, and θ the angle of incidence of the X−ray beam and the atomic planes. To satisfy Bragg's law, θ must change as d changes.

It is important that the powder or polycrystalline sample have a smooth plane surface for XRD measurement. Samples should be ground to particles of about 0.002 mm to 0.0005 mm diameter if possible. The sample is usually pressed into a sample holder so that a smooth flat surface is obtained. However powder diffraction has some limitations including: peak overlaps which makes individual peak identification difficult; inaccurate intensities and difficulty to determine crystal symmetry (Woodward, 2004). Therefore for comprehensive analysis, other analytical techniques are required for the target material in addition to XRD. In this research XRD was used to examine the crystallinity of TiO_2.

3.4.7. Thermogravimetric Analysis

Thermogravimetric analysis (TGA) is an analytical technique used for measuring the amount and rate of change in the weight of a material as a function of temperature or time in a controlled atmosphere. This controlled atmosphere is normally air or an inert gas such as nitrogen or helium. The

TA instrument used for this research allows both TGA and differential scanning calorimetry (DSC) analysis to be carried out simultaneously.
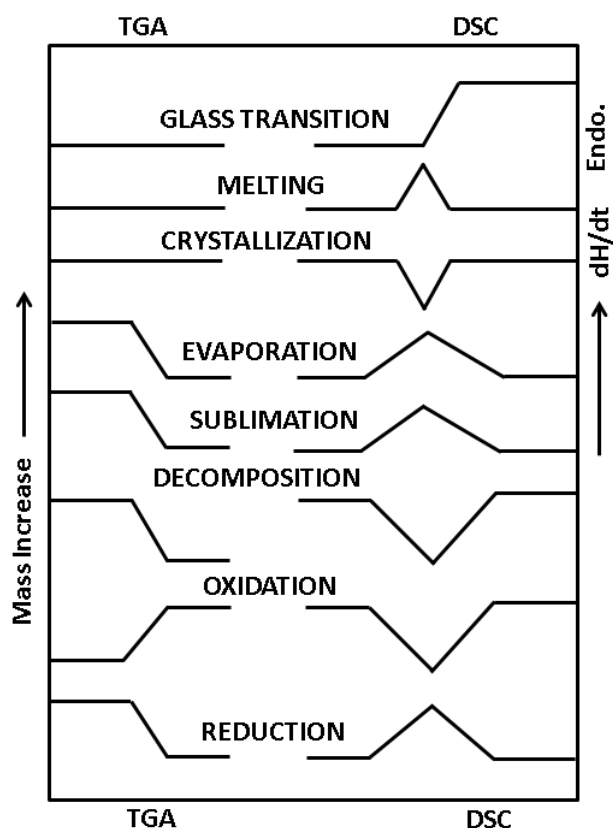
Figure 3.14: Typical TGA and DSC Results for various transitions (Stodghill S.P, 2010)

DSC works on the principle of measuring changes in heat flow as a function of temperature (Coats and Redfern, 1968). That is, the heat flow rate difference between a sample and a reference material (e.g. alumina) is measured, providing quantitative and qualitative information about physical and chemical changes that involve exothermic and endothermic processes, or changes in heat capacity.

Thermogravimetry can be used to characterize materials that exhibit weight loss or gain due to reduction, decomposition, oxidation, sublimation, evaporation as shown in Figure 3.14 (Hatakeyama and Quinn,

1994). However it cannot provide information on solid–state reactions that occur without change in weight (Coats and Redfern, 1963). TGA can also be used to predict the thermal stability of a material up to 1000 ºC. Composition, oxidative stability, decomposition kinetics, effects of reactive or corrosive atmospheres on materials, and volatile contents of materials can be measured by TGA-DSC instrument.

In a TGA, the maximum temperature is set so that all chemical reactions can be completed by the end of the experiment, when a stable specimen weight is obtained. In this research TGA was carried out to confirm the CNT-TiO_2 ratio content of the synthesised hybrid and possible transformations of the synthesised CNT-TiO_2 hybrids.

3.4.8. Brunauer-Emmett-Teller - Barrett-Joyner-Halenda Analysis

Brunauer-Emmett-Teller (BET) and Barrett-Joyner-Halenda (BJH) is a physical method for studying sample surface properties by a condensation or adsorption process of gas molecules (generally N_2, Ar or CO_2) with known sizes on the unknown material surface. The quantity of gas adsorbed and corresponding sample pressure are measured at a constant temperature (the boiling point of the adsorbed gas), to produce an adsorption-desorption isotherm and the subsequent porosity calculations.

In the current theories, BET model is the most common way to determine the specific surface area of sample (Brunauer et al., 1938), while Barrett-Joyner-Halenda (BJH) theorem is used to calculate the pore size distributions (Barrett et al., 1951).

The evaluation of BET theory is based on the capacity of the monolayer formed on a given surface (the number of adsorbed molecules in the

monolayer) by fitting the experimental adsorption data into the BET equation (equation 3.28).

$$\frac{P}{V(P_0 - P)} = \frac{1}{V_m C} + \frac{C-1}{V_m C}\left(\frac{P}{P_0}\right)$$

3.28

Where V is the volume of gas adsorbed by the sample, V_m the monolayer capacity, P the actual gas pressure, P_0 the vapour or saturation pressure of the gas at the temperature analysed, and C the constant related to the enthalpy of adsorption in the first adsorbed layer. The specific surface area can therefore be obtained by multiplying the monolayer capacity and the cross-sectional area of the individual molecule adsorbed.

The derivation of the above calculation (equation 3.28) is based on the following assumptions: the surface is flat; there are no lateral interactions present between adsorbed molecules; the adsorption energy on all adsorption sites is homogenous; the molecular adsorption energy is equal to the liquefaction energy except for the molecules in the first layer; and an infinite number of layers can be formed (Kruk and Jaroniec, 2001).

However, in the real case of adsorption on the porous solid, these assumptions will not usually be true. Hence, this method can only offer a rough approach to evaluate the material surface properties. Nevertheless, the BET method is currently a standard for specific surface area evaluation since other theories still cannot provide any significant advantages. More than the calculation of the sample surface area, the shape of gas adsorption-desorption isotherms can also be used as a source to classify the structural information on the sample surface. The experimental gas adsorption isotherms may be grouped into six categories as presented in Figure 3.15 (a).
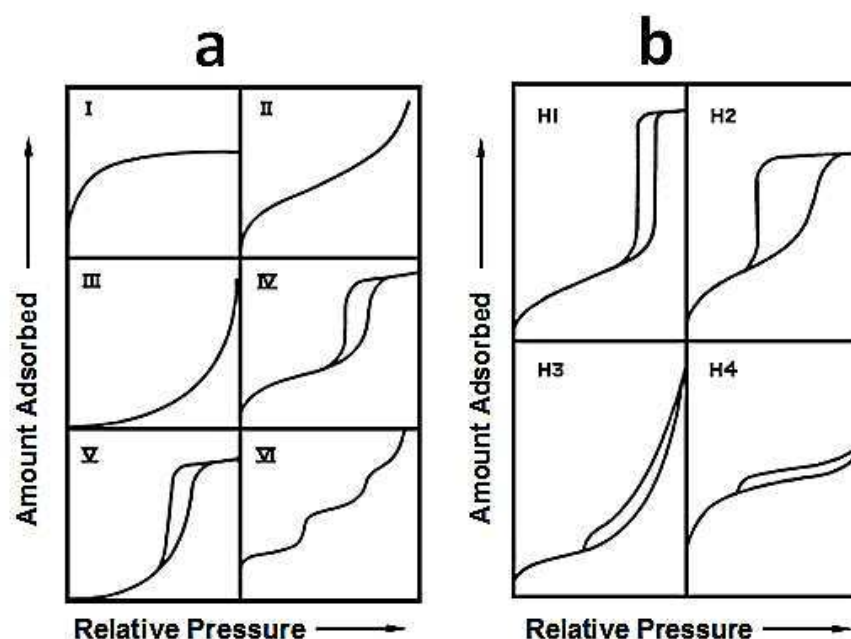
Figure 3.15: Classification of (a) type of gas adsorption isotherms and (b) adsorption-desorption hysteresis loops. (Kruk and Jaroniec, 2001, Sing et al., 1985, Rouquerol et al., 1994).

Type I isotherm is usually an indication of adsorption in micropores or monolayer adsorption; Type II demonstrates unrestricted monolayer-multilayer adsorption, which is due to the presence of non-porous or macroporous adsorbent; Type III can be observed when lateral interactions between adsorbed molecules play an important role in the system, but this is not common; Type IV is a normal indication of adsorption involving capillary condensation in mesopores; Type V indicates adsorbate-adsorbate interactions and is also uncommon; Type VI possess a step-liked shape related to the system and environmental temperature, corresponding to the stepwise adsorption on a uniform non-porous surface (Kruk and Jaroniec, 2001, Sing et al., 1985).

In mesoporous structures, the capillary condensation and capillary evaporation normally do not occur at the same pressures, which cause the emergence of hysteresis loops. The shape of such hysteresis loops may

exhibit a wide variety depending on the sorption meta-stabilities and/or pore connectivity of the sample. According to the IUPAC index, the hysteresis loops typically can be classified into four groups (Sing et al., 1985), as seen Figure 3.15 (b). The Type H1 loop is usually used to identify the materials with relatively high pore size homogeneity and simple pore network, which consist of assemblages of rigidly joint particles, or approximately uniform spheres formed in a fairly regular means and highly uniform cylindrical pore geometry (Kruk and Jaroniec, 2001). The Type H2 loops are often observed for many porous materials with a wide range of pore size distributions and an increase of irregular shapes. The pore geometries, such as ink-bottle pores or cage-like pores, are the main causes of this behaviour. Isotherms with a Type H3 hysteresis loop are found in materials with loose assemblages of plate-like particles leading to slit like pores. Finally, the features of Type H4 loops may be attributed to the presence of narrow slit-shaped pores, or a mesoporous array embedded with pores in relatively larger sizes.

Furthermore, some systems may cause low-pressure hysteresis arising from the adsorbent swelling or coexistence of irreversible chemical interactions during the adsorption process. Whatever the case, it should be noted that, in practical measurements, many samples tend to have ambiguous features. This makes interpretations difficult and requires further studies. In this research, the BET-BJH analysis was conducted using a fully automated analyser (Figure 3.16) to evaluate the CNT-TiO$_2$ nanohybrid surface properties in order to provide possible explanations for the appearance of catalyst profiles.

This involved three steps including sample preparation, adsorption analysis and interpretation. 1 mg of the sample was placed in the sample cell and outgassed for 16 hours using flowing helium gas. This removed surface

contaminants (gases and vapours) that may have become physically adsorbed during handling and storage.
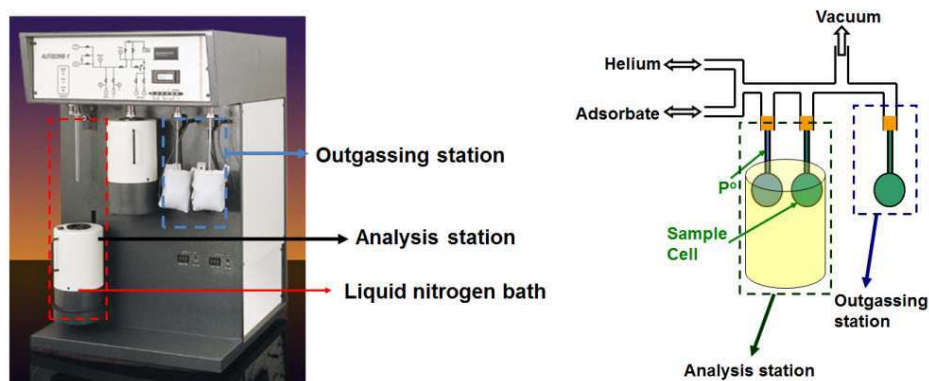
Figure 3.16: A typical BET analyser (Lab, 2013)

This step was critical for obtaining the required precision and accuracy of the specific surface area because of the sensitivity of the materials surface area. Full analysis was then carried out and the interpretation of the results obtained is presented in Chapter 5.

3.5. Conclusion

The experimental and analytical methodology followed in the investigation of treatment of produced water by simultaneous removal of heavy metals and PAH from produced water in a photoelectrochemical cell has been presented in this chapter alongside the techniques to characterise deposited metals and synthesised CNT-TiO_2 nanohybrids and to estimate PAH degradation. The main findings derived from the experimental approach to fulfil the research objectives are critically discussed in Appendix 1 and Chapters 4, 5, and 6.

Chapter 4: Cathodic processes

4.1. Introduction

Thermodynamic modelling show that copper, lead, iron and nickel exist predominantly as Cu(I), Pb(II), Fe(II) and Ni(II) in produced water and the electrodeposition of these heavy metals ions from synthetic produced water containing single or multiple metal ion(s) is feasible (Appendix A). Although thermodynamic modelling offers some understanding about the chemistry of synthetic produced water and possible electrode reactions at different pH values, it could not identify the electrode potentials at which hydrogen, oxygen or chlorine evolution will occur and the effect of different electrode materials on metal deposition. In this chapter the main experimental outcomes of the cathodic processes of heavy metal (lead, nickel, iron and copper) removal from synthetic produced water via electrodeposition are reported. Cyclic voltammetry (CV) and electrodeposition of individual and multiple heavy metal ions in synthetic produced water at different scan rates, pH and concentrations are presented in section 4.2. Faradaic estimation of the amount of metals deposited from synthetic produced water based on the CV result obtained in section 4.2 at different conditions are presented and discussed in section 4.3. In section 4.4, the growth and structure of electrodeposits or recovered heavy metals are characterised and analysed. A mechanism of electrodeposition of heavy metals from synthetic produced water containing multiple heavy metals is proposed based on these results. It should be noted that a series of knowledge gaps in the recovery of heavy metals from chloride solutions currently present in literature have been identified during the course of this research work.

4.2. Cyclic Voltammetry of produced water

CV was the first experimental study carried out on the removal of heavy metals from produced water via electrodeposition. Cyclic voltammograms were obtained for all synthetic produced water types (PW I, PW II, PW III,

PW IV, PW V and PW VI (cf. Table 3.3) used in this study. The kinetics of metal reduction processes, the deposition potentials and the potentials at which gases could evolve on the electrode surface are examined in this section. Three types of disk electrodes were employed for this study to determine the effect of electrode materials on electrodeposition of heavy metals from produced water.

4.2.1.   Electrode reactions in basic simulated produced water

To understand the electrode reactions in the basic simulated produced water, i.e. PW I which contained no heavy metal ions and organic pollutants (cf. Table 3.3), CV was carried out on different electrodes at three pH values. Figure 4.1 presents the cyclic voltammograms (CVs) obtained in PW I at pH 4. (In the following text, CV refers to either cyclic voltammetry or cyclic voltammogram, depending on the context.) These CVs show quite different features, suggesting the strong influence of the electrode substrate.

The CVs of the platinum electrode in Figure 4.1 (b) exhibit a couple of reduction and re-oxidation peaks clearly around -0.34 V, which can be attributed to the reduction of proton to adsorbed hydrogen atoms and the re-oxidation of the adsorbed hydrogen atoms. The fast increasing currents at the positive and negative potential ends should have resulted from the oxidation of the Cl^- ion to the Cl_2 gas and the reduction of proton and adsorbed hydrogen atom to the H_2 gas, respectively (Pletcher and Sotiropoulos, 1994). A small and broad reduction peak appeared between 0 and 0.4 V, which was likely due to the reduction of adsorbed chlorine atoms that were formed during the discharge of the Cl^- ion at the positive potential end. On the glassy carbon electrode, the CVs became sluggish in shape, but still present noticeably three electrode reactions.
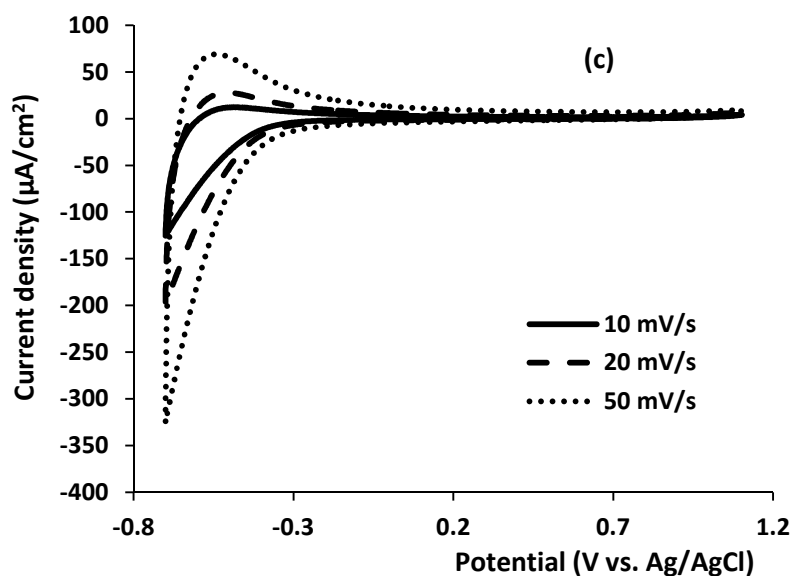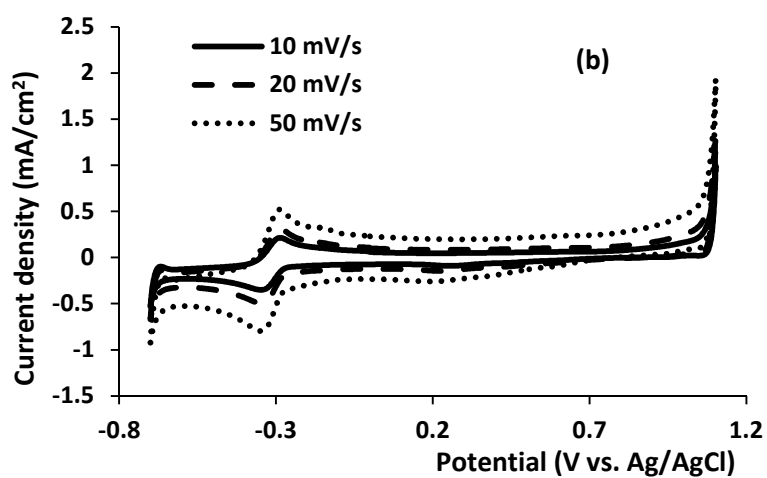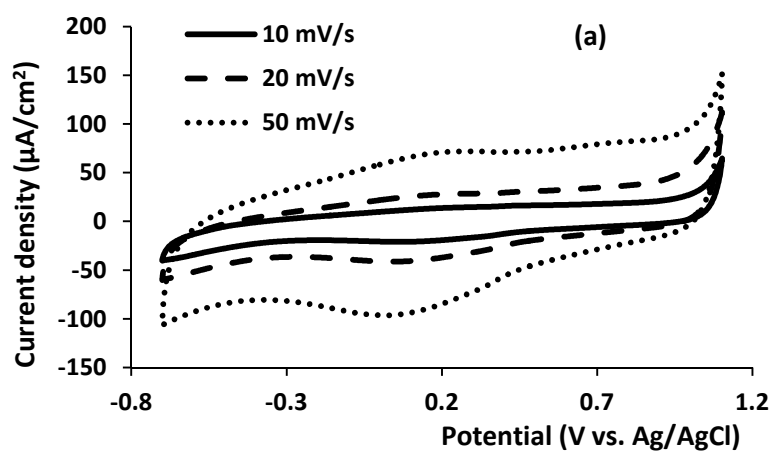
Figure 4.1: Cyclic voltammogram of PW I at pH 4 on (a) glassy carbon, (b) platinum and (c) titanium working electrodes

At the positive and negative potential ends, the current increases must have been due to the oxidation of the Cl$^-$ ion and the reduction of proton, respectively. The broad reduction and re-oxidation current peaks around 0.04 V should however have different origins. The reduction peak is more likely linked to the reduction of the adsorbed chlorine atoms, whilst the oxidation peak to the oxidation of the adsorbed hydrogen atoms.

In comparison with Figure 4.1b, the CVs of the glassy carbon electrode show comparable electrode reactions related with the Cl$^-$ ions, but very different features for the reduction of proton, which is known due to the high overpotential of proton reduction on carbon based electrodes.

The titanium electrode shows on the CVs in Figure 4.1c only the reduction of proton to adsorbed hydrogen atom, and the re-oxidation process at potentials near the negative potential end. Titanium metal has always a thin surface layer of TiO$_2$ which causes high overpotentials to both the oxidation of Cl$^-$ ions and water, and explains the absence of electrode reactions at positive potentials. Increasing the solution pH to 7 did not affect very much the CVs of the three electrodes (see Figures 4.2), except that the reduction currents decreased near the negative potential end, which is expected because of the decrease of proton activity in response to the pH increase. Note that the current scale of Figure 4.2c is much smaller than that in Figure 4.1c, which makes the small oxidation current at the positive potential end more pronounced.

When the pH of PW I was increased to 10, the significant change only occurred on the CVs of the platinum electrode as shown in Figure 4.3. The oxidation current plateau at 0.5 ~ 1.1 V can be associated with the oxidation of the OH$^-$ ion to adsorbed oxygen atom and the oxygen gas.
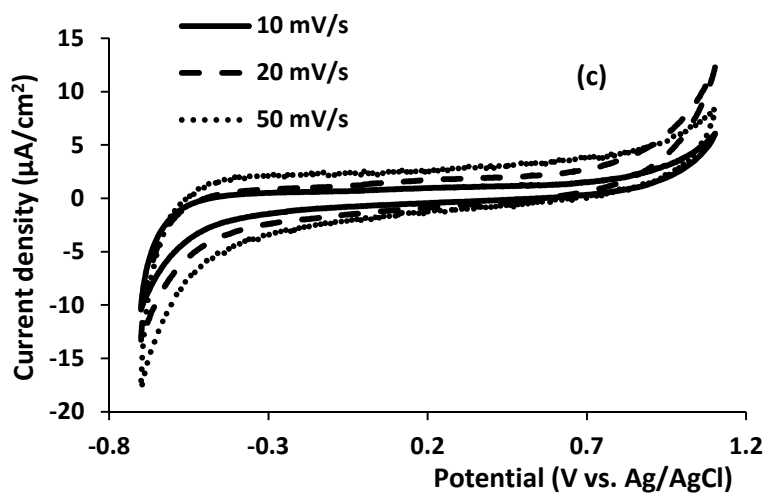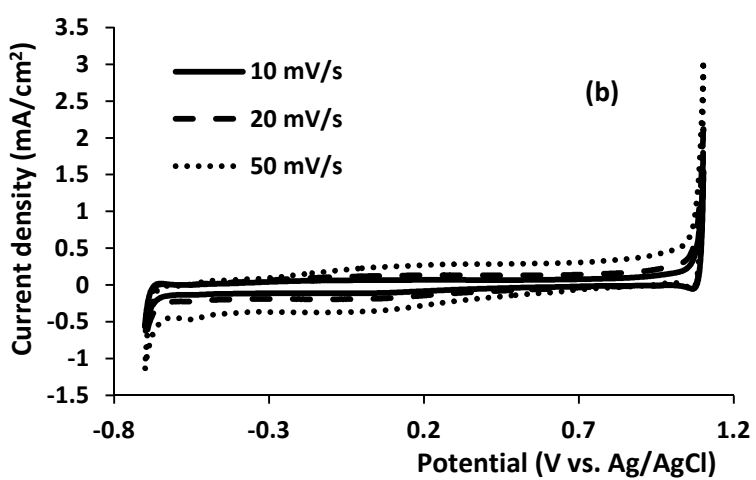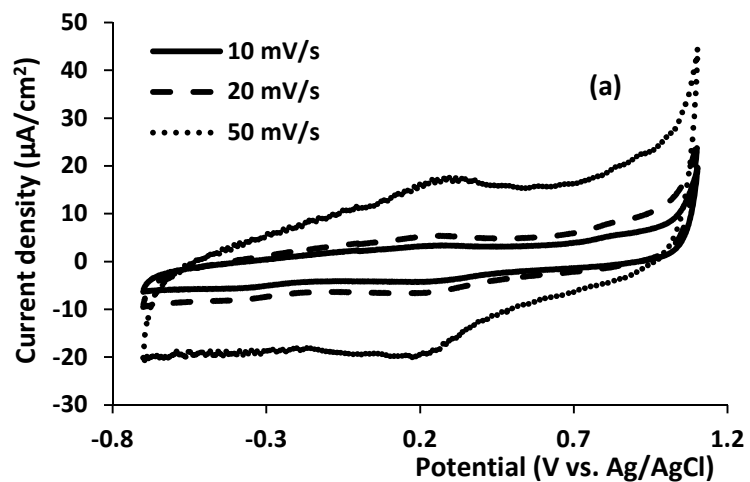
Figure 4.2: Cyclic voltammogram of PW I, at pH 7 on (a) glassy carbon, (b) platinum and (c) titanium working electrodes.
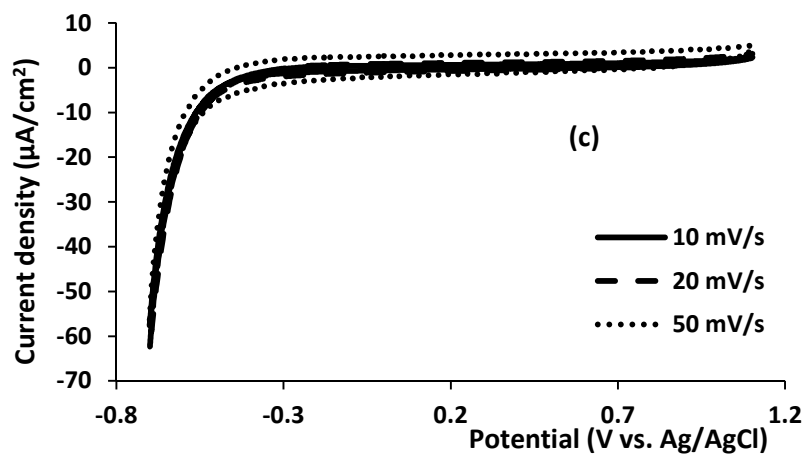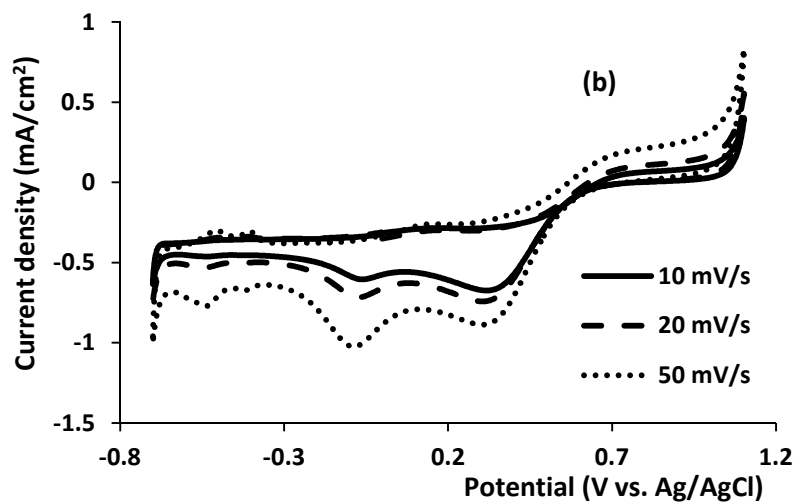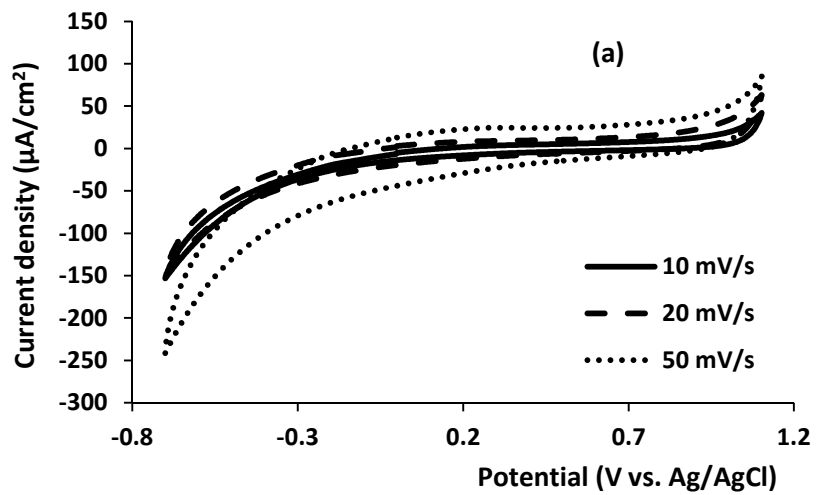
Figure 4.3: Cyclic voltammogram of PW I at pH 10 on (a) glassy carbon, (b) platinum and (c) titanium working electrodes

It was likely that the discharge of the OH$^-$ ion had suppressed that of the Cl$^-$ ion to some degree, because the oxidation current at the positive potential end was smaller than that at lower pH values as shown in Figure 4.1b and 4.2b. Interestingly, there are several reduction peaks on CVs in Figure 4.3b. The two reduction peaks at 0.38 V and -0.10 V may be due to the reduction of the adsorbed chlorine and oxygen atoms, respectively.

The smaller reduction peaks near the negative potential end were likely a result of the anodic discharge of the OH$^-$ ions which led to an increase of the proton activity near the electrode. It is worth mentioning that the reason why the CV changes only occurred on platinum is that platinum is a good catalyst for water (or OH$^-$) oxidation and proton reduction, whilst glassy carbon and titanium (with a thin surface layer of TiO$_2$) can retard these reactions.

The electrode reactions as discussed above in PW I are unwanted because they can cause a decrease in current efficiency. However, it can be noted in Figures 4.1 to 4.3 that the currents resulting from these reactions were fairly small (if compared with those on the CVs presented in the following sections), and hence should not be a great concern in practice.

4.2.2.   Cyclic voltammetry of copper in synthetic produced water

In this section, CV is used to investigate the kinetics of reduction reactions of the Cu^{2+} ion on platinum, glassy carbon and titanium electrodes in acidic, neutral and alkaline PW II (cf. Table 3.3). Two anodic and two cathodic peaks were observed on glassy carbon and platinum electrodes at pH 4 and pH 7 (Figures 4.4 - 4.5). This is consistent with the results obtained from thermodynamic studies in Appendix A.
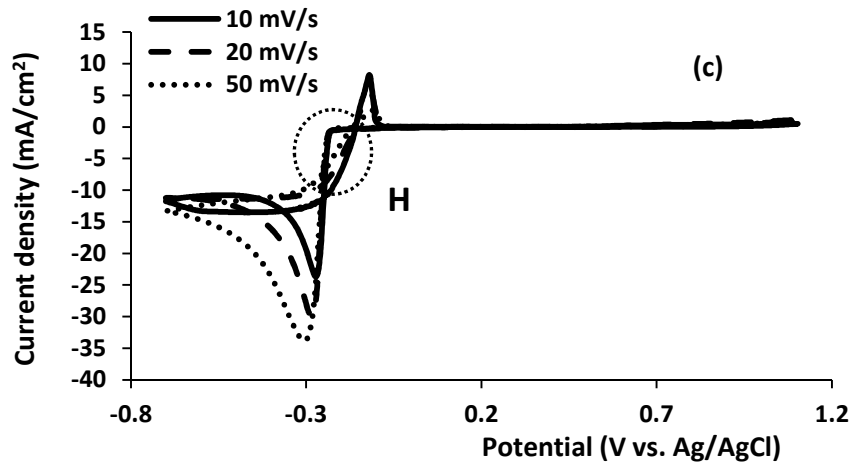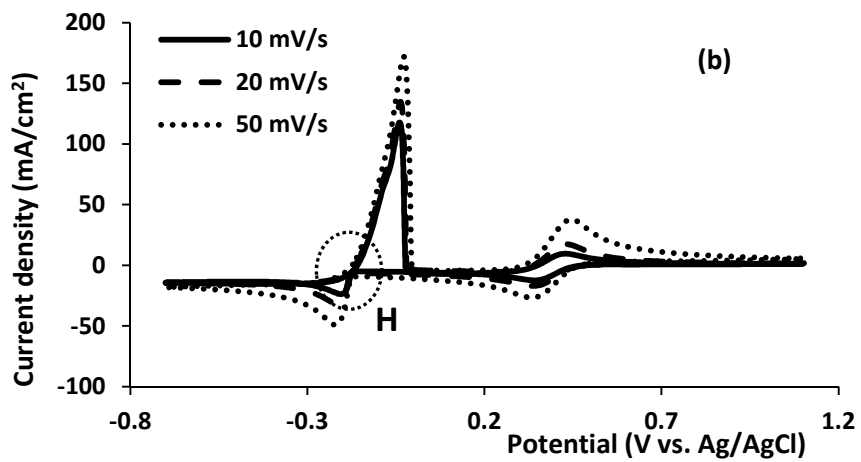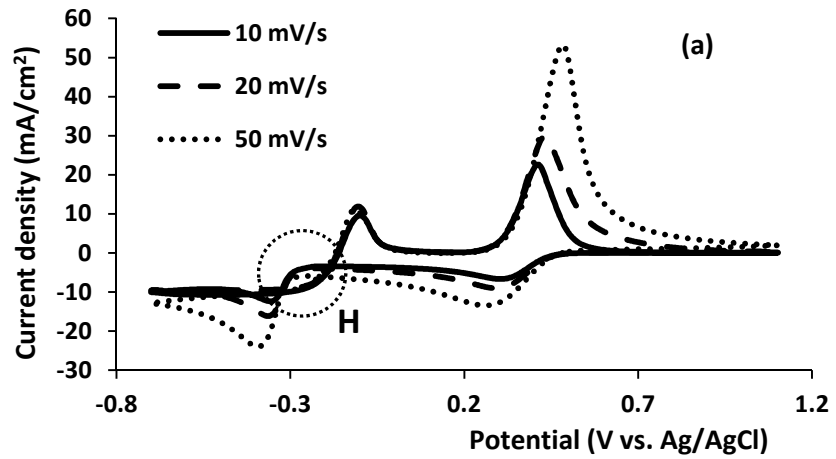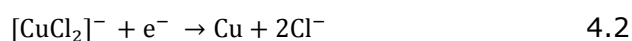
Figure 4.4: Cyclic voltammogram of PW II containing 0.02 mol/L Cu^{2+} at pH 4 on (a) glassy carbon, (b) platinum and (c) titanium working electrodes

The peaks formed at the negative potentials indicates that there was reduction of Cu(I) to Cu(0) and subsequently the re-oxidation of Cu(0) to Cu(I) as the direction of the sweep was reversed, while the peaks at the more positive potential were due to the oxidation of Cu(I) to Cu(II) and subsequent reduction of Cu(II) to Cu(I). There were no peaks observed when titanium electrode was made more positive at all pH values examined. This indicates that titanium electrode does not have affinity for oxidation of copper species. The appearance of a hysteresis loop (labelled H in Figure 4.4) is characteristic of a nucleation and growth process on the electrode surfaces (Alvarez and Salinas, 2010). This is an indication that $Cu_{(s)}$ was deposited on all three electrodes at pH 4, and on glassy carbon and titanium electrodes at pH 7. A slight shift of the cathodic peak potential was observed as the scan rate increased from 10 mV/s to 50 mV/s, which suggests that the reaction may be quasi-reversible, especially on the glassy carbon electrode at pH 7. The hysteresis loop did not appear on the platinum electrode at pH 7, and on all the three electrodes at pH 10. This change could be due to the conversion of free Cu^{2+} ion, at high pH values, to more stable complexes with the OH$^-$ and Cl$^-$ ions that could not be reduced to Cu metal in the applied potential range.

$$[CuCl_3]^{2-} + e^- \rightarrow Cu + 3Cl^- \qquad\qquad 4.1$$

$$[CuCl_2]^- + e^- \rightarrow Cu + 2Cl^- \qquad\qquad 4.2$$

Therefore based on thermodynamic and kinetic studies the mechanism of $Cu_{(s)}$ deposition on platinum, titanium and glassy carbon electrodes from PW II is shown in equations 4.1 and 4.2.
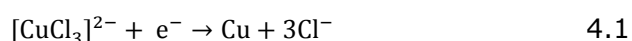
Figure 4.5: Cyclic voltammogram of PW II containing 0.02 mol/L Cu^{2+} at pH 7 on (a) glassy carbon, (b) platinum and (c) titanium working electrodes

Figure 4.6: Cyclic voltammogram of PW II containing 0.02 mol/L Cu²⁺ at pH 10 on (a) glassy carbon, (b) platinum and (c) titanium working electrodes

It is observed in Figures 4.4 - 4.5 that the current peak for Cu deposition is higher at pH 4 than at pH 7, and follows the order of platinum > titanium > glassy carbon at pH 4, and glassy carbon > titanium > platinum at pH 7. Therefore the amount of Cu deposit from synthetic produced water depends on the pH and the type of electrode material used. However, it is difficult to show a particular electrode pattern for Cu deposition at pH 10 (Figure 4.6). This shows that copper recovery/removal from synthetic produced water is difficult at pH 10 as explained earlier in section 4.2.1.

4.2.3. Cyclic voltammetry of lead in synthetic produced water

An anodic peak and a cathodic peak of approximately equal heights were observed on the CV of $Pb_{(s)}$ deposition from PW III as shown in Figures 4.7 and 4.8. The cathodic peak represents $Pb_{(s)}$ deposition while the anodic peak represents its dissolution. The peak current ratio (i_{pa}/i_{pc}) = 1 at all scan rates suggests that $Pb_{(s)}$ deposition is a reversible process. The peak current also increased with increasing scan rate which suggests that the reversible process is controlled by a surface step. Since only two peaks were obtained during the CV scan, this suggests that the mechanism of $Pb_{(s)}$ deposition from synthetic produced water follows equation 4.3 which agrees with the thermodynamic studies carried out (cf. Appendix A.3).

$$[PbCl_4]^{2-} + 2e^- \rightarrow Pb + 4Cl^- \qquad\qquad 4.3$$
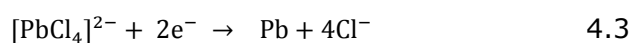
The $Pb_{(s)}$ deposition potential from synthetic produced water was -0.54 V vs. Ag/AgCl. However it is not clear what was happening on the titanium electrode at pH 7 (Figure 4.7c). The CV scan was repeated thrice and similar results were obtained each time. The two cathodic peaks and two anodic peaks observed are difficult to explain and are similar to results reported for the deposition of $Pb_{(s)}$ from chloride-based ionic liquids onto platinum electrodes (Golgovici, 2011). The cathodic peaks may correspond

to Pb$_{(s)}$ and PbOHCl$_{(s)}$ deposition based on thermodynamic calculations, and the anodic peaks to their re-oxidation.
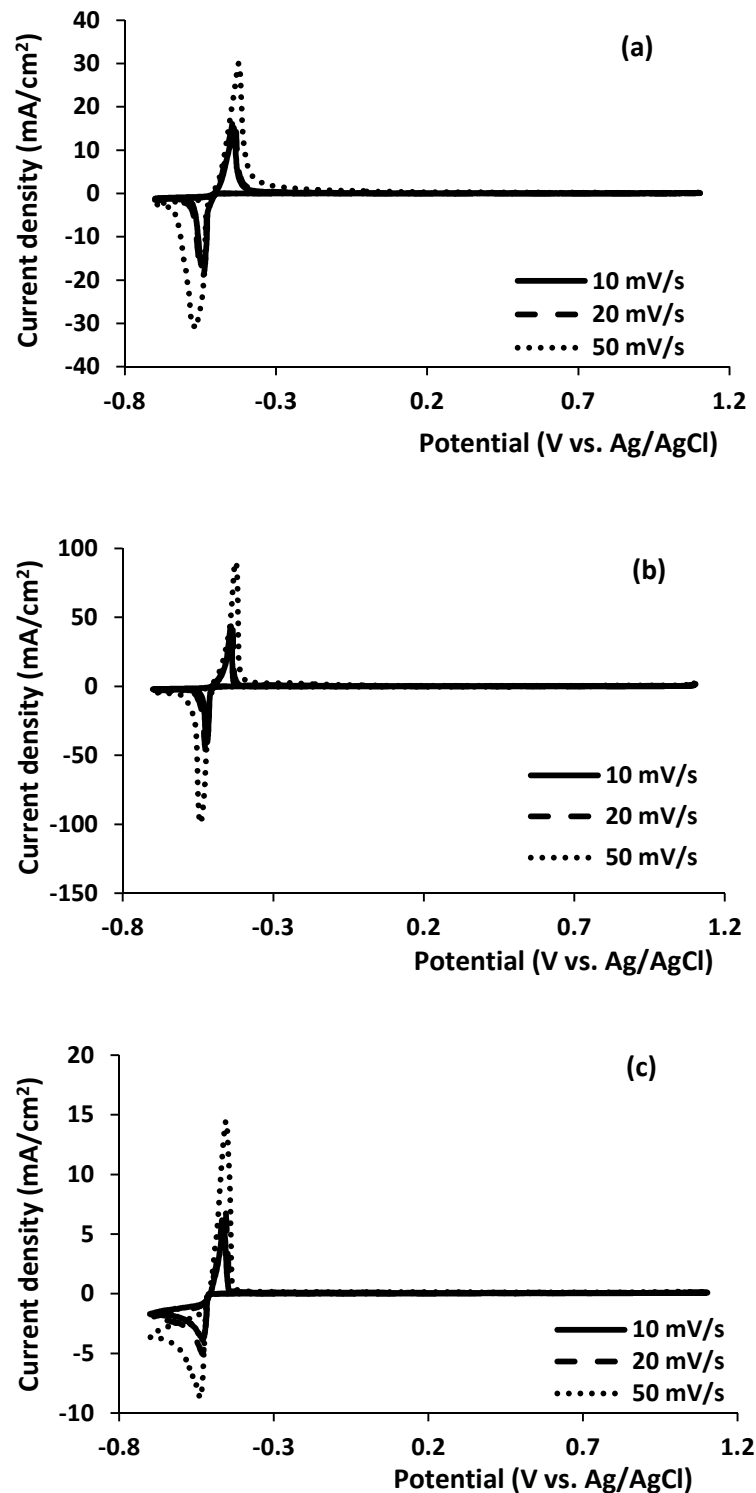
Figure 4.7: Cyclic voltammogram of PW III containing 0.02 mol/L Pb^{2+} at pH 4 on (a) glassy carbon, (b) platinum and (c) titanium working electrodes
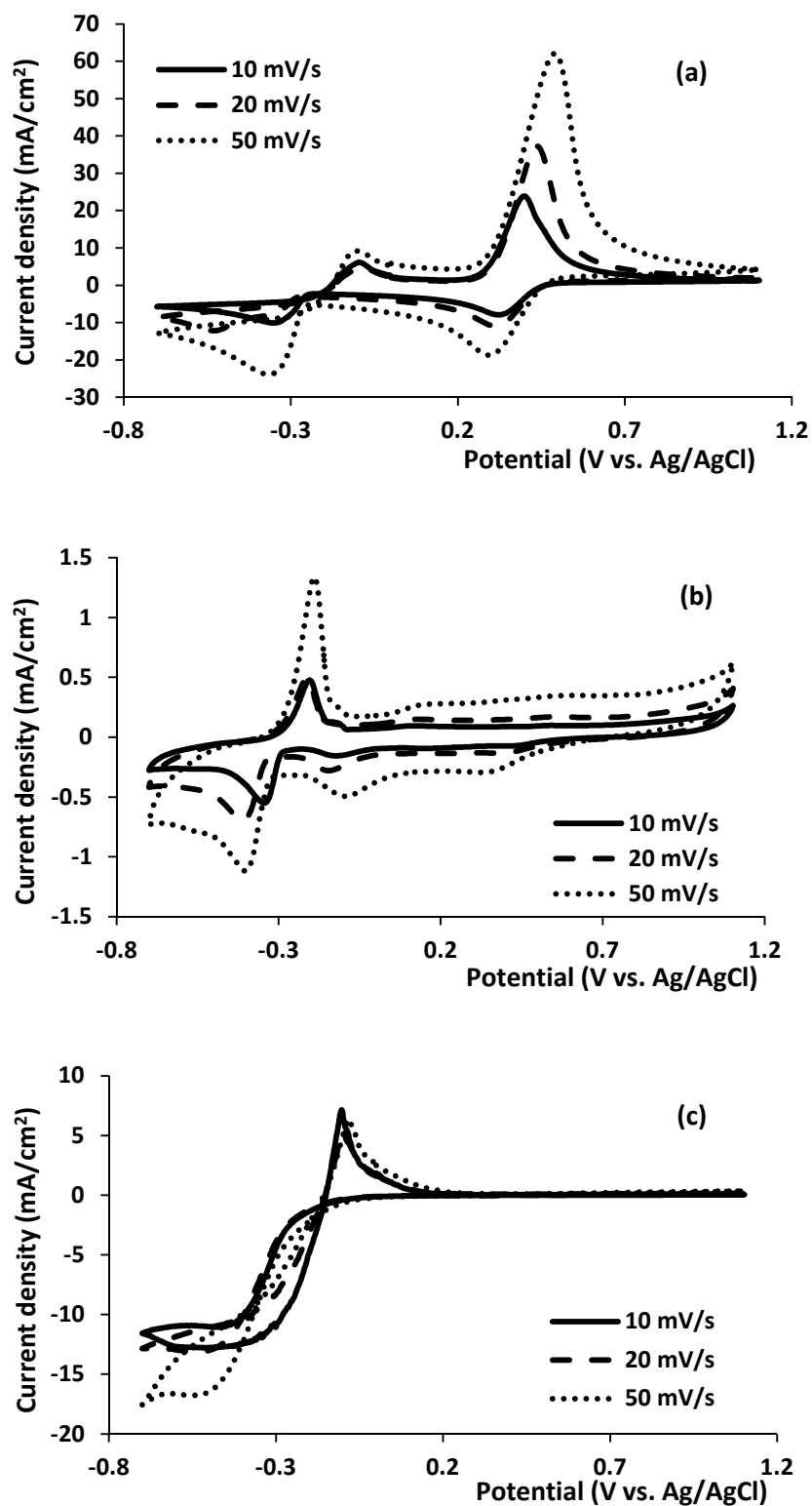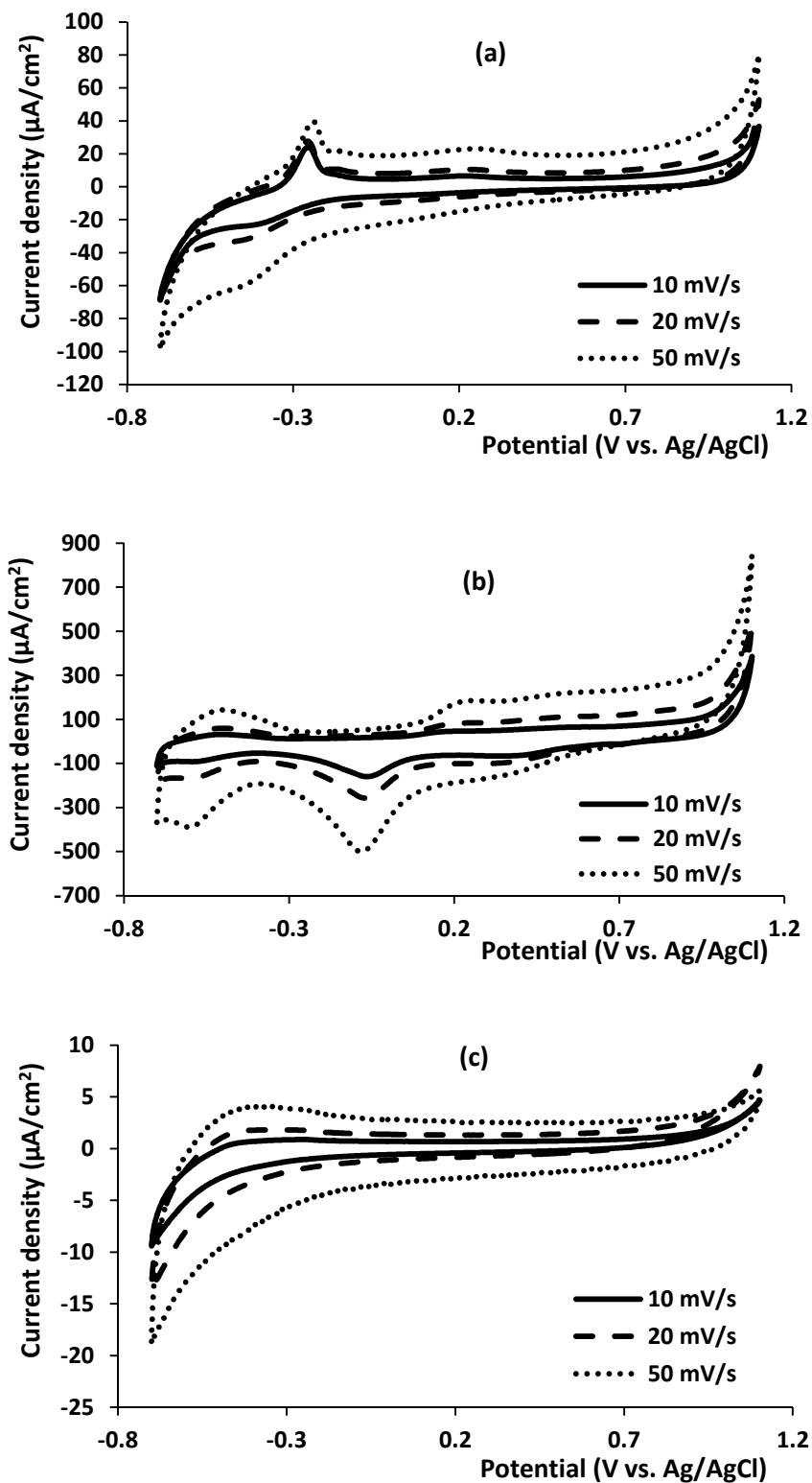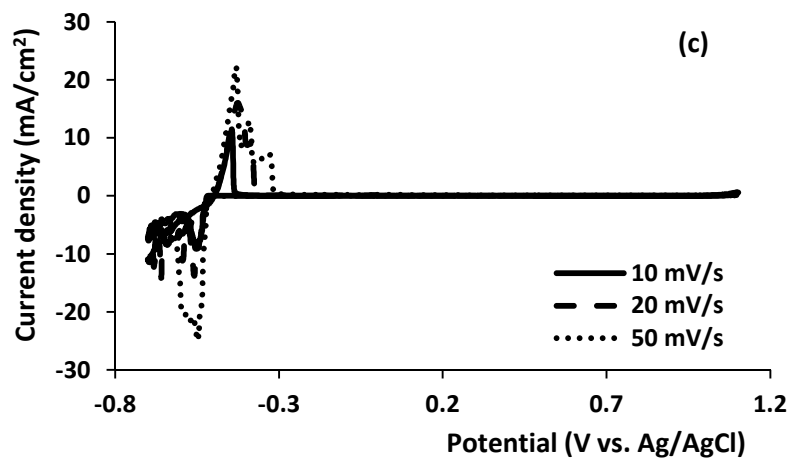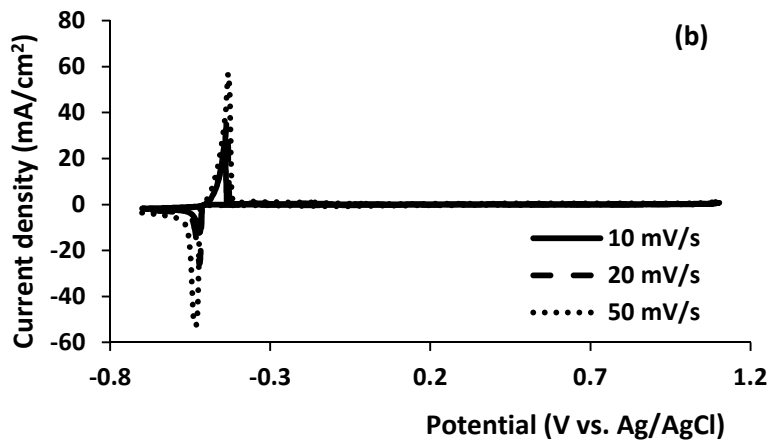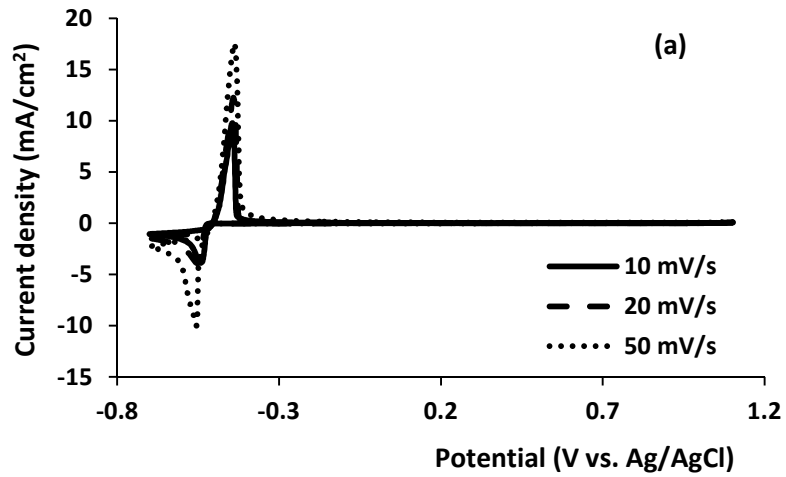
Figure 4.8: Cyclic voltammogram of PW III containing 0.02 mol/L Pb $^{2+}$ at pH 7 on (a) glassy carbon, (b) platinum and (c) titanium working electrodes
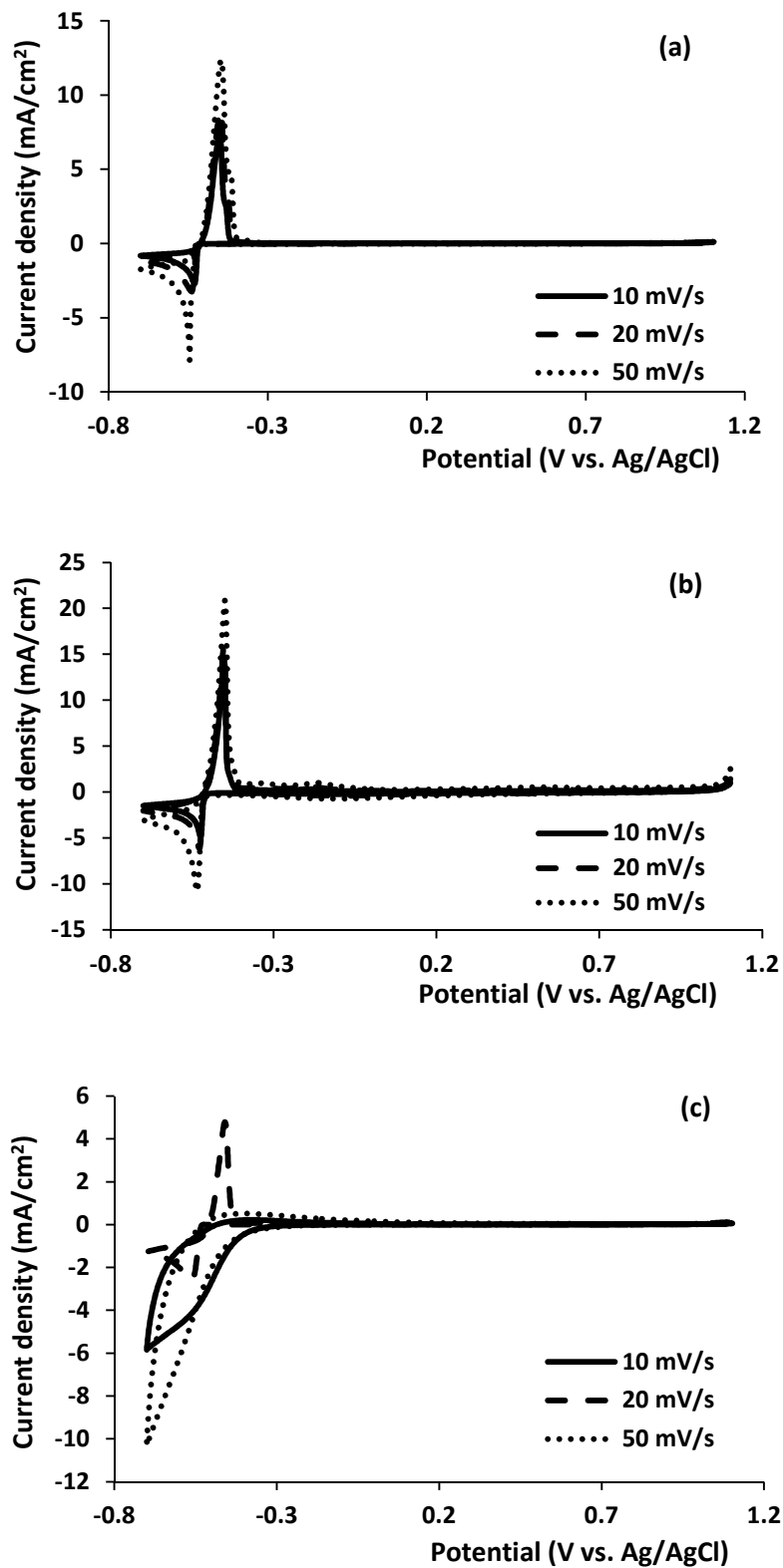
Figure 4.9: Cyclic voltammogram of PW III containing 0.02 mol/L Pb^{2+} at pH 10 on (a) glassy carbon, (b) platinum and (c) titanium working electrodes

According to Faraday's law the amount of Pb that can be deposited on each electrode is proportional to the current density of the cathodic peak, and current density of lead deposition increases in the order: platinum > glassy carbon > titanium. A comparison of the CVs in Figures 4.7 to 4.9 reveals that the amount of Pb that can be deposited from synthetic produced water increases with decreasing pH. This cannot be explained by equation 4.3 since the reaction is independent of pH. Therefore this indicates that the increase in the amount of Pb deposited from synthetic produced water is due to the formation of more stable complexes between the Pb^{4+} ions and the OH^- and Cl^- ions.

4.2.4. Cyclic voltammetry of nickel in synthetic produced water

Figures 4.10 and 4.11 show that it is difficult to deposit Ni metal from PW IV (cf. Table 3.3). The onset of a new reduction peak at pH 4 occurred at -0.21 V vs. Ag/AgCl and -0.31 V vs. Ag/AgCl on glassy carbon and platinum electrodes respectively. There was no new reduction occurring on the titanium electrode as shown in Figure 4.10c.

Further, there was no anodic peak observed on the glassy carbon electrode which suggests that reduction was (or was followed by) an irreversible process. It is also evident from CV results on the platinum electrode that as the sweep rate was increased from 10 mV/s to 50 mV/s, the anodic and cathodic peaks were slightly shifted to the more negative and more positive potentials respectively. This implies that the reduction is a kinetically slow process (Srinivasan and Ramesh Bapu, 2013). Equations 4.4 – 4.10 suggests the mechanism of the reduction in PW IV based on CV and thermodynamic studies. Nickel ions can exist as $NiCl_2$ and $[NiCl]^+$ in synthetic produced water (equations 4.4 and 4.8).
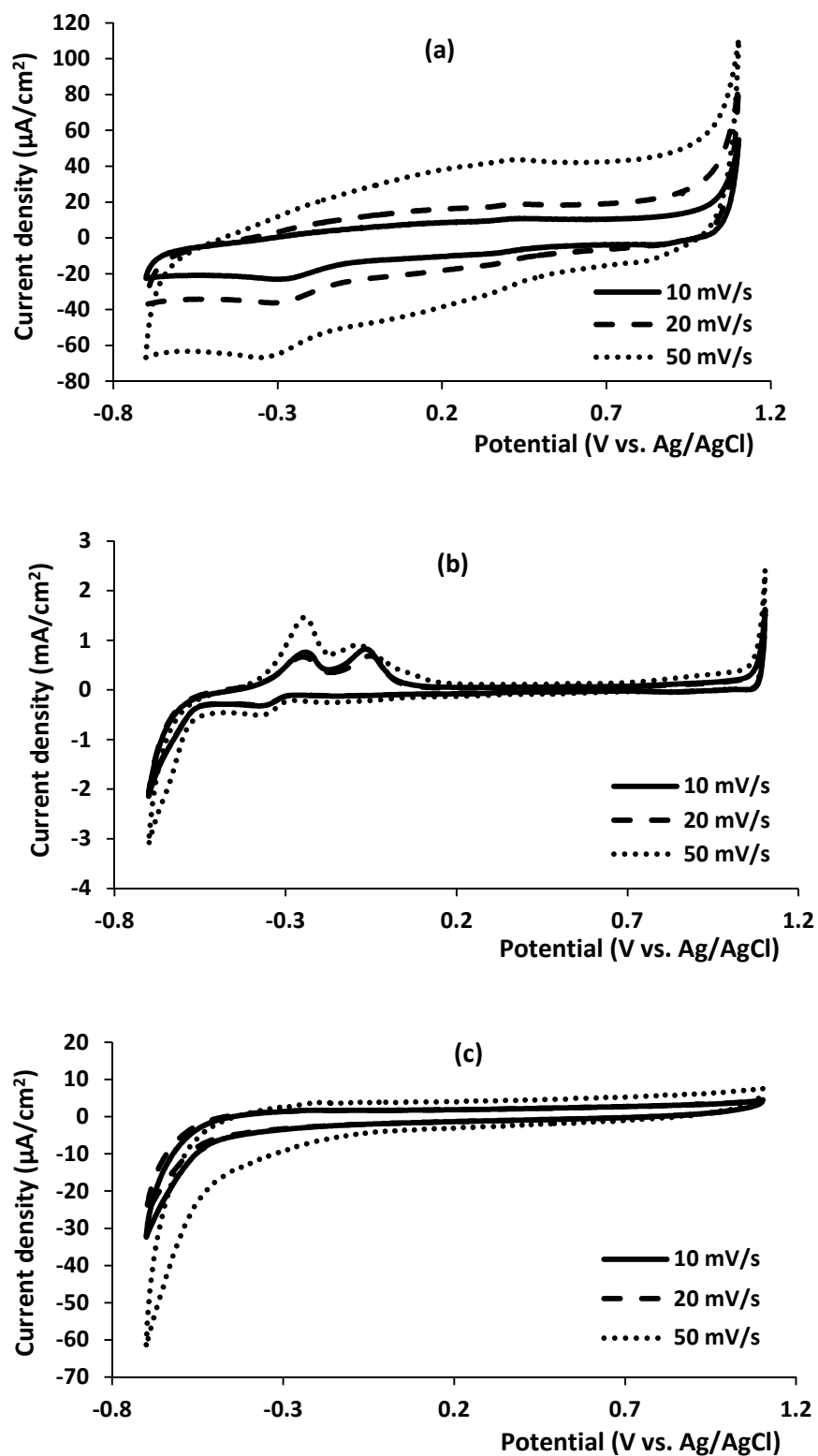
Figure 4.10: Cyclic voltammogram of PW IV containing 0.02 mol/L Ni^{2+} at pH 4 on (a) glassy carbon, (b) platinum and (c) titanium working electrodes

However two anodic peaks at -0.09 V vs. Ag/AgCl and -0.25 V vs. Ag/AgCl were observed on the platinum electrode at pH 4. This suggests that the reduction on the platinum electrode follows a two stage process i.e. the adsorption of Ni(OH)$_{ads}$ onto the electrode surface and subsequently the growth of Ni$_{(s)}$ (equations 4.9 and 4.10). Although the step in equation 4.8 is not visible on the CV it is believed to be the predominant step for the initiation of nickel formation on electrode surface (Srinivasan and Ramesh Bapu, 2013). The anodic peak at -0.25 V vs. Ag/AgCl disappeared from the CV at pH 7 (Figure 4.11 b) which suggests that Ni(OH)$_{2(s)}$ rather than Ni$_{(s)}$ was deposited on the platinum electrode (equation 4.6 and 4.8).

$$NiCl_2 \rightarrow Ni^{2+} + 2Cl^- \qquad\qquad 4.4$$

$$[NiCl]^+ \rightarrow Ni^{2+} + Cl^- \qquad\qquad 4.5$$

$$Ni^{2+} + H_2O \rightleftharpoons [Ni(OH)_{(aq)}]^+ + H^+ \qquad\qquad 4.6$$

$$[Ni(OH)_{(aq)}]^+ + 2e^- + H_2O \rightarrow Ni(OH)_2 + H^+ \qquad\qquad 4.7$$

$$[Ni(OH)_{(aq)}]^+ \rightleftharpoons [Ni(OH)_{(ads)}]^+ \qquad\qquad 4.8$$

$$[Ni(OH)_{(ads)}]^+ + e^- \rightarrow Ni(OH)_{(ads)} \qquad\qquad 4.9$$

$$Ni(OH)_{(ads)} + Ni^{2+} + 2e^- \rightarrow Ni(OH)_{(ads)} + Ni \qquad\qquad 4.10$$
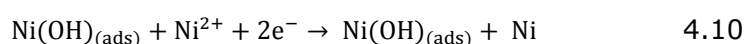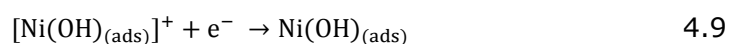
It is also noted that there was no conspicuous cathodic peak observed at pH 7 but there is an anodic peak at 0.09 V vs. Ag/AgCl on the platinum electrode which is similar to what has been reported in literature as nickel re-oxidation peak (Gomez et al., 1992, Vaskevich et al., 2005).

Figure 4.11: Cyclic voltammogram of PW IV containing 0.02 mol/L Ni^{2+} at pH 7 on (a) glassy carbon, (b) platinum and (c) titanium working electrodes

Figure 4.12: Cyclic voltammogram of PW IV containing 0.02 mol L-1 Ni^{2+} at pH 10 on (a) glassy carbon, (b) platinum and (c) titanium working electrodes

This suggests that the amount of nickel compound that can be removed from synthetic produced water at pH 7 is very small which is confirmed by the very low current density ($\mu A/cm^2$) at this pH. There was no nickel deposition on titanium electrode because there are no observed cathodic and anodic peaks during CV (Figures 4.10 c, 4.11 c and 4.12 c).

This may be one of the reasons why titanium is not usually used for commercial nickel electroplating apart from the fact that titanium usually dissolves in the electroplating bath (Dennis and Eugene, 1993). The evolution of hydrogen gas on titanium electrode might also be responsible for its inability to remove nickel from produced water via electrodeposition because Ni acts as a catalyst for hydrogen evolution (Papandrew and Zawodzinski Jr, 2014, Pshenichnikov, 1982, Selembo et al., 2010), thereby favouring hydrogen gas to be evolved on the electrode surface. Hence the quantity of nickel that can be deposited from PW IV is very small. For instance in Figure 4.10 (a) the current density of the reduction peak corresponds to 20 $\mu A/cm^2$ and to 100 $\mu A/cm^2$ in Figure 4.10 (b). Therefore electrodeposition of Ni from synthetic produced water would be more difficult compared to Cu and Pb.

4.2.5.   Cyclic voltammetry of iron in synthetic produced water

Four peaks were observed on the CV of Fe deposition from PW V, two cathodic peaks and two anodic peaks as shown in Figures 4.13 – 4.15. The peaks that occur at the positive potential range correspond to the oxidation-reduction of Fe(II) to Fe(III) while the ones at the negative potentials correspond to the oxidation-reduction of $Fe_{(s)}$ to Fe(II). Thermodynamic calculations indicated that Fe would exist in produced water as Fe^{2+} or $FeCl^+$ (cf. Appendix A.5).
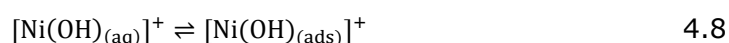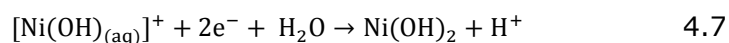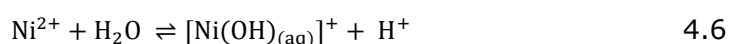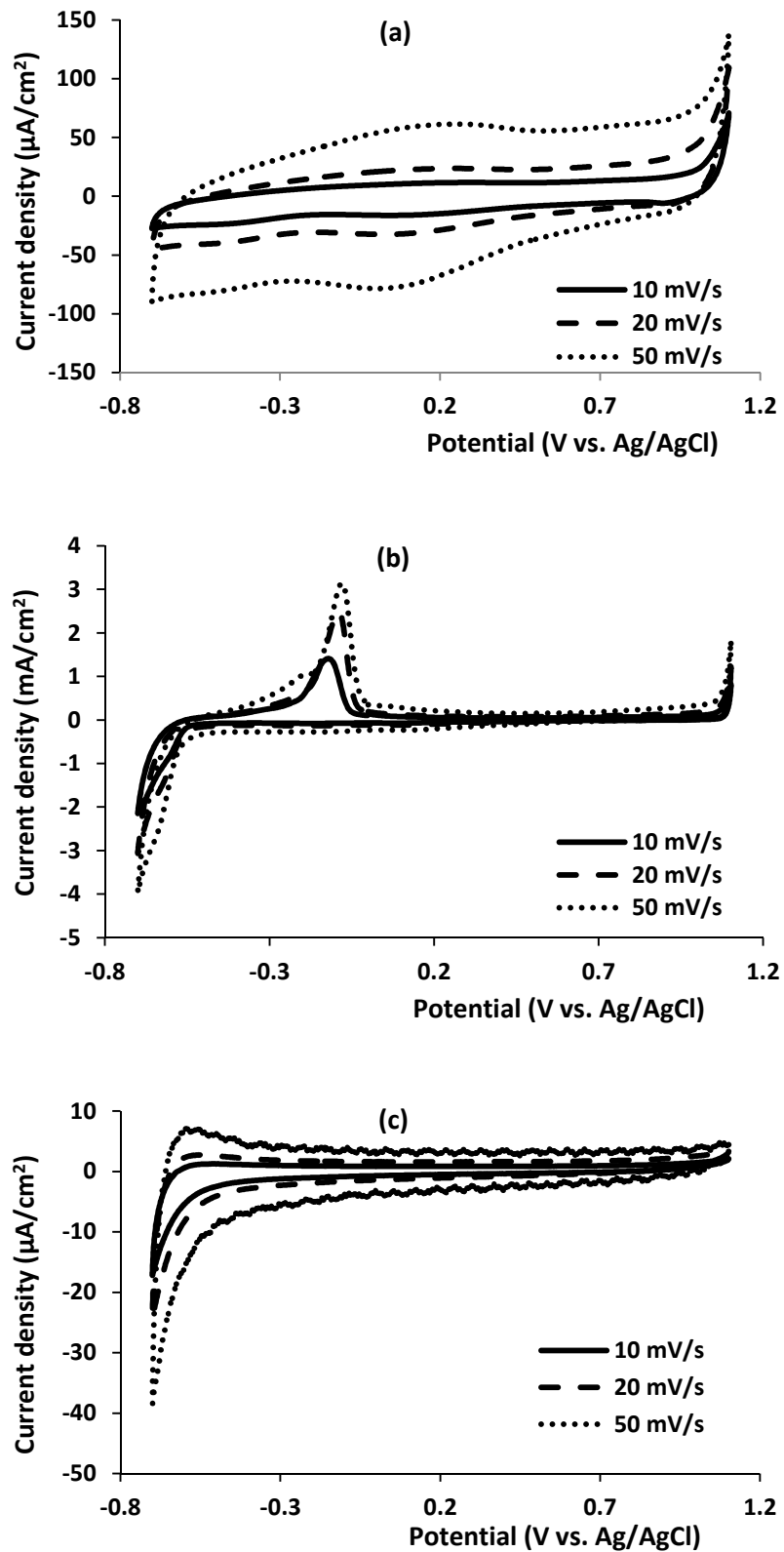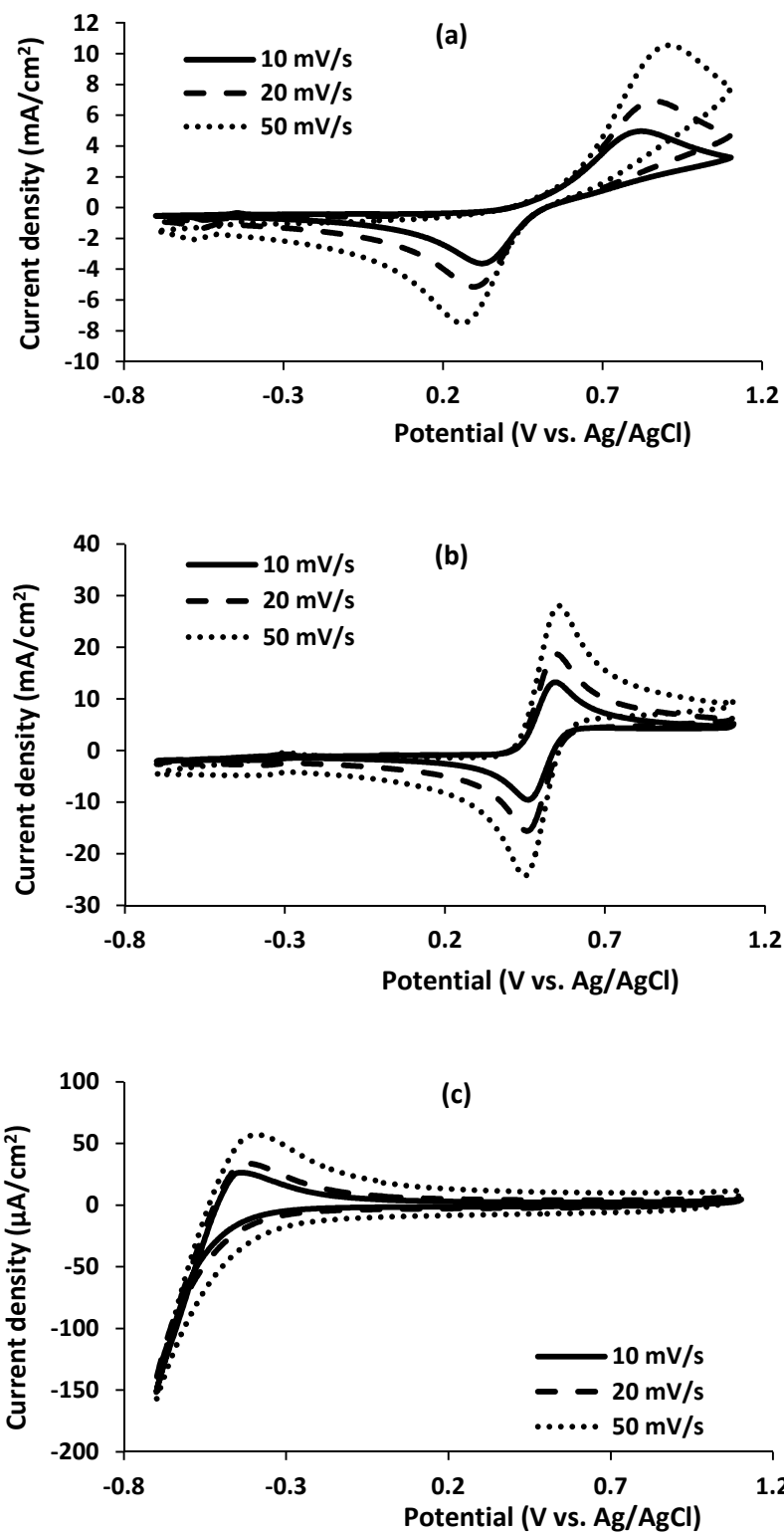
Figure 4.13: Cyclic voltammogram of PW V containing 0.02 mol L^{-1} Fe^{2+} at pH 4 on (a) glassy carbon, (b) platinum and (c) titanium working electrodes
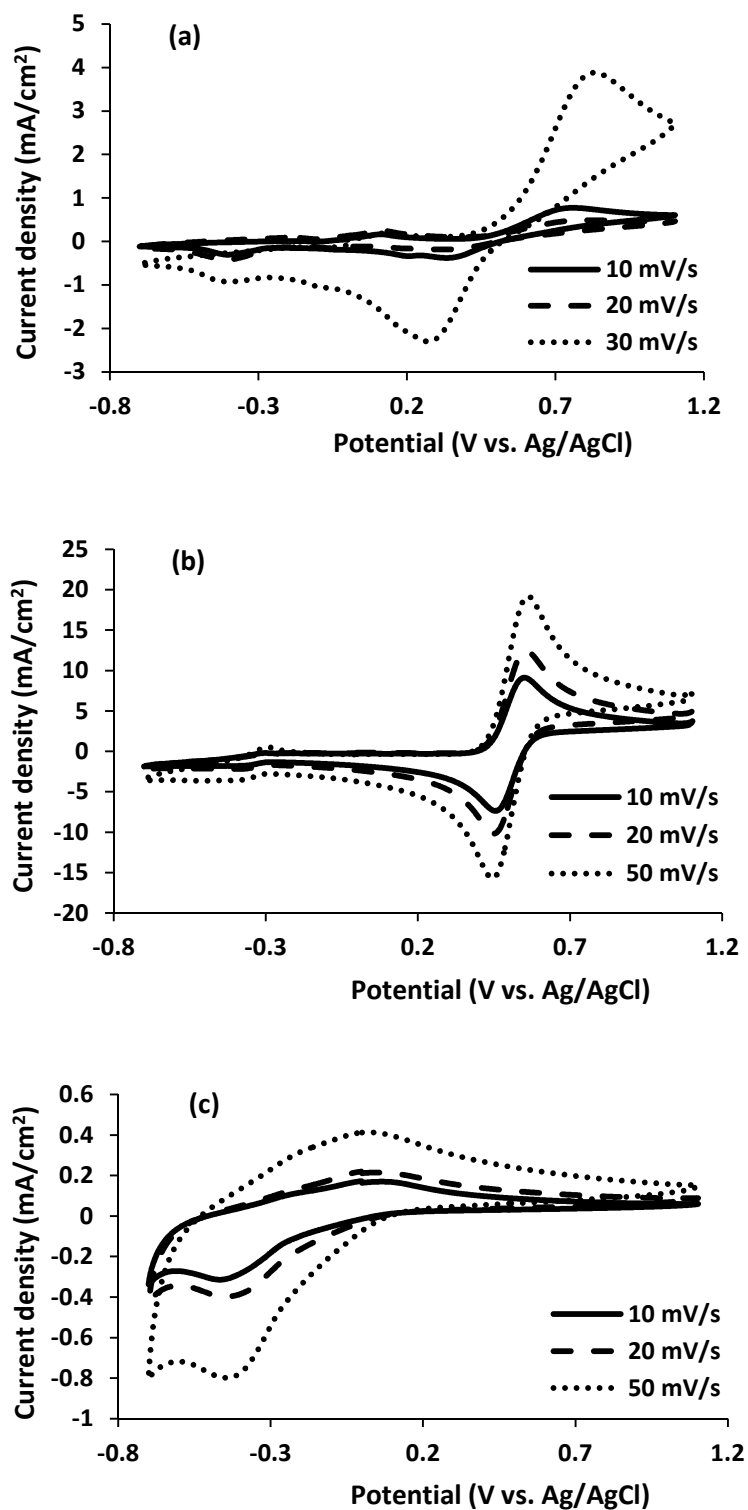
Figure 4.14: Cyclic voltammogram of PW V containing 0.02 mol L^{-1} Fe^{2+} at pH 7 on (a) glassy carbon, (b) platinum and (c) titanium working electrodes
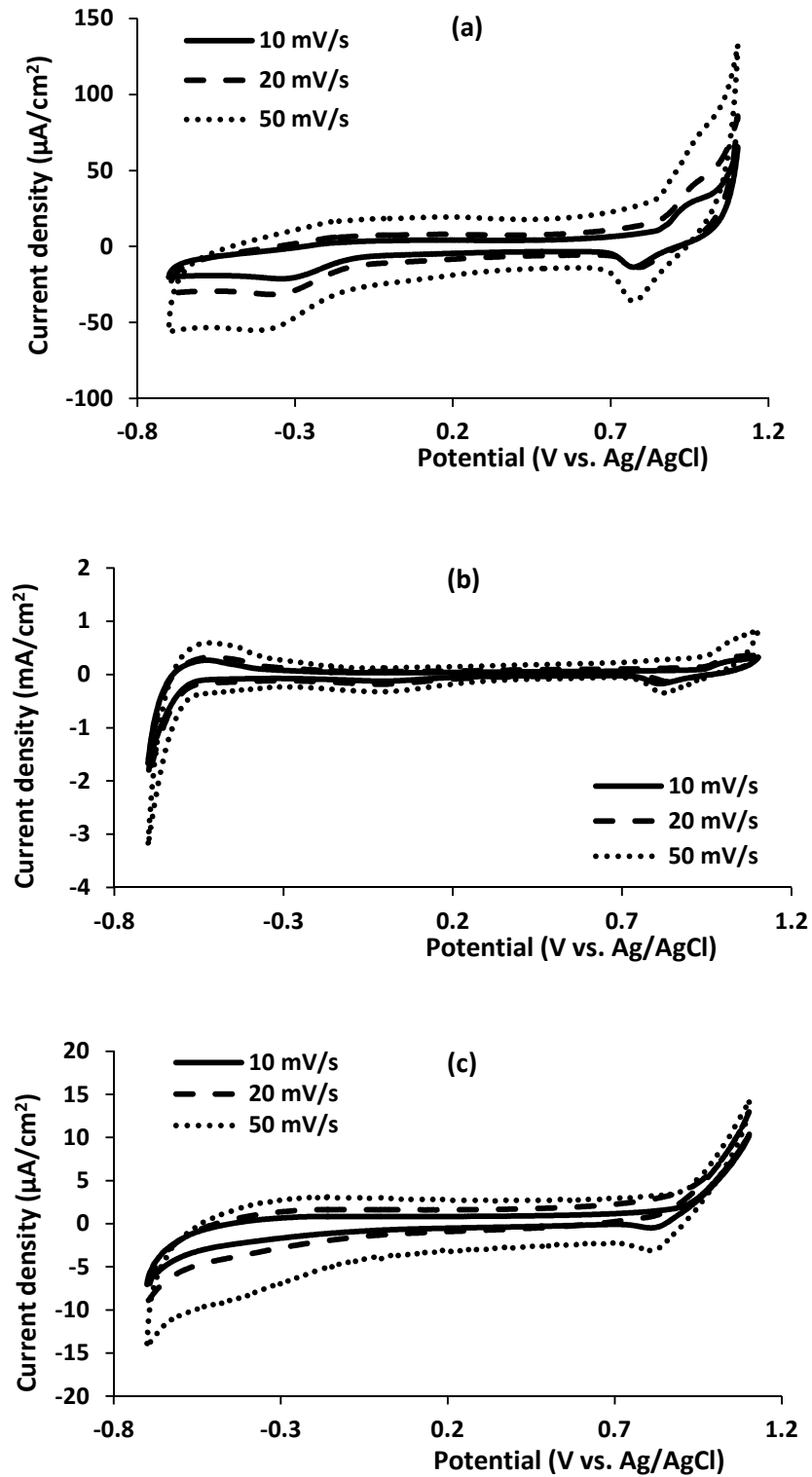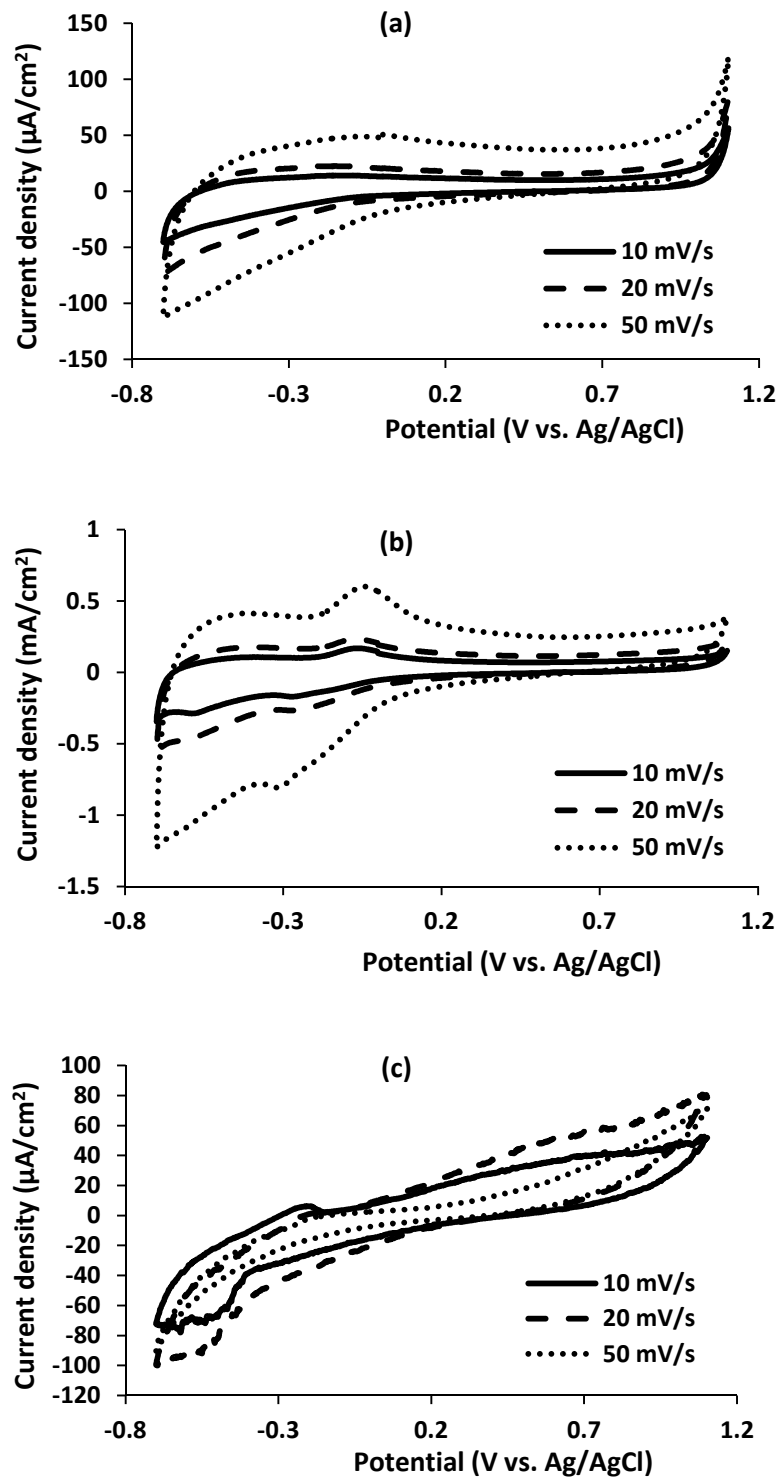
Figure 4.15: Cyclic voltammogram of PW V containing 0.02 mol L^{-1} Fe2$^+$ at pH 10 on (a) glassy carbon, (b) platinum and (c) titanium working electrodes

CV results therefore suggests that its mechanism of reduction in produced water at pH 4 and 7 can be illustrated by equations 4.11 and 4.12

$$Fe^{2+} + 2e^- \rightarrow Fe \qquad\qquad 4.11$$

$$[FeCl]^{\mp} + 2e^- \rightarrow Fe + Cl^- \qquad\qquad 4.12$$

The current density of the reduction peaks of the Fe (II) species are less than 0.5 mA/cm^2 which suggests that only a very small quantity of Fe would be deposited from the produced water. Therefore the deposition of Fe$_{(s)}$ from PW V is difficult. Cathodic peaks observed on glassy carbon and platinum electrodes at pH 10 only occurred when the scan rate was lowered to 20 mV/s. This suggests that the deposit at pH 10 may be Fe$_3$O$_{4(s)}$ or Fe$_{(s)}$ or other Fe compounds. Fe$_{(s)}$ deposition on the electrodes follows an irreversible process because the re-oxidation peak is mostly not identifiable on the cyclic voltammogram and where it is seen it is not of the same value as the reduction peak.

4.2.6. CV of multiple heavy metal ions in synthetic produced water

The cathodic peaks of PW VI (cf. Table 3.3) on glassy carbon (Figure 4.16 a) correspond to the deposition of Cu and Pb. The cathodic peaks at - 0.29 V, - 0.44 V and - 0.54 V vs. Ag/AgCl in Figure 4.16 (b) correspond Cu, Fe and Pb deposition on platinum electrode respectively. The anodic peaks at - 0.12 V, -0.18 V, - 0.44 V and - 0.47 V vs. Ag/AgCl correspond to Cu, Ni, Pb and Fe dissolution. It should be noted that although no deposition peak was observed for Ni, its dissolution peak indicates that Ni was removed from produced water. It is possible that its deposition peak overlapped with Fe peak or may be only a small quantity of Ni was removed under this condition.
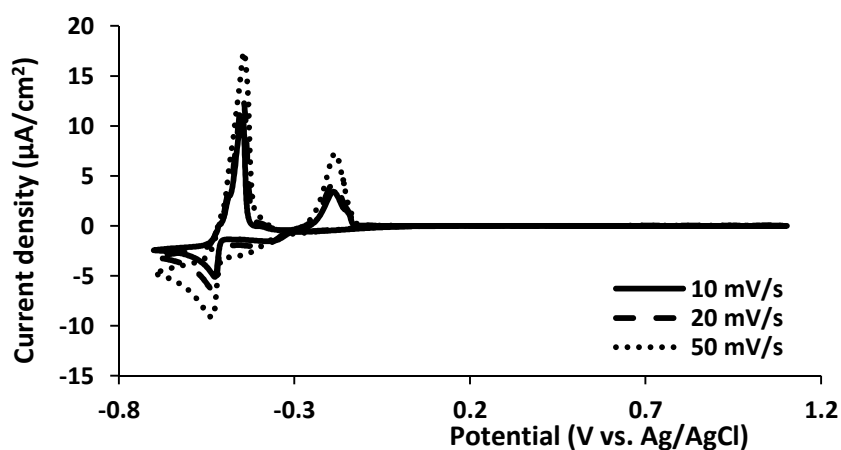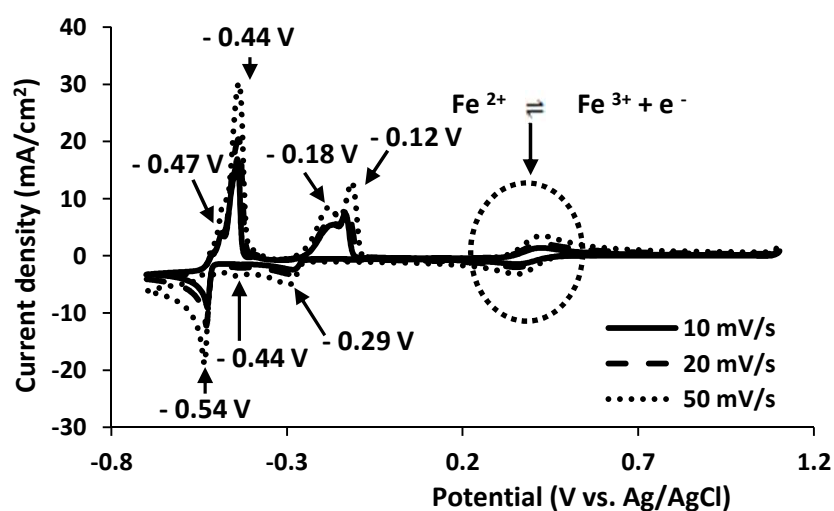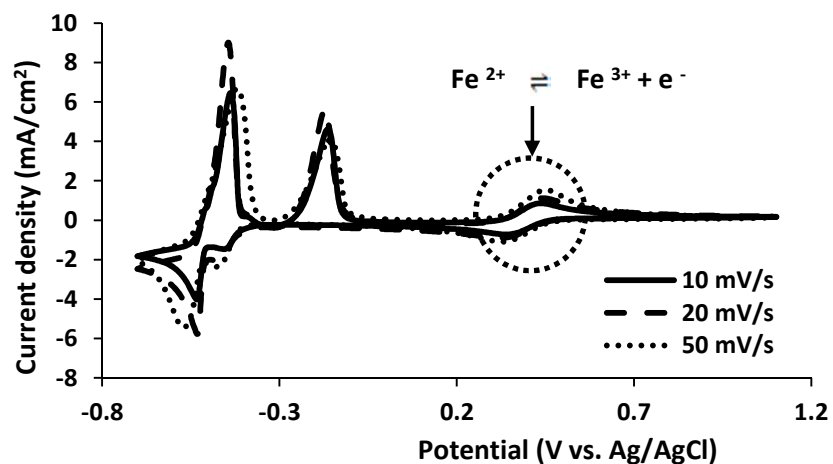
Figure 4.16: Cyclic voltammogram of PW VI containing 0.02 mol L^{-1} Cu^{2+}, 0.02 mol L^{-1} Pb^{2+} 0.02 mol L^{-1} Ni^{2+} 0.02 mol L^{-1} Fe^{2+} at pH 2 on (a) glassy carbon, (b) platinum and (c) titanium working electrodes
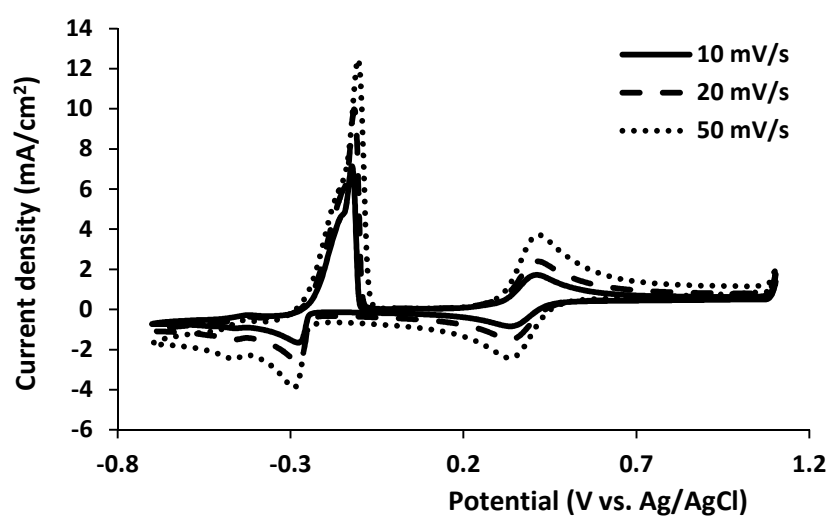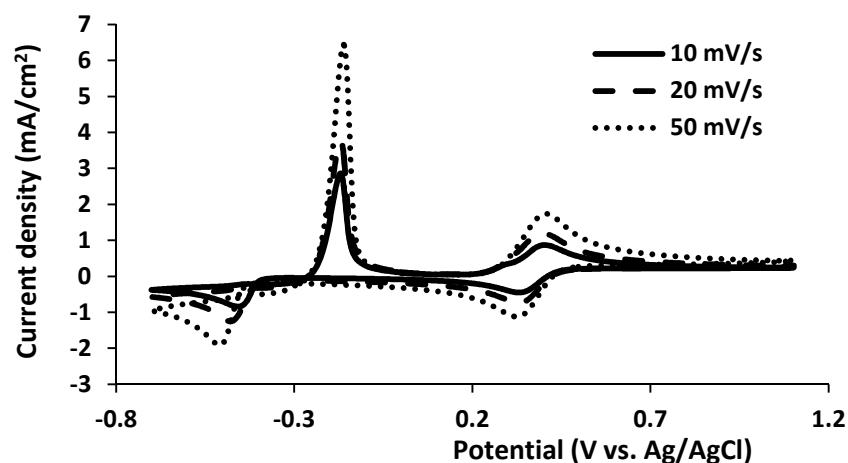
Figure 4.17: Cyclic voltammogram of PW VI containing 0.02 mol L^{-1} Cu^{2+}, 0.02 mol L^{-1} Pb^{2+} 0.02 mol L^{-1} Ni^{2+} 0.02 mol L^{-1} Fe^{2+} at pH 7 on (a) glassy carbon and (b) platinum working electrodes

Only Cu and Pb are deposited on platinum electrode at -0.29 V and -0.46 V vs. Ag/AgCl respectively from PW VI at pH 7 (Figure 4.17b). However on glassy carbon electrode (Figure 4.17a) three reduction peaks are seen and an increase in scan rate shifts the reduction peaks to a more negative potential with higher current contribution. This implies that electrodeposition of metals from PW VI on glassy carbon electrode at pH 7 is irreversible (Zhang et al., 2009b).
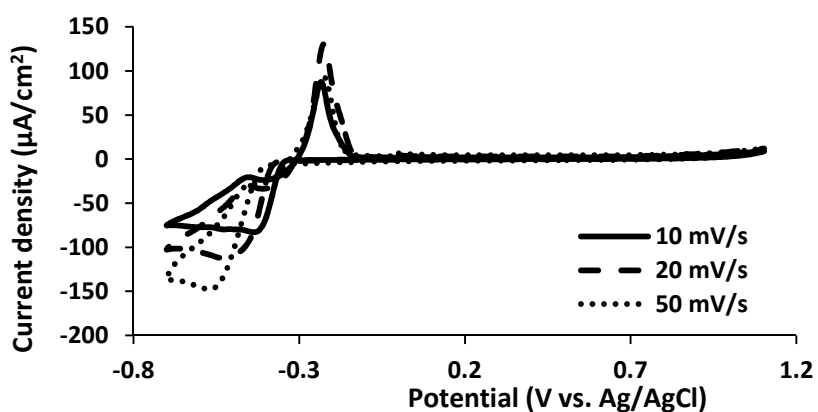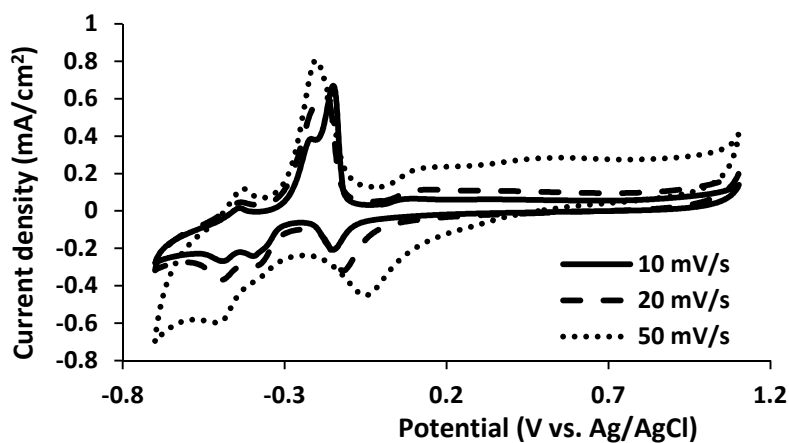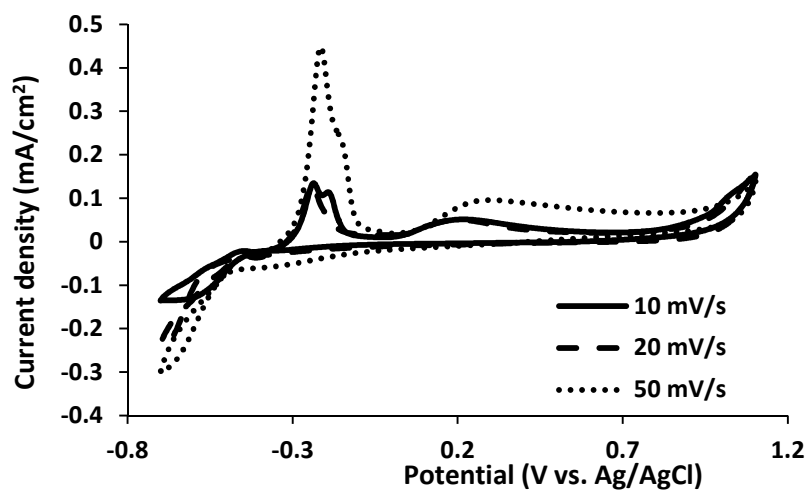
Figure 4.18: Cyclic voltammogram of PW VI containing 0.02 mol L^{-1} Cu^{2+}, 0.02 mol L^{-1} Pb^{2+} 0.02 mol L^{-1} Ni^{2+} 0.02 mol L^{-1} Fe^{2+} at pH 10 on (a) glassy carbon, (b) platinum and (c) titanium working electrodes

Figures 4.16 – 4.18 show that Pb and Cu are deposited on titanium electrode at pH 2 and only Pb is deposited on titanium electrode at pH 10. The comparison of CV results obtained in section 4.2.6 with those in sections 4.2.2 – 4.2.5 shows that the current densities of deposition peaks in PW VI are lower than what was observed in types II – V. This means that the quantity of a particular metal that can be deposited in the presence of other metal ions in produced water is limited. This is consistent with thermodynamic predictions made in Appendix A. CVs show that it is possible to remove Cu, Fe, Ni and Pb in acidic synthetic produced water whereas Cu and Pb deposition are favoured in synthetic produced water with pH 7. This may be due to the displacement reaction of Ni and Fe in PW IV which leads to formation of Ni-Fe complex. The CVs also indicate that the platinum electrode is better than glassy carbon and titanium electrodes for carrying out multiple heavy metal removal from produced water while titanium is least suitable for this purpose.

4.3.   Faradaic estimation of metal deposition from synthetic produced water

The CV results obtained at 20 mV/s were used to estimate the mass of heavy metals that can be deposited from synthetic produced water using Faraday's law (equation 4.13).

$$m = \frac{M}{nF} \text{ x } aI_d t \hspace{4cm} 4.13$$

Where m is the mass of metal deposited per cm^2, I_d the current density that flows through the reactor per cathode surface area (A/cm^2), a the

current efficiency (assumed to be 100% for all cases), M the molar mass, F the Faraday's constant (26.799 A-h or commonly 96,500 C), n the number of electrons transferred, and t the time in hours. The mass per cm^2 rather than the total mass was calculated because the quantity of deposit is a function of the electrode surface area (Di Bari, 2000). In produced water containing single metal ions it is almost impractical to recover Ni and Fe on the platinum, titanium and glass carbon electrodes as presented in Figures 4.19 – 4.21. However it is evident that platinum is the most suitable electrode of the three for this research and the best in an acidic medium. The amount of Cu and Pb that can be recovered on all electrodes at pH 4 after 24 hours of electrodeposition ranges from 0.6 to 1.2 g/cm^2, and 1.2 to 4.2 g/cm^2 respectively, while only 0.18 to 0.5 g/cm^2 of Pb can be recovered at pH 10. Also, at pH 7, $Pb_{(s)}$ is the main deposit on platinum and titanium electrodes however both $Cu_{(s)}$ and $Pb_{(s)}$ can still be deposited on glassy carbon at this pH. Generally a greater quantity of $Pb_{(s)}$ will be deposited on all electrodes at every pH, however at pH 4 more $Cu_{(s)}$ will be deposited on titanium electrode, the same will happen for glassy carbon at pH 7. There is no clear reason for this behaviour which is nevertheless supported by SEM and EDX analysis as discussed in section 4.3.

The mass of metals that can be recovered from produced water decreased with increasing pH in PW I – V. It appears that Ni and Fe deposition increased with time in PW VI (Figure 4.22). The presence of multiple metals might have aided this. According to Faradic calculations, there seems to be a linear relationship between time and mass of metal deposited from PW VI. Also the quantity of Cu is higher than all other metals in the deposit from PW VI, unlike in other cases (Figures 4.19 – 4.21) where Pb is the most favourably electrodeposited metal.
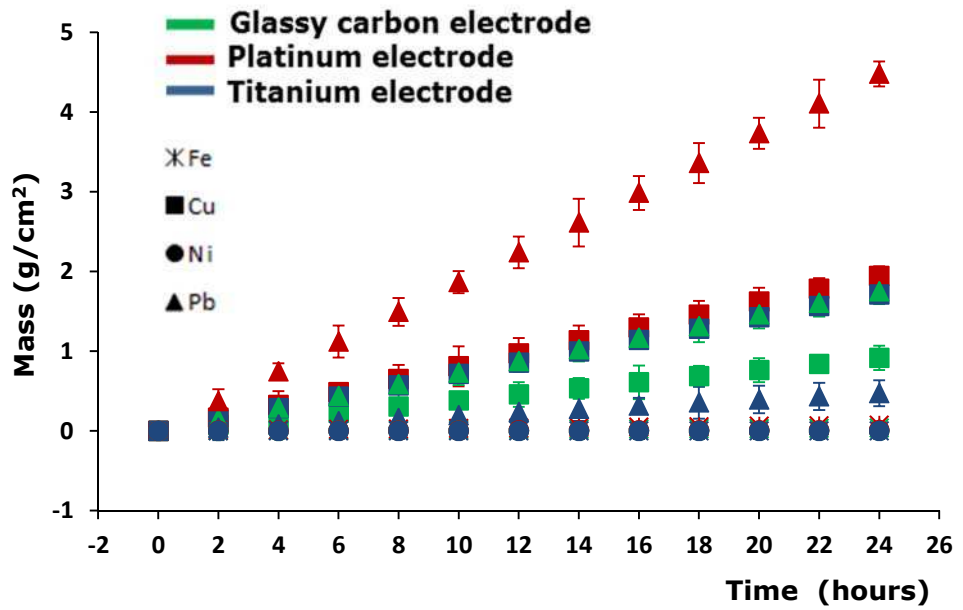
Figure 4.19: Rate of heavy metal recovery from different grades of synthetic produced water (PW I - V) at 20mV/s and pH 4
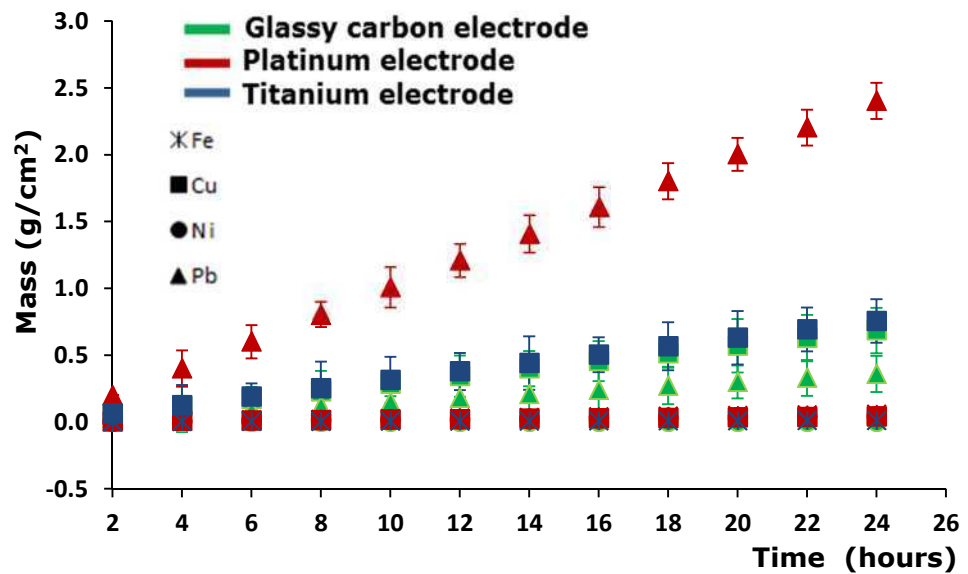
Figure 4.20: Rate of heavy metal recovery from different grades of synthetic produced water (PW I - V) at 20mV/s and pH 7
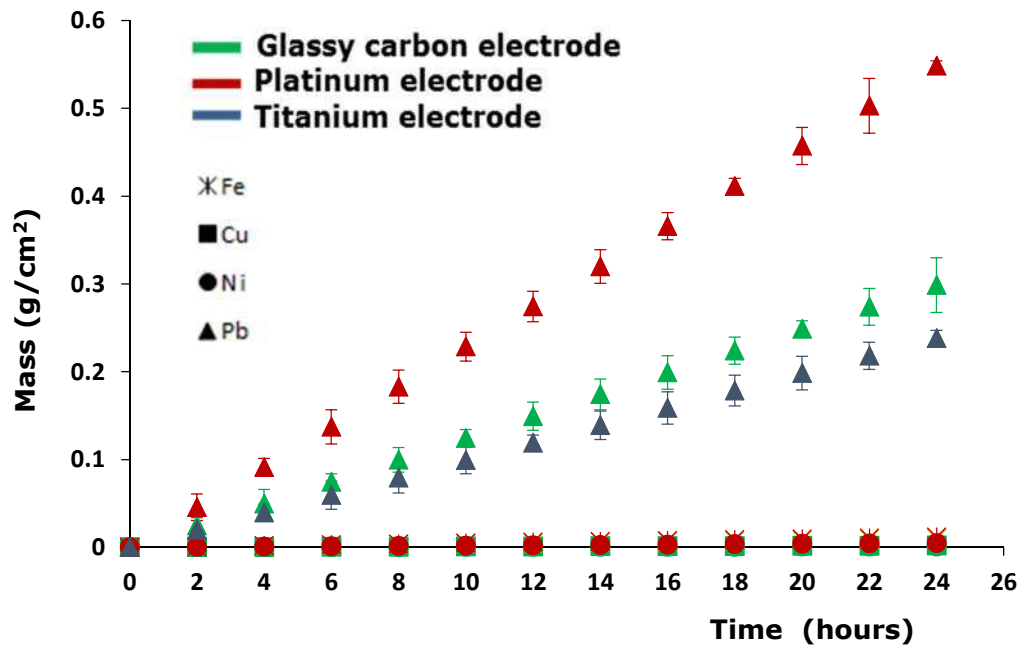
Figure 4.21: Rate of heavy metal recovery from different grades of synthetic produced water (PW I - V) at 20mV/s and pH 10
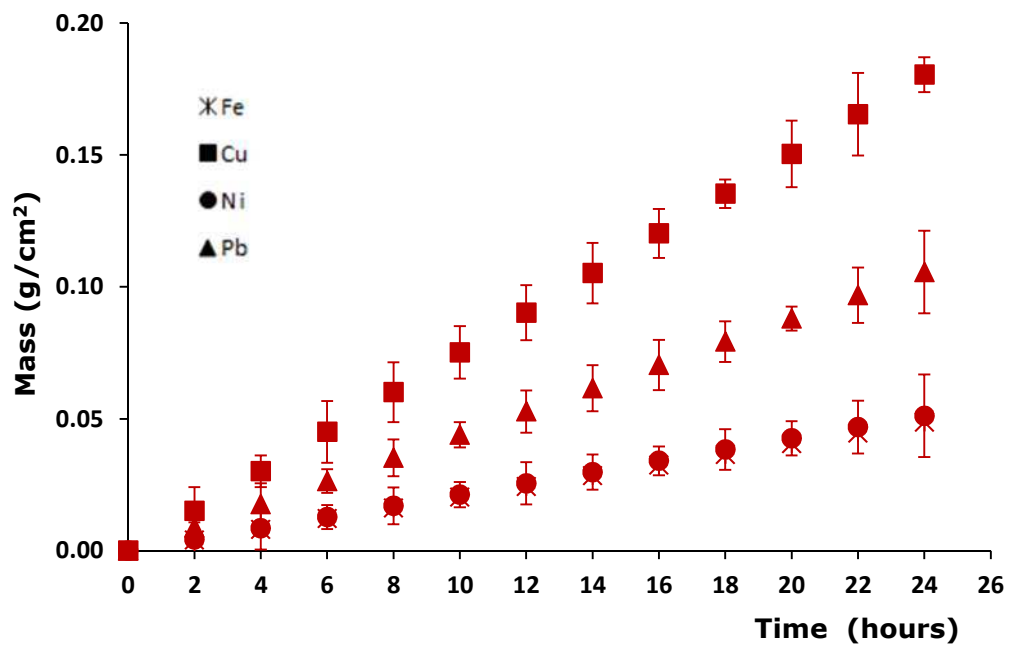
Figure 4.22: Rate of heavy metal recovery from synthetic produced water, PW VI on platinum electrode at 20mV/s and pH 4

The order of the quantity of metals deposited from PW VI suggests that metal reactivity is the dominant factor in recovery. It should be noted that although deposition of all metals are possible from produced water containing multiple heavy metals, the quantities of $Pb_{(s)}$ and $Cu_{(s)}$ that can be recovered were much lower than when the produced water contains just a single metal. For example at pH 4, 1.94 g/cm^2 of $Cu_{(s)}$ was deposited on platinum electrode after 24 hours in PW II, however only 0.18 g/cm^2 of $Cu_{(s)}$ could be deposited under the same condition in PW VI. Also 2.40 g/cm^2 of $Pb_{(s)}$ was recovered from PW III after 24 hours on the platinum electrode but only 0.1 g/cm^2 of $Pb_{(s)}$ could be recovered from PW VI under the same condition. This suggests more energy may be needed to remove all heavy metals present in PW VI.

4.4.   Growth, structure and mechanism of electrodeposition

Although CV has shown that metal recovery from produced water is feasible, chronoamperometry (CA), SEM and EDX were carried out to confirm the mechanism of deposition and determine if the heavy metals are removed as individual metals or alloys. The relevant results, analyses and discussions are presented in this section.

4.4.1.   Chronoamperometry of heavy metal deposition from produced water

Figure 4.23 shows a typical chronoamperogram (in the following text, CA refer to either chronoamperometry or chronoamperogram depending on the context) observed for heavy metal deposition. After the initial current spike which resulted likely from the double layer charging, the curve exhibits a slow increase of the current, which is in agreement with the electrodeposition occurring on an electrode with a growing surface area. Another major observation in CA study is that the applied potential needed

to cause noticeable metal deposition shifted negatively by around 0.25 V in all cases.
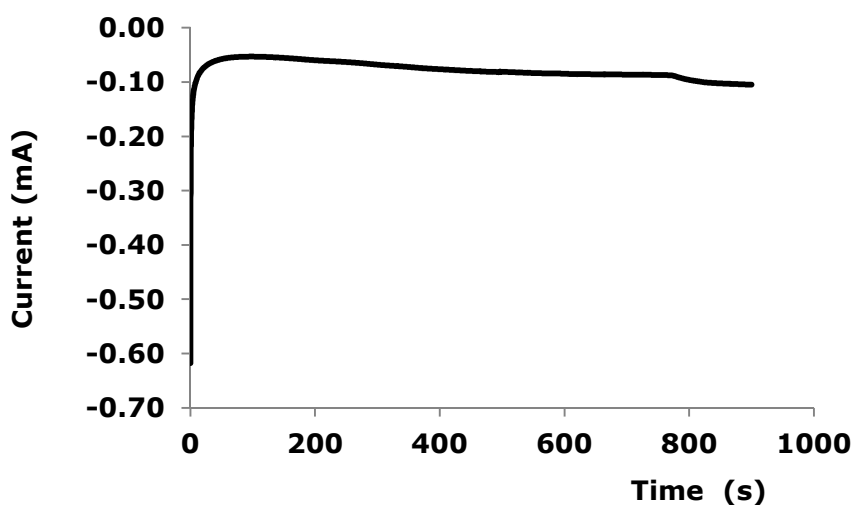
Figure 4.23: Chronoamperogram of metal deposition on glassy carbon electrode from PW VI at pH 1.5 and - 0.7 V vs. AgAgCl

For example, CV results (cf. Figure 4.4) indicate that Cu deposition on the platinum electrode at pH 4 would occur around - 0.2 V vs. Ag/AgCl. However, in CA, the noticeable deposition only started to occur on platinum around - 0.45 V vs. Ag/AgCl. Therefore overpotential of – 0.25 V vs. Ag/AgCl is required to drive the deposition of heavy metals from produced water under this condition. Otherwise, the results obtained from CA are consistent with those of CV.

4.4.2.   Structure and mechanism of metal recovery from synthetic produced water

After electrodeposition of heavy metals from synthetic produced water using CA methods, the morphology and elemental composition of the deposits were examined using SEM and EDX, and the effects of concentration, pH and applied potential were investigated.

4.4.2.1. Morphology of copper deposits recovered from produced water

Copper was successfully deposited on glassy carbon, platinum and titanium electrodes at pH 4 in PW II containing 1000 ppm of Cu (II) species after 15 minutes of CA at – 0.7 V vs. Ag/AgCl. However only traces of $Cu_{(s)}$ deposits were present on the electrodes at pH 7 at this concentration and no $Cu_{(s)}$ was deposited on any of the electrodes at pH 10. Electrodeposition was also carried out at 100 ppm and 500 ppm of Cu concentrations in PW II. As expected the amount of Cu deposit decreased with decreasing the concentration at pH 4. The morphology of Cu deposit obtained at pH 4 and 1000 ppm was studied.
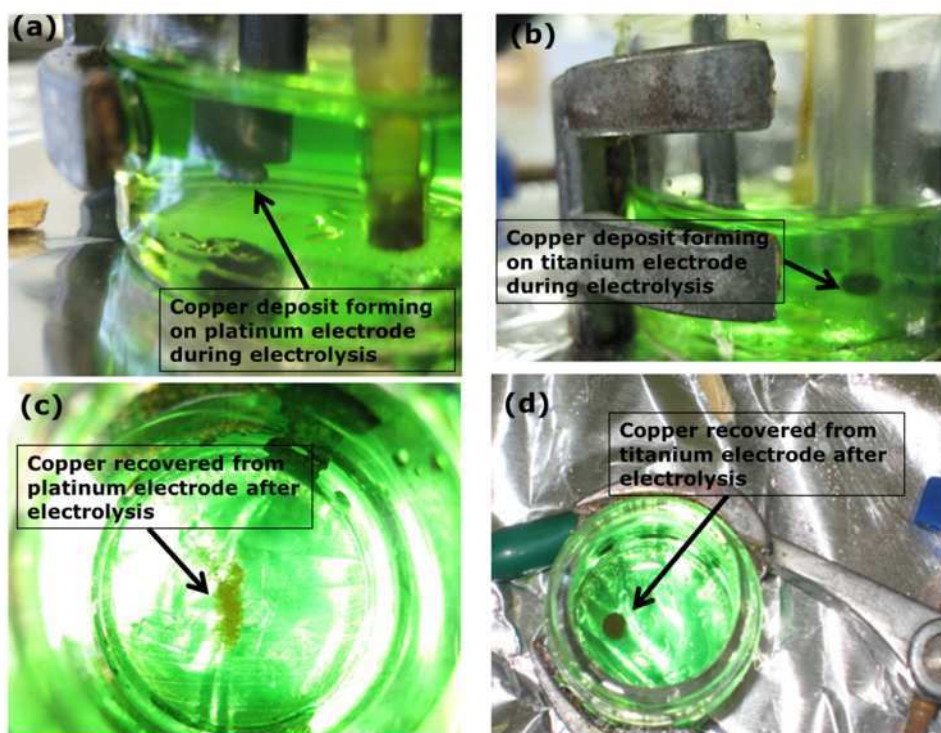
Figure 4.24: Images taking during deposition of Cu from PW III at -0.7 V and pH 4 on (a) Platinum and (b) titanium working electrodes and after 15 minutes deposition of Cu from synthetic produced water, PW II, at -0.7 V vs. Ag/AgCl and pH 4 on (c) Platinum and (d) titanium

The concentration of metals and the potential applied for metal deposition affect the nucleation and growth pattern of heavy metals from produced water. Figure 4.24 shows that after 15 minutes of electrodeposition of $Cu_{(s)}$ in PW II at - 0.7 V vs. Ag/AgCl and pH 4, a dendritic structure of Cu grew on the electrode which later fell off because it was too big for the electrode surface area. However when the electrode was viewed under SEM there was no trace of Cu deposit on platinum and titanium electrodes (Figure 4.25), even though dendritic copper structures were formed on both electrodes before falling off.
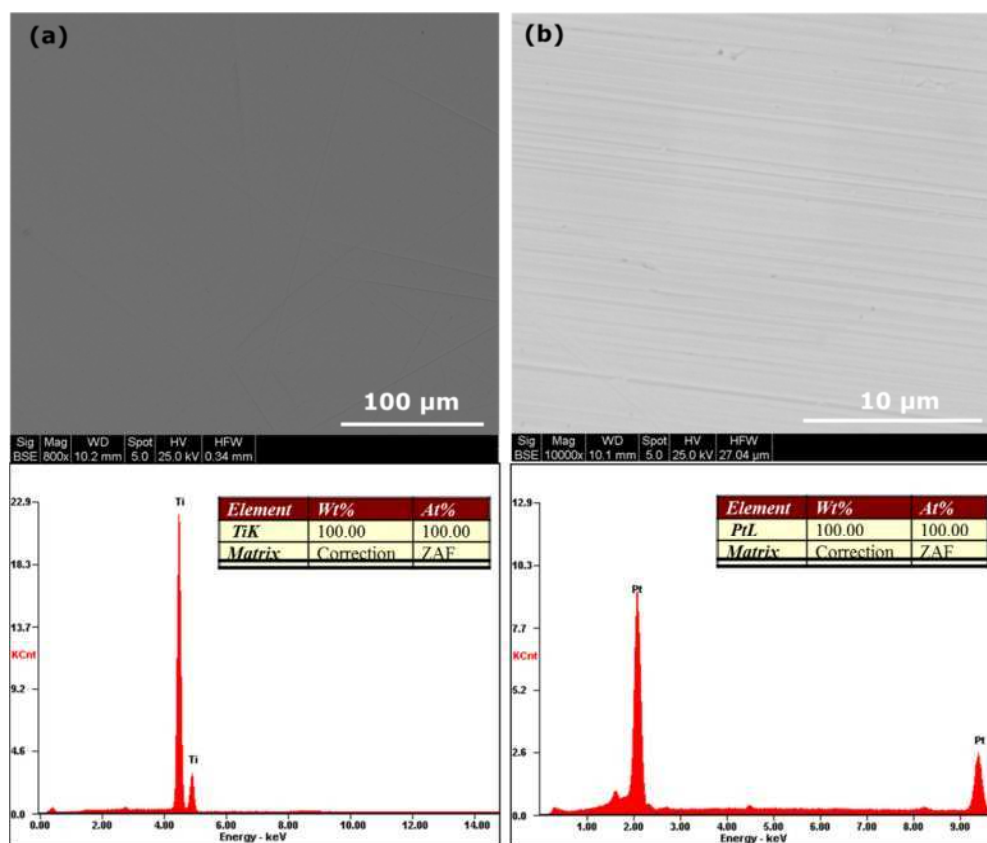
Figure 4.25: SEM/EDX images of (a) titanium electrode and (b) platinum electrode surfaces after 15 minutes of Cu deposition from PW II containing 0.02 mol/L Cu^{2+} at - 0.7 V vs. Ag/AgCl

It is also important to note that there was a very weak bonding/interaction between the electrode surfaces and deposited Cu. This is advantageous in

that stripping becomes easy and the deposited metal can be easily recovered without spending much energy, especially on an industrial scale.

A similar dendritic structure was formed when the electrodeposition was repeated at - 0.6 V vs. Ag/AgCl but Cu deposits can be seen on the electrodes this time as shown in Figure 4.26. This suggests that a more negative applied potential can lead to rapid growth of deposit since applied potential was proportional to the current passing through the cell. Therefore to reduce the time of deposition more negative potentials can be applied to the system.
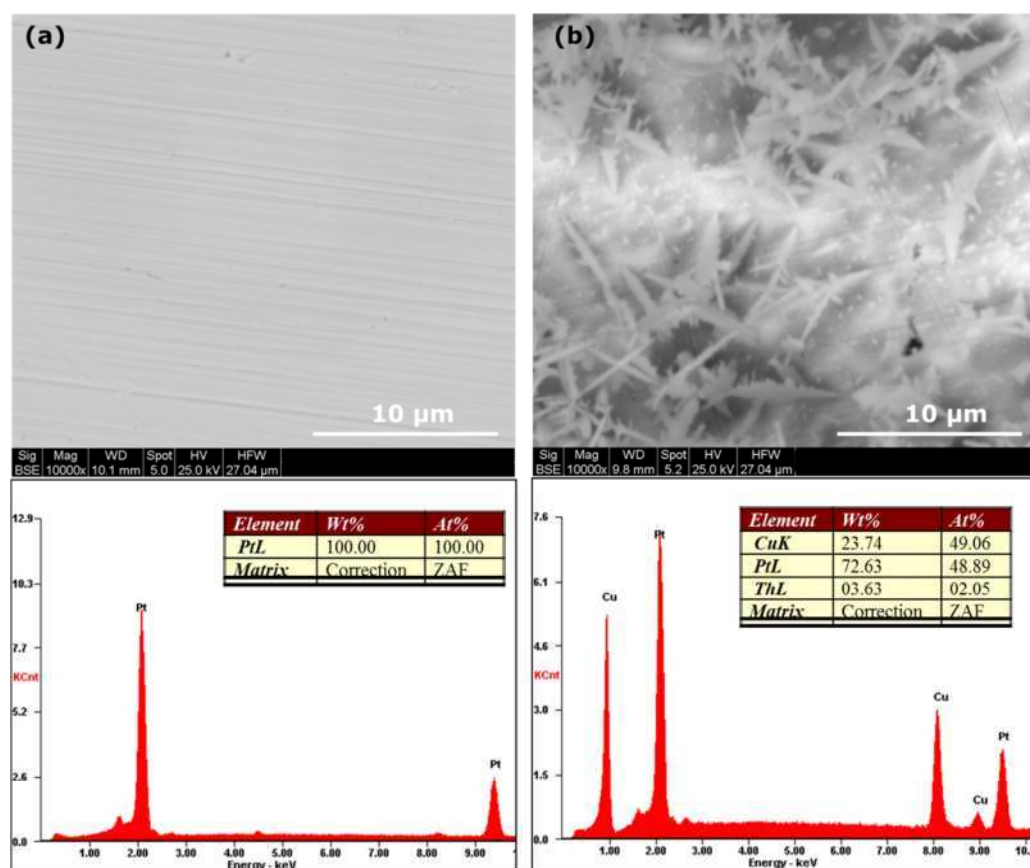
Figure 4.26: SEM/EDS images of platinum electrode surfaces after 15 minutes of Cu deposition from PW II (pH 4) containing 0.02 mol/L Cu^{2+} at (a) -0.7 V and (b) -0. 6 V vs. Ag/AgCl

The type of electrode and applied potential can equally affect the morphology of electrodeposits. Figure 4.27 shows that at - 0.7 V vs. Ag/AgCl copper deposits were closely knitted together forming a spongy structure while at - 0.6 V vs. Ag/AgCl they maintained the dendritic structure on glassy carbon as on platinum. These dendritic structures are typical of Cu deposits previously reported in literature (Shao and Zangari, 2009, Nebojša et al., 2007, Li et al., 2001).
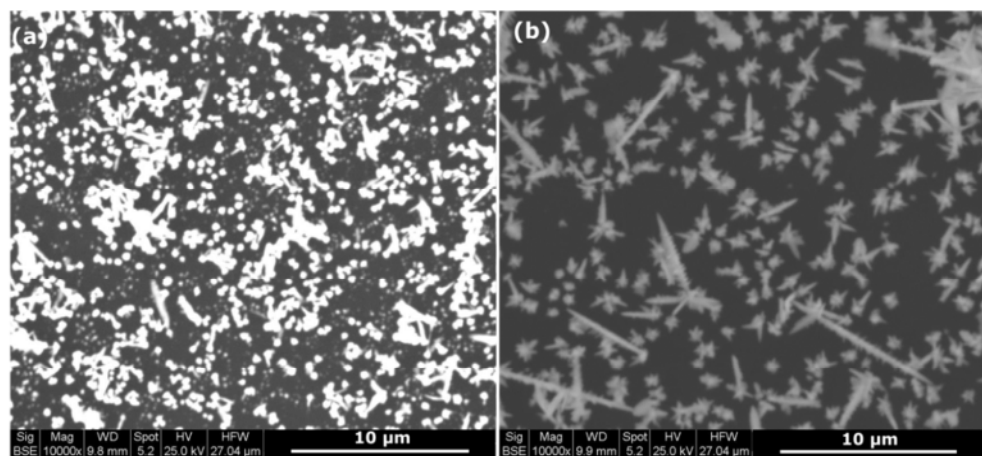
Figure 4.27: SEM images of glassy carbon surfaces after 15 minutes of Cu deposition from PW II (pH 4) containing 0.02 mol/L Cu^{2+} at (a) -0.7 V vs. Ag/AgCl and (b) -0.6 V vs. Ag/AgCl
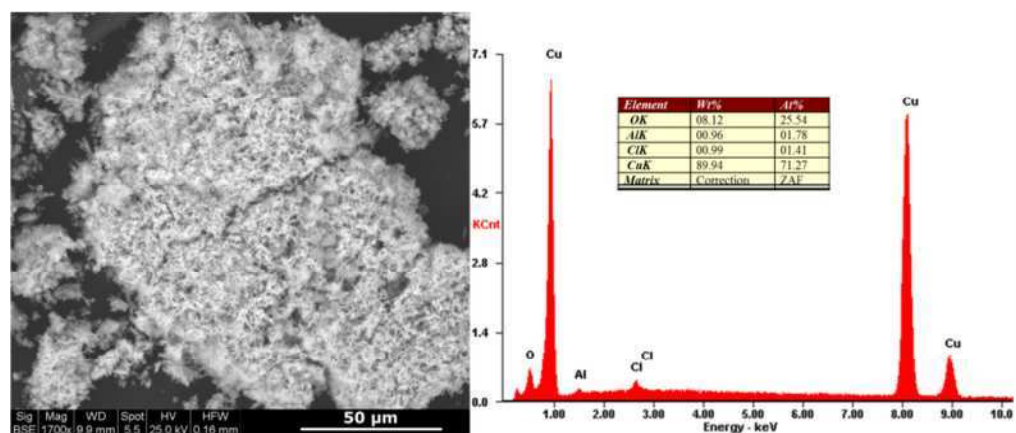
Figure 4.28: SEM/EDX of Cu from PW II containing 0.02 mol L-1 Cu^{2+} at - 0.7 V vs. Ag/AgCl

These changes in shape suggest that $Cu_{(s)}$ forms the dendritic structure initially during growth which later changes to the spongy structure as the dendrites were lumped together as the copper deposition continued. This is confirmed by the $Cu_{(s)}$ deposit that fell off from the titanium electrode (Figure 4.28). It contained about 90 wt. % Cu and formed a sponge of dendrites. This means that $Cu_{(s)}$ was recovered from PW II at pH 4 as indicated in both computational and CV results.

4.4.2.2. Morphology of lead deposits recovered from produced water

The electrodeposition of $Pb_{(s)}$ was also carried out successfully in PW III (cf. Table 3.3) at pH 4 and 1000 ppm of $PbCl_2$.
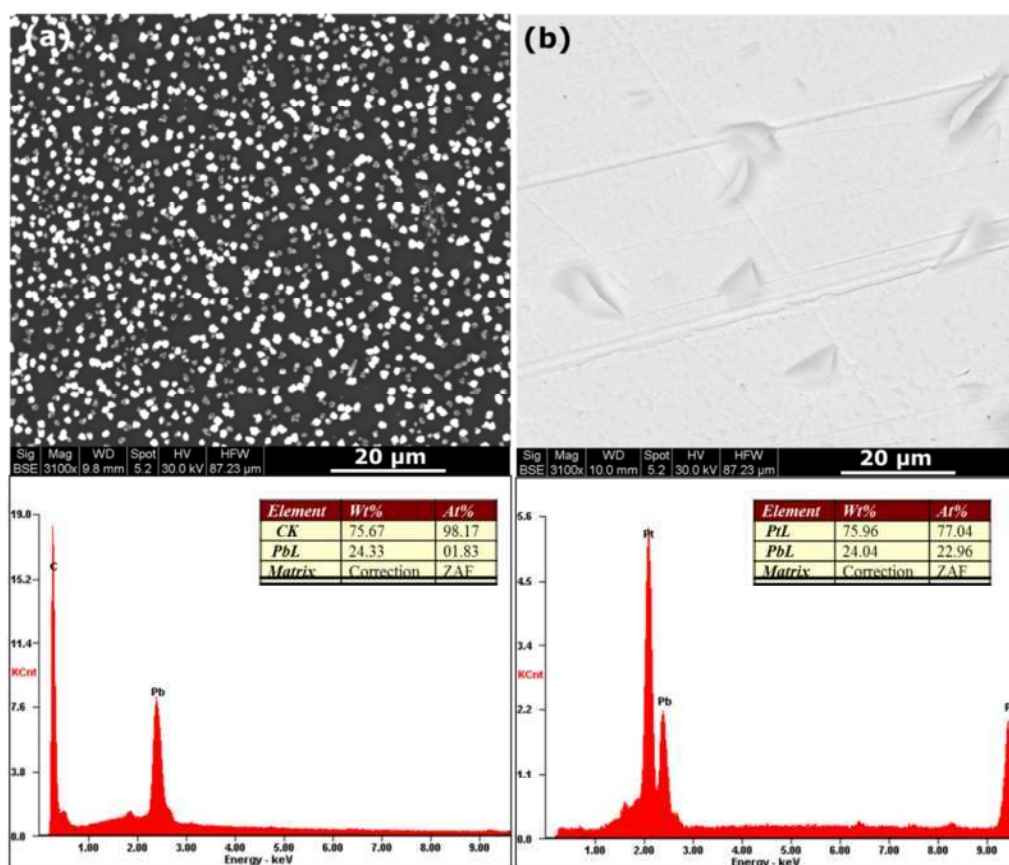
Figure 4.29: SEM/EDX spot analysis of Pb deposits on (a) glassy carbon electrode and (b) platinum electrode from PW III at − 0.7 V vs. Ag/AgCl after 15 minutes of electrodeposition

The structure of the $Pb_{(s)}$ deposit varied with the type of electrode used. Flakes of Pb were observed on the platinum electrode while crystal shaped lead particles were deposited on the glassy carbon electrode as presented in Figure 4.29. It should be noted that $Pb_{(s)}$ was not deposited on the titanium electrode at this concentration for the same deposition time. EDX analysis revealed that the amount of $Pb_{(s)}$ deposited on the electrode surface after 15 minutes was very small compared to that of Cu deposited under the same conditions, suggesting that nucleation of Pb would take a longer time than that of Cu in produced water.

4.4.2.3. Morphology of nickel deposits recovered from produced water

Nickel was successfully deposited from PW IV after the application of − 1 V vs. Ag/AgCl on titanium electrode for 15 minutes. It should be noted there was no Ni deposition at more positive potentials. This is consistent with CV, thermodynamic and Faradaic calculations that Ni deposition from produced water is difficult. There was no observed hydrogen evolution at this potential which suggests that the presence of other metal ions in the solution cause a negative shift in the hydrogen deposition potential. Scanning electron micrographs and EDX analysis showed that even under this condition, Ni was not deposited on glassy carbon; however there was Ni deposition on platinum and titanium as presented in Figure 4.30.

It should be noted that the cracked structure on platinum is similar to what was reported as Ni deposit in the literature (Cui and Lee, 1995). However considering the high oxygen content this may be $Ni(OH)_{ads}$ on the electrode surface as suggested in equation 4.8. It appears that nickel deposition followed a two stage process: An initiation process where $NiOH_{(ads)}$ was first adsorbed onto the surface of the electrode preceding further reduction and the growth of Ni crystals. Ni growth was more

favourable on titanium than on platinum or glassy carbon. Hence, under this experimental condition, globular Ni crystals were already grown on the titanium electrode (Figure 4.30).
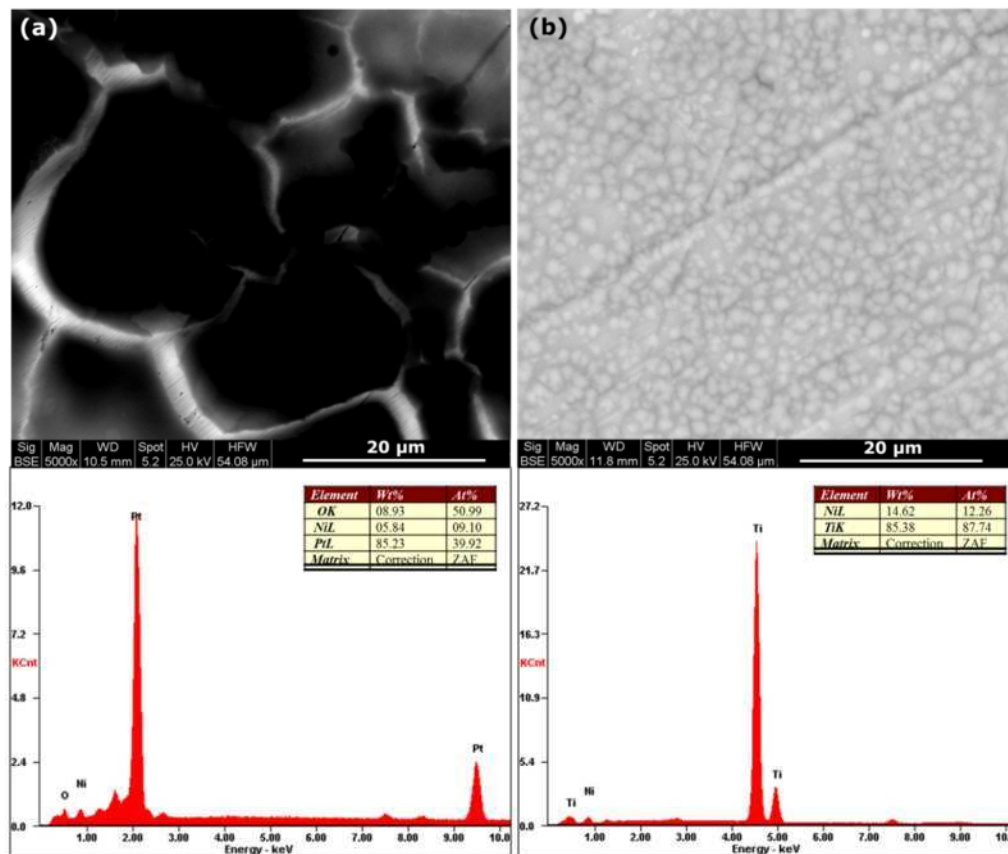
Figure 4.30: Scanning electron micrographs of Ni deposit on (a) platinum and (b) titanium electrode from PW IV at pH 4 and − 0.7 V vs. Ag/AgCl

4.4.2.4. Morphology of Iron deposits recovered from produced water

The deposition of Fe from PW V (cf. Table 3.3) was found to be difficult as presented in Chapter 4 and in Section 4.2. SEM/EDX analyses revealed that $Fe_{(s)}$ was not deposited on glassy carbon and titanium after 15 minutes of CA at pH 4 and -0.8 V vs. Ag/AgCl. However $Fe_{(s)}$ was deposited on the platinum electrode under this condition as presented in Figure 4.31. It is difficult to study the morphology of the Fe deposit other than that it appeared like black dots on the platinum surface.
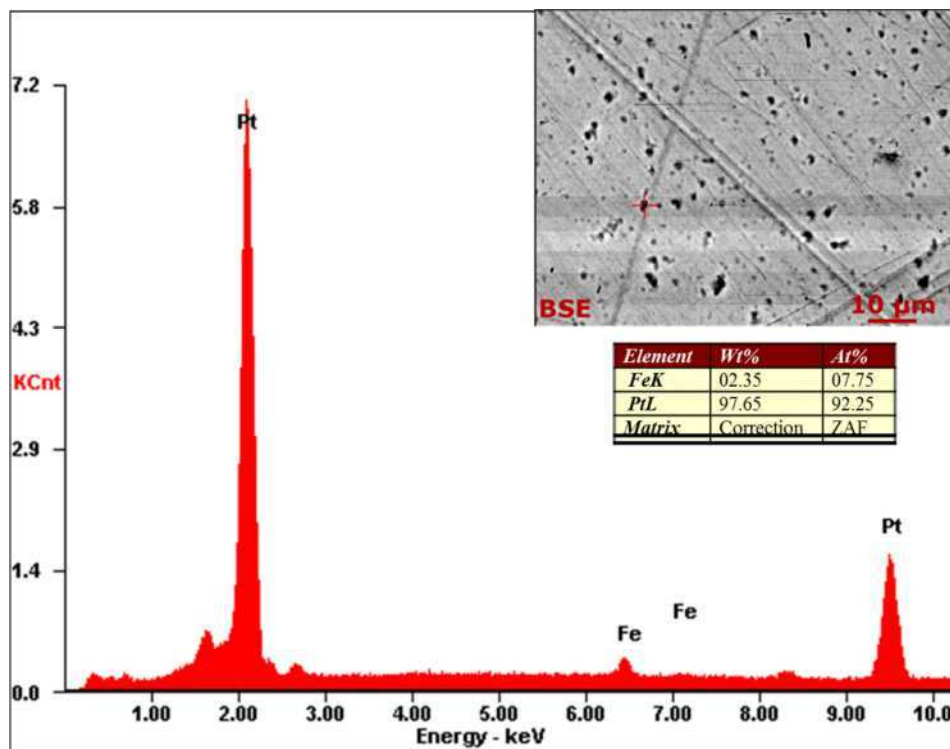
Figure 4.31: SEM/EDX spot analysis of Fe deposit from PW V on platinum electrode at − 0.8 V vs. Ag/AgCl at pH 4

It is possible that the deposited $Fe_{(s)}$ could have reacted with protons and dissolved back into solution at this pH, even at higher pH there was no $Fe_{(s)}$ observed. SEM/EDX analysis suggest the process of Fe deposition from produced water may be the most difficult and complicated of the four heavy metals studied in this research.

4.4.2.5. Mechanism of electrodeposition of multiple metals from produced water

SEM and EDX were used to investigate the structure of the deposits from synthetic produced water with multiple heavy metal ions, and to understand the mechanisms of the growth of the deposits on the electrode surface. Electrodeposition was carried out for 15 minutes at three different concentrations of PW VI and the atomic percentage of each element in the deposit was counted as presented in Table 4.1.

This table can help reveal the mechanism of metal deposition from synthetic produced water. In the deposition process of Cu, the Cu adatoms are the first to be attached to the electrode surface, after which the deposit starts to grow. This was evident by the results achieved when 100 ppm of each metal was present in produced water. As the concentration of the multiple metal ions increased, Ni adatoms started to attach on the surface of the electrode. Further growth of deposited Ni is evident by the Ni atomic percentage on the electrode surface when 500 ppm of each metal ion was present in PW VI. As Ni growth was initiated on electrode surface, copper growth continued. At 500 ppm Pb adatoms began to form on the surface of the electrode as evident by small atomic percentage of Pb observed on glassy carbon and titanium electrodes.

Table 4.1: Percentage of elements deposited on electrode surface from PW VI at different concentrations at pH 2.5

Electrode	Elements	At % (Matrix: ZAF)		
		100 ppm	500 ppm	1000 ppm
Glassy carbon	C	99.47	91.55	-
	Cu	0.53	6.22	30.27
	Pb	-	0.92	19.54
	Ni	-	1.06	16.54
	Fe	-	-	4.66
	O	-	-	28.99
Platinum	Pt	94.18	74.49	6.61
	Cu	5.82	19.73	26.83
	Pb	-	-	21.07
	Ni	-	5.78	16.09
	Fe	-	-	4.86
	O	-	-	24.53
Titanium	Ti	94.38	75.79	18.37
	Cu	5.62	11.74	25.2
	Pb	-	0.98	17.02
	Ni	-	2.46	12.22
	Fe	-	-	4.01
	O	-	-	22.17

When the concentration of each of the multiple metal ions was increased to 1000 ppm, all metals were deposited on the electrode surface; however it appeared that the growth of Fe just began at this concentration as evident by the relatively low atomic percentage of Fe.

It should be noted that although Pb growth was initiated after nickel, the growth rate of Pb appeared to be very high. The order in which heavy metals were deposited on electrode surface followed this trend: Cu → Ni → Pb → Fe. It is hard to claim a particular reason for this behaviour because this order does not follow the metal reactivity series. However, as shown in Table 4.1, both Ni and Pb began to form on the electrodes at 500 ppm, and since it has been established that Ni followed a two – stage deposition process, the Ni atomic percentage observed at 500 ppm should have been $Ni(OH)_{ads}$. Hence the trend of metal electrodeposition from PW VI can be changed to Cu → Pb → Ni → Fe in line with their standard reduction potential and metal reactivity series. The formation of Ni-Fe complex in solution as shown in Appendix A may be responsible for the slow growth rate of Ni and Fe on the electrode surface and subsequently their small deposition mass per cm^2 after an extended electrodeposition time (cf. Figure 4.22). This EDX analysis is supported by scanning electron micrographs images presented in Figure 4.32.

The behaviour of metal deposition from a produced water sample containing multiple metal ions such as PW VI is quite different from the synthetic produced water sample containing a single metal. Every metal component in the complex produced water can be deposited in an acidic medium (Figure 4.32). However, the quantity of each metal that could be experimentally recovered was significantly lower compared to when only a single metal was present in the water. This may be due to a theoretical reduction in the current efficiency needed to deposit each metal. The

deposition of $Ni_{(s)}$ and $Fe_{(s)}$ was significantly improved in the presence of multiple heavy metal ions.
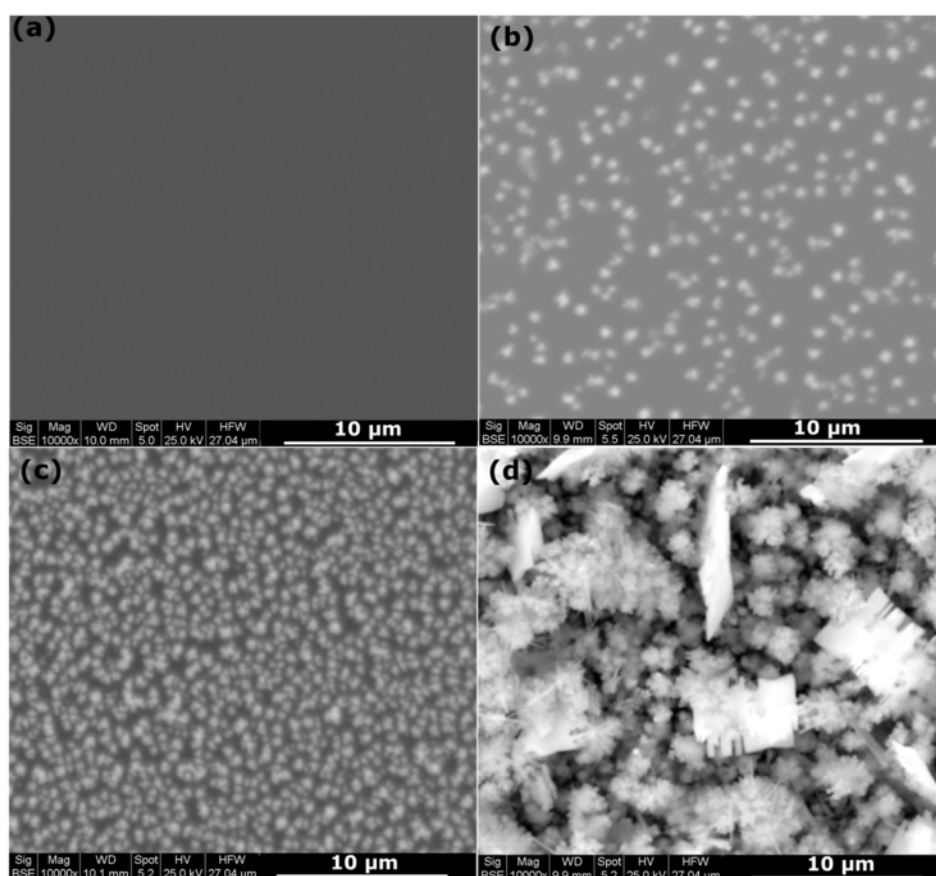
Figure 4.32: Scanning electron micrographs showing growth of pattern of metal deposition from synthetic produced water with heavy metal concentrations of (a) 0 ppm (b) 100 ppm (c) 500 ppm and (d) 1000 ppm on glassy carbon electrode at pH 2.5

Also in the complex produced water, $Cu_{(s)}$ rather than $Pb_{(s)}$ was the most favoured for electrodeposition. The atomic percentages of the deposits from EDX analysis suggests that multiple metals were removed from produced water as individual metals rather than as alloys. This is supported by scanning electron micrographs (Figure 4.33). A similar image was obtained for deposits on the titanium electrode. Distinct and consistent shapes similar to what was obtained for individual metals can be seen on the electrode surfaces. Since these were not joined together, it implies

individual metals rather than alloys were deposited from produced water containing multiple metal ions.
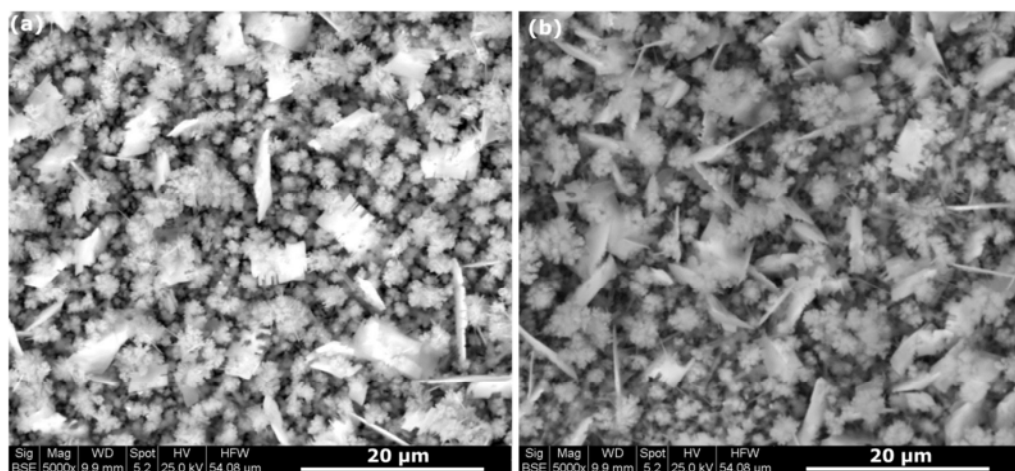
Figure 4.33: Scanning electron micrograph of deposits from PW VI on (a) Glassy carbon and (b) platinum from synthetic produced water after 15 minutes at -0.7 V vs. Ag/AgCl and pH 2.5.

4.5. Conclusion

In this chapter it has been shown that metals can be recovered from produced water containing multiple heavy metals via electrodeposition. The deposition is a function of metal reactivity, electrode surface area, type of electrode, pH, applied potential and concentrations of metal ions in solution. The more reactive the metal ion in the produced water, the better its recovery. Also the larger/higher the electrode surface area and the applied potential; the greater the quantity of metals which can be recovered from produced water. Platinum electrode was found to be the most suited for deposition of individual metals except for Ni. However, the titanium electrode was most suited for Ni electrodeposition, and platinum and glassy carbon for recovery of multiple metals from produced water. High metal concentrations in produced water are good for metal recovery via electrodeposition however the concentration could be too high as shown in Appendix A. The lower the pH, the better the recovery of heavy metals

from produced water. In conclusion this chapter has demonstrated that $Cu_{(s)}$, $Pb_{(s)}$, $Ni_{(s)}$ and $Fe_{(s)}$ can be recovered from produced water containing multiple heavy metal ions. These can be selectively removed as individual metals based on their reactivity and deposition potential or as a mixture of metals on platinum, glassy carbon and titanium in acidic, neutral, or alkaline media, but most effectively in the acidic medium.

Chapter 5: Photoanodic processes

5.1. Introduction

In the previous chapter it was demonstrated that multiple metal ions can be recovered as metal deposits from produced water, and that the best conditions for lead, iron, nickel and copper recovery on various cathode materials from produced water with low heavy metal concentrations should be at potentials more negative than -0.7 V vs. Ag/AgCl and pH 4. The aim of this chapter is to study the reactions that will take place on the anode in the dual purpose photoelectrochemical (PEC) cell for produced water treatment.

In this chapter the feasibility of photocatalytic degradation of dissolved phenanthrene in produced water via a photoanode of synthesised MWCNT-TiO_2 is presented. The vast majority of research in this field only report a heavily diluted suspension, ≤ 1 mg-CNT/mL-H_2O, (Rastogi et al., 2008, Yu et al., 2007) which is not practical for making a photoanode both in the laboratory and the industry. To address this concern, the dispersion of a highly concentrated MWCNT suspension using anionic surfactant (NaDDBS) was studied in this work and the results are presented and analysed in Section 5.2. After obtaining the optimum CNT–to-surfactant ratio from the suspension studies, CNT-TiO_2 nanohybrids were synthesised as described in Chapter 3. The characterization of the synthesised CNT-TiO_2 nanohybrid was carried out using TGA, TEM, SEM, BET and EDX analyses and discussed in section 5.3. The photocatalytic activities of the nanohybrids compared with commercial TiO_2 is presented in section 5.4. Finally and more importantly, section 5.5 presents the performance of photoanode made from the synthesised CNT-TiO_2 nanohybrid as a photocatalyst in the degradation of phenanthrene at appropriate anodic potentials.

5.2. Dispersion of MWCNTs in NaDBBS

The majority of the current techniques of CNT fabrication cannot be used to fabricate short, rigid and isomerically pure CNTs, although applications including nanocomposite, optics, electronics, and sensing require pure and well isolated individual CNTs (Scott et al., 2012, Uddin et al., 2012).

Chemical functionalization and mechanical interactions are often employed to disperse CNTs in an appropriate liquid medium. Although the chemical functionalization technique has been found effective, it introduces defects on the wall of CNTs which deteriorates their intrinsic properties (Wang et al., 2003). Mechanical interactions such as ultrasonication and high-shear mixing on the other hand have been able to unbundle CNTs while maintaining the integrity and intrinsic properties of individual CNTs (Sandler et al., 1999, Qian et al., 2000, Xie et al., 2005, Wang, 2009, Uddin et al., 2012). However a major drawback of mechanical interactions is the re-aggregation of CNTs due to van der Waals interactions which may lower the efficiency of load transfer. Several studies have shown that surfactants act as dispersing agents which limits CNT agglomeration and improve CNTs dispersion in aqueous solutions (Madni et al., 2010, Gong et al., 2000, O'Connell et al., 2001, Moore et al., 2003).

Sodium dodecylbenzenesulfonate (NaDDBS) is an excellent anionic surfactant and one of the most widely used surfactants for CNT dispersion in an aqueous medium. Several studies have been carried out on its effectiveness in dispersing CNTs (Islam et al., 2003, Matarredona et al., 2003), however the most important parameter affecting nanotube dispersion using surfactant is the CNT-surfactant ratio (Rastogi et al., 2008). To the best of the author's knowledge all aqueous CNT dispersion studies reported in literature up till now are based on very diluted CNT suspension (0.0001 – 1 mg-CNT/mL-H_2O). Therefore in this section

dispersion study of MWCNT in a highly concentrated CNT suspension (14.5 mg–CNT/mL-H$_2$O) by NaDDBS is presented.

5.2.1. Effect of NaDDBS on dispersion of CNTs in solution

Individual CNTs are active in the (ultraviolet-visible) UV-Vis region exhibiting characteristic bands (Kataura et al., 1999, Hamada et al., 1992). However, the photoluminescence is quenched for bundled CNTs which are hence rarely photoactive due to carrier tunnelling between the nanotubes (Yu et al., 2007). Therefore, it is possible to establish a linear relationship between the amounts of individual CNTs dispersed in solution and the intensity of their corresponding absorption spectrum. Thus, UV-Vis spectroscopy was used to monitor the dynamics of CNT dispersion process, hence the determination of the optimal CNT to TiO$_2$ ratio and sonication time to achieve the best MWCNT dispersion.

Figure 5.1 presents the UV-Vis spectra of CNT-NaDDBS suspensions obtained after continuous sonication at 100 kJ for 67 minutes at different CNT to NaDDBS concentration (mg/L) ratios. Two absorbance peaks were observed at 224 nm and 260 nm corresponding to NaDDBS and dispersed CNT absorbance respectively. This is because the absorbance peak at 224 nm is the same as what is obtained when a pure solution of NaDDBS was measured and it also increases linearly as the concentration of NaDDBS increases. It can be observed from Figure 5.1 that the absorbance of CNT suspensions shows a maximum around 260 nm and gradually diminishes from UV to near-IR, partly due to scattering especially in the lower wavelength range. A similar UV-Vis absorption spectra has been reported in literature for dispersed SWCNTs and MWCNTs (Grossiord et al., 2005, Jiang et al., 2003, Yu et al., 2007).
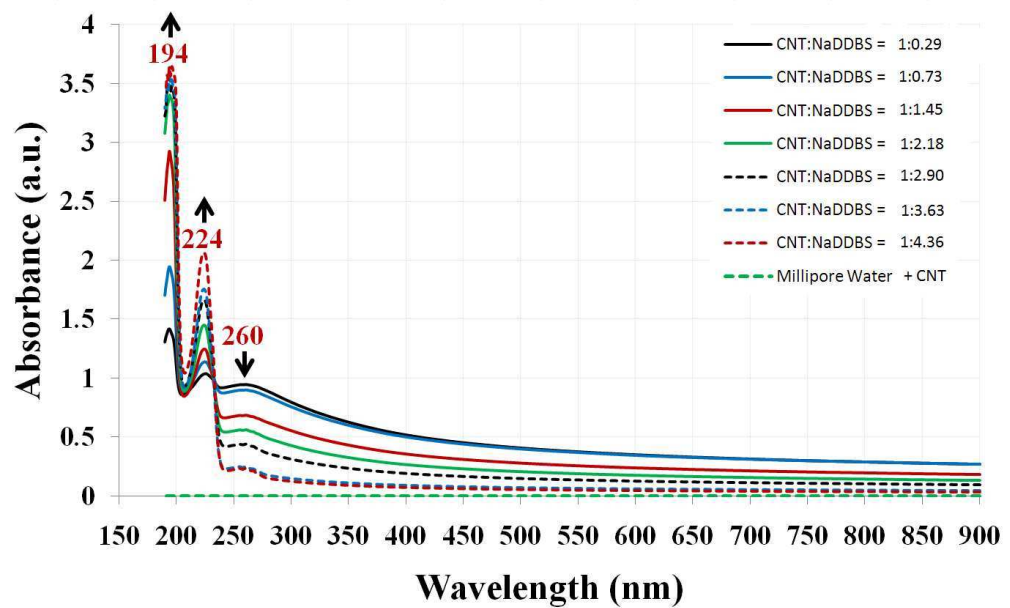
Figure 5.1: UV-Vis spectra of an aqueous MWCNT suspension as a function of CNT to NaDDBS concentration (mg/L) ratio after continuous sonication at 100 KJ for 67 minutes. Note that the peak at 224 nm corresponds to NaDDBS in solution while the peak at 260 nm corresponds to dispersed CNT. (The CNT suspension was diluted by a factor of 100 in the UV-Vis measurements)

MWCNTs exist as entangled aggregates as-produced, and should remain so at the beginning of sonication (Yu et al., 2007). Thus, no absorption was observed as shown in the UV-Vis spectrum (Millipore water + CNT). However upon sonication, the mechanical energy overcomes the van der Waals interactions in the CNTs aggregates, leading to extrication and dispersion. The increasing spectrum lines area and absorbance is a result of the increasing amount of dispersed CNTs. It is evident that the concentration ratio of CNT to NaDDBS is important in CNT dispersion in water. As observed in Figure 5.1, the general trend appears to be that dispersion increases with a reduction in the concentration of NaDDBS in solution; however there is no significant difference in CNT dispersion between CNT to NaDDBS concentration ratios at 1:4.36 and 1:3.63, and also between CNT to NaDDBS concentration ratios at 1:0.29 and 1:0.73.

The maximum MWCNT dispersion was obtained at CNT to NaDDBS concentration ratio 1:0.29 and this was only slightly more dispersed than when the ratio was 1: 0.73. This implies that the optimum CNT to NaDDBS ratio for MWCNT dispersion in water may be 1:0.29. This knowledge is important in the industry and in environmental management as it helps to minimise the amount of surfactants discharged into the environment.

Also, a change of CNT to NaDDBS ratio from 1:3.63 to 1:4.36 has little or no effect on CNT dispersion. As a matter of fact, there is a subsequent increase in the amount of NaDDBS not used for CNT dispersion (see NaDDBS peak at 224nm in Figure 5.1) in the suspension as the concentration ratio of CNT to NaDDBS is changed from 1:0.29 to 1:0.4.36. There was formation of micelles in the suspension when the CNT-NaDDBS concentration ratio was changed from 1:4.36 to 1:4.90. Sonication does not result in efficient dispersion at this ratio even after very long sonication time. This behaviour can be ascribed to the reduction of electrostatic repulsion forces between the CNTs and NaDDBS. An increase in the NaDDBS concentration results in the formation of very large amount of NaDDBS micelles in water. The osmotic pressure of these micelles around the CNT aggregates creates an effective attraction which results in depletion-induced aggregation of MWCNTs (Vigolo et al., 2000, Yu et al., 2007, Matarredona et al., 2003).

5.2.2. Effect of Energy on dispersion of MWCNTs in solution

The trend observed in Figure 5.1 implies that the lower the concentration of NaDDBS in the suspension the better the CNT dispersion. Therefore in order to determine the optimum CNT to NaDDBS ratio for MWCNT dispersion, the dispersion obtained at CNT to NaDDBS concentration ratio 1:0.29 (where the maximum CNT dispersion was recorded) was compared to that at ratio 1:0.15 (where the concentration of NaDDBS is further

reduced) as presented in Figure 5.2. The mechanical energy employed for sonication is a function of power and time, and due to voltage fluctuations, the sonication power cannot be kept constant throughout the experiments. Therefore in order to monitor the dispersion dynamics of MWCNTs in solution, a plot of the absorbance versus the total energy supplied was used instead of sonication time. It was verified that during sonication process, the area under the spectrum is proportional to the relative absorbance value at a specific wavelength.
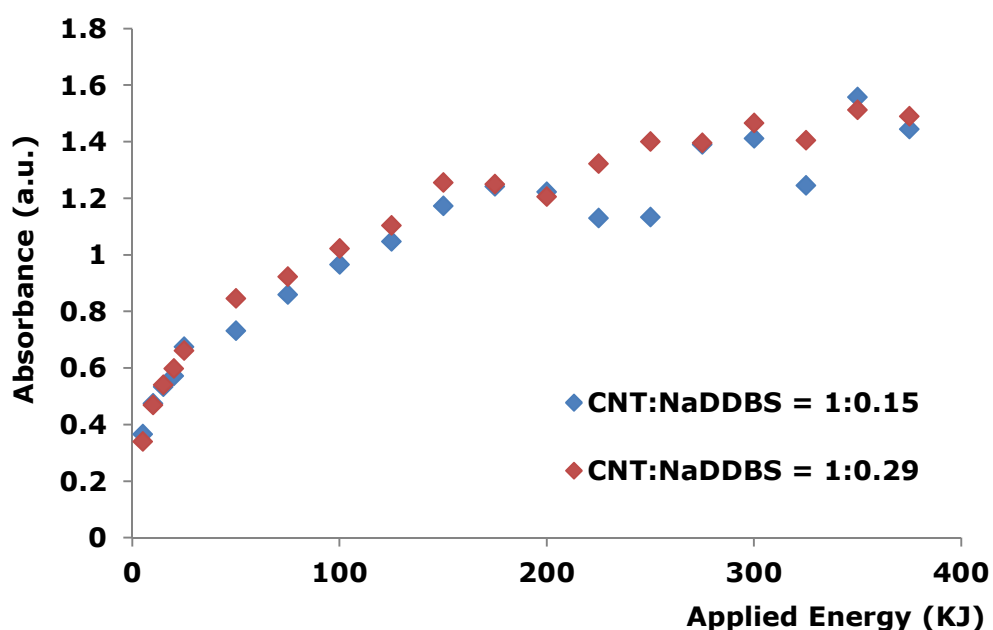
Figure 5.2: Effect of applied energy and CNT to NaDDBS concentration ratio on the dispersion of MWCNTs. The error bars are so small they do not appear in this graph

The absorbance maximum value around 260 nm is determined and plotted against the total energy supplied to the solution after baseline subtraction. This shows the development of the maximum absorbance as a function of the total energy supplied to the solution, describing the dispersion dynamics of different CNT to NaDDBS concentration ratios in aqueous suspension. The trend of the UV absorbance versus total energy curves obtained for both CNT to NaDDBS concentration ratios is similar.

The value of maximum absorbance increases at the beginning of sonication but reaches a plateau after a certain amount of supplied energy, which corresponds to the maximum achievable degree of dispersion of the MWCNTs in the aqueous NaDDBS solutions. Therefore from Figure 5.2 it can be concluded that the optimum dispersion of MWCNT in a suspension containing NaDDBS surfactant is at a CNT to NaDDBS concentration ratio of 1:0.29 and applied energy of 250 KJ. This indicates that the NaDDBS molecules can exert an unzippering force to disperse MWCNTs in the suspension, which is supported by high shear provided by sonication. The unzippering mechanism of MWCNT by NaDDBS is similar to that of SWCNT , where the bundled end of the CNTs frayed by high local shear during sonication becomes the site for additional surfactant molecules. The surfactant molecules then gradually exfoliate the CNTs bundle in an unzippering mechanism (Strano et al., 2003).

It should be noted that the energy required for the dispersion of highly concentrated MWCNTs suspension (14.5 mg–CNT/mL-H_2O) is significantly higher than what is needed to disperse low MWCNTs concentrations (0.0001 – 1 mg-CNT/mL-H_2O). It was reported that 60 kJ is necessary to reach maximum degree of CNT dispersion for 0.1 wt. % MWCNTs suspension (Yu et al., 2007), whereas about 250 kJ is required for optimum dispersion of CNT in 3.4 wt. % MWCNT suspension (Figure 5.2).

Prolonged sonication is energy consuming and may damage CNTs (Liu et al., 1999, Yu et al., 2007), therefore the minimum energy and minimum NaDDBS required to optimally disperse a certain amount of MWCNTs in aqueous CNT suspension must be determined, and the sonication process should be stopped when maximum dispersion of the CNTs has been achieved. Likewise excess NaDDBS surfactant in the suspension does not only limit the dispersion of MWCNT by the formation of micelles, it also amounts to waste of surfactants. It is therefore necessary to use the exact

amount of CNT to NaDDBS ratio needed for optimum dispersion. Several concentrations of MWCNT in suspension were tested at CNT to NaDDBS concentration ratio 1:0.29 in order to determine the optimum mg-CNT/mL-H_2O suspension at which the maximum CNT dispersion can be obtained as presented in Figure 5.3.
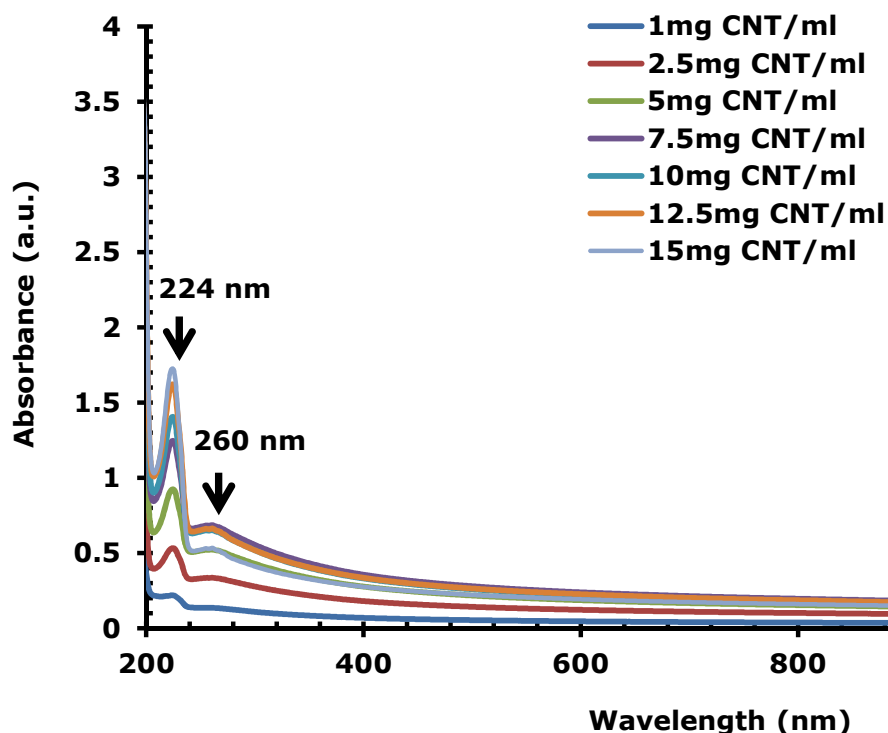
Figure 5.3: The effect of MWCNT concentration (mg−CNT/mL-H$_2$O) on CNT dispersion at CNT to NaDDBS concentration ratio 1:0.29

The highest dispersion occurred at 7.5 mg-CNT/mL-H_2O because it showed the highest absorbance at 260 nm. It should also be noted that the amount of unused NaDDBS at this concentration is relatively low. Therefore the optimum condition for MWCNT dispersion in highly concentrated suspension containing NaDDBS surfactant is to have a suspension of 7.5 mg-CNT/mL-H_2O, CNT to NaDDBS concentration ratio of 1:0.29 and applied energy of about 250 KJ in 67 minutes.

5.3. Characterization of CNT–TiO$_2$

MWCNT-TiO$_2$ nanohybrids based on the optimum conditions determined in section 6.2 were synthesised by a modified sol-gel method as described in Chapter 3. The characterization of these synthesised hybrids by various techniques is discussed in this section. TGA was used to determine the carbon content of nanohybrids, BET, SEM and TEM measurements were used to observe their surface state and structure. XRD was used for crystal phase identification and estimation of the anatase-to-rutile ratio while EDX was used for the elemental analysis of the hybrids.

5.3.1. Structures and morphology

The carbon content of the synthesised nanohybrids determined by TGA is presented in Table 5.1 and Figure 5.4.

Table 5.1: Carbon content of CNT-TiO$_2$ samples from Thermogravimetric analysis

Thermogravimetric Analysis	
Sample	Carbon content (wt. %)
Raw MWCNT	94.69
Calcined MWCNT-TiO$_2$ (wt. % 1: 0.9)	35.61
Uncalcined MWCNT-TiO$_2$ (wt. % 1: 0.9)	30.63
Calcined MWCNT-TiO$_2$ (wt. % ratio 2:1)	64.42
Uncalcined MWCNT-TiO$_2$ (wt. % ratio 2:1)	57.90

As expected, there was no appreciable degradation of the CNT and the determined carbon content agrees very well with the calculated value from initial ratio. However it was observed that the carbon content in the calcined samples is more than that in the uncalcined samples as shown in Figure 5.1.

This suggests that for the same amount of calcined and uncalcined MWCNT-TiO$_2$ nanohybrids, there are more impurities in the uncalcined samples. Since calcination was carried out at 500 ^{O}C, water and other organic impurities have been evaporated from the calcined samples,

leaving basically CNT and TiO_2. Therefore the carbon contents of calcined nanohybrids are higher than the uncalcined ones of the same weight due to the presence of water molecules and other impurities (from the synthesis process) present in the uncalcined nanohybrids as shown in the TGA plot in Figure 5.4.
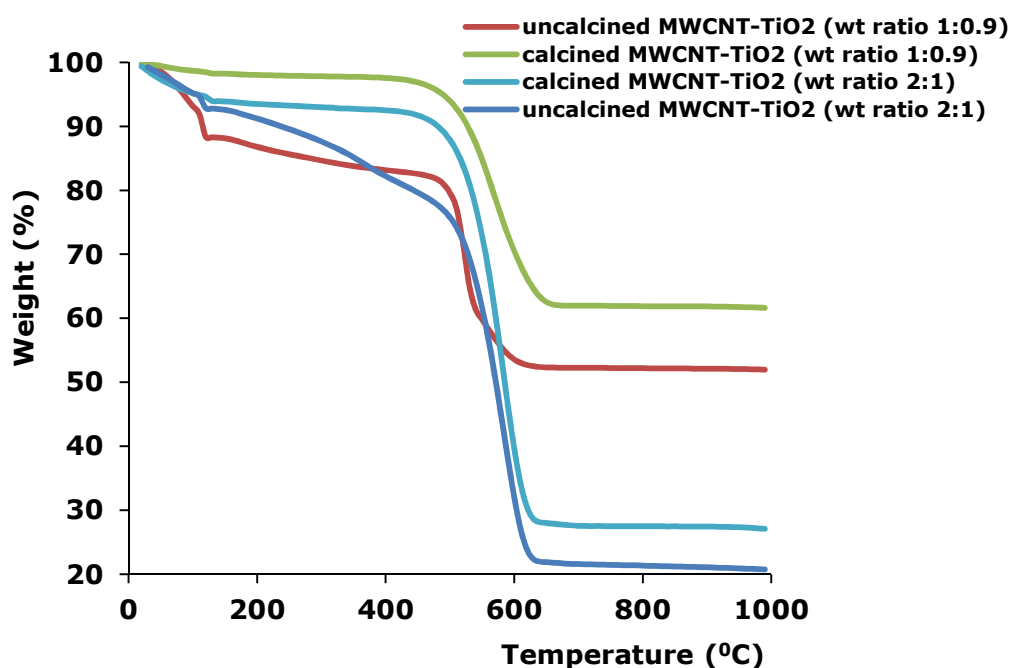
Figure 5.4: TGA plots showing the carbon content in raw MWCNT, calcined and uncalcined MWCNT-TiO$_2$ nanohybrids at different weight percent ratios

This observation is different from what is generally reported in literature for calcined and uncalcined CNT-TiO_2 composites (Gao et al., 2009b). Although there is an increase in the carbon content of calcined nanohybrids, some carbon was lost at 500 ^{O}C because carbon burns off in air or nitrogen at 450 – 650 ^{O}C (Zhenga et al., 2003). This carbon lost is responsible for a slight variation in the calculated carbon content and that of the synthesised calcined nanohybrids. The result is similar when the weight ratio of CNT to TiO_2 in the hybrid was changed from 1:0.9 to 2:1 as

shown in Table 5.1 and Figure 5.4. A CNT-TiO$_2$ (wt. % ratio 0.9:1) was chosen for this research because it gave the highest photo response value compared to other CNT-TiO$_2$ nanohybrids of different ratios (Li, 2013). Also a CNT-TiO$_2$ (wt. % ratio 2:1) to ensure that the synthesis method employed is precise and to establish that the conclusions drawn from literature about CNT-TiO2 (wt. % 1:0.9) nanohybrid performance is reliable.
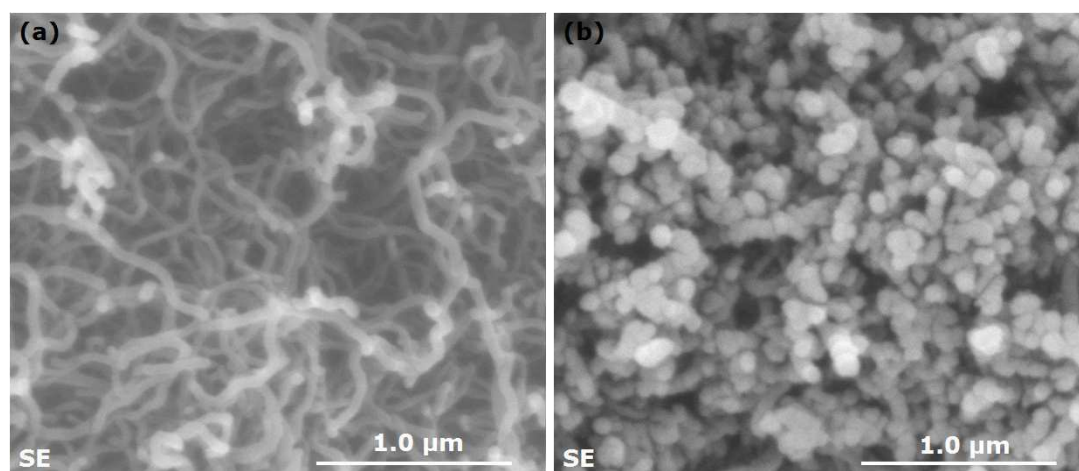
Figure 5.5: SEM images of (a) raw MWCNT and (b) calcined MWCNT-TiO$_2$ (wt. % ratio 1:0.9)

The SEM images of raw MWCNT, and calcined MWCNT– TiO$_2$ (wt. % ratio 1:0.9) hybrids are presented in Figure 5.5. Figure 5.5 (b) shows that the CNT surfaces is uniformly coated by TiO$_2$, which are also typical images of acid treated MWCNT and other synthesised hybrids used in this research. The images are similar to what was reported in literature (Li et al., 2011, Gao et al., 2009a, Li, 2013). This establishes the fact that nanohybrids were synthesised. However it is difficult to properly understand the structure of the hybrids, therefore TEM was used to obtain more detailed observations of the synthesised nanohybrids.

Figure 5.6 shows the TEM images of the synthesised MWCNT-TiO$_2$ hybrids, TiO$_2$ (P25), raw and acid treated MWCNTs. It is evident that TiO$_2$ particles are homogeneously distributed on the MWCNT in both synthesised hybrids; but nanohybrid of wt. % ratio 1:0.9 shows better homogeneous distribution.
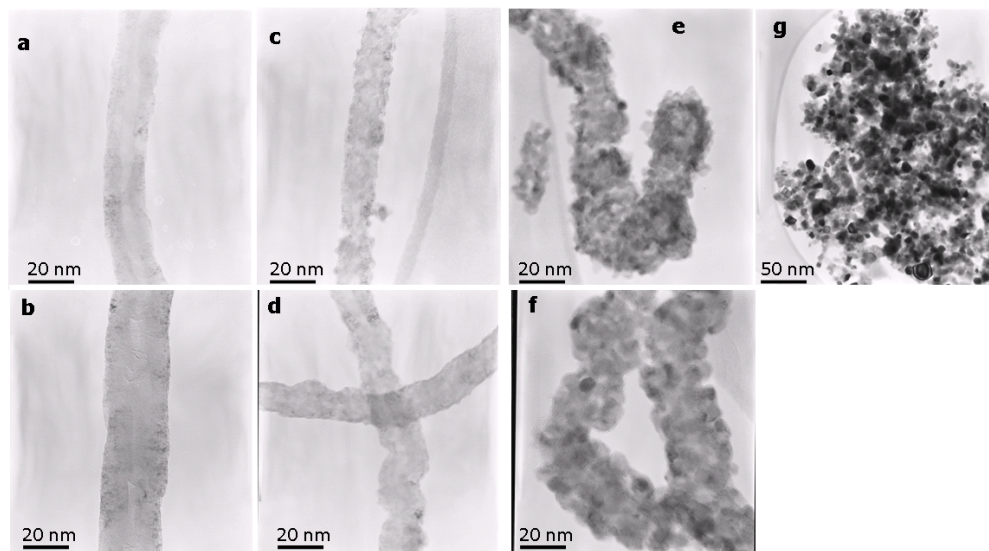
Figure 5.6: TEM images of (a) acid treated MWCNT (b) raw MWCNT (c) calcined MWCNT-TiO$_2$ (wt. % ratio 2:1) (d) uncalcined MWCNT-TiO$_2$ (wt. % ratio 2:1) (e) calcined MWCNT-TiO$_2$ (wt. % ratio 1:0.9) (f) uncalcined MWCNT-TiO$_2$ (wt. % ratio 1:0.9) and (g) TiO$_2$

TiO$_2$ is well known to have photocatalytic properties but its particles are agglomerated together as shown in Figure 5.6 (g), but good dispersion of small particles could provide more reactive sites for the reactants than aggregated particles. Therefore TEM results suggest that MWCNT-TiO$_2$ nanohybrid will possess greater photocatalytic activity than TiO$_2$ for the degradation of phenanthrene in produced water.

The electron diffraction pattern of each sample was also examined to determine the crystallinity and hence photocatalytic activities of the samples as presented in Figure 5.7. It is evident that TiO$_2$ is crystalline and

homogeneously covers the CNT in the synthesised MWCNT-TiO$_2$ (wt. % ratio 0.9:1) hybrid as the diffraction pattern of the TiO$_2$ is maintained in the hybrid (cf. Figure 5.7 b-d).
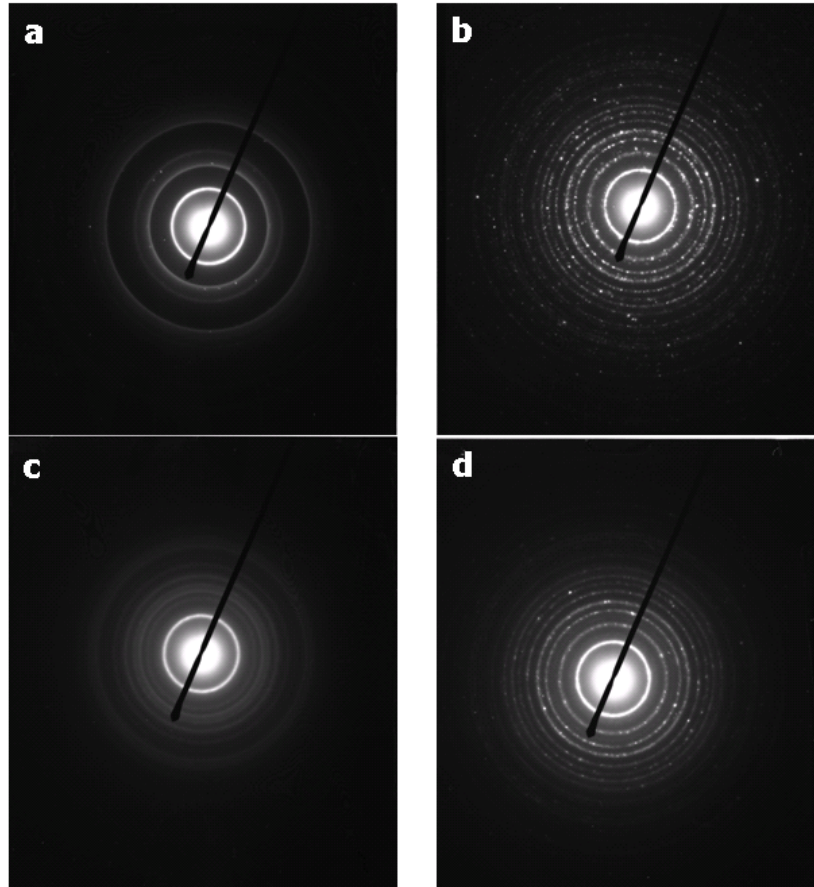
Figure 5.7: Diffraction patterns (at 200KV, 100cm) of (a) raw MWCNT (b) TiO$_2$ (c) MWCNT-TiO$_2$ (wt. % ratio 2:1) and (d) MWCNT-TiO$_2$ (wt. % ratio 1:0.9)

The recorded diffraction pattern of the hybrid is similar to what was obtained in previous studies for a good anatase crystal structure of TiO$_2$ spheres (Dai, 2006). The diffraction lines of TiO$_2$ were almost undetectable in the MWCNT-TiO$_2$ (wt. % ratio 2:1) hybrid as it shows a similar pattern to raw MWCNT (cf. Figure 5.7 a-b). This indicates that the CNT in MWCNT-TiO$_2$ (wt. % ratio 2:1), is not well covered by TiO$_2$, and will not be as good a photocatalyst as MWCNT-TiO$_2$ (wt. % ratio 0.9:1). SEM and TEM image analyses show that MWCNT-TiO$_2$ (wt. % ratio 0.9:1) hybrid features a good

homogeneous embedding of CNT in the TiO$_2$ matrix without apparent agglomeration of the TiO$_2$ particles.

The XRD analysis of the synthesised MWCNT-TiO$_2$ hybrids and raw MWCNT are presented in Figure 5.8. In the hybrid samples, peaks at 2θ = 25.35º, 38.05º, 48.05º, 53.95º, and 62.75º are due to anatase TiO$_2$ while peak at about 44.3º 2θ is due to machine error and is to be ignored. In the raw MWCNT sample peaks at 2θ = 25.75º and 42.85º are due to carbon peaks. The XRD patterns reveal that only anatase TiO$_2$ can be identified for in MWCNT-TiO$_2$ hybrids. The rutile (2θ = 35.15º, 54.96º, 44.54º and 61.34º) and brookite phases of TiO$_2$ were not observed. This further confirms that MWCNT-TiO$_2$ hybrid was successfully synthesised.
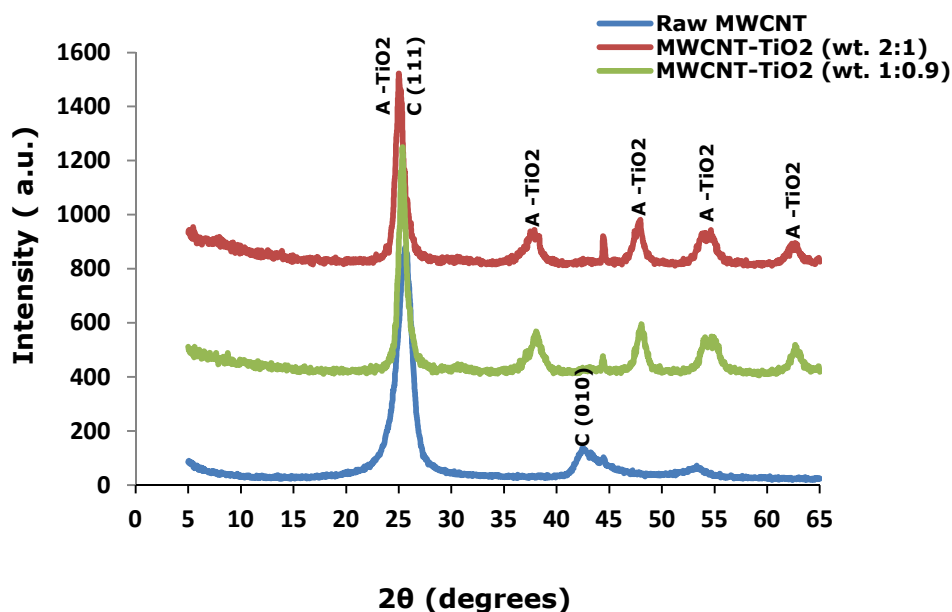
Figure 5.8: XRD patterns of MWCNT and MWCNT-TiO$_2$ hybrid

It was observed that no peaks from impurities existed in the XRD patterns of the MWCNT-TiO$_2$ hybrids, indicating the high purity of the hybrids. It should also be noted that the characteristic peaks of MWCNT can hardly be identified in the MWCNT–CNT hybrid. It could be considered that the small amount of carbon content in the nanohybrids and the disappearance of

MWCNTs characteristic peaks in the XRD patterns may indicate that the hybrid has no aggregated pores. These results are similar to what was obtained previously and reported in literature (Wang et al., 2005, Chen et al., 2011, Oh and Chen, 2008, Zhang et al., 2013). EDX spectra of the synthesised MWCNT-TiO$_2$ hybrid catalysts presented in Figure 5.9 (which is typical for all hybrids synthesised in this research) also confirm only the presence of C, O and Ti elements. The structure and morphology analysis therefore indicates that homogeneously coated MWCNT-TiO$_2$ hybrids were synthesised.

Element	Wt%	At%
CK	21.97	36.68
OK	36.73	46.03
TiK	41.29	17.29
Matrix	Correction	ZAF
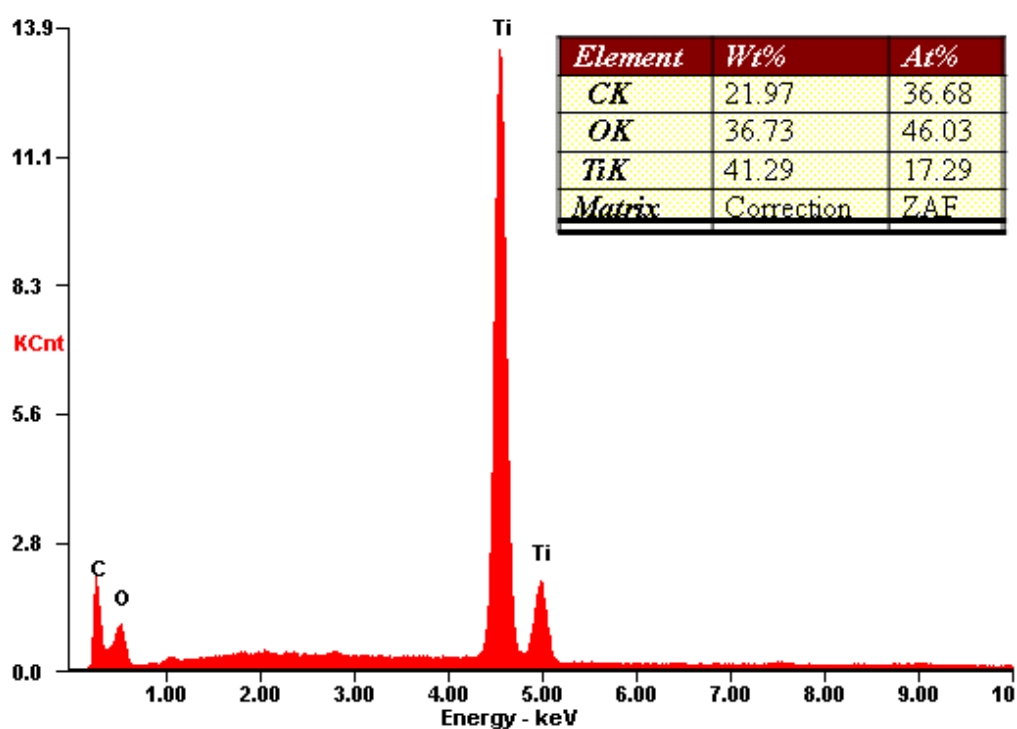
Figure 5.9: EDX spectra of synthesised calcined MWCNT-TiO$_2$ hybrid (wt. % ratio 1:0.9)

5.3.2.   BET surface area and pore distributions

The BET surface areas of neat TiO$_2$ and MWCNT are 53.4 m^2/g and 122.2 m^2/g respectively, while that of the hybrids vary between 5.7 m^2/g and 57.4 m^2/g (Table 5.2). These results suggest that TiO$_2$ introduced into CNT

matrix are dispersed on the surface of the MWCNT and could clog the pores of MWCNT which prevents TiO_2 particles from agglomeration, thus decreasing the surface area. The average pore sizes of different hybrids obtained from N_2 isotherm are also given in Table 5.2. Studies have shown that the pores in MWCNT can be divided into narrowly distributed inner hollow cavities (3 - 10 nm), narrowly distributed external walls cavities (10 - 20nm) and widely distributed aggregated pores of 20 – 100 nm formed by the interactions of isolated MWCNTs (Serp et al., 2003).

Table 5.2: Textural Properties of MWCNT, TiO_2 and MWCNT-TiO_2 hybrids

Samples	S_{BET} (m²/g)	Average diameter (nm)
TiO_2	53.4	21
Raw MWCNT	122.2	25
Calcined MWCNT-TiO_2 (wt. ratio % 1: 0.9)	5.7	16
Uncalcined MWCNT-TiO_2 (wt. ratio % 1: 0.9)	31.6	15
Calcined MWCNT-TiO_2 (wt. ratio % 2:1)	57.4	20
Uncalcined MWCNT-TiO_2 (wt. ratio % 2:1)	24.8	15

In this study, TiO_2 used has an average pore size of 21 nm, while the average pore size of the MWCNT was 25 nm which decreased greatly to about 16 nm and 20 nm in calcined MWCNT-TiO_2 hybrids containing weight percent ratios 1:0.9 and 2:1 respectively. It is considered that the average pore diameter of the hybrids decreased a lot and this indicates that TiO_2 are homogeneously distributed on the MWCNT. It should be noted from Table 5.2 that all surface textural parameters for the hybrids are considerably lower than that of pristine CNT due to surface structural modification by an increase in TiO_2 weight ratio. The absence of MWCNT aggregate pores in the calcined nanohybrids proves that a homogeneous coating of MWCNT by TiO_2 was achieved. This claim is supported by the disappearance of MWCNT characteristic peaks observed in the XRD patterns. Therefore a well coated nanohybrid was synthesised which can

act as a catalyst in a photoanodic process for the degradation of PAH in produced water.

5.4. Photocatalytic activity of CNT-TiO$_2$ hybrids

In an ordinary photocatalytic test performed at 25 $^{\circ}$C, a photoanode was made by forming a paste of 2.5 mg/cm^2 nanohybrid with Millipore water and loaded onto a titanium plate, which was then allowed to dry at room temperature for 12 hours. The response of the photoanode in light and dark conditions in PW I (cf. Table 3.3) was determined as presented in Figure 5.10.
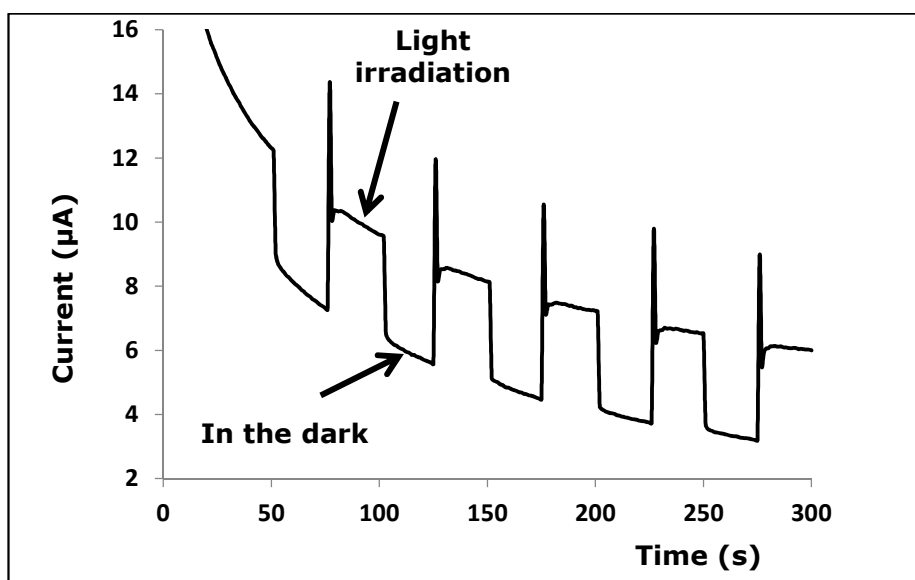
Figure 5.10: Chronoamperogram showing photocurrent generated by MWCNT-TiO$_2$ photoanode in PW I using a three electrode cell in dark and light at 0.125 V vs. Ag/AgCl (OCP)

Photocurrent was generated when the solar light was shone onto the electrode and a sharp decrease in the current was observed in the dark. This indicates that electrons and holes are generated on the photoanode. The sharp spikes on the graph correspond to the point when the light was switched on. The reason for this spike is not reported in literature however

this may be caused by the initial response following the excitation of electrons from the conduction band to the valence band of the TiO_2 semiconductor in the photoanode, however the recombination of some electron-hole pair might have led to a sharp decrease in the current since the full separation of electron-hole pair cannot be maintained. The consistent decrease in current may indicate a reaction on the surface of the photoanode or may be result from a non-equilibrium state between the surface of the photoanode and the produced water. There is no definite conclusion to this behaviour as it was observed each time every time the experiment (Figure 5.10) was carried out.

The photocurrent generated from the photoanode is significant because photocatalytic activity of MWCNT-TiO_2 often reported in literature is carried out by suspension of the powder catalyst in the solution (Zhou et al., 2010, Zhang et al., 2013, Zhang and Oh, 2010, Dai, 2006). However this experimental set-up is neat because the catalyst was immobilised in on a titanium plate (photoanode). Hence it eliminates the problem of catalyst powder clean-up after the reaction. This is a significant contribution to the industrial process of wastewater treatment using immobilized titania-based CNT hybrid photoanode. This experiment was repeated in PW I (cf. Table 3.3) containing 0.5 mg/L of phenanthrene and a similar increase in current was observed under irradiation with simulated sunlight. This was then repeated at different applied potential vs. Ag/AgCl using MWCNT-TiO_2 photoanode and TiO_2 photoanode. It was observed that the photocurrent generated increased with increasing applied potential.

In Figure 5.11 the difference in the current generated in light and dark conditions are plotted against the applied potential. It is evident from the result that the MWCNT-TiO_2 (wt. % ratio 1:0.9) photoanode shows the best photocatalytic response and its photocurrent increased with increasing applied potential. This increase is due to the separation of the

photogenerated electron-hole pair by the applied potential. The applied potential creates an electric field region between the conduction band and the valence band in the TiO$_2$ which reduce the rate of electron-hole recombination, hence higher photocurrent generation. This electron-hole separation is improved with increasing applied potential. The photocurrent generated on the MWCNT-TiO$_2$ (wt. % ratio 1:0.9) photoanode is better than that obtained for TiO$_2$ and MWCNT-TiO$_2$ (wt. % ratio 2:1) photoanodes.
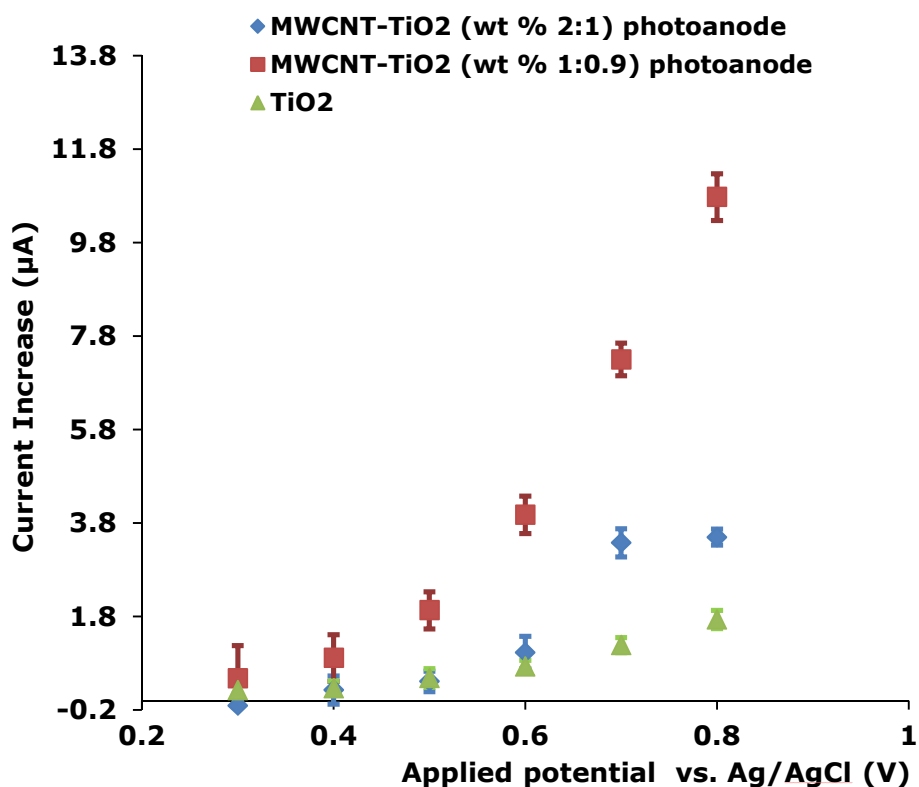
Figure 5.11: Comparison of photocatalytic response of 2.5 mg/cm^2 of MWCNT-TiO$_2$ (wt. % ratio 1:0.9) photoanode with 2.5 mg/cm^2 of MWCNT-TiO$_2$ (wt. % ratio 2:1) photoanode and 2.5 mg/cm^2 of TiO$_2$ in PW I, containing 0.5 mg/L phenanthrene

Therefore MWCNT-TiO$_2$ (wt. % ratio 1:0.9) photoanode shows a better photocatalytic activity than other photoanodes tested in PW I and PW I

191

containing organic pollutants. This is consistent with the discussions in section 5.3. Figure 5.11 also suggests that there is an optimum applied voltage to enhance the separation of photogenerated electrons-hole pair beyond which applied potential has no significant effect on photocatalytic activity. When the applied voltage was > 0.7V vs. Ag/AgCl, there was no increase in the photocurrent generated on the MWCNT-TiO$_2$ (wt. % 2:1) photoanode which was not the case for MWCNT-TiO$_2$ (wt. % 1:0.9) photoanode at this condition. This suggests that the optimum potential for MWCNT-TiO$_2$ (wt. % 2:1) photoanode has been reached. Therefore the photocatalytic activity of MWCNT-TiO$_2$ photoanode is also a function of applied potential and CNT to TiO$_2$ ratio.

5.5. Photocatalytic degradation of phenanthrene in produced water

The catalytic activity of MWCNT-TiO$_2$ (wt. % ratio 1:0.9) photoanode has been established as discussed in section 6.4. In this section its ability to remove phenanthrene from produced water is examined. Previous works on the photocatalytic degradation of phenanthrene was carried out in organic solvents because the solubility of phenanthrene is very low (0.6 - 1.6 mg/L) in water (Chae and Chen, 2012, Chen, 2013, Gong et al., 2005, Zhang et al., 2003). There is little or no attention given to phenanthrene dissolved in water even though environmental impact of dissolved PAH as low as 2 ppb is very significant as discussed in Chapters 1 and 2. Therefore the novelty of this study is that it focuses on the photocatalytic degradation of dissolved phenanthrene at extremely low concentrations in produced water. A calibration curve was obtained after measuring the absorbance of different concentrations of dissolved phenanthrene in water using UV-Vis spectrophotometer.
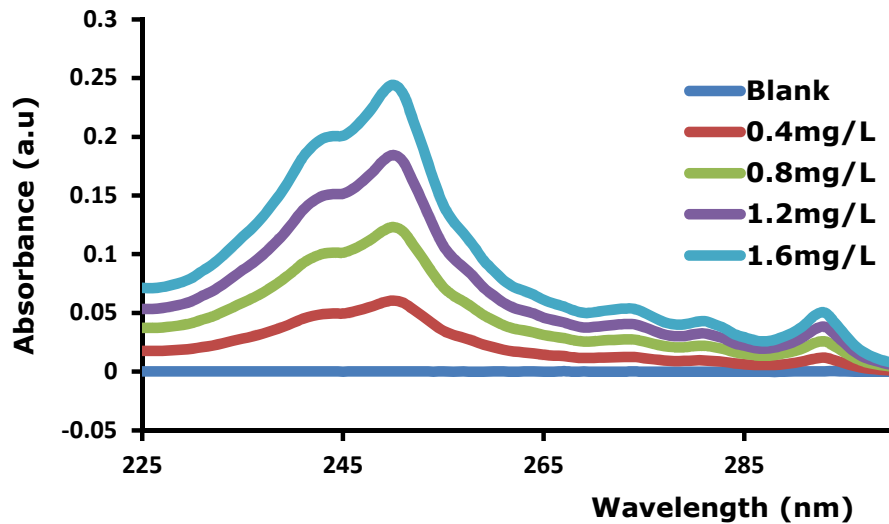
Figure 5.12: UV-Vis absorbance spectra of different concentrations of dissolved phenanthrene in Millipore water
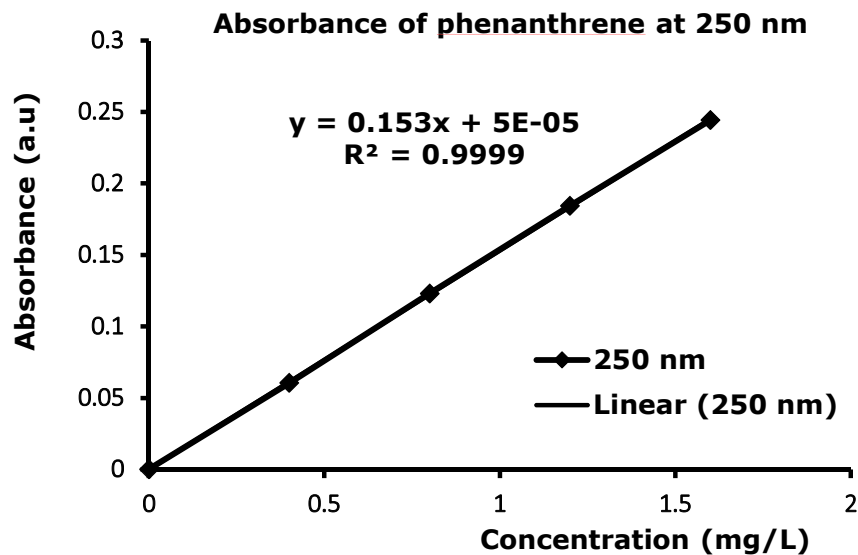
Figure 5.13: Calibration of dissolved phenanthrene concentration in water measured by UV-Vis spectrophotometer

Phenanthrene peak appears at 250 nm in both Millipore water and synthetic produced water as presented in Figure 5.12. Figure 5.13 shows a calibration curve obtained for dissolved phenanthrene in water based on the absorbance value obtained in Figure 5.12 at 250nm. The calibration shows a straight line (R^2 = 0.9999) passing through zero. This indicates

193

that we can reliably trust the results of subsequent phenanthrene degradation in water or synthetic produced water.

Photocatalytic degradation of phenanthrene dissolved in synthetic produced water on MWCNT-TiO$_2$ (wt. % 1:0.9) photoanode was measured at different starting concentrations as shown in Figure 5.14. It is important to note that at least 20% of dissolved phenanthrene concentration was removed after 10 minutes of irradiation with simulated sunlight. This confirms that dissolved phenanthrene may be removed from produced water via photocatalysis. The photogenerated holes attack the adsorbed water on the photoanode to form hydroxyl radicals which in turn oxidise phenanthrene.
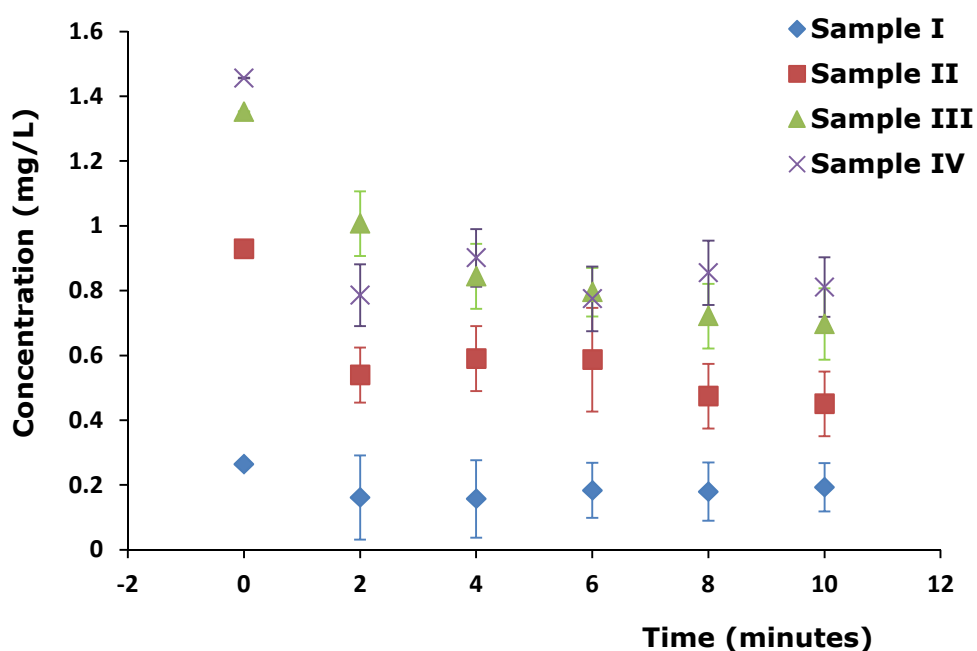
Figure 5.14: Photocatalytic degradation of phenanthrene dissolved in synthetic produced water, PW I, after irradiation of 2.5 mg/cm^2 of MWCNT-TiO$_2$ (wt. % 1:0.9) photoanode with simulated light at an applied potential of 0.125 V vs. Ag/AgCl

The oxidation of oxygen or chlorine on the anode is remote because the energy levels of the holes in the valence band are more positive than those of Cl-/Cl$_2$ of H$_2$O/O$_2$. It should be noted that after 2 minutes of irradiation

about 40% of the phenanthrene appeared to have been removed from the produced water. However this percentage then decreases before it then starts to increase again as can be seen at the starting phenanthrene concentrations of 1.46 mg/L and 0.8 mg/L in Figure 5.14.

This suggests that the phenanthrene was first adsorbed onto the MWCNT-TiO_2 photoanode prior to photocatalysis. It was observed that after the first two minutes the rate of degradation then appears to be slower. This is consistent with the arguments made in literature that pollutants are first adsorbed on CNT-TiO_2 before degradation (Turchi and Ollis, 1990, Chatterjee and Dasgupta, 2005). This is very interesting because it means the translational mobility of phenanthrene molecules is considerably reduced. This potentially extends the range of excitation energies of the photoanode into the visible region, thereby making a more complete use of the solar energy and hence enhancing the photocatalytic process. The adsorption of phenanthrene onto the photoanode was confirmed by EDX measurement of the carbon content of the photoanode after various degradation times as presented in Table 5.3.

Table 5.3: Carbon content of MWCNT-TiO_2 (wt. % ratio 1:0.9) photoanode after degradation of phenanthrene obtained from EDX

Time(minutes)	Carbon (wt. %)
0	36.68
2	70.89
4	43.86
8	42.72
10	39.59
15	36.72
30	39.59

The increase in carbon content in the photoanode after 2 minutes of the experiment as shown in Table 5.3 can be attributed to the adsorption phenanthrene. This result is consistent with the degradation of phenanthrene presented in Figure 5.14 indicating that adsorption of

phenanthrene onto the photoanode is very key to its degradation. Since phenanthrene is a hydrocarbon, it is expected that the carbon content will increase if it is adsorbed into the photoanode. The carbon content had increased by about 100% after 2 minutes, which indicates that the MWCNT-TiO$_2$ (wt. % ratio 1:0.9) photoanode has excellent surface area and pore volume for the adsorption of so much phenanthrene after 2 minutes.
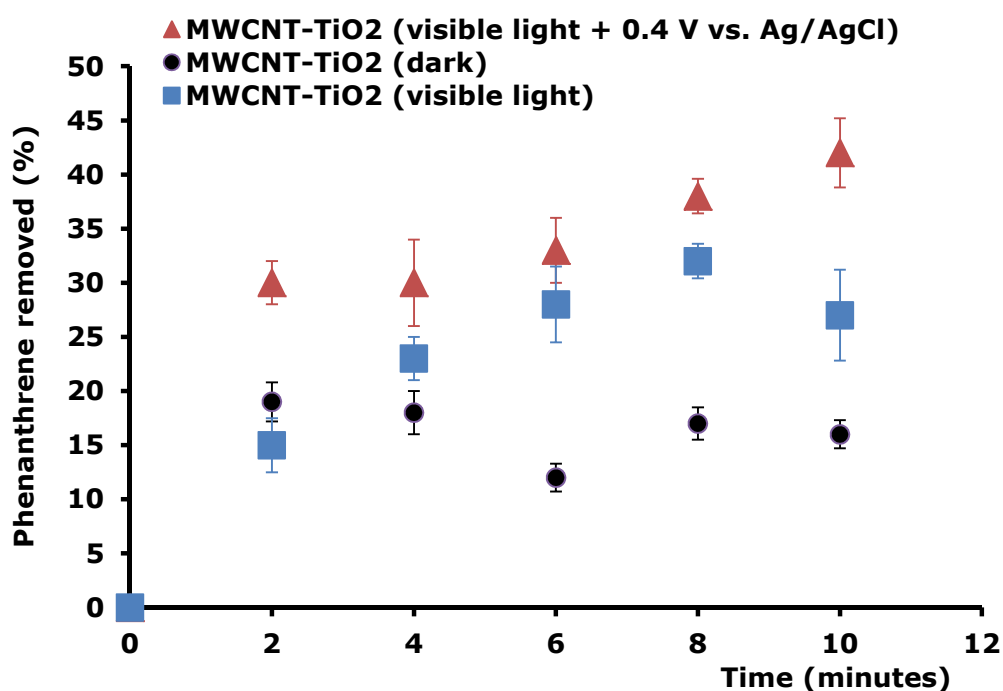
Figure 5.15: Effect of MWCNT-TiO$_2$ on degradation of dissolved phenanthrene in synthetic produced water under only visible light, only dark, and in visible light with applied potential.

The percentage of phenanthrene that can be removed from produced water increases with time and as the applied potential increases as presented in Figure 5.15. In the dark, it appears phenanthrene is only removed by adsorption onto the photoanode. Its percentage removal remained constant which suggests there is nothing practically happening in the dark other than adsorption.

However when the photoanode is irradiated with solar light there is a steady increase in percentage of phenanthrene removed, which suggests that phenanthrene degradation happens via photocatalytic degradation. By applying 0.4 V vs. Ag/AgCl potential to the system under light the percentage of phenanthrene removed increased as shown in Figure 5.15. This result is consistent with what is reported earlier in Figure 5.11. Therefore phenanthrene degradation can happen via a photocatalytic or a photoelectrocatalytic process however photoelectrocatalytic process is more efficient. The percentage of phenanthrene removed after 30 minutes of irradiation with simulated sunlight (with and without applied potential)from the produced water was practically the same with the highest percentage removal obtained within the first 10 minutes of reaction. This may be due to loading effects of the photoanode.

Element	Wt%	At%
CK	22.24	40.12
OK	27.39	37.09
TiK	50.38	22.79
Matrix	Correction	ZAF
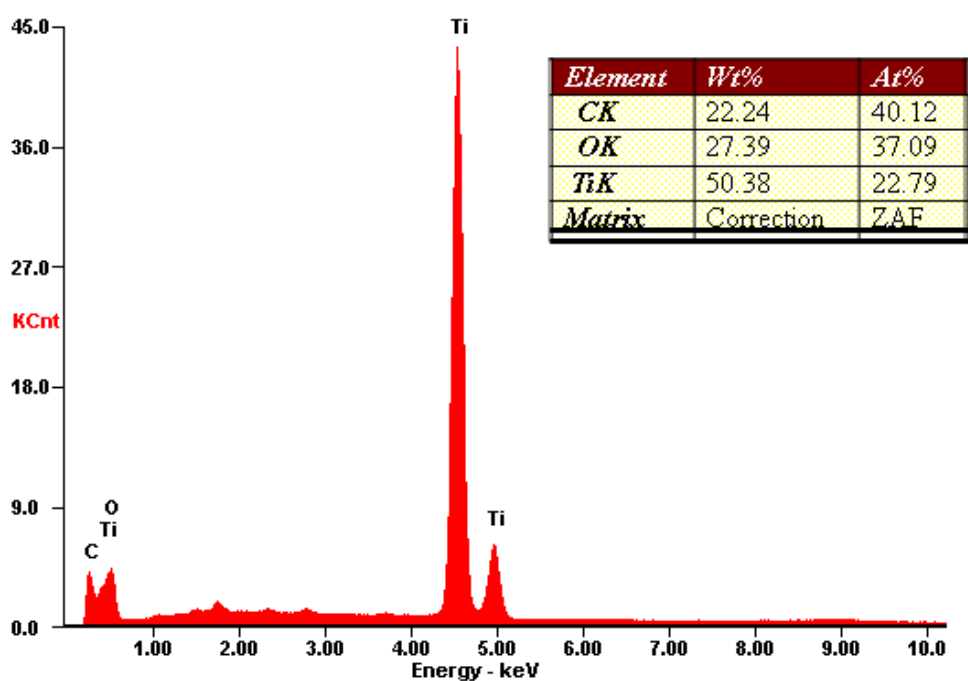
Figure 5.16: EDX spectra of MWCNT-TiO$_2$ photoanode after 18 hours of irradiation with visible light in synthetic produced water, PW I

It is possible that a loading of 2.5 mg/cm^2 was too small for the reaction or that there was degradation of MWCNT-TiO$_2$. The latter is most likely to have occurred because after 18 hours of irradiation under visible light the carbon content of the photoanode measured using EDX shows a weight percent of 22.24 % (Figure 5.16) down from the initial 36.68 % recorded before the experiment. In this research the effect of MWNCT-TiO$_2$ catalyst loading and electrode surface area were not fully examined, although it is expected that an increase in surface area and loading will lead to an increase in photocatalytic degradation of phenanthrene. On the other hand, an excess of phenanthrene adsorbed into the photoanode may have inhibited the transport of electrons and increased the probability of electron trapping by the crystal defects. Moreover, the shielding and scattering effects of excess carbon in the pores of the photoanode might have prevented the photo absorption of other visible light active species (e.g. by-product of phenanthrene photo-decomposition) since there is an optimal carbon loading at which the generated photocurrent can be maximized (Zhang et al., 2009a).

5.5.1. Mechanism of photocatalytic degradation of phenanthrene in produced water

As explained below in this section, there are three predominant steps involved in the photocatalytic degradation of phenanthrene on MWCNT-TiO$_2$ photoanode under visible light in synthetic produced water. First, the MWCNTs absorb over almost the entire visible light spectrum and act as photosensitizers, endowing the MWCNT-TiO$_2$ photoanode with an electron transfer mechanism similar to that of dye-sensitized TiO$_2$ (Richards et al., 2012, Bisquert et al., 2002). The excited electrons from the MWCNTs are transferred to the conduction band of the TiO$_2$ when illuminated with sunlight, thereby increasing the photocurrent. Secondly, the conductivity of

MWCNTs is superior to that of TiO_2; therefore, a high transport rate of electrons in the MWCNT-TiO_2 photoanode is expected. Thirdly, the MWCNT-TiO_2 photoanode possesses high surface areas, pore sizes, and pore volumes, which enhanced visible light absorption and interfacial charge transfer, thereby improving the efficiency. This accounts for the synergetic effect induced by MWCNT in the photoanode. Therefore phenanthrene degradation can be attributed to both the effects between photocatalysis of the supported TiO_2 and adsorptivity of the MWCNTs.

It was difficult to track the photo-products of phenanthrene degradation in synthetic produced water because the medium was not an organic solvent. Therefore GC-MS analysis was not done for this work. However no other peak was noticed when the effluent produced water was analysed using UV-Vis spectroscopy. The major intermediate products identified during photocatalytic degradation of phenanthrene reported in literature are 9,10,-phenanthrenquinone, (a group of hydroxyphenanthrene), 2,2'-biphenyldialdehyd, 2,2'-biphenyldicarbonic acid and 2-biphenylbenzaldehyde (Wangl et al., 1995). Since none of these products was identified via UV-Vis spectroscopy in this work, it can be concluded that the toxicity of dissolved phenanthrene in produced water can be reduced significantly via photocatalysis or photoelectrocatalysis using MWCNT-TiO_2 (wt. % ratio 1:0.9) photoanode.

5.6.   Conclusion

In this chapter we have established that for a good dispersion of MWCNT in a highly concentrated MWCNT aqueous suspension using anionic surfactant (NaDDBS), a CNT to NaDDBS concentration ratio of 1:0.29 and ultrasonication at 250KJ is required. The optimum CNT/mL H_2O concentration at this condition was determined to be 7.5mg/mL. The MWCNT-TiO_2 nanohybrids synthesised at this conditions via a modified sol-

gel method are homogeneously coated. The photocatalytic property of the MWCNT-TiO$_2$ (wt. % ratio 1:0.9) was found to be superior to MWCNT-TiO$_2$ (wt. % ratio 2:1) and TiO$_2$. Degradation of dissolved phenanthrene in synthetic produced was successfully carried out on MWCNT-TiO$_2$ (wt. % ratio 1:0.9) photoanode under irradiation by simulated sunlight, and this process was improved by applied potential. This proves that independently the photoanode of the proposed PEC cell can remove up to 45% dissolved phenanthrene from produced water in 10 minutes. These results are very impressive and form the basis of the design of the PEC cell discussed in Chapter 6.

Chapter 6: The photoelectrochemical cell

6.1. Introduction

In Chapters 4, it was demonstrated that multiple heavy metals can be removed from synthetic produced water, and in Chapter 5 that when made into a photoanode, the MWCNT-TiO$_2$ hybrid possesses photo-electro-catalytic activity towards degradation of dissolved phenanthrene, which is a typical polycyclic aromatic hydrocarbon (PAH), in produced water. In this chapter the combination of both methods used in Chapters 4 and 5 into a single dual purpose photoelectrochemical (PEC) cell is presented (which demonstrates the novelty of this research). In section 6.2 the principle of the dual purpose PEC for the simultaneous removal of heavy metals and PAH is discussed. The details of the PEC cell are presented in section 6.3, and the experimental results demonstrating the removal of heavy metals and phenanthrene in PEC cell are presented and discussed in sections 6.4 - 6.8.

6.2. Principle of dual purpose PEC cell

Light energy can be utilised as additional energy for reactions in a PEC cell, but it can also be stored as chemical energy when ΔG>0. In this system, light energy can trigger nonspontaneous reactions if the electrochemical potentials of two redox couples (e.g. O/R and O'/R') are located between the conduction band minimum (CBM) and the valence band maximum (VBM) of a semiconductor. Figure 6.1 shows a PEC cell where the electrochemical potential of one of the redox couples is more negative than the semiconductor's CBM. Under dark condition (Figure 6.1 (a)); a depletion layer (a space charge region) is formed within the semiconductor near its surface due to the electrochemical potential difference between the semiconductor and the redox (O/R) in the electrolyte.
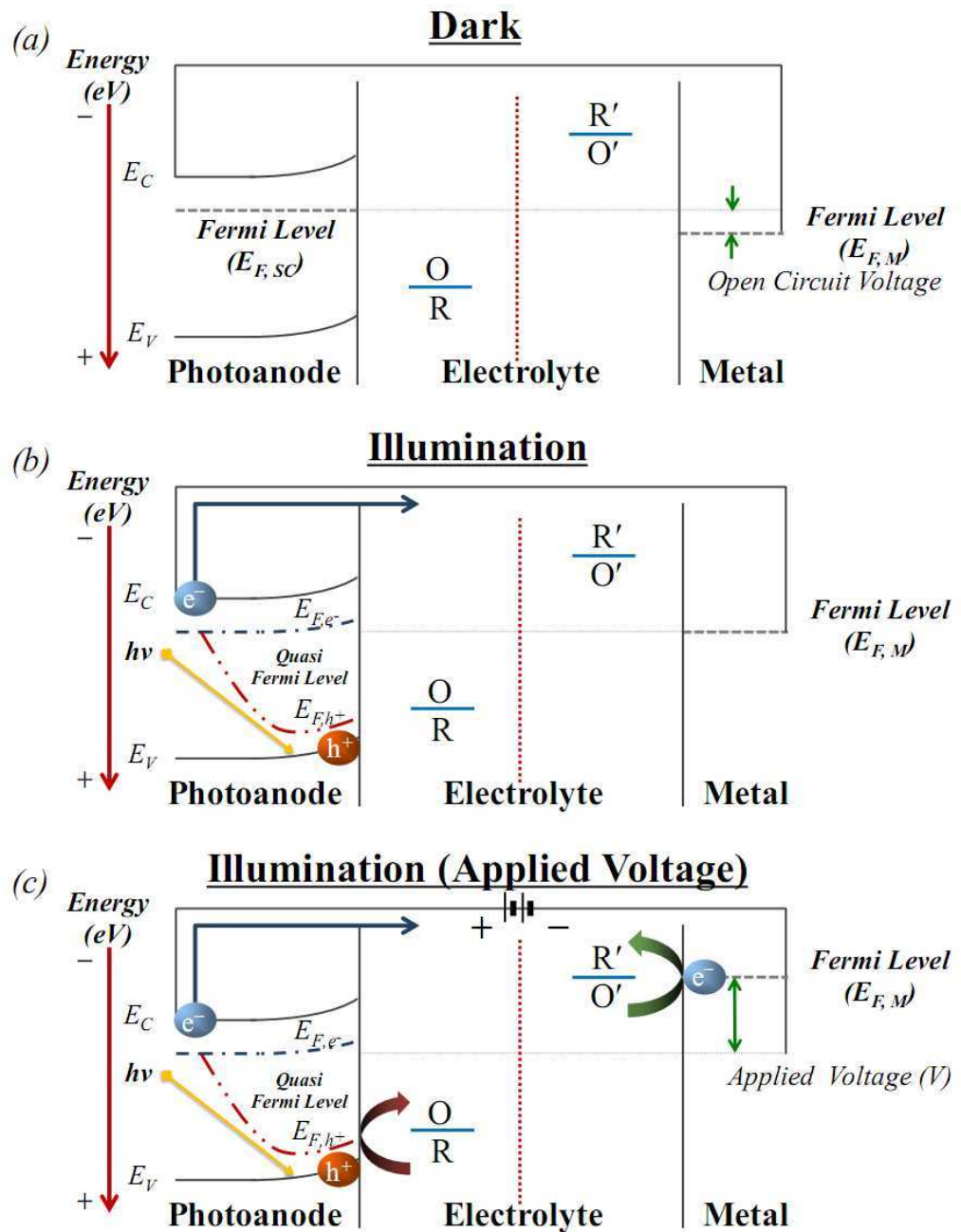
Figure 6.1: A schematic representation of a PEC in different situations (Kim et al., 2014)

Under illumination, electron-hole pairs are created in the semiconductor by optical energy. However, only those generated within the space charge region can be effectively separated by the electric field across the space charge region. The addition of charge carriers (electrons and holes) in the depletion layer leads to a concentration gradient over the semiconductor,

forming a diffuse layer. Therefore, a current will flow due to a combined effect of drift and diffusion by photogenerated electrons which are in turn collected at the counter electrode.

The creation of charge carriers by illumination can disturb a system at equilibrium. Under this condition, a semiconductor's Fermi level ($E_{F,SC}$) is no longer able to describe carrier populations. Thus, a quasi-Fermi level (E_{F,e^-} and E_{F,h^+}) for each charge carrier should be taken into consideration (Gerischer, 1977). E_{F,e^-} and E_{F,h^+} are the same as $E_{F,SC}$ in the bulk of a semiconductor. However, they start to deviate as carrier density within the space charge region changes under illumination. Due to the low minority carrier density of a n-type semiconductor, the addition of photo-generated holes induces a drastic change in E_{F,h^+} as shown in Figure 6.1 (b). This shows that illumination does not induce a continuous photocurrent across the circuit.

In this system, the electrochemical potential of photogenerated electrons that have been transferred to the counter electrode is not negative enough to reduce O′ to R′. The electrons are just accumulated at the counter electrode leading to an increase of metal Fermi level ($E_{F,M}$), which gives a limited capacitive current until the system reaches a new equilibrium. That is, some amount of light energy can be stored as electrical energy and the stored energy could be utilised for a desired reaction with an extra electrical energy as shown in Figure 6.1 (c). The MWCNT in the photoanode acts as a scavenger to limit the recombination of the photogenerated electron-hole pair as discussed in Chapters 2 and 5.

6.3. PEC cell design

The materials of construction selected for the PEC cell were selected to meet certain requirements including ability to withstand a certain range of

temperatures, chemical inertness to solvents and reactants, excellent rigidity and durability. Optical transparency was also a highly desirable property because it allows direct observation of the electrodes and solution. Based on the criteria mentioned above, a cubic PEC cell with a quartz window was designed and constructed as illustrated in Figure 6.2.
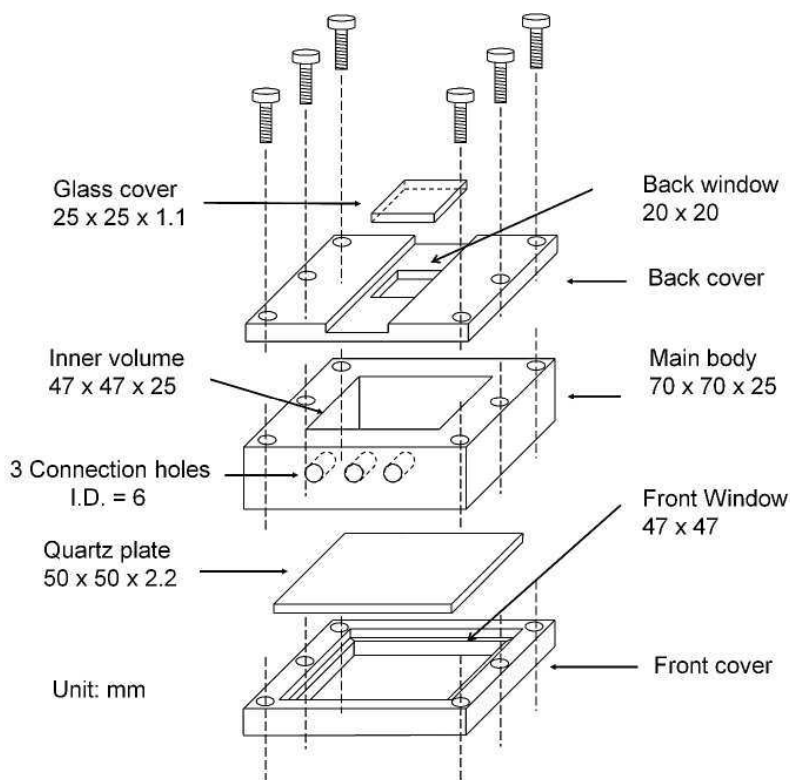
Figure 6.2: Design drawing of a proposed PEC cell (Li, 2013)

The reactor, which was made of PTFE, consisted of three parts including the front cover, the main body and the back cover. These parts were held together by a total of twelve plastic screws, six in the front and six at the back. The cell was sealed with two O-rings made of silicone to prevent electrolyte leakage from the reactor, and the quartz plate and glass cover were also fixed by silicone. This sandwich-type assembly allowed great flexibility to dismantle for cleaning and maintenance and for later modifications as interchangeable parts could be readily made and installed

for different purposes. For example, a second compartment could be added easily for dual chamber experiments.
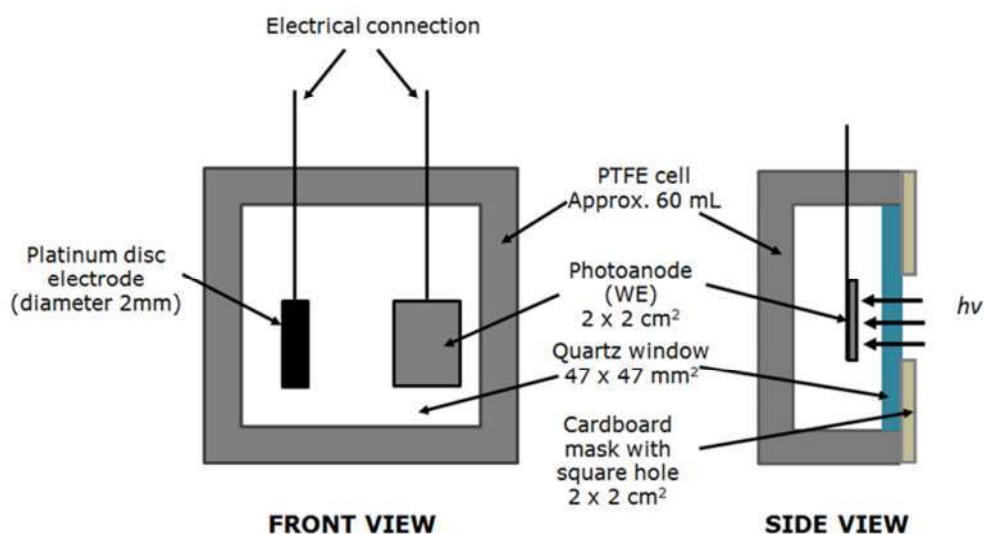
Figure 6.3: Schematic diagram of the PEC cell used for produced water treatment

The reactor has three holes with a diameter of 6 mm on the top of the cell, which allow the two electrodes to be inserted and in turn connected to the potentiostat as illustrated in Figure 6.3. The third hole serves as a sampling channel from where the electrolyte could be extracted out. It may also serve as a point where the electrolyte could be purged by an inert gas. Although the proposed PEC cell configuration is similar to a previously reported photocatalytic cell, there are differences in the electrodes arrangements, the type and dimensions of the photoanode (Figure 6.3), the source of light, the electrolytes employed and the aim of research.

6.4. Determination of metal deposition potentials in the PEC cell

Cyclic Voltammetry (CV) was carried out to determine the deposition potential of heavy metals in synthetic produced water, PW VI (cf. Table 3.3), containing 1.6 mg/L dissolved phenanthrene. Figure 6.4 shows the CVs obtained from different configurations of a two-electrode cell. The

cathode (platinum disc electrode) had a diameter of 2 mm and the dimensions of the photoanode (MWCNT-TiO$_2$) were 2 cm x 2 cm with a loading of 2.5 mg/cm^2. A Pt - graphite configuration was also used to monitor the experiment. These selections were based on the results discussed in chapters 4 and 5. The electrode voltage scan started from 0 V and was reversed at -1.2 V when all of the metal deposition voltages have been obtained. As shown in Figure 6.4, the deposition voltages of metals were the same in both Pt-graphite and Pt-Photoanode configurations (dark condition).

In dark condition the deposition of copper [Cu(I)/Cu(0)] occurred around -0.57 V showing a peak at -0.61 V, and lead deposition (Pb(II)/Pb(0)) occurred around -0.88 V showing a peak at -0.94 V. It was difficult to determine the exact deposition voltage of iron and nickel but there was a small plateau around -0.81 V which indicated deposition of nickel or iron may have occurred. During the return scan, oxidation peaks were observed at −0.79 V, -0.73 V, and −0.44 V, corresponding to oxidation of lead, nickel and copper deposits on the platinum electrode respectively.

There is a positive shift in heavy metals deposition voltages when the Pt - Photoanode configuration was irradiated with simulated sunlight. Under irradiation the deposition of copper [Cu(I)/Cu(0)] occurred around -0.52 V showing a peak at -0.57 V, lead deposition (Pb(II)/Pb(0) occurred around - 082 V showing a peak at - 0.88 V and nickel disposition occurred around - 0.79 V. During the return scan, oxidation peaks were observed at −0.77 V, -0.71 V, and − 0.44 V which can be attributed to oxidation of lead, nickel and copper deposited on the platinum electrode respectively. It is worth mentioning that these metal ions are only stable as complexes as shown in chapter Appendix A.

It is important to note that the behaviour of metal deposition was similar in both light and dark conditions; however a voltage shift of about 40 mV was observed when the Pt-Photoanode cell was irradiated with solar light. This may be attributed to photogenerated electrons on the photoanode as illustrated in Figure 6.1. The light energy leads to photogenerated electrons-holes pairs in the TiO_2, which are separated by the aid of MWCNT in the photoanode. The photogenerated electrons then travel through the circuit to the cathode (platinum); hence there is an increase in the electron density at the Pt-electrolyte (PW VI) interface leading to an improved metal deposition in terms of quantity and energy supplied.
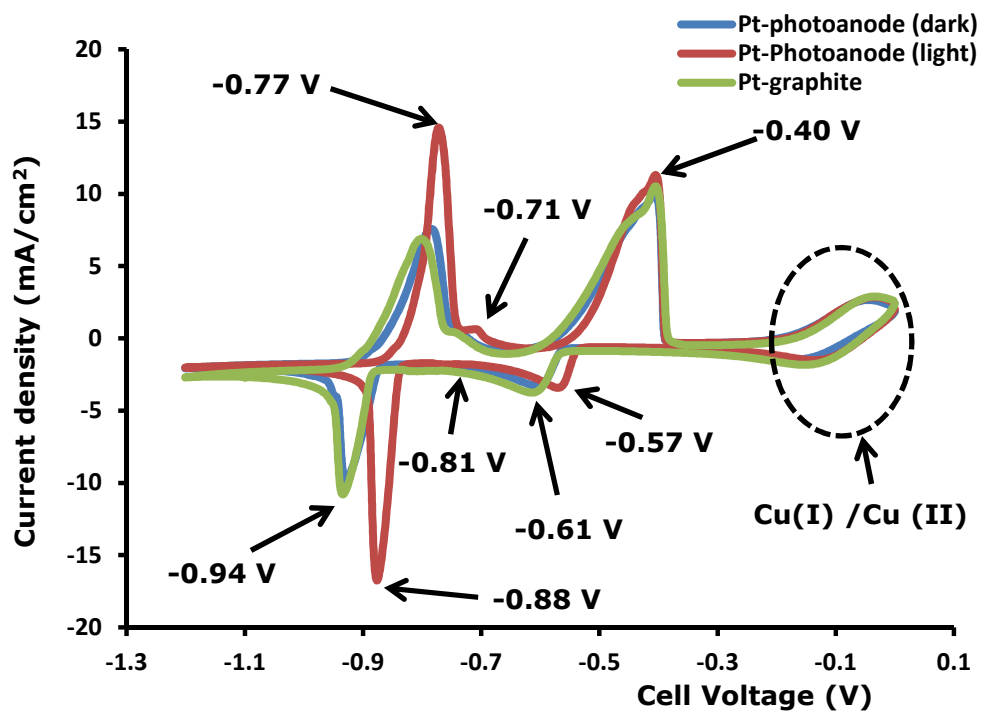
Figure 6.4: Cyclic voltammogram of PW VI containing 1.6 mg/L of phenanthrene at 20 mV/s electrode potential scan rate and pH 4 in a PEC of different cell configurations

CVs were also recorded to determine the deposition voltages of individual heavy metals in PW II – PW VI (where each type of produced water contained 1.6 mg/L dissolved phenanthrene). The results obtained in all

cases are similar to what is presented in Figure 6.4. However the voltage shift observed when individual metal ions were present in synthetic produced water increased to about 120 mV as illustrated in Figure 6.5.

This shift is particularly beneficial for metal electrodeposition since it makes cathodic reactions more favourable to occur. The increase in voltage shift may be attributed to the fact that the photogenerated electrons are now available for the reduction of just a single metal ion unlike the case in Figure 6.4 where multiple metal ions (Pb^{2+}, Fe^{2+}, Ni^{2+} and Cu^{2+}) depended on the same amount of photogenerated electrons.
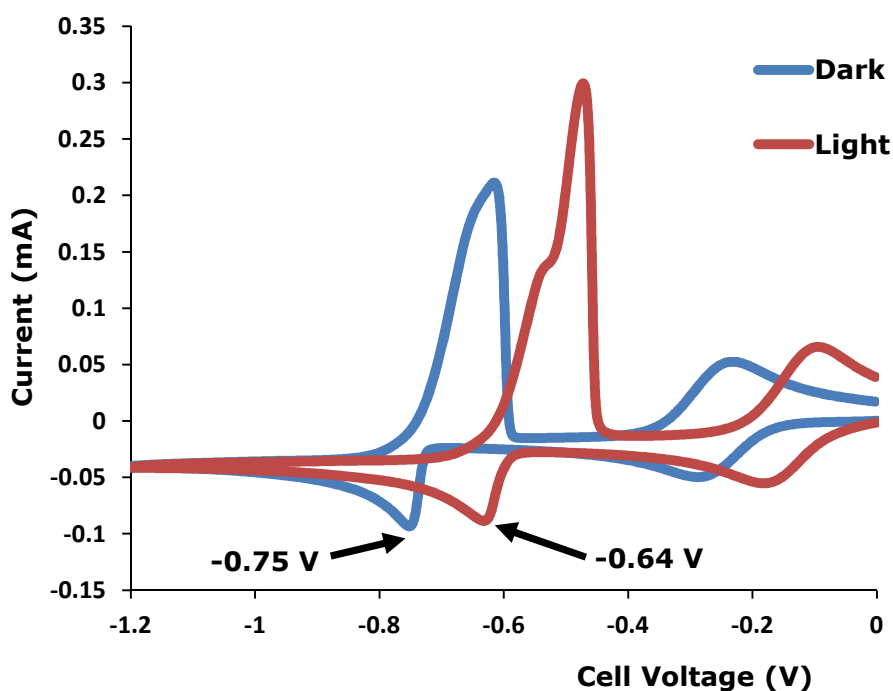
Figure 6.5: Cyclic voltammogram of PW VI containing 1.6 mg/L of phenanthrene conditions at 20 mV/s Pt/CNT-TiO$_2$ electrode potential scan rate and pH 4 in a PEC cell under light and dark.

Although the voltage shift when only Cu(I) was present in produced water increased from 40 mV to 120 mV, the deposition voltage of copper in the dark shifted negatively from -0.69 V to -0.75 V. This suggests that in a PEC

cell for produced water treatment, the concentration of phenanthrene and other metal ions affects metal deposition. This effect is examined later in this chapter. However it was generally observed that the deposition of heavy metals occurred at lower cell voltages in synthetic produced water containing phenanthrene and multiple heavy metal ions.

6.5. Electrodeposition of heavy metals from produced water in the PEC cell

Electrodeposition of heavy metals in the PEC cell was tested at cell voltages 0.7 V, 1.0 V and 1.2 V in dark and light conditions to confirm the data obtained in Figure 6.4. At 0.7 V, only copper was deposited on the platinum electrode surface whereas at both 1.0 V and 1.2 V copper, nickel and lead were deposited as shown in Figure 6.6.
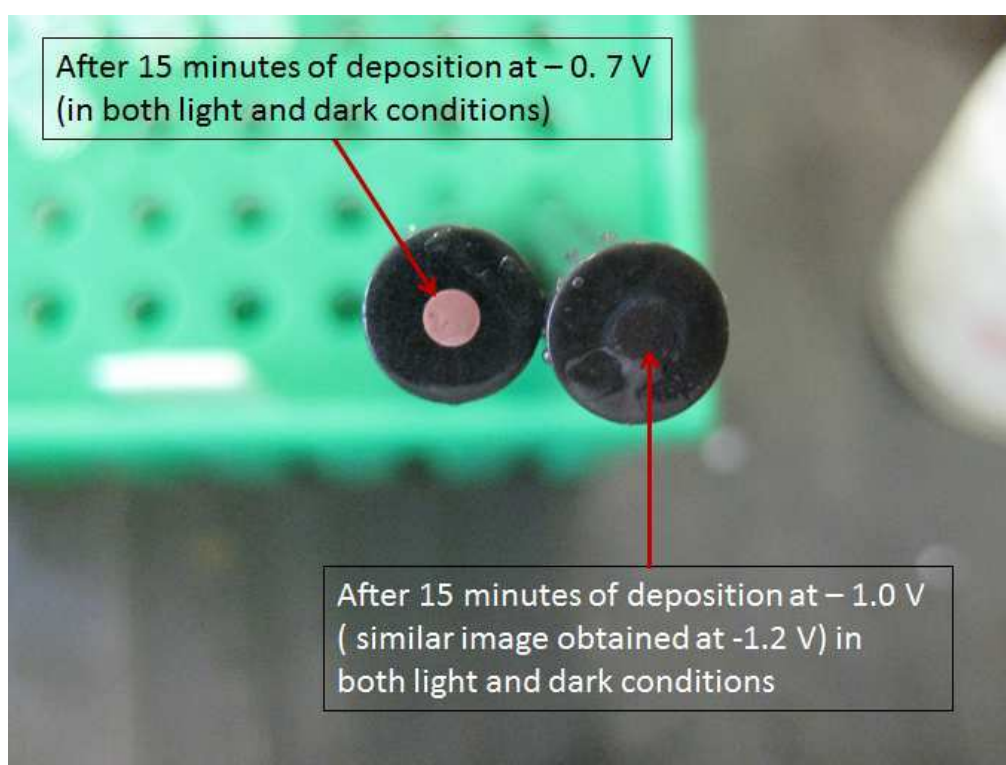
Figure 6.6: Effect of applied voltage on metal deposition from PW VI containing 1.6 mg/ L of dissolved phenanthrene

The current-time plots obtained for heavy metal deposition at cell voltage 1.0 V and 1.2 V are presented in Figure 6.7. The Pt-graphite configuration showed similar deposition curve as the Pt-photoanode configuration (dark condition). However, when the Pt-Photoanode configuration was irradiated with light there was an increase of 1.2 mA/cm^2 in the current density. This suggests that without solar light the quantity of a mixture of heavy metals that can be deposited from synthetic produced water in a PEC cell is significantly diminished.
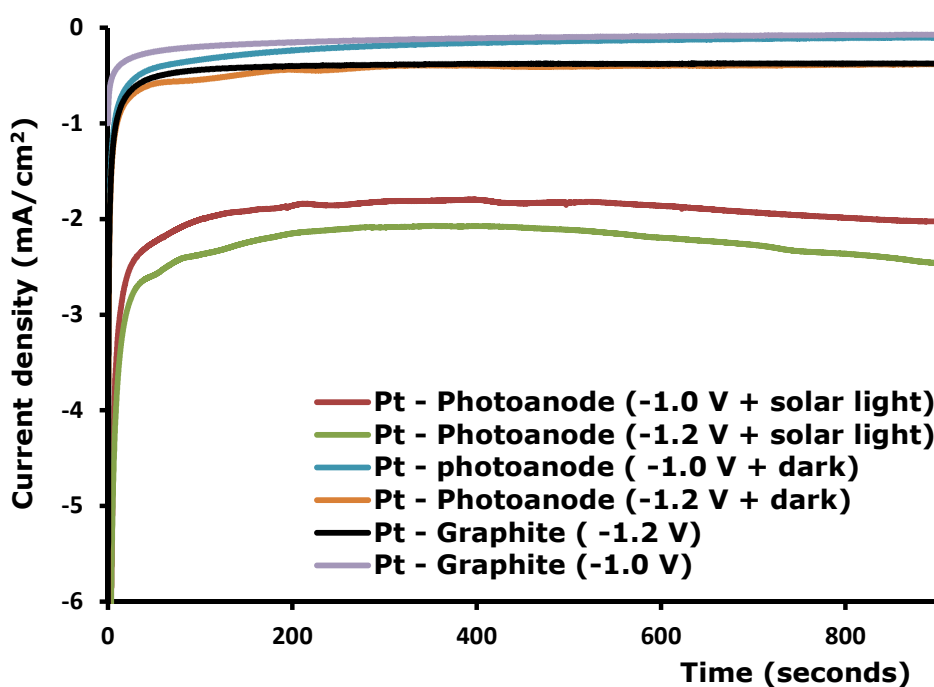
Figure 6.7: Chronoamperograms of PW VI containing 1.6 mg/L of phenanthrene in a Pt/CNT-TiO$_2$ PEC cell at applied cell voltages of 1.0 V and 1.2 V and pH 4 compared to conventional Pt- graphite cell

Although heavy metals can be removed from produced water, the energy required for their removal can be drastically reduced by the use of the dual purpose PEC cell irradiated with solar light, because the required cell voltage can be lowered by as much as 60 % than what is obtainable in a

conventional Pt-graphite configuration. Also the charge efficiency for metal deposition of the PEC cell can be as high as 100 %.

6.6. Characterization of electrodeposited heavy metals from produced water

The metal obtained after 15 min of electrodeposition at a cell voltage of 1.0 V was analysed by SEM and EDX. The SEM image obtained under light, Figure 6.8 (b), is similar with those reported in Figure 4.33 (b) where the deposition was carried out in a three-electrode cell under the chronoamperometric control, where no PAH was present in the PW VI. The distinct morphology of each deposited metal is not clear in Figure 6.8 (a) and the surface of the platinum electrode is not well covered by the deposits when the PEC cell was not irradiated compared to when it was irradiated as shown in Figure 6.8 (b).
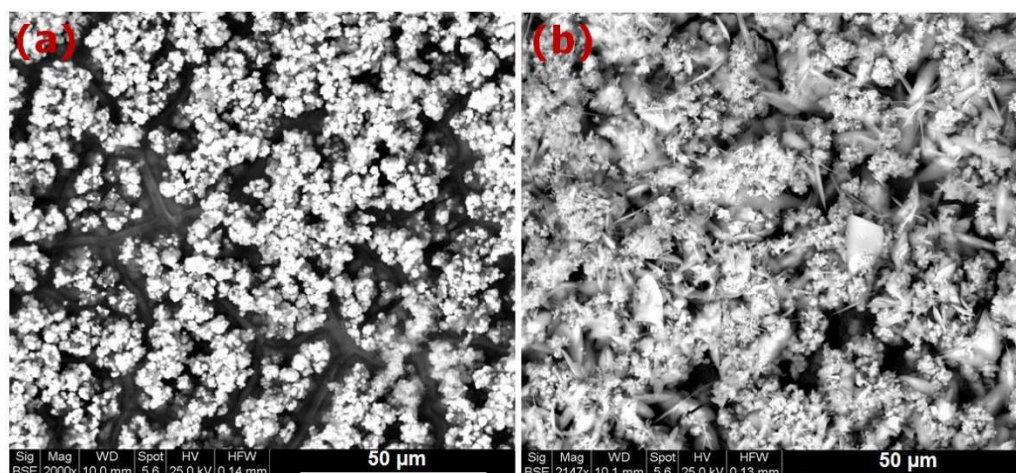
Figure 6.8: SEM images of metals deposited on Pt after 15 minutes in a Pt/CNT-TiO$_2$ PEC when -1.0 V was applied in (a) dark and (b) simulated sunlight.

This implies that the quantity of heavy metal that can be recovered from produced water is significantly increased when the PEC cell was used under

irradiation. The EDX spectra and elemental composition of the deposited heavy metals are presented in Figures 6.9 and 6.10.

Element	Wt%	At%
OK	27.41	78.34
NiK	03.76	02.93
CuK	06.70	04.82
PtL	15.04	03.52
PbL	47.10	10.39
Matrix	Correction	ZAF
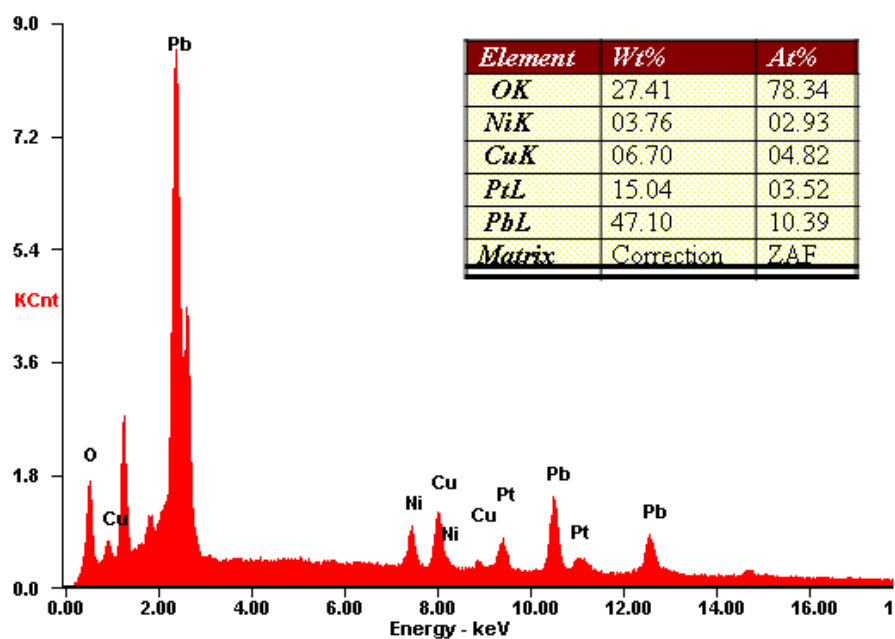
Figure 6.9: EDX spectra and elemental composition of Pt–Photoanode surface after applying – 1.0 V cell voltage in dark for 15 minutes

The large weight percentage of the platinum peak in dark (Figure 6.8) indicates that the thickness of the deposited layer was thin enough for an electron beam from EDX to penetrate through in order to detect the platinum electrode. The platinum weight percentage was significantly reduced under light because the surface was well covered. Also the weight percentage of heavy metals deposited increases significantly when the Pt-Photoanode cell was irradiated by light. The weight of nickel increased from 3.76 % to 8.16 %, copper from 6.7% to 22.73%, and lead from 47.10% to 56.88%.

213

The higher oxygen content in the dark is due to the very thin metal deposit. All metal surfaces are covered by an oxide layer whose thickness is more or less the same for each metal. Thus, the oxygen content detected by EDX was relatively higher in a thin metal layer than in a thicker one. The porous nature of the thin deposit results in an increased surface area, and a higher oxygen content than that of a dense thin layer.

Element	Wt%	At%
OK	07.82	38.12
NiK	08.16	10.83
CuK	22.73	27.89
PtL	04.41	01.76
PbL	56.88	21.40
Matrix	Correction	ZAF
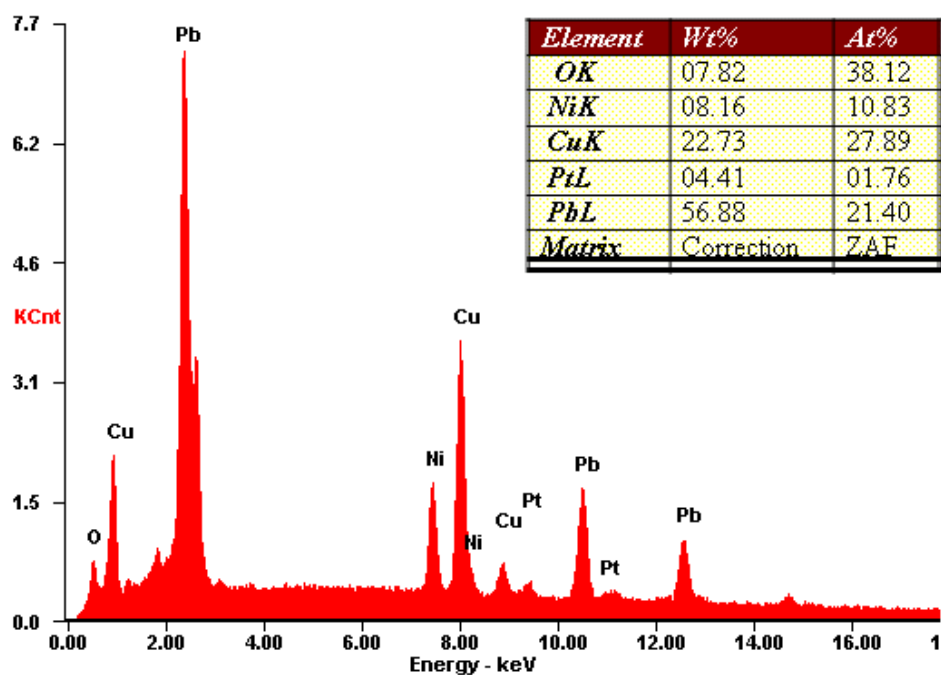
Figure 6.10: EDX spectra and elemental composition of Pt– photoanode surface after applying – 1.0 V cell voltage in light for 15 minutes

Therefore since the oxygen content was significantly reduced under light as the quantity of the deposits increase on the surface of the electrode, it implies that metals rather than metal oxides are recovered from the produced water. Hence nickel, lead and copper can be recovered from produced water containing dissolved phenanthrene and dissolved multiple heavy metal ions/complexes.

6.7. Effect of phenanthrene on electrodeposition of heavy metals

The electrodeposition of heavy metals from synthetic produced water, PW VI, containing no phenanthrene was discussed in chapter 4. The CV obtained showed deposition peaks of all four metals present in PW VI. However no deposition/re-oxidation peak of iron was observed when 1.6 mg/L phenanthrene was dissolved in PW VI as shown in Figure 6.4. To investigate if iron was present in the PW VI containing dissolved phenanthrene, CV was carried out with an increased voltage window which scanned in both positive and negative directions as presented in Figure 6.11.
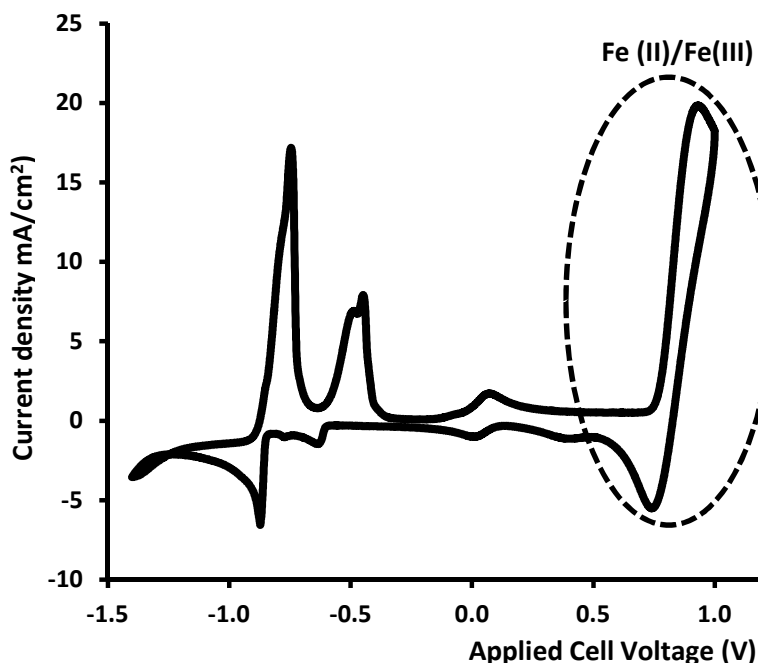

Figure 6.11: Cyclic voltammogram of PW VI containing 1.6 mg/L of phenanthrene in a PEC at 20 mV/s electrode potential scan rate and pH 4 from 0.8 V to – 1.2 V

At around 0.7 V, Fe (II)/Fe (III) oxidation-reduction peaks can be observed. This suggests that iron was present in the solution. SEM/EDX analysis presented in Figures 6.8 – 6.10 however show that iron was not

deposited at all from PW VI containing dissolved phenanthrene. This suggests that iron deposition from produced water may not occur in the presence of phenanthrene. Thermodynamic studies show that Fe exists as Fe(II) in PW VI (Appendix A.5). However there is a strong interaction between iron and phenanthrene which leads to the formation of ferroin (Carter, 1971). Three molecules of phenanthrene can easily bind a Fe(II) cation to form the ferroin ion ($Fe(phen)_3^{2+}$). This may be a probable explanation for the absence of the iron deposition peaks on the CV (Figure 7.4), and its non-detection by EDX and SEM analysis as shown in Figures 7.9 and 7.10. Although in an acidic medium the Fe(II) cation should be free in the electrolyte as illustrated in equation 6.1 (Abrash, 2013). However it appears that pH 4 is not sufficient for such dissociation. Therefore since produced water had a pH range of 4 – 10, iron recovery from produced water containing dissolved phenanthrene would be difficult if not impossible.

$$Fe(phen)_3^{2+} + 3H_3O^+{}_{(aq)} \rightarrow Fe^{2+}{}_{(aq)} + 3phenH^+{}_{(aq)} + 3H_2O_{(l)} \qquad 6.1$$
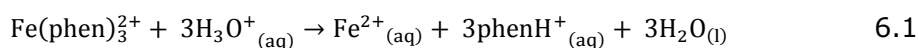
phen stands for phenanthrene in this equation

In the presence of phenanthrene, the order of metal deposition changed from what was observed in its absence (cf. Figure 4.22). The peak current of lead was higher under light than in the dark or when the Pt-graphite configuration was used (Figure 6.4). This result is different from the conclusion made in chapter 5 about the quantity of metal deposition in PW VI free of PAH.

It was observed in a three electrode cell that more copper than lead could be deposited from PW VI. However in the PEC cell, more lead was deposited than copper. Also, while the amount of deposited copper remained the same in both light and dark, the amount of lead was

significantly increased under light. The mass of copper deposited was higher than that of lead when there was no dissolved phenanthrene in PW VI; however this order was reversed in the presence of phenanthrene. It was also noted that there was no significant change in the amount of copper and nickel deposited when the PEC cell was irradiated with solar light as shown in (cf. Figure 6.12 and Figure 4.22).
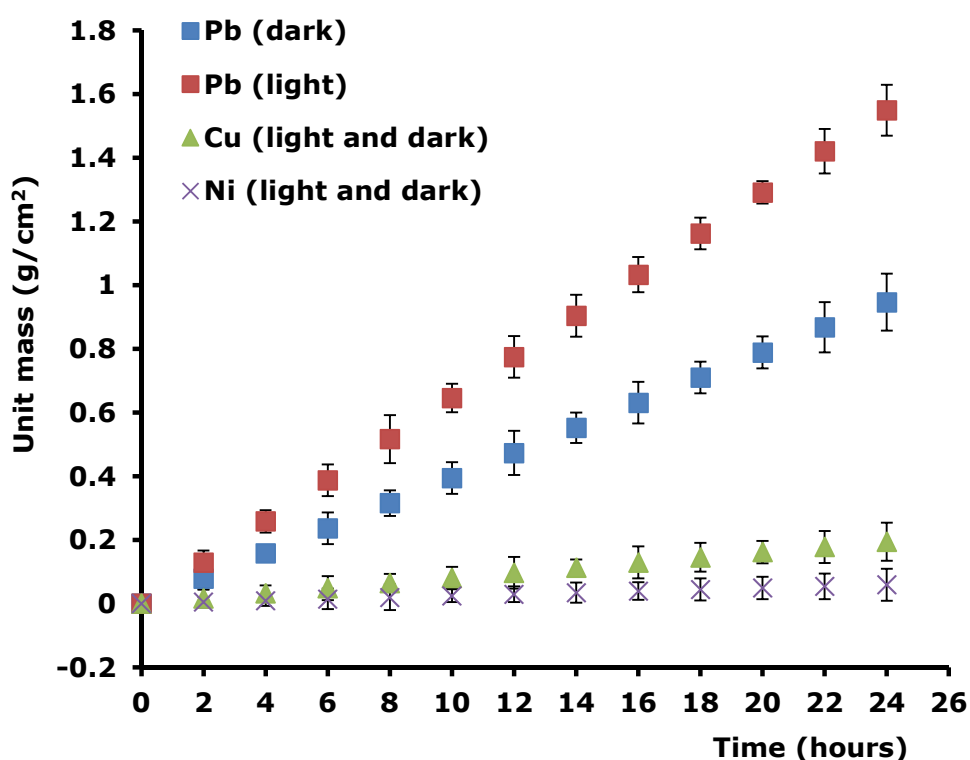
Figure 6.12: Faradic Rate of heavy metal recovery from synthetic produced water, PW VI in a PEC cell at pH 4 and applied potential of 20mV/s

The behaviour of copper and nickel in the presence of phenanthrene may be due to interactions between these metals and phenanthrene. In a previous study it was concluded that there existed potential interactions between copper and modified PAHs and that these interactions could involve reactive oxygen species (Xie et al., 2006). Therefore the reduction in the mass of copper deposited from PW VI containing phenanthrene could

be due to reactions between Cu(I) ions and phenanthrene molecules leading to a decrease of free Cu(I) ions that can be reduced to $Cu_{(s)}$ on the platinum electrode. It may have also been the case that Ni(II) ions react with phenanthrene molecules Since there was little or no interaction between Pb(II) ions and phenanthrene in this case, it means that more free Pb(II) ions would then be available in PW VI containing dissolved phenanthrene, which may be responsible for the high quantity of lead deposited from the synthetic produced water containing phenanthrene. It is well reported in literature that lead and PAH could coexist in soil independently, and could even be removed simultaneously from a mixture (Zhang et al., 2010, Wang et al., 2010). Therefore the order of removal of heavy metals from produced water containing PAHs is based on the interaction of the metal with the PAH present in the water. In this study the order of removal of heavy metals from PW VI containing phenanthrene follows Pb > Cu > Ni > Fe.

6.8. Degradation of phenanthrene in the PEC cell

It is evident that photoelectrons are generated on the MWCNT-TiO_2 photoanode and are transferred to the cathode where it improves the deposition of metals as discussed in earlier sections. However the holes generated are very unstable and powerful oxidants. These holes generated at a very high energy level (3.2 eV for TiO_2) can react with water molecules or dissolved oxygen to generate hydroxyl radicals as illustrated in equations 7.2 – 7.3 (Zigah et al., 2012). The hydroxyl radicals are powerful oxidants which can then react with phenanthrene (equation 6.4). However since there is no way to control the holes generated it is important to examine if the holes are actually involved in phenanthrene degradation or in other reactions in the synthetic produced water such as breaking down

of water to liberate oxygen or the evolution of chlorine which are also possible reactions (see Figure 6.14).

$$TiO_2 + hv \rightarrow e^- + h^+ \qquad\qquad 6.2$$

$$H_2O + h^+ \rightarrow {}^\bullet OH_{(ads)} + H^+ \qquad\qquad 6.3$$

$${}^\bullet OH_{(ads)}{}^\bullet + phenanthrene \rightarrow degraded\ products \qquad\qquad 6.4$$

The potential of each electrode was simultaneously monitored by a multi-channel potentiostat (IviumnStat) while applying a cell voltage to the PEC cell in both light and dark to understand whether the anodic current or the cathodic current is the total controlling cell current.
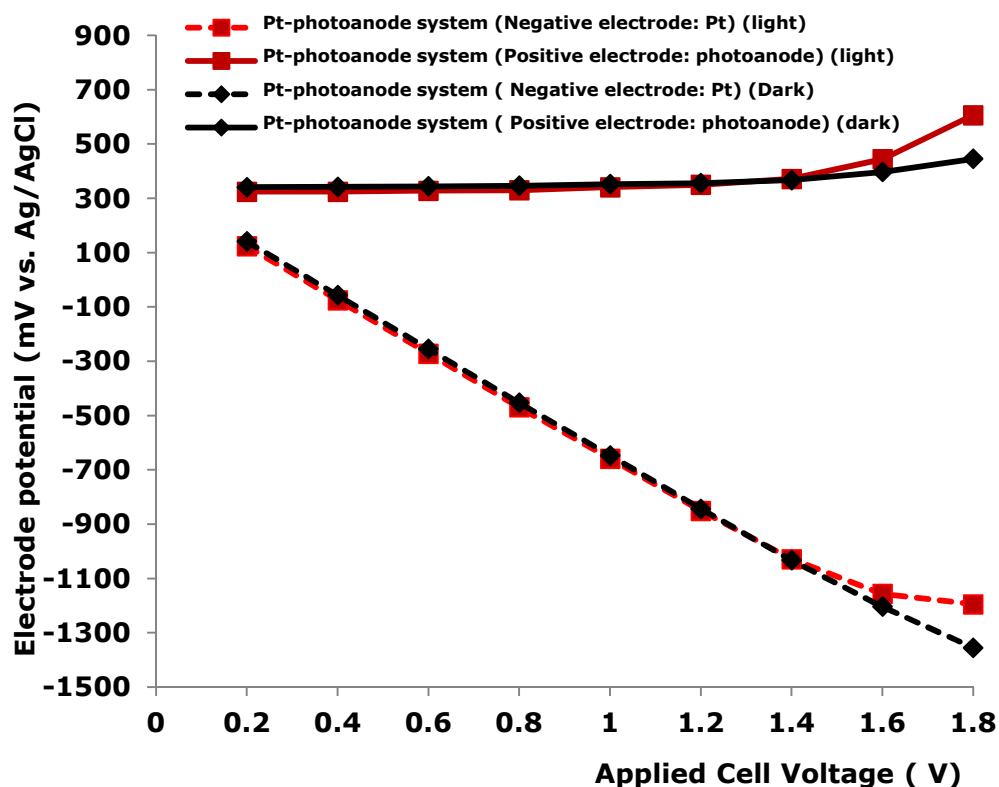
Figure 6.13: The potential of positive and negative electrode at the set cell voltages in the PEC cell. Electrode potentials were measured after conducting CA for 150s at the set cell voltages

The electrode potential of the cathode (platinum) increased with increasing cell voltage both in the light and in the dark. The potential of the photoanode also increases with increasing cell voltage in the dark. In light, a similar behaviour was recorded as the cell voltage increased from 0 V to 1.4 V. However when the applied cell voltage was greater than 1.4 V under light, the potential of the photoanode increases with increasing cell voltage. This implies that in the dark the cathodic current controlled the overall cell current but under solar light irradiation the overall cell current may be controlled by the cathodic current or the anodic current. In Figure 6.13, the cathodic current controlled the overall cell current when applied cell voltage was 0 – 1.4 V and the anodic current controlled the overall cell current when the cell voltage is greater than 1.4 V. Although the overall cell current is controlled by the cathodic current when the cell voltage is 0 - 1.4 V, this does not mean that there are no reactions on the photoanode.
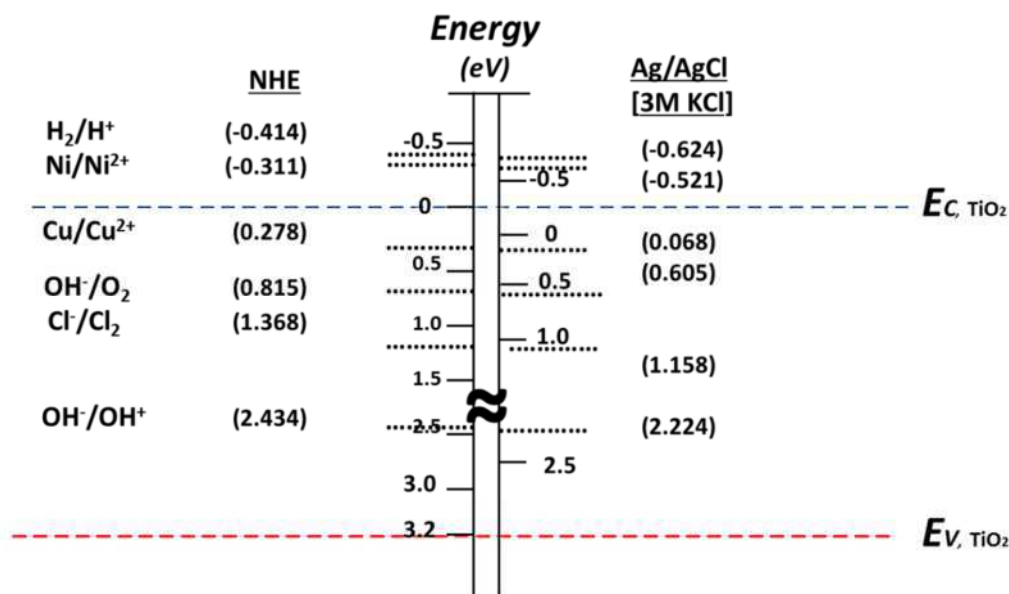
Figure 6.14: Energy band diagram of electrolytes with reference to the normal hydrogen scale (NHE) and in 3M KCl Ag/AgCl scale based on thermodynamic calculations

It implies that the cell cannot fully utilise the photogenerated electrons (and subsequently holes) and that phenanthrene oxidation is driven solely by photogenerated holes at this voltage range. This may be the effect of the cathode size. Since any of the three reactions within the energy band gap of the TiO_2 semiconductor (Figure 6.14) can take place on the photoanode irrespective of its potential, it was important to determine whether the photogenerated holes degraded phenanthrene in the PEC cell. To achieve this, a portion of the electrolyte (PW VI containing phenanthrene) was taken out of the cell every two minutes and analysed by UV-vis.
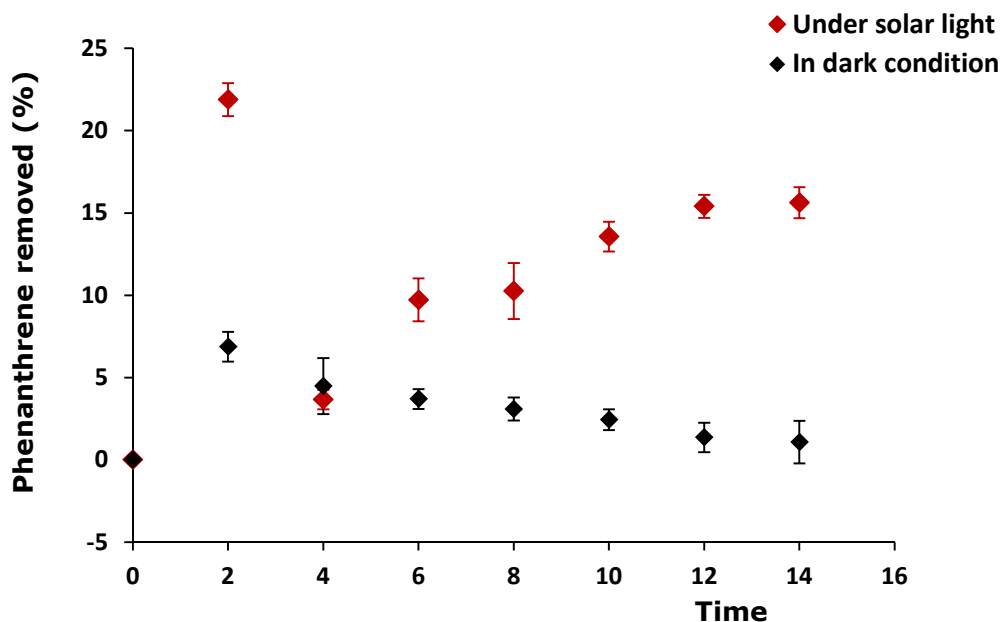
Figure 6.15: Degradation of phenanthrene in PW VI containing phenanthrene at pH 4 via a PEC at an applied cell voltage of -1.0 V

The results obtained from this measurement are presented in Figure 6.15. In the dark, about 6 % of the phenanthrene appeared to have been removed within the first two minutes. However this percentage decreased to about 3 % with time. The increase in the percentage of phenanthrene

removed was caused by adsorption of dissolved phenanthrene unto the photoanode, however beyond two minutes the system came back to equilibrium, which implies no phenanthrene was removed under this condition. It should be noted that although heavy metals were deposited on the platinum cathode at this voltage; there was no evidence of simultaneous phenanthrene degradation.

However when the system was irradiated with simulated sunlight, phenanthrene degradation occurred as shown in Figure 6.15. This confirms that phenanthrene degradation can occur on the photoanode at cell voltage 0 - 1.4 V under light irradiation despite the constant photoanode potential recorded in Figure 6.13. The high percentage of phenanthrene degradation observed after two minutes was due to adsorption as explained in chapter 5. The amount of phenanthrene removed from PW VI in sunlight continued to increase steadily until it peaked after 12 minutes. It should be noted that, heavy metals were simultaneously deposited on the platinum electrode under this condition as discussed in section 6.5. Therefore, recovery of lead, nickel and copper metals by photo-generated electrons on the cathode, and phenanthrene decomposition by hydroxyl radicals at the photoanode could be accomplished in the PEC cell under irradiation at a cell voltage of 1.0 V

6.8.1.   Effect of heavy metal ions on phenanthrene degradation

Since it has been established from the results of this study that the photogenerated holes are basically responsible for phenanthrene degradation in produced water, the effect of multiple heavy metal species in produced water was examined as presented in Figure 6.16. Within 14 minutes of irradiation under sunlight 16% of phenanthrene was remove from PW VI, 37% from PW II and 46% from PW I all containing 1.6 mg/L of dissolved phenanthrene. The results show that the percentage of

phenanthrene degradation was highest when no metal ions were present in PW VI, and lowest when copper, iron, nickel and lead ions were all present. This may be due to the interactions between the metal ions and phenanthrene which should result in a decrease in the overall phenanthrene concentration in solution. Metal ions may also be adsorbed unto the photoanode, leading to a reduction in the quantity of phenanthrene that can interact with the photogenerated holes, thus limiting the amount of phenanthrene degraded.
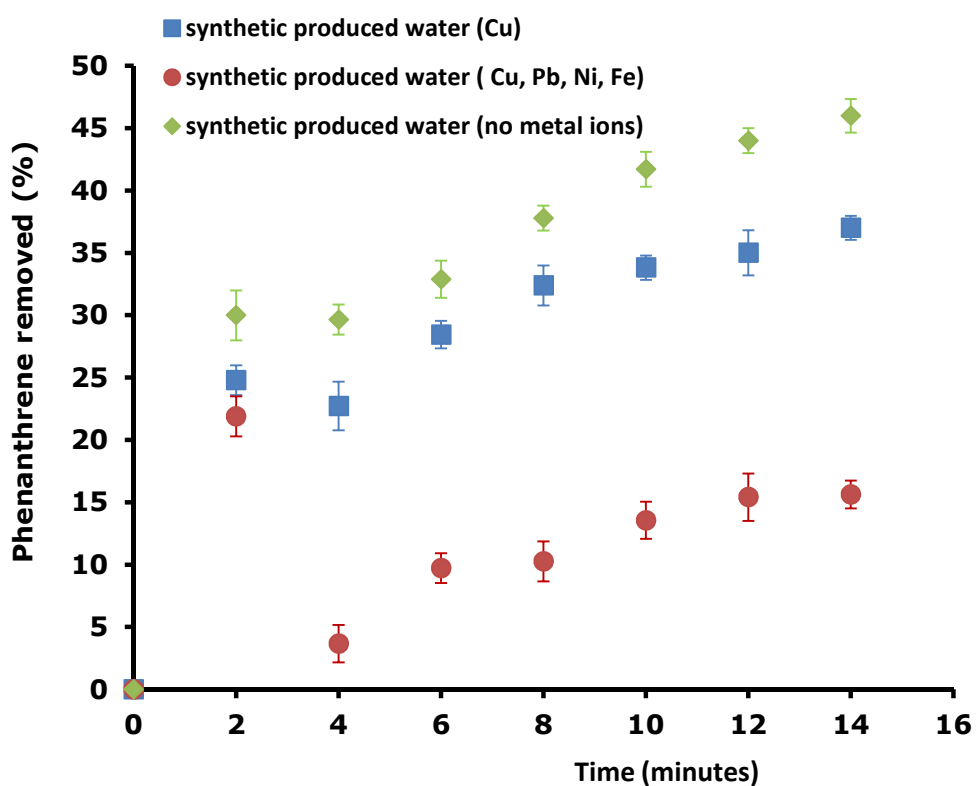
Figure 6.16: Rate of phenanthrene degradation in synthetic produced water [PW I (no metals), PW II (Cu) and PW VI (Cu, Pb, Ni, and Fe)] under irradiation in a PEC at a cell voltage of 1.0 V and pH 4

There is no possibility of any reduction reactions (of adsorbed metal species or hydrogen evolution) occurring on the photoanode at a cell voltage < 1.4 V because a reduction by photogenerated electrons can only occur when the reduction potential of a species is located at more positive

position than the semiconductor's CBM as shown in Figure 6.14. Since, the reduction potentials of most heavy metal ions are similar to or even more negative than the CBM of the photoanode (MWCNT-TiO$_2$), it is very unlikely to reduce metal ions into metals on the photoanode.

Figure 6.16 shows that when only copper ions were present in the synthetic produced water the percentage of phenanthrene removed increased from when the four metal ions are present. This result further indicates that there are interactions between phenanthrene and metal ions in the synthetic produced water, especially iron and copper as discussed earlier. Therefore phenanthrene degradation in produced water via a PEC cell will decrease with increasing concentration of multiple heavy metal ions.

6.8.2.   Effect of phenanthrene concentration on degradation

The effect of phenanthrene concentration on its degradation in PW VI was examined by varying the concentration of phenanthrene as shown in Figure 6.17. There is no significant change in the amount of phenanthrene removed at various starting concentrations of phenanthrene, however the higher the concentration of dissolved phenanthrene the higher the percentage of phenanthrene removed from the produced water. Since adsorption is the determining step for phenanthrene oxidation, it follows that at higher concentrations of phenanthrene more phenanthrene molecules are adsorbed unto the photoanode; hence the hydroxyl radical can interact with more phenanthrene pollutants leading to higher current efficiency. It should be noted that it is difficult to determine the optimum phenanthrene concentration for maximum degradation under this condition, because phenanthrene has a very poor solubility in aqueous medium.
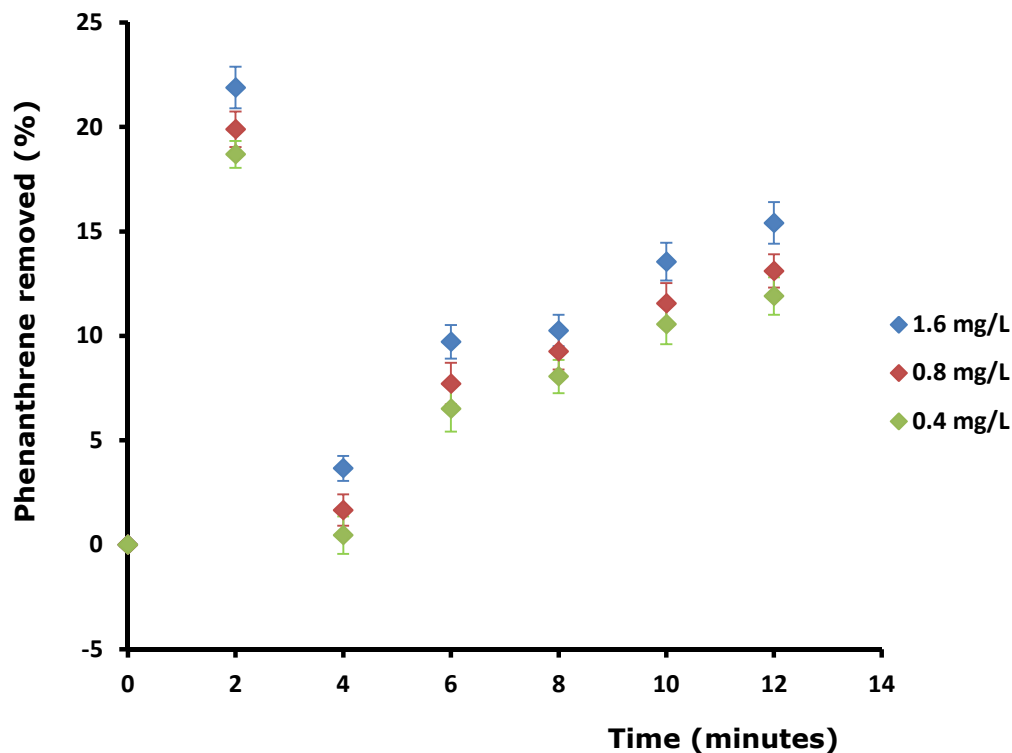
Figure 6.17: Rate of phenanthrene degradation in synthetic produced water, PW VI, at different phenanthrene concentration (under irradiation in a PEC at a cell voltage of 1.0 V and pH 4.

6.8.3. Effect of cell voltage on phenanthrene degradation

The effect of an increase in voltage on phenanthrene degradation was examined during the operation of the PEC. The percentage of phenanthrene degradation slightly increased from 14.9 % to 15.4 % after 12 minutes of irradiation when the applied cell voltage was increased from 1.0 V to 1.2 V respectively as presented in Figure 6.18.

Although the cathodic current is the controlling cell current at applied cell voltage < 1.4 V, which means applied cell voltage has no direct effect on phenanthrene degradation, the slight increase in the percentage of phenanthrene degradation at cell voltage of 1.2 V indicates that increasing the cell voltage can help to increase the electric field strength in the space

charge region, which leads to a reduction in the electron-hole pair recombination, hence allowing more holes to participate in the oxidation process. It should be noted that it is difficult to determine the efficiency of holes generated for phenanthrene oxidation because the holes cannot be controlled and can participate in other oxidation reactions as discussed earlier.
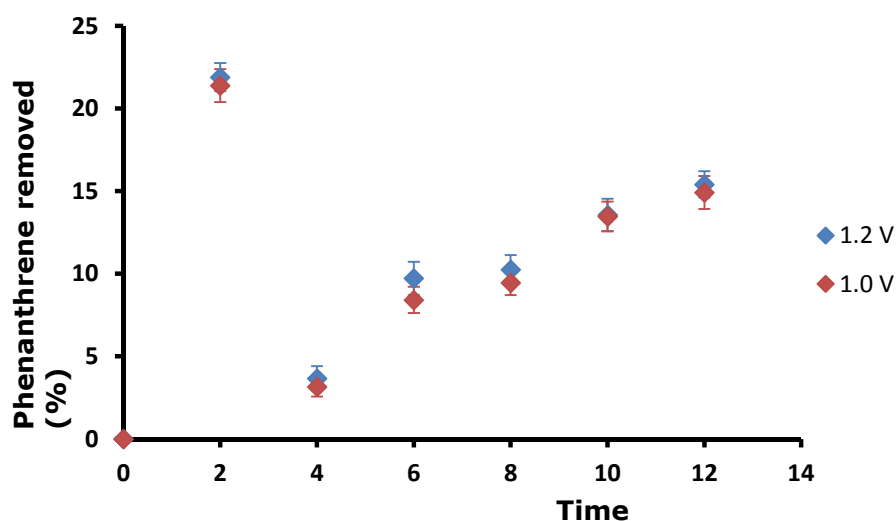
Figure 6.18: Effect of applied cell voltage on phenanthrene degradation in PW VI containing 1.6 mg/L phenanthrene under irradiation in a PEC cell at a cell voltage of 1.0 V and pH 4

This study shows that the anodic current is a function of the size of the photoanode and their photocatalytic performance while the cathodic current is a function of the concentration of the species to be reduced in an electrolyte, the cell voltage and the photogenerated electrons. Therefore an increase in the photoanode surface area coupled with a corresponding increase in the cathode size could lead to higher phenanthrene degradation in synthetic produced water.

6.9. Conclusion

A dual purpose PEC cell has been demonstrated to successfully and simultaneously remove heavy metals and phenanthrene in synthetic produced water under sunlight irradiation. The applied cell voltage is mainly responsible for the metal deposition while the photogenerated holes are the main driving force for phenanthrene degradation. To maximise this process reasonable sizes of the cathode and photoanode are required. Lead, nickel and copper was successfully deposited from synthetic produced water in a PEC cell at an applied voltage of 1.0 V accompanied by simultaneous degradation of phenanthrene. However, iron could not be deposited in this reactor due to the interaction of Fe(II) and phenanthrene to form ferroin ions. Selective deposition of metals from synthetic produced water was also achieved in the PEC cell. The presence of heavy metal ions in synthetic produced water is shown to limit the amount of phenanthrene degradation, and this limitation increased with an increase in the concentrations of multiple metal ions present in the produced water. Although further studies are needed to do a full techno-economic analysis of this process, heavy metals recovered can be sold which is advantageous in terms of reducing the total operational cost. This technology can be a profit making sustainable engineering process in the future if the efficiency of metal recovery and phenanthrene degradation is significantly improved..

Table 6.1. Estimated global profit from metal recovery at various operational efficiency of PEC cell

Heavy metals		Lead	Copper	Nickel	TOTAL
Estimated annual global value of input produced water per tonnne		$ 2,050.30	$ 6,657.97	$ 16,402.34	$ 25,110.61
Estimated global input of produced water (tonne)		$ 120.00	$ 70.00	$ 520.00	$ 710.00
Estimated global value at various efficiency of PEC cell	20%	$ 49,207.20	$ 93,211.60	$ 1,705,843.20	$ 1,848,262.00
	40%	$ 98,414.40	$ 186,423.20	$ 3,411,686.40	$ 3,696,524.00
	60%	$ 147,621.60	$ 279,634.80	$ 5,117,529.60	$ 5,544,786.00
	80%	$ 196,828.80	$ 372,846.40	$ 6,823,372.80	$ 7,393,048.00
	100%	$ 246,036.00	$ 466,058.00	$ 8,529,216.00	$ 9,241,310.00

For example if the produced water discharged from the oil and gas platforms in the North Sea (cf. Table 2.4) accounts for 1% of the total yearly global discharge of produced water into the environment, then Table 6.1 shows the potential value of heavy metals that can be recovered from the photoelectrochemical process developed in this research at various operational efficiencies. Therefore this process has the potential to shape the future of produced water treatment technology since it utilises sunlight to drive phenanthrene degradation while simultaneously recovering heavy metals. The energy from sunlight is cheap and the recovered metals can be sold, suggesting that the process would be energy efficient and cost effective.

The design of the PEC and scale up of this process to commercial throughput is a major engineering issues not fully addressed in this work because the aim of this research was to lay the foundation for the feasibility of a simultaneous removal of heavy metals and polycyclic aromatic hydrocarbons from produced water. It is important to note that attention must be given to an effective way to collect deposited metals from the PEC in a continuous engineering operation. The shape of the cathode and photoanode will play an important role in the design of a concise and highly efficient commercial PEC reactor. It may be important to explore a tube shaped cathode for easier collection of metals. It should be noted that re-oxidation of deposited heavy metals is a major challenge to metal recovery in this process. Therefore selective deposition of heavy metals at various potentials must be explored in addition to electrode design in scaling up this process to a commercial throughput. Overall the simultaneous removal of heavy metals and PAH via the photo-electrochemical technology is realistic, clean, beneficial to the environment and potentially cost effective.

Chapter 7: Conclusions and Future work

7.1. Introduction

The development of a photoelectrochemical process for the treatment of produced water has been undertaken in this research. The process benefits from low temperatures and sustainable sources of electrolyte and energy. A computer model has been implemented and assessed to predict solution speciation and elucidate observed trends. The work was organised in three main experimental chapters. Chapter 5 describes the electrodeposition process for the recovery of heavy metals from various grades of synthetic produced water. The photoanodic process for degradation of dissolved phenanthrene (a model of PAH) on the MWCNT-TiO$_2$ photoanode was studied in Chapter 5. Chapter 6 describes the overall conceptual photoelectrochemical process for the treatment of produced water derived from this research. The summary of the main conclusions extracted from the aforementioned chapters are described in sections 7.2, 7.3 and 7.4 and recommendation for future works are presented in section 7.5.

7.2. Recovery of metals from produced water

Several grades of produced water were prepared following extensive literature search and understanding of real produced water. They all have sufficiently high conductivity that makes them suitable electrolytes for electrodeposition. Lead, copper, iron and nickel can be recovered from produced water via electrodeposition at an applied potential of - 0.7 V vs. Ag/AgCl and pH 4 in a three-electrode cell. However only lead and copper were successfully recovered as metals from synthetic produced water containing a single metal ion at this condition. It is difficult to remove nickel and iron from produced water containing their single metal ions because -1.2 V vs. Ag/AgCl is needed to overcome their energy barrier which automatically results in competing reactions between hydrogen production and nickel or iron deposition on the cathode. Furthermore when

multiple metal ions are present in produced water the potential of hydrogen evolution is significantly shifted to more negative potential of -1.6 V vs. Ag/AgCl which makes deposition of all metals possible even at -1.2 V vs. Ag/AgCl without hydrogen evolution. Electrodepositions of metals are improved as the pH decreased and was best carried out on platinum and glassy carbon electrodes. Titanium electrode was the least suitable because of the passivation of its surface by titanium dioxide. Therefore recovery of metals from synthetic produced water is a function of produced water quality, concentration of metal ions, pH and quality of electrode surface.

7.3. Oxidation of dissolved phenanthrene from produced water

MWCNT-TiO_2 (0.9:1 mass ratio) was synthesised by a modified sol gel method after determining the optimum CNT-surfactant molar ratio, CNT suspension concentration and sonication time. The synthesised composite was homogeneously coated and loaded onto a 2 cm x 2 cm titanium plate to make a photoanode. The photoanode shows a superior photocatalytic activity compared to the commercial TiO_2 (P25), which is enhanced by the application of applied potential. The photoanode was able to remove 32% of phenanthrene under irradiation by sunlight and this improved to 42% when assisted with a potential of 0.4 V vs. Ag/AgCl in 15 minutes of operation. The application of potential to the photoanode helps the separation of the photogenerated electron-hole pair which makes more holes available to carry out oxidation of phenanthrene by limiting electron-hole pair recombination. It was observed that the percentage of phenanthrene removal remained constant after 15 minutes. Therefore photocatalytic degradation of phenanthrene in produced water is feasible but depends on the size of, and the amount of photocatalyst loaded onto

the photoanode, the concentration of the dissolved phenanthrene, and the time of light irradiation.

7.4. Simultaneous removal of metals and phenanthrene from produced water

A photoelectrochemical cell was built for the simultaneous removal of metals and phenanthrene on the cathode and anode of the cell based on the knowledge derived from electrodeposition and photoanodic process studies. Copper, lead and nickel were successfully recovered from synthetic produced water at a cell voltage of 1.0 V and the quantity of metal deposited increased under light irradiation. Photoelectrons generated on the photoanode travel to the cathode where it increased the charge density at the cathode-electrolyte interface, hence causing a positive shift in the metal deposition voltage. There was no degradation of phenanthrene in the dark however 15% of phenanthrene was degraded under light irradiation. This percentage is half of what was obtained when no heavy metal ions are present in the produced water. The reaction of phenanthrene and iron to form ferroin ions is attributed to the non-deposition of iron in the PEC cell and also the low amount of copper deposition in the cell is attributed to reactions between copper ions and phenanthrene in solution. These metals–PAH reactions are also one of the reasons attributed to the lower percentage of phenanthrene degradation in the PEC cell. The potential of the photoanode was monitored by a multichannel potentiostat and there was no significant change in its potential even when 1.4 V was applied to the cell. This implies that the small surface area of the platinum electrode used in the PEC cell does not allow the full utilization of the photogenerated electron-hole pair therefore reducing the efficiency of the photoanode. Although phenanthrene and heavy metals were successfully removed from synthetic produced water via

the photoelectrochemical process, the size of electrodes, quality of produced water, pH and applied cell voltage are major factors responsible for the simultaneous removal of heavy metals and phenanthrene from produced water via a PEC cell.

This thesis provides the essential experimental data needed to perform a feasibility study. Future work is nevertheless required to demonstrate the industrial-scale feasibility of the treatment approach developed in this work, particularly the PEC cell design and operation.

7.5.   Future work

As a consequence of the results and conclusions of this work, a series of avenues of research are recommended for further investigation.

➤ It would be interesting to have a test on the longevity of the nanohybrid, i.e., to examine the influence of long-term irradiation on the composite structure and morphology, which is a very important index for its application as a catalyst in industrial processes.

➤ The effect of electrode sizes and composite loading on the performance of the PEC cell in terms of metal deposition and phenanthrene degradation should be investigated to determine the optimum loading and size of electrode needed to improve this process.

➤ It will be interesting to check the effect of carrying out this treatment by arranging several photoanodes and cathodes in series in order to optimise selective deposition of metals from synthetic produced water at different voltages.

- ➢ It is important to study the effect of mass transport of charged species via convection and migration by using a stirred tank or a rotating electrode to carry out the treatment.

- ➢ The effect of other light sources (e.g. UV) and intensity on metal deposition and phenanthrene degradation should be studied.

- ➢ It is important to check the performance of different types of photoanodes in the PEC cell especially semiconductors sensitive in the visible region e.g. WO_3.

- ➢ It is necessary to construct a batch and a continuous pilot scale photoelectrochemical treatment unit with real samples of produced water using the process developed in this research. This would allow for a preliminary commercial viability study of the process on an industrial scale.

References

Abdul, G., Saifullah, M. & Mhulam, M. 2000. Estimation of ionic strength from electrical conductivity of Punjab ground waters. *Pakistani Journal of Agricultural Sciences,* 37**,** 113 - 115.

Abrash 2013. Chemistry 141 Laboratory Lab Lecture Notes for Kinetics Lab. *University of Richmond.*

Adams, M., Campbell, I. & Robertson, P. K. J. 2008. Novel Photocatalytic Reactor Development for Removal of Hydrocarbons from Water International. *Journal of Photoenergy***,** 1 - 7

Aessopos, A., Berdoukas, V. & Tsironi, M. 2008. The heart in transfusion dependent homozygous thalassaemia today – prediction, prevention and management. *European Journal of Haematology,* 80**,** 93-106.

Ajayan, P. M. 1999. Nanotubes from carbon. *Chemical Reviews,* 99**,** 1787-1799.

Akzo Nobel MPP systems 2004. Macro-porous polymer extraction for offshoreproduced water removes dissolved and dispersed hydrocarbons. *Business Briefing: Exploration & Production: The Oil & Gas Review***,** 1-4.

All 2003. Handbook on Coal Bed Methane Produced Water: Management and Beneficial Use Alternatives. *In:* Ground Water Protection Research Foundation, U. S. D. O. E., and U.S. Bureau Of Land & Management (eds.). ALL Consulting.

Allen, E. W. 2008. Process water treatment in Canadas oil sands industry: II. A review of emerging technologies. *Journal of Environmental Engineering and Science,* 7**,** 499-524.

Altelarain[TM] System 2007. ARS-4000: New patented technology for cleaning produced water on-site. *Altela Information,* 26 January.

Alvarez, A. E. & Salinas, D. R. 2010. Formation of Cu/Pd bimetallic crystals by electrochemical deposition. *Electrochimica Acta,* 55**,** 3714-3720.

Anders R. Johnsen, A. W., Ulrich Karlson, Peter Roslev 2002. Linking of Microorganisms to Phenanthrene Metabolism in Soil by Analysis of 13C-Labeled Cell Lipids *Appl. Environ. Microbiol.,* 68**,** 6106-6113.

Arthur, J. D., Langhus, B. G. & Patel, C. 2005. Technical Summary of Oil & Gas Produced Water Treatment Technologies. *ALL Consulting, LLC***,** 1-52.

Ashokkumar, M. 1998. An overview on semiconductor particulate systems for photoproduction of hydrogen. *International Journal of Hydrogen Energy,* 23**,** 427-438.

Azetsu-Scott, K., Yeats, P., Wohlgeschaffen, G., Dalziel, J., Niven, S. & Lee, K. 2007. Precipitation of heavy metals in produced water: Influence on contaminant transport and toxicity. *Marine Environmental Research,* 63**,** 146-167.

Baath, E. 1989. Effects of heavy metals in soil on microbial processes and populations (a review). *Water, Air, and Soil Pollution,* 47**,** 335-379.

Banks, C. E., Ji, X., Crossley, A. & Compton, R. G. 2006. Understanding the Electrochemical Reactivity of Bamboo Multiwalled Carbon Nanotubes: the Presence of Oxygenated Species at Tube Ends May not Increase Electron Transfer Kinetics. *Electroanalysis,* 18**,** 2137-2140.

Barratt, P. A., Feng, X., Arne, B. & Neil 1997. Chemical Oxidation: Technologies for the Nineties. *In:* Eckenfelder, W. W., Bowers, A. R. & Roth, J. A. (eds.). Lancaster: Technomic Publishing Co. Inc.,6,1 - 12

Barrett, E. P., Joyner, L. G. & Halenda, P. P. 1951. The Determination of Pore Volume and Area Distributions in Porous Substances. I.

Computations from Nitrogen Isotherms. *Journal of the American Chemical Society, 73*, 373-380.

Batchelor-Mcauley, C., Wildgoose, G. G., Compton, R. G., Shao, L. D. & Green, M. L. H. 2008. Copper oxide nanoparticle impurities are responsible for the electroanalytical detection of glucose seen using multiwalled carbon nanotubes. *Sensors and Actuators B-Chemical, 132*, 356-360.

Bessa, E., Sant'anna, G. L. & Dezotti, M. 2001. Photocatalytic/H_2O_2 treatment of oil field produced waters. *Applied Catalysis B: Environmental, 29*, 125-134.

Bilstad, T. & Espedal, E. 1996. Membrane separation of produced water. *Water Science and Technology, 34*, 239-246.

Bisquert, J., Zaban, A. & Salvador, P. 2002. Analysis of the Mechanisms of Electron Recombination in Nanoporous TiO2 Dye-Sensitized Solar Cells. Nonequilibrium Steady-State Statistics and Interfacial Electron Transfer via Surface States. *The Journal of Physical Chemistry B, 106*, 8774-8782.

Blanton, R. H., Lyte, M., Myers, M. J. & Bick, P. H. 1986. Immunomodulation by Polyaromatic Hydrocarbons in Mice and Murine Cells. *Cancer Research, 46*, 2735 - 2739.

Blanton, R. H., Myers, M. J. & Bick, P. H. 1988. Modulation of immunocompetent cell populations by benzo[a]pyrene. *Toxicology and Applied Pharmacology, 93*, 267-274.

Borba, C. E., Guirardello, R., Silva, E. A., Veit, M. T. & Tavares, C. R. G. 2006. Removal of nickel(II) ions from aqueous solution by biosorption in a fixed bed column: Experimental and theoretical breakthrough curves. *Biochemical Engineering Journal, 30*, 184-191.

Boysen, J. 2007. The Freeze-Thaw/Evaporation (FTE) Process for Produced Water Treatment, Disposal and Beneficial Uses. *14th Annual International Petroleum Environmental Conference.* Houston, TX.

Boysen, J. E., Harju, J. A., B. Shaw, M. Fosdick, A. Grisanti & Sorensen, J. A. 1999. The Current Status of Commercial Deployment of the Freeze Thaw Evaporation Treatment of Produced Water. *SPE/EPA 1999 Exploration and Production Environmental Conference.* Austin, TX.

Brunauer, S., Emmett, P. H. & Teller, E. 1938. Adsorption of Gases in Multimolecular Layers. *Journal of the American Chemical Society,* 60**,** 309-319.

Bryan, G. W. 1971. The effects of heavy metals (other than mercury) on marine and estuarine organisms. *Proceedings of the Royal Society,* 1048**,** 389 - 410.

Budevski, E., Staikov, G. & Lorenz, W. J. 2000. Electrocrystallization: Nucleation and growth phenomena. *Electrochimica Acta,* 45**,** 2559-2574.

Buller, A. T., Johnsen, S. & Frost, K. 2003a. Offshore produced water management - knowledge, tools and procedures for assessing environmental risk and selecting remedial measures. *Statoil Research and Technology Offshore,* Memoir 3.

Buller, A. T., Johnsen, S. & Frost, K. 2003b. Offshore produced water management: knowledge, tools and procedures for assessing environmental risk and selecting remedial measures. *Memoir 3. Statoil Research and Technology Offshore***,** 1-4.

Burritt, D. J. 2008. The polycyclic aromatic hydrocarbon phenanthrene causes oxidative stress and alters polyamine metabolism in the aquatic liverwort Riccia fluitans L. *Plant, Cell & Environment,* 31**,** 1416-1431.

Çakmakce, M., Kayaalp, N. & Koyuncu, I. 2008. Desalination of produced water from oil production fields by membrane processes. *Desalination,* 222**,** 176-186.

Carls, M. G., Rice, S. D. & Hose, J. E. 1999. Sensitivity of fish embryos to weathered crude oil: Part I. Low-level exposure during incubation causes malformations, genetic damage, and mortality in larval pacific herring (Clupea pallasi). *Environmental Toxicology and Chemistry,* 18**,** 481-493.

Carter, P. 1971. Spectrophotometric determination of serum iron at the submicrogram level with a new reagent (ferrozine). *Analytical Biochemistry,* 40**,** 450-458.

Cassidy, A. L. 1993. Advances in flotation unit design for produced water treatment. *SPE 25472 Production Operations Symposium.* Oklahoma.

Chae, J. H. & Chen, G. Z. 2012. 1.9 V aqueous carbon-carbon supercapacitors with unequal electrode capacitances. *Electrochimica Acta,* 86**,** 248-254.

Chan, L.-H., StarinskY, A. & Katz, A. 2002. The behavior of lithium and its isotopes in oilfield brines: evidence from the Heletz-Kokhav field, Israel. *Geochimica et Cosmochimica Acta,* 66**,** 615-623.

Chao, K.-J., Cheng, W.-Y., Yu, T.-H. & Lu, S.-Y. 2013. Large enhancements in hydrogen production of TiO2 through a simple carbon decoration. *Carbon,* 62**,** 69-75.

Charlier, J. C. 2002. Defects in carbon nanotubes. *Accounts of Chemical Research,* 35**,** 1063-9.

Chatterjee, D. & Dasgupta, S. 2005. Visible light induced photocatalytic degradation of organic pollutants. *Journal of Photochemistry and Photobiology C: Photochemistry Reviews,* 6**,** 186-205.

Chen, G. Z. 2013. Understanding supercapacitors based on nano-hybrid materials with interfacial conjugation. *Progress in Natural Science: Materials International,* 23**,** 245-255.

Chen, M.-L., Bae, J.-S., Yoon, H.-S., Lim, C.-S. & Oh, W.-C. 2011. The Photodegradation Effect of Organic Dye for Metal Oxide (Cr2O3, MgO and V2O3) Treated CNT/TiO2 Composites. *Bulletin of the Korean Chemical Society,* 32**,** 815-820.

Chen, Y., Huang, G.-F., Huang, W.-Q., Zou, B. S. & Pan, A. 2012. Enhanced visible-light photoactivity of La-doped ZnS thin films. *Applied Physics A,* 108**,** 895-900.

Chou, A., Bocking, T., Singh, N. K. & Gooding, J. J. 2005. Demonstration of the importance of oxygenated species at the ends of carbon nanotubes for their favourable electrochemical properties. *Chemical Communications***,** 842-844.

Clifford, D. A. 1999. Ion exchange and Inorganic Adsorption. *In:* LETTERMAN, R. D. (ed.) *Water Quality and Treatment.* Fifth Edition ed. New York: McGraw-Hill.

Cline, J. T. 1998. Treatment and Discharge of Produced Water for Deep Offshore

Disposal. *API Produced Water Management Technical Forum and Exhibition.* Lafayette, LA.

Commoner, B. & Lipkin, D. 1949. The Application of the Beer-Lambert Law to Optically Anisotropic Systems. *Science,* 110**,** 41-43.

CSM 2009. Technical assessment of produced water treatment technologies *Colorado School of Mines RPSEA Project* 071222-12**,** 1-157.

Cui, C. Q. & Lee, J. Y. 1995. Nickel deposition from unbuffered neutral chloride solutions in the presence of oxygen. *Electrochimica Acta,* 40**,** 1653-1662.

Dai, L. 2006. *Carbon Nanotechnology: Recent Development in Chemistry, Physics, Materials Science and Device Applications,* Amsterdam, Elsevier B. V.

Darwish, M. A., AL Asfour, F. & Al-Najem, N. 2003. Energy consumption in equivalent work by different desalting methods: case study for Kuwait. *Desalination,* 152**,** 83-92.

Dasgupta, P. S. & Lahiri, T. 1992. Alteration of brain catecholamines during growth of benzo(a)pyrene induced murine fibrosarcoma. *Neoplasma,* 39**,** 163-5.

Dennis, J. K. & Eugene, T. 1993. *Nickel and chromiumplating,* Third edition, Woodhead Publishing Ltd, Cambridge, 50 - 56.

Di Bari, G. A. 2000. *Electrodeposition of nickel,* New Jersey, Wiley & Sons Inc, New Jersey.

Doran, G. F., Williams, K. L., Drago, J. A., Huang, S. S. & Leong, L. Y. C. Pilot-study results to convert oilfield produced water to drinking-water or reuse quality. Proceedings of the SPE Annual Technical Conference, 1998 New Orleans, LA. Production Operations and Engineering/General, New Orleans, La. 403 - 417, 403 - 417.

EIA 2009. International energy outlook. *US Department of Energy, Energy Information Administration,* DOE/EIA-0484**,** www.eia.doe.gov/oiaf/ieo/index.html.

Eriksson 1979. An algorithm for the computation of aqueous multicomponent, multiphase equilibria. *Anal. Chim. Acta,* 112**,** 375-383.

Ettouney, H. M., El-Dessouky, H. T., Faibish, R. S. & Gowin, P. J. 2002. Evaluating the economics of desalination. *Chemical Engineering Progress,* 98**,** 32 - 39.

Faibish, R. S. & Cohen, Y. 2001a. Fouling-resistant ceramic-supported polymer membranes for ultrafiltration of oil-in-water microemulsions. *Journal of Membrane Science,* 185**,** 129-143.

Faibish, R. S. & Cohen, Y. 2001b. Fouling and rejection behavior of ceramic and polymer-modified ceramic membranes for ultrafiltration of oil-in-water emulsions and microemulsions. *Colloids and Surfaces A: Physicochemical and Engineering Aspects,* 191**,** 27-40.

Fakhru'l-Razi, A., Pendashteh, A., Abdullah, L. C., Biak, D. R. A., Madaeni, S. S. & Abidin, Z. Z. 2009. Review of technologies for oil and gas produced water treatment. *Journal of Hazardous Materials,* 170**,** 530-551.

Feng, W., Feng, Y., Wu, Z., Fujii, A., Ozaki, M. & Yoshino, K. 2005. Optical andelectrical characterizations of nanocomposite film of titania adsorbed onto oxidized multiwalled carbon nanotubes. *Journal of Physics: Condensed matter,* 17**,** 4361-4368.

Fu, F. & Wang, Q. 2001. Removal of heavy metal ions from wastewaters: A review. *Journal of Environmental Management,* 92**,** 407-418.

FujishimA, A. & Honda, K. 1972. Electrochemical Photolysis of Water at a Semiconductor Electrode. *Nature,* 238**,** 37-38.

Gao, B. 2008. *The Synthesis and Characterization of TiO_2 and $CNTs/TiO_2$ Nano-catalysts.* University of Nottingham, PhD thesis.

Gao, B., Chen, G. Z. & Li Puma, G. 2009a. Carbon nanotubes/titanium dioxide (CNTs/TiO2) nanocomposites prepared by conventional and novel surfactant wrapping sol-gel methods exhibiting enhanced photocatalytic activity. *Applied Catalysis B: Environmental,* 89**,** 503-509.

Gao, B., Chen, G. Z. & Li Puma, G. 2009b. Carbon nanotubes/titanium dioxide (CNTs/TiO2) nanocomposites prepared by conventional and novel surfactant wrapping sol–gel methods exhibiting enhanced

photocatalytic activity. *Applied Catalysis B: Environmental,* 89**,** 503-509.

Gaya, U. I. & Abdullah, A. H. 2008. Heterogeneous photocatalytic degradation of organic contaminants over titanium dioxide: A review of fundamentals, progress and problems. *Journal of Photochemistry and Photobiology C: Photochemistry Reviews,* 9**,** 1-12.

Gerischer, H. 1977. On the stability of semiconductor electrodes against photodecomposition. *Journal of Electroanalytical Chemistry and Interfacial Electrochemistry,* 82**,** 133-143.

Godshall, N. A. 2006. AltelaRain[SM] produced water treatment technology: Making water from waste. *International Petroleum Environmental Conference.* Houston, Texas: ALTELA[TM].

Golgovici, F. 2011. Cathodic deposition of Pb from ionic liquids based on chlorine chloride. *Chemical Bulletin of Politehnica University of Timisoara,* 56**,** 62-66.

Gomez, E., Muller, C., Proud, W. G. & Valles, E. 1992. Electrodeposition of nickel on vitreous carbon: Influence of potential on deposit morphology. *Journal of Applied Electrochemistry,* 22**,** 872-876.

Gong, K., Yan, Y., Zhang, M., Su, L., Xiong, S. & Mao, L. 2005. Electrochemistry and electroanalytical applications of carbon nanotubes: a review. *Analytical Sciences,* 21**,** 1383-1393.

Gong, X., Liu, J., Baskaran, S., Voise, R. D. & Young, J. S. 2000. Surfactant-Assisted Processing of Carbon Nanotube/Polymer Composites. *Chemistry of Materials,* 12**,** 1049-1052.

Grini, P. G., Hjelsvold, M. & Johnsen, S. Choosing produced water treatment technologies based on environmental impact reduction. HSE Conference, 2002 Kuala Lumpur, Malaysia. SPE paper 74002.

Grossiord, N., Regev, O., Loos, J., Meuldijk, J. & Koning, C. E. 2005. Time-Dependent Study of the Exfoliation Process of Carbon Nanotubes in

Aqueous Dispersions by Using UVâˆ'Visible Spectroscopy. *Analytical Chemistry,* 77**,** 5135-5139.

Gutierrez, G., Lobo, A., Allende, D., Cambiella, A., Pazos, C., Coca, J. & Benito, J. M. 2008. Influence of Coagulant Salt Addition on the Treatment of Oil-in-Water Emulsions by Centrifugation, Ultrafiltration, and Vacuum Evaporation. *Separation Science and Technology,* 43**,** 1884 - 1895.

GWI 2006. IDA worldwide desalting plants inventory report no 19. *Global water intelligence,* Gnarrenburg, Germany.

Hahon, N. & Booth, J. A. 1986. Coinhibition of viral interferon induction by benzo[a]pyrene and chrysotile asbestos. *Environmental Research,* 40**,** 103-109.

Hamada, N., Sawada, S.-I. & Oshiyama, A. 1992. New one-dimensional conductors: Graphitic microtubules. *Physical Review Letters,* 68**,** 1579-1581.

Han, R., Zhang, S., Xing, D. & Jian, X. 2010. Desalination of dye utilizing copoly(phthalazinone biphenyl ether sulfone) ultrafiltration membrane with low molecular weight cut-off. *Journal of Membrane Science,* 358**,** 1-6.

Hansen, B. R. & Davies, S. R. H. 1994. Review of potential technologies for the removal of dissolved components from produced water. *Chemical Engineering Research & Design,* 72**,** 176-188.

Harris, P. J. F. 2007. Solid state growth mechanisms for carbon nanotubes. *Carbon,* 45**,** 229-239.

Hayes, A. T. D. 2004. Overview of emerging produced water treatment technologies. *The 11th Annual International Petroleum Environmental Conference.* Albuquerque, NM.

He, Y. & Jiang, Z.-W. 2008. Technology review: Treating oilfield wastewater. *Filtration & Separation,* 45**,** 14-16.

Heins, B. 2005. World's First SAGB Facility Using Evapoorators, Drum Boilers, and Zero Discharge Crystallizers to Treat Produced Water. *Efficiency and Innovation Forum for Oil Patch.* Calgary, Alberta.

Heins, W. F. & McneilL, R. 2007. Vertical-tube evaporator system provides SAGD-quality feed water. *World Oil Magazine* 228.

Heintz, R. A., Rice, S. D., Wertheimer, A. C., Bradshaw, R. F., Thrower, F. P., Joyce, J. E. & Short, J. W. 2000. Delayed effects on growth and marine survival of pink salmon Oncorhynchus gorbuscha after exposure to crude oil during embryonic development. *Marine Ecology Progress Series,* 208**,** 205-216.

Hoffmann, M. R., Martin, S. T., Choi, W. & Bahnemann, D. W. 1995. Environmental Applications of Semiconductor Photocatalysis. *Chemical Reviews,* 95**,** 69-96.

Hofmann, S., Sharma, R., Ducati, C., Du, G., Mattevi, C., Cepek, C., Cantoro, M., Pisana, S., Parvez, A., Cervantes-Sodi, F., Ferrari, A. C., Dunin-Borkowski, R., Lizzit, S., Petaccia, L., GoldonI, A. & Robertson, J. 2007. In situ observations of catalyst dynamics during surface-bound carbon nanotube nucleation. *Nano Letters,* 7**,** 602-608.

Hou, P.-X., Liu, C. & Cheng, H.-M. 2008. Purification of carbon nanotubes. *Carbon,* 46**,** 2003-2025.

Huang, G.-F., Ma, Z.-L., Huang, W.-Q., Tian, Y., Jiao, C., Yang, Z.-M., WAN, Z. & PAN, A. 2013. Ag_3PO_4 semiconductor photocatalyst: possibilities and challenges. *Journal of Nanomaterials,* 2013**,** http://dx.doi.org/10.1155/2013/371356.

Hudgins, C. M. & Petrotech, C. I. 1994. Chemical Use in North Sea Oil and Gas E&P. *Journal of Petroleum Technology,* 46**,** 67 - 74.

Igunnu, E. T. & Chen, G. Z. 2012. Produced water treatment technologies. *International Journal of Low-Carbon Technologies,* doi:10.1093/ijlct/cts049**,** 1 - 21.

Iijima, S. 1991. Helical microtubules of graphitic carbon. *Nature,* 354**,** 56-58.

Ingri, N., Kakolowicz, W., Sillen L.G. & Warnqvist B. 1967. High-speed computers as a supplement to graphical methods - V. HALTAFALL, a general program for calculating the composition of equilibrium mixtures. . *Talanta,* 14**,** 1261-1286.

Ingri, N., Kakolowicz, W., Sillén, L. G. & Warnqvist, B. 1968. High-speed computers as a supplement to graphical methods - V. HALTAFALL, a general program for calculating the composition of equilibrium mixtures. *Errata,* 15**,** xi-xii.

Islam, M. F., Rojas, E., Bergey, D. M., Johnson, A. T. & Yodh, A. G. 2003. High Weight Fraction Surfactant Solubilization of Single-Wall Carbon Nanotubes in Water. *Nano Letters,* 3**,** 269-273.

Jarup, L. 2003. Hazards of heavy metal contamination. *British Medical Bulletin,* 68: **,** 167-182.

Jerez Vegueria, S. F., Godoy, J. M. & Miekeley, N. 2002. Environmental impact studies of barium and radium discharges by produced waters from the "Bacia de Campos" oil-field offshore platforms, Brazil. *Journal of Environmental Radioactivity,* 62**,** 29-38.

Ji, X., Banks, C. E., Crossley, A. & Compton, R. G. 2006. Oxygenated Edge Plane Sites Slow the Electron Transfer of the Ferro-/Ferricyanide Redox Couple at Graphite Electrodes. *ChemPhysChem,* 7**,** 1337-1344.

Jiang, L., Gao, L. & Sun, J. 2003. Production of aqueous colloidal dispersions of carbon nanotubes. *Journal of Colloid and Interface Science,* 260**,** 89-94.

Jiang, T., Zhang, L., Ji, M., Wang, Q., Zhao, Q., Fu, X. & Yin, H. 2013. Carbon nanotubes/TiO2 nanotubes composite photocatalysts for efficient degradation of methyl orange dye. *Particuology*.

Johnsen, A. R., Winding, A., Karlson, U. & Roslev, P. 2002. Linking of microorganisms to phenanthrene metabolism in soil by analysis of (13)C-labeled cell lipids. *Applied and Environmental Microbiology,* 68**,** 6106-13.

Judd, S., Simon, J. & Bruce, J. 2003. Chapter 2 - Membrane technology. *Membranes for Industrial Wastewater Recovery and Re-use.* Amsterdam: Elsevier Science.

Karacik, B., Okay, O. S., Henkelmann, B., Bernhoft, S. & Schramm, K. W. 2009. Polycyclic aromatic hydrocarbons and effects on marine organisms in the Istanbul Strait. *Environment International,* 35**,** 599-606.

Kataura, H., Kumazawa, Y., Maniwa, Y., Umezu, I., Suzuki, S., Ohtsuka, Y. & Achiba, Y. 1999. Optical Properties of Single-Wall Carbon Nanotubes. *Synthetic Metals,* 103**,** 2555-2558.

Kaur, G., Mandal, A. K., Nihlani, M. C. & LAL, B. 2009. Control of sulfidogenic bacteria in produced water from the Kathloni oilfield in northeast India. *International Biodeterioration & Biodegradation,* 63**,** 151-155.

Khawaji, A. D., Kutubkhanah, I. K. & Wie, J.-M. 2008. Advances in seawater desalination technologies. *Desalination,* 221**,** 47-69.

Khemakhem, S., Larbot, A. & Ben Amar, R. 2009. New ceramic microfiltration membranes from Tunisian natural materials: Application for the cuttlefish effluents treatment. *Ceramics International,* 35**,** 55-61.

KhosravI, J. & Alamdari, A. 2009. Copper removal from oil-field brine by coprecipitation. *Journal of Hazardous Materials,* 166**,** 695-700.

Kim, G., Igunnu, E. T. & Chen, G. Z. 2014. A sunlight assisted dual purpose photoelectrochemical cell for low voltage removal of heavy metals and organic pollutants in wastewater. *Chemical Engineering Journal,* 244**,** 411-421.

Kim, H., Senthil, K. & Yong, K. 2010. Photoelectrochemical and photocatalytic properties of tungsten oxide nanorods grown by thermal evaporation. *Materials Chemistry and Physics,* 120**,** 452-455.

Kim, P., Shi, L., Majumdar, A. & Mceuen, P. L. 2001. Thermal Transport Measurements of Individual Multiwalled Nanotubes. *Physical Review Letters,* 87**,** Art. No. 215502.

Kimura, K., Hata, S., Matsumura, S., Tomokiyo, Y., MoritanI, T. & Doi, M. 2005. Tomographic Dark-Field TEM Observation of Ordered and Disordered Precipitates in Ni-Al-Ti Alloy. *Microscopy and Microanalysis,* 11**,** 344-345.

Konieczny, K., Bodzek, M. & Rajca, M. 2006. A coagulation-MF system for water treatment using ceramic membranes. *Desalination,* 198**,** 92-101.

Kou, J., Li, Z., Guo, Y., Gao, J., Yang, M. & Zou, Z. 2010. Photocatalytic degradation of polycyclic aromatic hydrocarbons in GaN:ZnO solid solution-assisted process: Direct hole oxidation mechanism. *Journal of Molecular Catalysis A: Chemical,* 325**,** 48-54.

Kraemer, T. F. & Reid, D. F. 1984. The occurenece and behaviour of radium in saline formation water of the U.S. gulf coast region. *Isotope Geoscience,* 2**,** 153-174.

Krishna, V., Pumprueg, S., Lee, S. H., Zhao, J., Sigmund, W., Koopman, B. & Moudgil, B. M. 2005. Photocatalytic Disinfection with Titanium Dioxide Coated Multi-Wall Carbon Nanotubes. *Process Safety and Environmental Protection,* 83**,** 393-397.

Kruk, M. & Jaroniec, M. 2001. Gas Adsorption Characterization of Ordered Organic-Inorganic Nanocomposite Materials. *Chemistry of Materials,* 13**,** 3169-3183.

Kruusma, J., Mould, N., Jurkschat, K., Crossley, A. & Banks, C. E. 2007. Single walled carbon nanotubes contain residual iron oxide impurities which can dominate their electrochemical activity. *Electrochemistry Communications,* 9**,** 2330-2333.

Kuhn, A., Ballach, H.-J. & Wittig, R. D. 2004. Studies in the Biodegradation of 5 PAHs (Phenanthrene, Pyrene, Fluoranthene, Chrysene und Benzo(a)pyrene) in the Presence of Rooted Poplar Cuttings. *Environmental Science and Pollution Research,* 11**,** 22-32.

Lawless, D., Serpone, N. & Meisel, D. 1991. Role of OH radicals and trapped holes in photocatalysis. A pulse radiolysis study. *Journal of physical Chemistry,* 95**,** 5166-5170.

Lawrence, A. W., Miller, J. A., Miller, D. L. & Hayes, T. D. 1995. A regional assessment of produced water treatment and disposal practices and research needs. *SPE/EPA Exploration and Production Environmental Conference.* Houston, TX, 373 -392.

Lee, S.-H., Pumprueg, S., Moudgil, B. & Sigmund, W. 2005. Inactivation of bacterial endospores by photocatalytic nanocomposites. *Colloids and Surfaces B: Biointerfaces,* 40**,** 93-98.

Leng, W. H., ZhU, W. C., Ni, J., Zhang, Z., Zhang, J. Q. & Cao, C. N. 2006. Photoelectrocatalytic destruction of organics using TiO2 as photoanode with simultaneous production of H2O2 at the cathode. *Applied Catalysis A: General,* 300**,** 24-35.

Li, X. Z., Li, F. B., Yang, C. L. & Ge, W. K. 2001. Photocatalytic activity of WOx-TiO2 under visible light irradiation. *Journal of Photochemistry and Photobiology A: Chemistry,* 141**,** 209-217.

Li, Z. 2013. *A Photoelectrochemical Study of CNT/TiO2 Nanocomposites Synthesised by Surfactant-aided Sol-gel Method.* PhD thesis, University of Nottingham, PhD thesis.

Li, Z., Gao, B., Chen, G. Z., Mokaya, R., Sotiropoulos, S. & Li Puma, G. 2011. Carbon nanotube/titanium dioxide (CNT/TiO_2) core-shell nanocomposites with tailored shell thickness, CNT content and photocatalytic/photoelectrocatalytic properties. *Applied Catalysis B: Environmental,* 110**,** 50-57.

Lin, S. H., Shyu, C. T. & Sun, M. C. 1998. Saline wastewater treatment by electrochemical method. *Water Research,* 32**,** 1059-1066.

Lindquist, S. E., Fell, C., X00fc & Rgen, G. 2009. FUELS - HYDROGEN PRODUCTION | Photoelectrolysis. *Encyclopedia of Electrochemical Power Sources.* Amsterdam: Elsevier, 369-383.

Linsebigler, A. L., Lu, G. & Yates, J. T. 1995. Photocatalysis on TiO_2 surfaces: Principles, mechanisms, and selected results. *Chemical Reviews,* 95**,** 735-758.

Liu, J., Casavant, M. J., Cox, M., Walters, D. A., BouL, P., LU, W., Rimberg, A. J., Smith, K. A., Colbert, D. T. & Smalley, R. E. 1999. Controlled deposition of individual single-walled carbon nanotubes on chemically functionalized templates. *Chemical Physics Letters,* 303**,** 125-129.

Lobo, A., Cambiella, Á., Benito, J. M., Pazos, C. & Coca, J. 2006. Ultrafiltration of oil-in-water emulsions with ceramic membranes: Influence of pH and crossflow velocity. *Journal of Membrane Science,* 278**,** 328-334.

Ma, H. & Wang, B. 2006. Electrochemical pilot-scale plant for oil field produced wastewater by M/C/Fe electrodes for injection. *Journal of Hazardous Materials,* 132**,** 237-243.

Madaeni, S. S. 1999. The application of membrane technology for water disinfection. *Water Research,* 33**,** 301-308.

Madni, I., Hwang, C.-Y., Park, S.-D., Choa, Y.-H. & Kim, H.-T. 2010. Mixed surfactant system for stable suspension of multiwalled carbon nanotubes. *Colloids and Surfaces A: Physicochemical and Engineering Aspects,* 358**,** 101-107.

Malato, S., Blanco, J., Richter, C., Braun, B. & Maldonado, M. I. 1998. Enhancement of the rate of solar photocatalytic mineralization of organic pollutants by inorganic oxidizing species. *Applied Catalysis B: Environmental,* 17**,** 347-356.

Maliszewska-Kordybach, B. & Smreczak, B. E. 2003. Habitat function of agricultural soils as affected by heavy metals and polycyclic aromatic hydrocarbons contamination. *Environment International,* 28**,** 719-728.

Malmgren, R. A., Bennison, B. E. & MC, K. T., JR. 1952. Reduced antibody titers in mice treated with carcinogenic and cancer chemotherapeutic agents. *Proceedings of the Society for Experimental Biology and Medicine,* 79**,** 484-8.

Mark, W. 2007. *The Guidebook to Membrane Desalination Technology: Reverse Osmosis, Nanofiltration and Hybrid Systems Process, DE Design, Applications and Economic*, L'Aquila desalination publications, 160 -180

Matarredona, O., Rhoads, H., LI, Z., Harwell, J. H., Balzano, L. & Resasco, D. E. 2003. Dispersion of Single-Walled Carbon Nanotubes in Aqueous Solutions of the Anionic Surfactant NaDDBS. *The Journal of Physical Chemistry B,* 107**,** 13357-13367.

Meijer, D. T., Karup, H. & Kuijvenhoven cor at 2004. Results from the latest MPPE field trials at NAM and total installations. *NEL Produced Water Workshop.* Aberdeen, UK.

Meijer, D. T. & Madin, C. 2010. Removal of dissolved and dispersed hydrocarbons from oil and gas produced water with mppe technology to reduce toxicity and allow water reuse. *Australian Petroleum Production and Exploration Association Journal***,** 1-11.

Mellendorf, M., Soja, G., Gerzabek, M. H. & Watzinger, A. 2010. Soil microbial community dynamics and phenanthrene degradation as affected by rape oil application. *Applied Soil Ecology,* 46**,** 329-334.

Merkoçi, A. 2006. Carbon Nanotubes in Analytical Sciences. *Microchimica Acta,* 152**,** 157-174.

Michel, J. 1990. Relationship of radium and radon with geological formations. *In:* COTHERN, C. R. & RIBERS, P. A. (eds.) *Uranium in drinking water.* Chelsea, MI: Lewis publishers, 83-95.

Mills, A. & LE Hunte, S. 1997. An overview of semiconductor photocatalysis. *Journal of Photochemistry and Photobiology A: Chemistry,* 108**,** 1-35.

Mondal, S. & Wickramasinghe, S. R. 2008. Produced water treatment by nanofiltration and reverse osmosis membranes. *Journal of Membrane Science,* 322**,** 162-170.

Moore, V. C., Strano, M. S., Haroz, E. H., Hauge, R. H., Smalley, R. E., Schmidt, J. & Talmon, Y. 2003. Individually Suspended Single-Walled Carbon Nanotubes in Various Surfactants. *Nano Letters,* 3**,** 1379-1382.

Nadav, N. 1999. Boron removal from seawater reverse osmosis permeate utilizing selective ion exchange resin. *Desalination,* 124**,** 131-135.

Nakata, K. & Fujishima, A. 2012. TiO2 photocatalysis: Design and applications. *Journal of Photochemistry and Photobiology C: Photochemistry Reviews,* 13**,** 169-189.

Nebojša, D. N., Ljubica, J. P., Miomir, G. P. & Konstantin, I. P. 2007. Effect of temperature on the electrodeposition of disperse copper deposits. *Journal of the Serbian Chemical Society,* 72**,** 1369-1381.

Neff, J. M., Johnsen, S., Frost, T. K., Utvik, T. I. & Durell, G. S. 2006. Oil well produced water discharges to the North Sea. Part II: comparison of deployed mussels (Mytilus edulis) and the DREAM model to predict ecological risk. *Marine Environment Research,* 62**,** 224-46.

Nicolaisen, B. & Lien, L. 2003. Treating oil and gas produced water using membrane filtration technology. *Produced water workshop.* Aberdeen, Scotland

NTG 2005. Introduction to produced water treatment. *Nature Technology Solutions,* 2-18**,** <http://naturetechsolution.com/images/introduction_to_produced_ water_treatment.pdf>.

O'connell, M. J., Boul, P., Ericson, L. M., Huffman, C., Wang, Y., HAROZ, E., KUPER, C., TOUR, J., AUSMAN, K. D. & SMALLEY, R. E. 2001. Reversible water-solubilization of single-walled carbon nanotubes by polymer wrapping. *Chemical Physics Letters,* 342**,** 265-271.

OGP 2005. Fate and effects of naturally occuring substances in produced water on the marine environment. *International Association of Oil & Gas Producers Publications,* Report No. 364**,** 1-35.

Oh, W.-C. & Chen, M.-L. 2008. Synthesis and Characterization of CNT/TiO2 Composites Thermally Derived from MWCNT and Titanium(IV) *n*-Butoxide. *Bulletin of the Korean Chemical Society,* 29**,** 159-164.

Oliveira, E. P., Santelli, R. E. & Cassella, R. J. 2005. Direct determination of lead in produced waters from petroleum exploration by electrothermal atomic absorption spectrometry X-ray fluorescence using Ir-W permanent modifier combined with hydrofluoric acid. *Analytica Chimica Acta,* 545**,** 85-91.

OSPAR 2008. Discharges, spills and emissions from offshore oiland gas installations in 2008. *OSPAR Commission Offshore Industry Series***,** 1-53.

Panizza, M., Bocca, C. & Cerisola, G. 2000. Electrochemical treatment of wastewater containing polyaromatic organic pollutants. *Water Research,* 34**,** 2601-2605.

Papandrew, A. B. & Zawodzinski JR, T. A. 2014. Nickel catalysts for hydrogen evolution from CsH2PO4. *Journal of Power Sources,* 245**,** 171-174.

Pars, H. M. & Meijer, D. T. 1998. Removal of dissolved hydrocarbons from production water by macro porous polymer extraction (MPPE). *SPE International Conference on Health, Safety and Environment in Oil and Gas Exploration and Production.* SPE paper no. 46577, Caracas, Venezuela.

Partovi-Azar, P. & Namiranian, A. 2012. Stone-Wales defects can cause a metal-semiconductor transition in carbon nanotubes depending on their orientation. *Journal of Physics: Condensed Matter,* 24**,** 035301.

Pelizzetti, E., Pramauro, E., Minero, C. & Serpone, N. 1990. Sunlight photocatalytic degradation of organic pollutants in aquatic systems. *Waste Management,* 10**,** 65-71.

Pletcher, D. & Sotiropoulos, S. 1994. Hydrogen adsorption-desorption and oxide formation-reduction on polycrystalline platinum in unbuffered aqueous solutions. *Journal of the Chemical Society, Faraday Transactions,* 90**,** 3663-3668.

Pletcher, D. & Walsh, F. C. 1990. *Industrial electrochemistry.*, Chapman & Hall.

Pollestad, A. The Troll oil case—practical approach towards zero discharge. Produced Water Conference, 2005 Tekna

Pramauro, E., Prevot, A. B., Vincenti, M. & Gamberini, R. 1998. Photocatalytic degradation of naphthalene in aqueous TiO_2 dispersions: effect of nonionic surfactants. *Chemosphere,* 36**,** 1523-1542.

Pshenichnikov, A. G. 1982. Hydrogen evolution on cathodes with a surface skeleton catalyst. *International Journal of Hydrogen Energy,* 7**,** 51-59.

Pumera, M. 2007a. Carbon nanotubes contain residual metal catalyst nanoparticles even after washing with nitric acid at elevated temperature because these metal nanoparticles are sheathed by several graphene sheets. *Langmuir,* 23**,** 6453-6458.

Pumera, M. 2007b. Electrochemical properties of double wall carbon nanotube electrodes. *Nanoscale Research Letters,* 2**,** 87 - 93.

Pumera, M. 2009. The Electrochemistry of Carbon Nanotubes: Fundamentals and Applications. *Chemistry – A European Journal,* 15**,** 4970-4978.

Pumera, M., Sasaki, T. & Iwai, H. 2008. Relationship between Carbon Nanotube Structure and Electrochemical Behavior: Heterogeneous Electron Transfer at Electrochemically Activated Carbon Nanotubes. *Chemistry-an Asian Journal,* 3**,** 2046-2055.

Pyrgiotakis, G., Lee, S.-H. & Sigmund, W. 2005. Advanced Photocatalysis with Anatase Nano-coated Multi-walled Carbon Nanotubes. . *MRS Proceedings,* 876, R5.7 doi:10.1557/PROC-876-R5.7.

Qian, D., Dickey, E. C., Andrews, R. & Rantell, T. 2000. Load transfer and deformation mechanisms in carbon nanotube-polystyrene composites. *Applied Physics Letters,* 76**,** 2868-2870.

Rajkumar, D. & Palanivelu, K. 2004. Electrochemical treatment of industrial wastewater. *Journal of Hazardous Materials,* 113**,** 123-129.

RastogI, R., Kaushal, R., Tripathi, S. K., Sharma, A. L., Kaur, I. & BHARADWAJ, L. M. 2008. Comparative study of carbon nanotube dispersion using surfactants. *Journal of Colloid and Interface Science,* 328**,** 421-428.

Ray, J. P. & Engelhardt, F. R. 1992. Produced water: technological/environmental issues and solutions. *Environmental Science Research,* 46**,** 1-5.

Reich, S., Thomsen, C. & Maultzsch, J. 2004. *Carbon Nanotubes: Basic concepts and physical properties,* Wiley-VCH, Weinheim, Germany.

Reid, D. F. 1983. Radium in formation waters: How much and is it of concern? *Proceedings 4th Annual MMS Gulf of Mexico Regional Office Information Transfer Meetings,* New Orleans, Louisiana**,** 187 - 191.

Reynolds, R. R. 2003. Produced Water and Associated Issues. *A manual for the independent operator* 6**,** 1- 56.

Rice, S. D., Thomas, R.E., Heintz, R.A., Moles, A., Carls, M.G., Murphy, M.L., Short, J.W., Wertheimer, A.C. 1999. Synthesis of longterm impacts to pink salmon following the Exxon Valdez oil spill: persistence, toxicity, sensitivity and controversy. Exxon Valdez Oil Spill Restoration Project Final Report US. *In:* DEPARTMENT OF COMMERCE NATIONAL OCEANIC AND ATMOSPHERIC ADMINISTRATION (ed.). Auke Bay laboratory, Juneau, Alaska: National Marine Fisheries Service.

Richards, C. E., Anderson, A. Y., Martiniani, S., Law, C. & O'regan, B. C. 2012. The Mechanism of Iodine Reduction by TiO2 Electrons and the Kinetics of Recombination in Dye-Sensitized Solar Cells. *The Journal of Physical Chemistry Letters,* 3**,** 1980-1984.

Roach, R. W., Carr, R. S. & Howard, C. L. 1992. An Assessment of Produced Water Impacts at Two Sites in the Galveston Bay System. *Unpublished report of Galveston Bay Information Center Texas***,** 133 - 151

Roe, T. I. 1998. *Produced water discharges to the North Sea: a study of bioavailability of organic produced water compounds to marine organisms.* PhD, Norwegian University of Science and Technology.

Rubin, H. 2001. Synergistic mechanisms in carcinogenesis by polycyclic aromatic hydrocarbons and by tobacco smoke: a bio-historical perspective with updates. *Carcinogenesis,* 22**,** 1903-1930.

Russell, C. 1995. Ionic Strength of Groundwaters as a Function of Conductivity. *unpublished study for NMSU Agronomy Dept.*

Salt, D. E., Blaylock, M., Kumar, N. P. B. A., Dushenkov, V., Ensley, B. D., Chet, I. & Raskin, I. 1995. Phytoremediation: A novel strategy for the removal of toxic metals from environment using plants. *Biotechnology,* 13**,** 468 - 474.

Sandler, J., Shaffer, M. S. P., Prasse, T., Bauhofer, W., Schulte, K. & Windle, A. H. 1999. Development of a dispersion process for carbon nanotubes in an epoxy matrix and the resulting electrical properties. *Polymer,* 40**,** 5967-5971.

Schmidt, C. J., Boyle, W. C., Clements, E. V., Otis, R. J., Bauer, D. H., Siegrist, R. L., Tyler, E. J., Stewart, D. E. & Converse, J. C. 1980. Design Manual: Onsite Wastewater Treatment and Disposal Systems *United States Environmental Protection Agency,* EPA 625/1-80-012 1-366.

Sclafani, A. 1996. Comparison of the photoelectronic and photocatalytic activities of various anatase and rutile forms of titania in pure liquid organic phases and in aqueous solutions. *Journal of physical Chemistry,* 100**,** 13655-13661.

Sclafani, A. & Herrmann, J.-M. 1998. Influence of metallic silver and of platinum-silver bimetallic deposits on the photocatalytic activity of titania (anatase and rutile) in organic and aqueous media. *Journal of Photochemistry and Photobiology A: Chemistry,* 113**,** 181-188.

Scott, L. T., Jackson, E. A., Zhang, Q., Steinberg, B. D., Bancu, M. & LI, B. 2012. A short, rigid, structurally pure carbon nanotube by stepwise chemical synthesis. *J Am Chem Soc,* 134**,** 107-10.

Selembo, P. A., Merrill, M. D. & Logan, B. E. 2010. Hydrogen production with nickel powder cathode catalysts in microbial electrolysis cells. *International Journal of Hydrogen Energy,* 35**,** 428-437.

Serp, P., Corrias, M. & Kalck, P. 2003. Carbon nanotubes and nanofibers in catalysis. *Applied Catalysis A: General,* 253**,** 337-358.

Shackelford, C., Malusis, M., Majeski, M. & Stern, R. 1999. Electrical Conductivity Breakthrough Curves. *Journal of Geotechnical and Geoenvironmental Engineering,* 125**,** 260-270.

Shao, W. & Zangari, G. 2009. Dendritic Growth and Morphology Selection in Copper Electrodeposition from Acidic Sulfate Solutions Containing Chlorides. *The Journal of Physical Chemistry C,* 113**,** 10097-10102.

Shi, W., Becker, J., Bischoff, M., Turco, R. F. & Konopka, A. E. 2002. Association of microbial community composition and activity with lead, chromium, and hydrocarbon contamination. *Applied and Environmental Microbiology,* 68**,** 3859-66.

Shi W., B. J., Bischoff M., Turco R. F AND Konopka1 A. E. 2002. Association of Microbial Community Composition and Activity with

Lead, Chromium, and Hydrocarbon Contamination. *Appl. Environ. Microbiol.,* 68**,** 3859-3866

Sing, K. S. W., Everett, D. H., Haul, R. A. W., Moscou, L., PierottI, R. A., Rouquerol, J. & Siemieniewska, T. 1985. Reporting Physisorption Data for Gas/Solid Systems with Special Reference to the Determination of Surface Area and Porosity. *Pure and Applied Chemistry,* 57**,** 603-619.

Sirivedhin, T., Mccue, J. & Dallbauman, L. 2004. Reclaiming produced water for beneficial use: salt removal by electrodialysis. *Journal of Membrane Science,* 243**,** 335-343.

Snoeyink, V. L. & Jenkins, D. 1980. Water Chemistry. John

Wiley & Sons, New York**,** 435.

Spellman, F. R. 2003. *Handbook of water and wastewater treatment plant operations*, CRC Press, 3-630.

Spence, J. C. H. 1988. *Experimental High-Resolution Electron Microscopy,* New York, NY, Oxford University Press, Inc.

Spiegler, K. S. & Kedem, O. 1966. Thermodynamics of hyperfiltration (reverse osmosis): criteria for efficient membranes. *Desalination,* 1**,** 311-326.

Srinivasan, R. & Ramesh Bapu, G. N. K. 2013. Effect of additives on electrodeposition of nickel from acetate bath: cyclic voltammetric study. *Transactions of the Institute of Metal Finishing,* 91**,** 52-56.

Srivastava, N. K. & Majumder, C. B. 2008. Novel biofiltration methods for the treatment of heavy metals from industrial wastewater. *Journal of Hazardous Materials,* 151**,** 1-8.

Stephenson, M. T. 1992. A survey of produced water studies. *In:* Ray, J. P. & Engelhardt, F. R. (eds.) *Produced Water: Technological/Environmental Issues and Solutions.* New York: Plenum Publishing Corp.

Strandwitz, N. C., Good, J. & Lewis, N. S. 2011. Photoelectrochemistry of semiconductors. *Electrochemistry Encyclopedia,* http://electrochem.cwru.edu/encycl/art-p06-photoel.htm.

Strano, M. S., Moore, V. C., Miller, M. K., Allen, M. J., Haroz, E. H., Kittrell, C., Hauge, R. H. & SmalleY, R. E. 2003. The role of surfactant adsorption during ultrasonication in the dispersion of single-walled carbon nanotubes. *J Nanosci Nanotechnol,* 3**,** 81-6.

Strømgren, T., Sørstrøm, S. E., Schou, L., Kaarstad, I., Aunaas, T., Brakstad, O. G. & Johansen, Ø. 1995. Acute toxic effects of produced water in relation to chemical composition and dispersion. *Marine Environmental Research,* 40**,** 147-169.

Su, D., Wang, J., Liu, K. & Zhou, D. 2007. Kinetic Performance of Oil-field Produced Water Treatment by Biological Aerated Filter. *Chinese Journal of Chemical Engineering,* 15**,** 591-594.

Suppan, V. P. 1994. *Chemistry and Light*, Royal Society of Chemistry,Cambridge, 5.

Svarovsky, L. 1992. *Hydrocyclones: analysis and applications,* Dordrecht, The Netherlands, Kluwer Academic Publishers, 1-3.

Terrones, M. 2003. SCIENCE AND TECHNOLOGY OF THE TWENTY-FIRSTCENTURY: Synthesis, Properties, and Applications of Carbon Nanotubes. *Annual Reviews of Materials Research,* 33**,** 419-501.

Tien, H. T. & Chen, J. W. 1992. Photoelectrolysis of water in semiconductor septum electrochemical photovoltaic cells. *Solar Energy,* 48**,** 199-204.

Tissue, B. M. 2000. *Activity -coefficients.xls* [Online]. [Accessed May 1 2013].

Tryk, D. A., Fujishima, A. & Honda, K. 2000. Recent topics in photoelectrochemistry: achievements and future prospects. *Electrochimica Acta,* 45**,** 2363-2376.

Turchi, C. S. & Ollis, D. F. 1990. Photocatalytic degradation of organic water contaminants: Mechanisms involving hydroxyl radical attack. *Journal of Catalysis,* 122**,** 178-192.

Uddin, N. M., Capaldi, F. M. & Farouk, B. 2012. Molecular dynamics simulations of carbon nanotube dispersions in water: Effects of nanotube length, diameter, chirality and surfactant structures. *Computational Materials Science,* 53**,** 133-144.

UNEP 1997. Environmental management in oil and gas exploration and production: An overview of issues and management approaches. *Joint E&P Forum/UNEP Technical publication***,** 1-7.

USEPA. 2011. *Toxic and priority pollutants* [Online]. http://water.epa.gov/scitech/methods/cwa/pollutants.cfm. [Accessed July 2 2013].

Utvik, T. I. R. 2003. Composition, Characteristics of produced water in the North Sea. *Produced Water Workshop.* Aberdeen, Scotland.

Van Hattum, B., Cofino, W. P. & Feenstra, J. F. 1992. Environmental Aspects of Produced Water Discharges from Oil and Gas Production on the Dutch Continental Shelf. *Institute for Environmental Studies***,** 2-4.

Vaskevich, A., Sinapi, F., Mekhalif, Z., Delhalle, J. & Rubinstein, I. 2005. Underpotential Deposition of Nickel on {111}-Textured Gold Electrodes in Dimethyl Sulfoxide. *Journal of The Electrochemical Society,* 152**,** C744-C750.

Veil, J. A., Puder, M. G., Elcock, D. & Robert J. Redweik, J. 2004. A White Paper Describing Produced Water from Production of Crude oil, Natural Gas, and Coal Bed Methane. *In:* ENERGY, U. D. O. (ed.). Argonne National Laboratory.

Velmurugan, V. & Srithar, K. 2008. Prospects and scopes of solar pond: A detailed review. *Renewable and Sustainable Energy Reviews,* 12**,** 2253-2263.

Vigolo, B., Penicaud, A., Coulon, C., Sauder, C., Pailler, R., Journet, C., Bernier, P. & Poulin, P. 2000. Macroscopic Fibers and Ribbons of Oriented Carbon Nanotubes. *Science,* 290**,** 1331-1334.

Walsh, F. C. & Herron, M. E. 1991. Electrocrystallization and electrochemical control of crystal growth: fundamental considerations and electrodeposition

of metals. *Journal of Physics D: Applied Physics,* 24**,** 217-225.

Wang, G., Zhou, Y., Wang, X., Chai, X., Huang, L. & Deng, N. 2010. Simultaneous removal of phenanthrene and lead from artificially contaminated soils with glycine-beta-cyclodextrin. *Journal of Hazardous Materials,* 184**,** 690-5.

Wang, H. 2009. Dispersing carbon nanotubes using surfactants. *Current Opinion in Colloid and Interface Science,* 14**,** 364-371.

Wang, W. D., Serp, P., Kalck, P. & Faria, J. L. 2005. Visible light photodegradation of phenol on MWCNT-TiO$_2$ composite catalysts prepared by a modified sol-gel method. *Journal of Molecular Catalysis A,* 235**,** 194-199.

Wang, Y., Wu, J. & Wei, F. 2003. A treatment method to give separated multi-walled carbon nanotubes with high purity, high crystallization and a large aspect ratio. *Carbon,* 41**,** 2939-2948.

Wangl, C. X., Yediler, A., Peng, A. & Kettrup, A. 1995. Photodegradation of phenanthrene in the presence of humic substances and hydrogen peroxide. *Chemosphere,* 30**,** 501-510.

Watson, I. C., Morin JR, O. J. & Henthorne, L. 2003. Desalting Handbook for planners. *Desalting and Water Purification Research and developement Program Report No. 72,* 3rd edition**,** 1-200.

WHO 1995. Lead. *World Health Organisation: Envronmental Health Criteria,* 165.

Wilcke, W. 2007. Global patterns of polycyclic aromatic hydrocarbons (PAHs) in soil. *Geoderma,* 141**,** 157-166.

Winand, R. 1992. Electrocrystallization - theory and applications. *Hydrometallurgy,* 29**,** 567-598.

Woan, K., Pyrgiotakis, G. & Sigmund, W. 2009. Photocatalytic Carbon-Nanotube–TiO_2 Composites. *Advanced Materials,* 21**,** 2233-2239.

Xie, F., Koziar, S. A., Lampi, M. A., Dixon, D. G., Warren, N. P., Borgmann, U., Huang, X. D. & Greenberg, B. M. 2006. Assessment of the toxicity of mixtures of copper, 9,10-phenanthrenequinone, and phenanthrene to Daphnia magna: evidence for a reactive oxygen mechanism. *Environ Toxicol Chem,* 25**,** 613-22.

Xie, X. L., Mai, Y. W. & Zhou, X. P. 2005. Dispersion and alignment of carbon nanotubes in polymer matrix: A review. *Materials Science and Engineering R: Reports,* 49.

Xu, P. & Drewes, J. E. 2006. Viability of nanofiltration and ultra-low pressure reverse osmosis membranes for multi-beneficial use of methane produced water. *Separation and Purification Technology,* 52**,** 67-76.

Yang, Y., Zhang, G., Yu, S. & Shen, X. 2010. Efficient removal of organic contaminants by a visible light driven photocatalyst $Sr_6Bi_2O_9$. *Chemical Engineering Journal,* 162**,** 171-177.

Yao, Y., Li, G., Ciston, S., Lueptow, R. M. & Gray, K. A. 2008. Photoreactive TiO2/Carbon Nanotube Composites: Synthesis and Reactivity. *Environmental Science & Technology,* 42**,** 4952-4957.

Yu, J., Grossiord, N., Koning, C. E. & Loos, J. 2007. Controlling the dispersion of multi-wall carbon nanotubes in aqueous surfactant solution. *Carbon,* 45**,** 618-623.

Zhang, B., Shi, R., Zhang, Y. & Pan, C. 2013. CNTs/TiO2 composites and its electrochemical properties after UV light irradiation. *Progress in Natural Science: Materials International,* 23**,** 164-169.

Zhang, F.-J., Chen, M.-L. & Oh, W.-C. 2009a. Fabrication and Electro-photolysis Property of Carbon Nanotubes/Titanium Composite Photocatalysts for Methylene Blue. *Bulletin of the Korean Chemical Society,* 30**,** 1798-1801.

Zhang, F.-J. & Oh, W.-C. 2010. Characterization and Photonic Effect of Novel Ag-CNT/TiO2 Composites and their Bactericidal Activities. *Bulletin of the Korean Chemical Society,* 31**,** 1981-1988.

Zhang, J., An, M. & Chang, L. 2009b. Study of the electrochemical deposition of Sn-Ag-Cu alloy by cyclic voltammetry and chronoamperometry. *Electrochimica Acta,* 54**,** 2883-2889.

Zhang, J., Lee, J. K., Wu, Y. & Murray, R. W. 2003. Photoluminescence and Electronic Interaction of Anthracene Derivatives Adsorbed on Sidewalls of Single-Walled Carbon Nanotubes. *Nano Letters,* 3**,** 403-407.

Zhang, W., Cao, J., Huang, H. & Zhang, R. 2010. Effect of Coexisting Lead and Phenanthrene on Their Individual Sorption on a Clayish Soil. *Soil and Sediment Contamination: An International Journal,* 19**,** 322-337.

Zhao, X. L. 1990. Effects of benzo(a)pyrene on the humoral immunity of mice exposed by single intraperitoneal injection. *Zhonghua Yu Fang Yi Xue Za Zhi,* 24**,** 220-2.

Zhenga, J., Songa, C., Pana, W., Suna, L., Natarajb, S., Wilhelmb, F. & ARMOR, J. N. 2003. Comparative study of carbon formation on supported ni catalysts during ch4 reforming using TEOM, TPO-IR, TPD-IR and TGA techniques. *Preprints of Papers- American Chemical Society, Division of Fuel Chemistry,* 48**,** 801-803.

Zhou, W., PAN, K., QU, Y., Sun, F., Tian, C., Ren, Z., Tian, G. & FU, H. 2010. Photodegradation of organic contamination in wastewaters by bonding TiO_2/single-walled carbon nanotube composites with enhanced photocatalytic activity. *Chemosphere,* 81**,** 555-561.

Zigah, D., Rodriguez-Lopez, J. & Bard, A. J. 2012. Quantification of photoelectrogenerated hydroxyl radical on TiO2 by surface interrogation scanning electrochemical microscopy. *Physical chemistry chemical physics,* 14**,** 12764-72.

Appendix

Appendix A: Thermodynamic Modelling

Computational thermodynamic model was developed and applied to calculate solution speciation. This constitutes the first step in the development of a dual purpose photoelectrochemical treatment of produced water. The results of thermodynamic modelling of activity coefficient, solution equilibria equations, solubility, ionic strength, effect of pH and applied potential on solution equilibria and speciation using the MEDUSA software are presented This step is important for experimental design and analysis of the cathode and the associated processes. Each condition is set to suit the synthetic produced water used for this work as described in Chapter 3 (cf. Table 3.3).

A.1. Behaviour of copper ions in PW II

I= 7.000 M
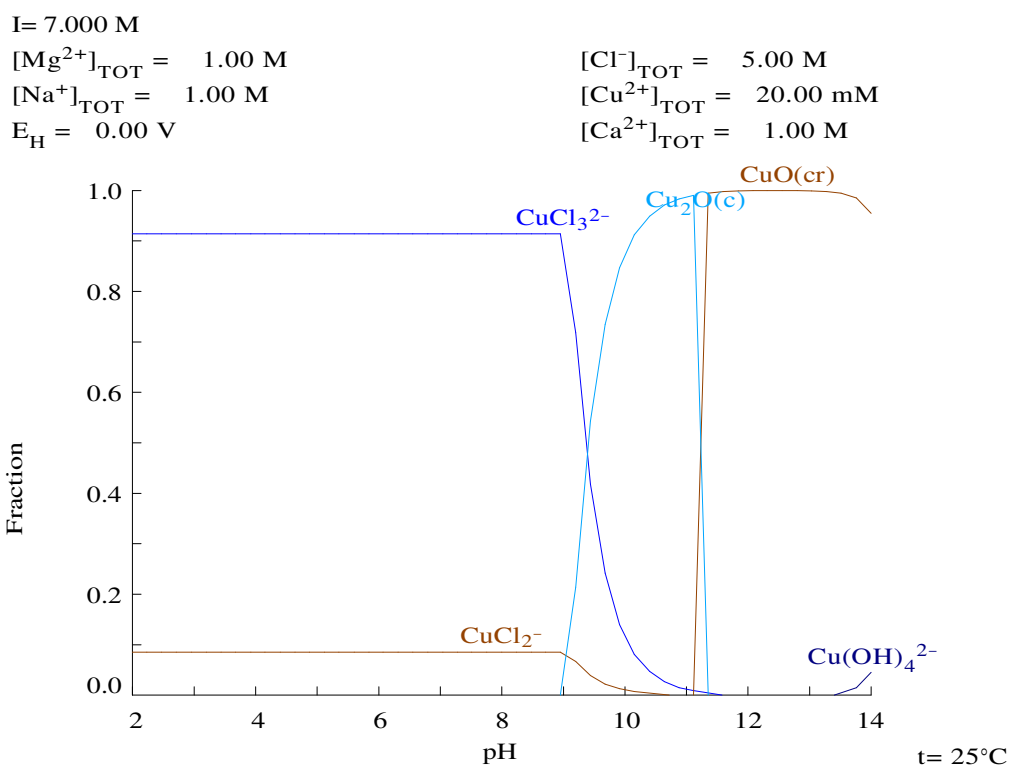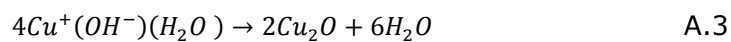$[Mg^{2+}]_{TOT} = $ 1.00 M $[Cl^-]_{TOT} = $ 5.00 M
$[Na^+]_{TOT} = $ 1.00 M $[Cu^{2+}]_{TOT} = $ 20.00 mM
$E_H = $ 0.00 V $[Ca^{2+}]_{TOT} = $ 1.00 M

Figure A.1: States of Cu species in PW II at different pH

$$Cu^{2+} + OH^- \rightleftarrows Cu^{2+}(OH^-) \qquad\qquad\qquad\text{A.1}$$

$$Cu^{2+}(OH^-) + H_2O \rightarrow Cu^+(OH^-)(H_2O) \qquad\qquad\text{A.2}$$

$$4Cu^+(OH^-)(H_2O) \rightarrow 2Cu_2O + 6H_2O \qquad\qquad\text{A.3}$$

I= 7.000 M

[Mg^{2+}]$_{TOT}$ =   1.00 M   [Cl$^-$]$_{TOT}$ =   5.00 M

[Na$^+$]$_{TOT}$ =   1.00 M   [Cu^{2+}]$_{TOT}$ =   20.00 mM

E$_H$ =   0.00 V   [Ca^{2+}]$_{TOT}$ =   1.00 M

t= 25°C

Figure A.2: Solubility of species in PW II

I= 7.000 M

[Na$^+$]$_{TOT}$ = 1.00 M [Cl$^-$]$_{TOT}$ = 5.00 M
E$_H$ = 0.00 V [Ca^{2+}]$_{TOT}$ = 1.00 M
pH = 10.00 [Mg^{2+}]$_{TOT}$ = 1.00 M
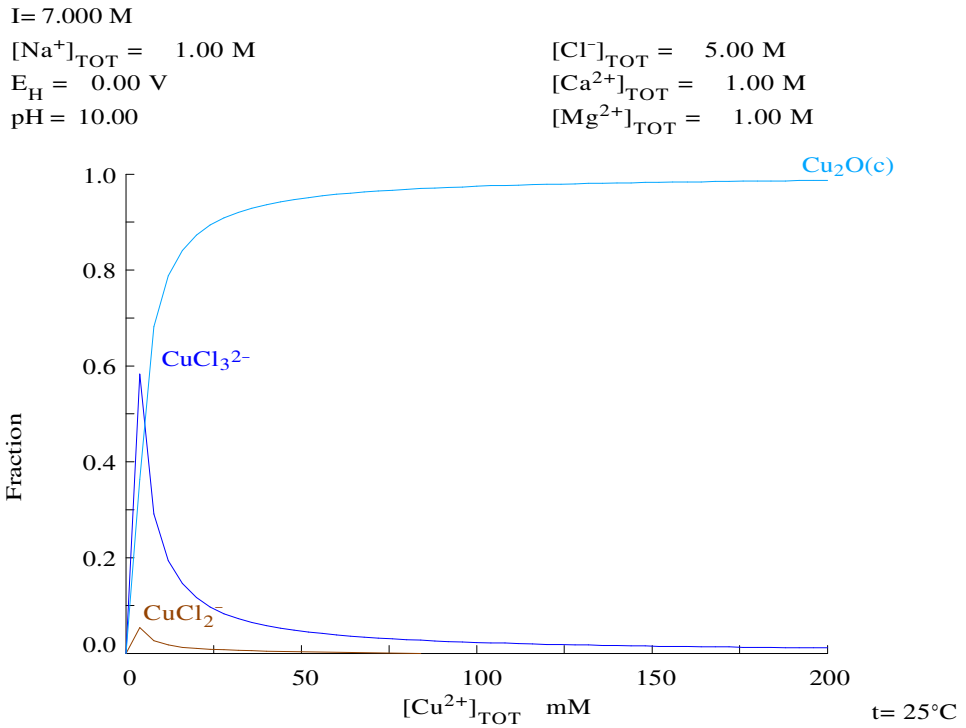
Figure A.3: Effect of concentration of Cu species in PW II at pH 10

I= 7.000 M

[Na$^+$]$_{TOT}$ = 1.00 M [Cl$^-$]$_{TOT}$ = 5.00 M
E$_H$ = 0.00 V [Ca^{2+}]$_{TOT}$ = 1.00 M
pH = 4.00 [Mg^{2+}]$_{TOT}$ = 1.00 M
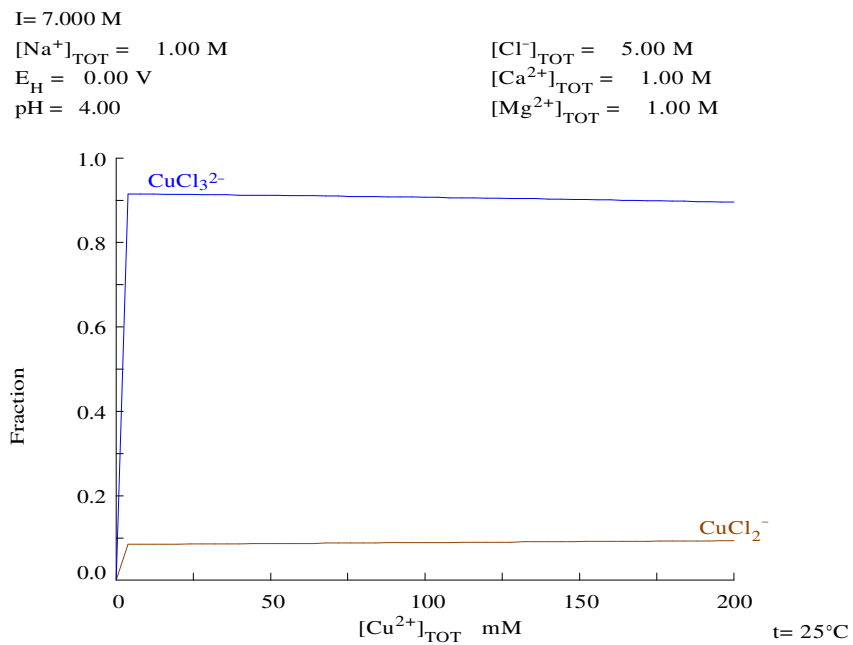
**Figure A.4: Typical effect of concentration on Cu species in PW II at pH 4
and pH 7**

A.1.1. Effect of applied potential on copper deposition from PW II

I= 7.000 M
$[Mg^{2+}]_{TOT} =$ 1.00 M $[Cl^-]_{TOT} =$ 5.00 M
$[Na^+]_{TOT} =$ 1.00 M $[Cu^{2+}]_{TOT} =$ 20.00 mM
pH = 4.00 $[Ca^{2+}]_{TOT} =$ 1.00 M

Figure A.5: State of Cu species under applied potential in PW II at pH 4

I= 7.000 M
$[Mg^{2+}]_{TOT} =$ 1.00 M $[Cl^-]_{TOT} =$ 5.00 M
$[Na^+]_{TOT} =$ 1.00 M $[Cu^{2+}]_{TOT} =$ 20.00 mM
pH = 7.00 $[Ca^{2+}]_{TOT} =$ 1.00 M
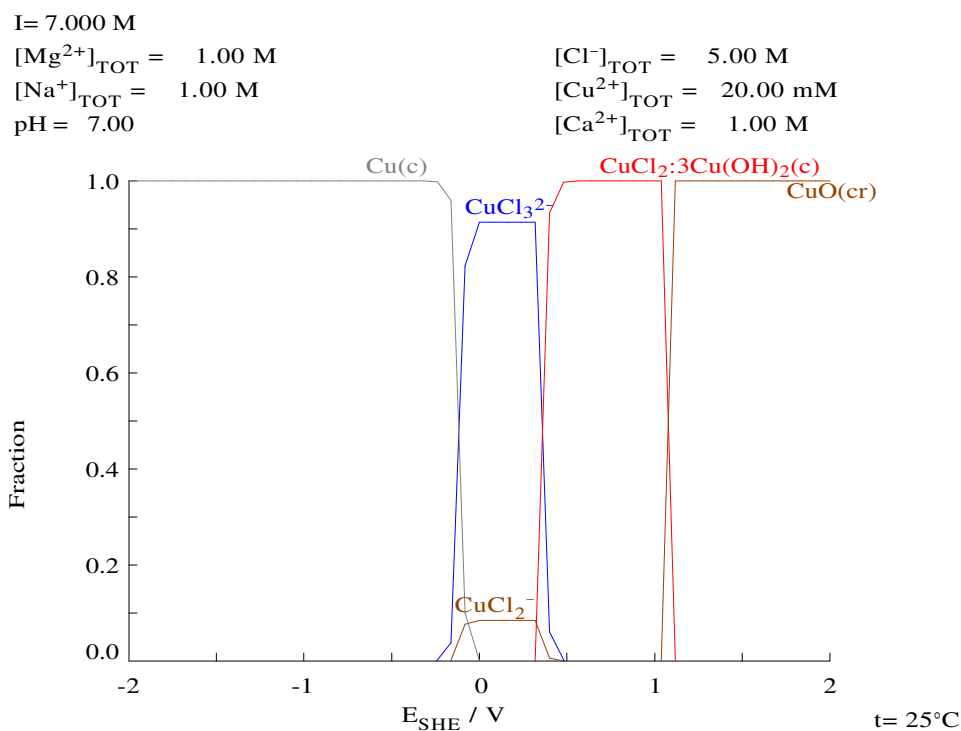
Figure A.6: State of Cu species under applied potential in PW II at pH 7

I= 7.000 M
[Mg^{2+}]$_{TOT}$ = 1.00 M
[Na$^+$]$_{TOT}$ = 1.00 M
pH = 10.00

[Cl$^-$]$_{TOT}$ = 5.00 M
[Cu^{2+}]$_{TOT}$ = 20.00 mM
[Ca^{2+}]$_{TOT}$ = 1.00 M

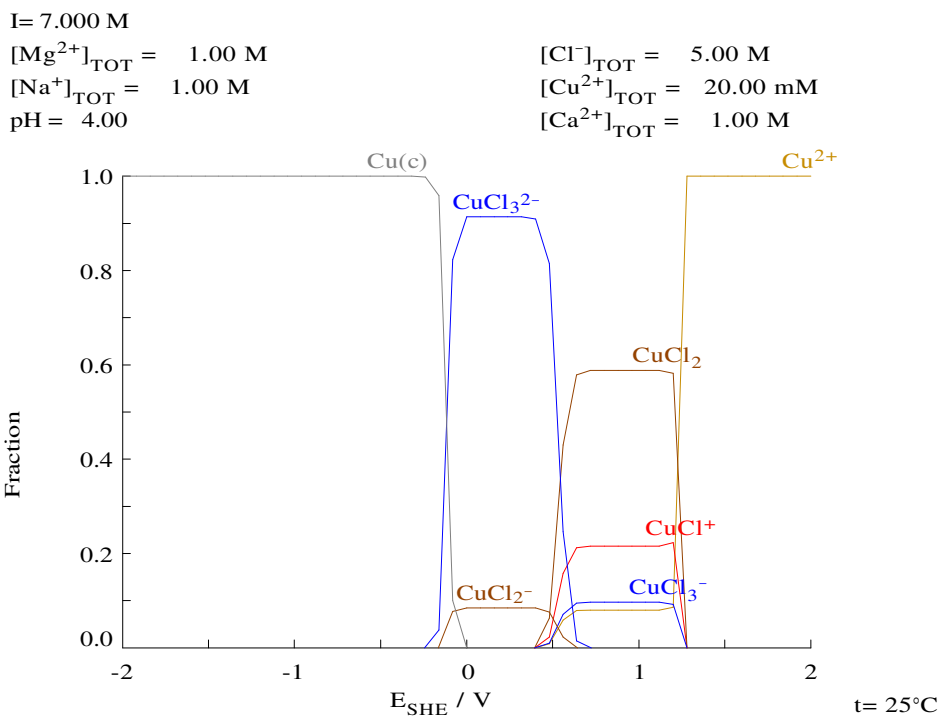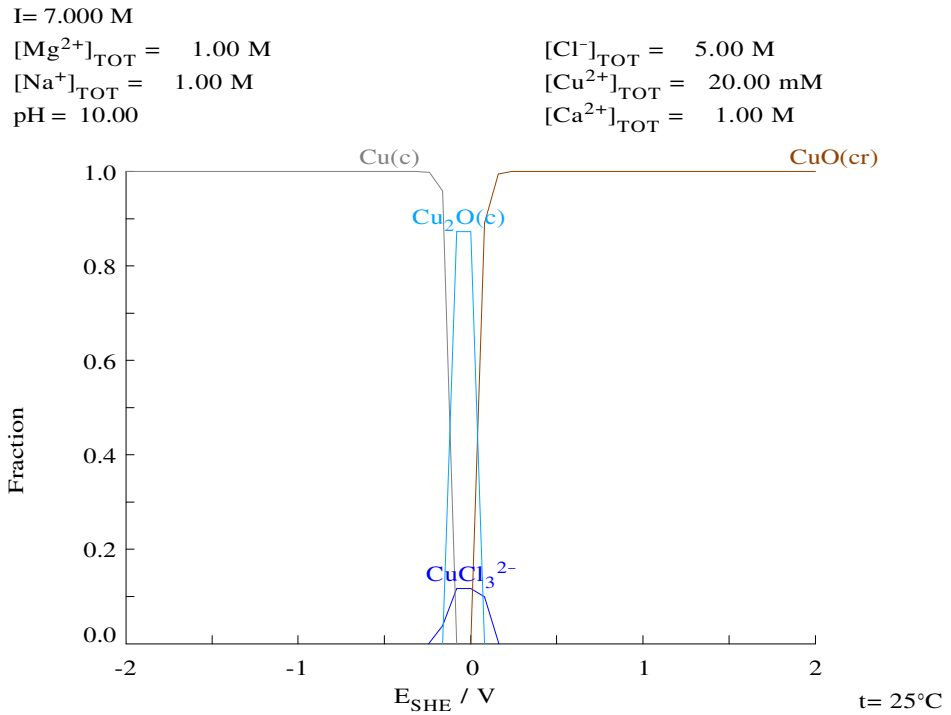**Figure A.7: State of Cu species under applied potential in PW II at pH 10**
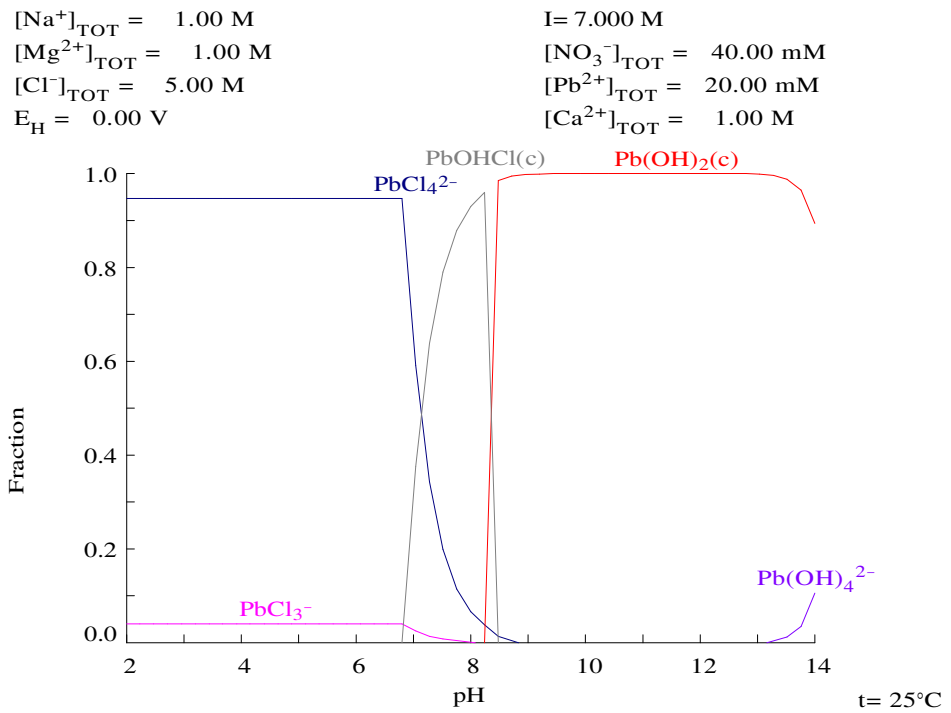
A.2.   Lead behaviour in PW III

[Na$^+$]$_{TOT}$ = 1.00 M
[Mg^{2+}]$_{TOT}$ = 1.00 M
[Cl$^-$]$_{TOT}$ = 5.00 M
E$_H$ = 0.00 V

I= 7.000 M
[NO$_3$$^-$]$_{TOT}$ = 40.00 mM
[Pb^{2+}]$_{TOT}$ = 20.00 mM
[Ca^{2+}]$_{TOT}$ = 1.00 M

Figure A.8: Pb oxidation states in PW III at different pH

[Na$^+$]$_{TOT}$ =   1.00 M
[Mg^{2+}]$_{TOT}$ =   1.00 M
[Cl$^-$]$_{TOT}$ =   5.00 M
E$_H$ =   0.00 V

I= 7.000 M
[NO$_3^-$]$_{TOT}$ =   40.00 mM
[Pb^{2+}]$_{TOT}$ =   20.00 mM
[Ca^{2+}]$_{TOT}$ =   1.00 M

Figure A.9: Solubility distribution of Pb ions in PW III

[Mg^{2+}]$_{TOT}$ =   1.00 M
[Cl$^-$]$_{TOT}$ =   5.00 M
E$_H$ =   0.00 V
pH =   7.00

I= 7.000 M
[NO$_3^-$]$_{TOT}$ =   40.00 mM
[Ca^{2+}]$_{TOT}$ =   1.00 M
[Na$^+$]$_{TOT}$ =   1.00 M

Figure A.10: Effect of concentration of Pb species in PW III at pH 7

$[Mg^{2+}]_{TOT} = 1.00 \text{ M}$ $I = 7.000 \text{ M}$
$[Cl^-]_{TOT} = 5.00 \text{ M}$ $[NO_3^-]_{TOT} = 40.00 \text{ mM}$
$E_H = 0.00 \text{ V}$ $[Ca^{2+}]_{TOT} = 1.00 \text{ M}$
$pH = 10.00$ $[Na^+]_{TOT} = 1.00 \text{ M}$

$t = 25°C$

Figure A.11: Effect of concentration of Pb species in PW III at pH 10

$[Mg^{2+}]_{TOT} = 1.00 \text{ M}$ $I = 7.000 \text{ M}$
$[Cl^-]_{TOT} = 5.00 \text{ M}$ $[NO_3^-]_{TOT} = 40.00 \text{ mM}$
$E_H = 0.00 \text{ V}$ $[Ca^{2+}]_{TOT} = 1.00 \text{ M}$
$pH = 4.00$ $[Na^+]_{TOT} = 1.00 \text{ M}$

$t = 25°C$
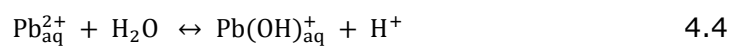
Figure A.12: Effect of concentration of Pb species in PW III at pH 4

A.2.1. Effect of Applied potential on lead species in PW III

$[Na^+]_{TOT} = 1.00\ M$

$[Mg^{2+}]_{TOT} = 1.00\ M$

$[Cl^-]_{TOT} = 5.00\ M$

pH = 7.00

I= 7.000 M

$[NO_3^-]_{TOT} = 40.00\ mM$

$[Pb^{2+}]_{TOT} = 20.00\ mM$

$[Ca^{2+}]_{TOT} = 1.00\ M$

Figure A.13: Thermodynamic prediction of Pb species behaviour in PW III in applied potential window -2 V to 2 V vs. SHE at pH 7

$$Pb_{aq}^{2+} + H_2O \leftrightarrow Pb(OH)_{aq}^+ + H^+ \qquad 4.4$$

$$Pb(OH)_{(aq)}^+ + Cl_{(aq)}^- \rightarrow Pb(OH)Cl_{(s)} \qquad 4.5$$
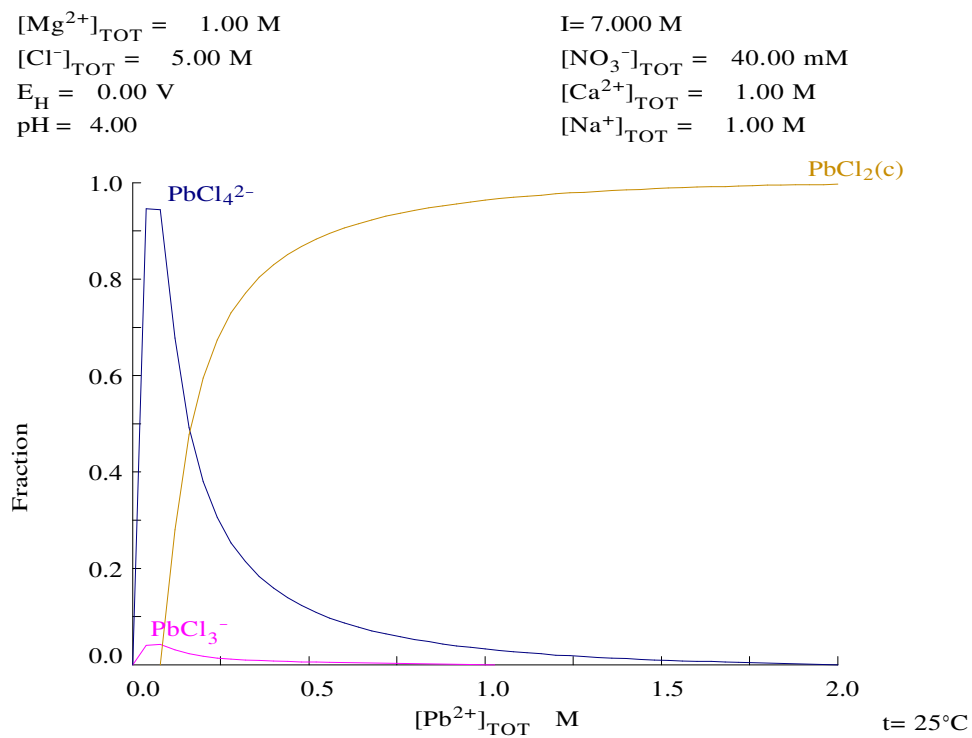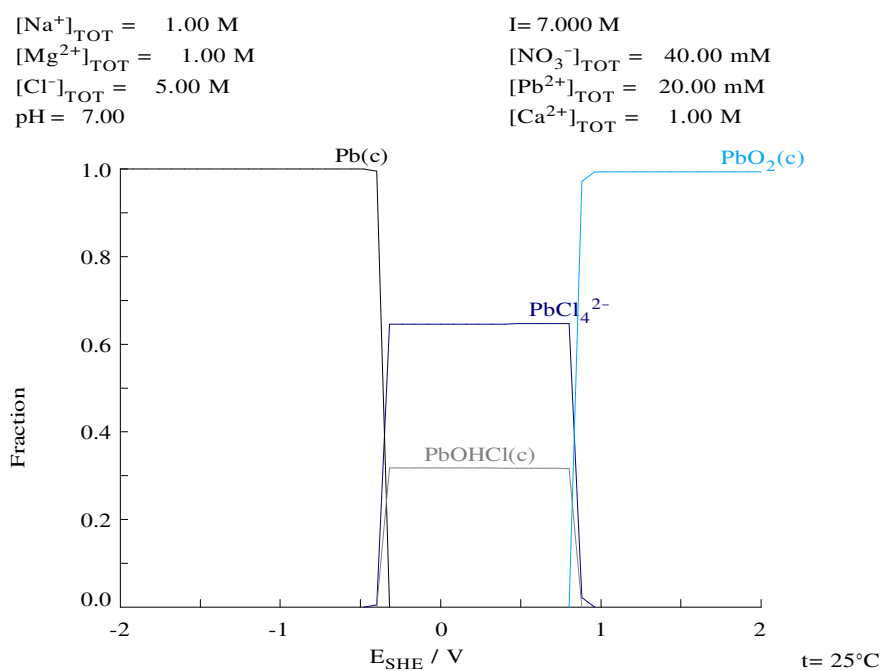
$[Na^+]_{TOT} = 1.00$ M
$[Mg^{2+}]_{TOT} = 1.00$ M
$[Cl^-]_{TOT} = 5.00$ M
pH = 4.00

I= 7.000 M
$[NO_3^-]_{TOT} = 40.00$ mM
$[Pb^{2+}]_{TOT} = 20.00$ mM
$[Ca^{2+}]_{TOT} = 1.00$ M

t= 25°C

Figure A.14: Thermodynamic prediction of Pb species behaviour in PW III in applied potential window -2 V to 2 V vs. SHE at pH 4

$[Na^+]_{TOT} = 1.00$ M
$[Mg^{2+}]_{TOT} = 1.00$ M
$[Cl^-]_{TOT} = 5.00$ M
pH = 10.00

I= 7.000 M
$[NO_3^-]_{TOT} = 40.00$ mM
$[Pb^{2+}]_{TOT} = 20.00$ mM
$[Ca^{2+}]_{TOT} = 1.00$ M

t= 25°C

Figure A.15: Thermodynamic prediction of Pb species behaviour in PW III in applied potential window -2 V to 2 V vs. SHE at pH 10

[NO$_3^-$]$_{TOT}$ = 40.00 mM
[Pb^{2+}]$_{TOT}$ = 20.00 mM   [Ca^{2+}]$_{TOT}$ = 1.00 M
[Cl$^-$]$_{TOT}$ = 5.00 M   [Mg^{2+}]$_{TOT}$ = 1.00 M
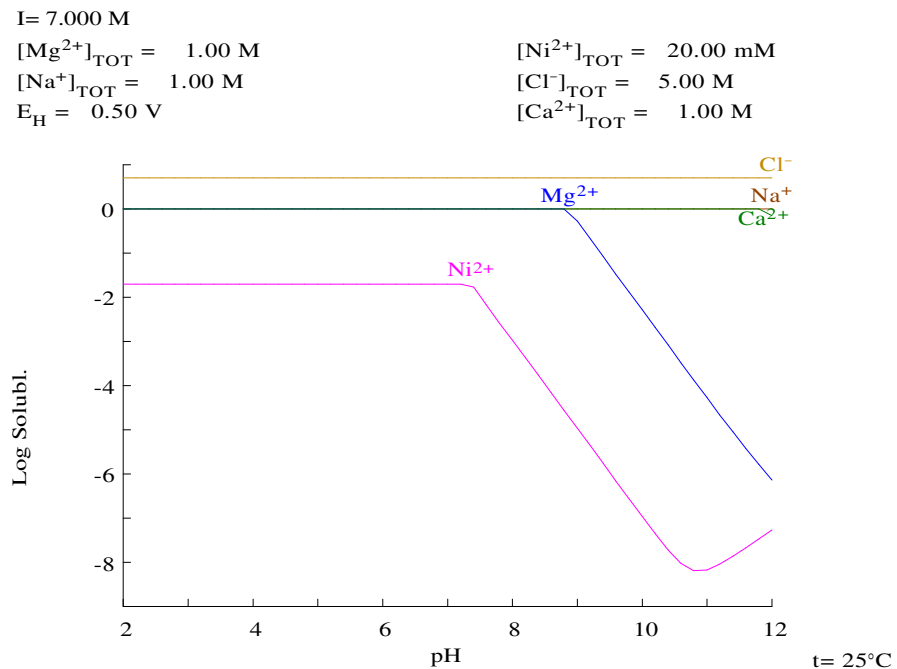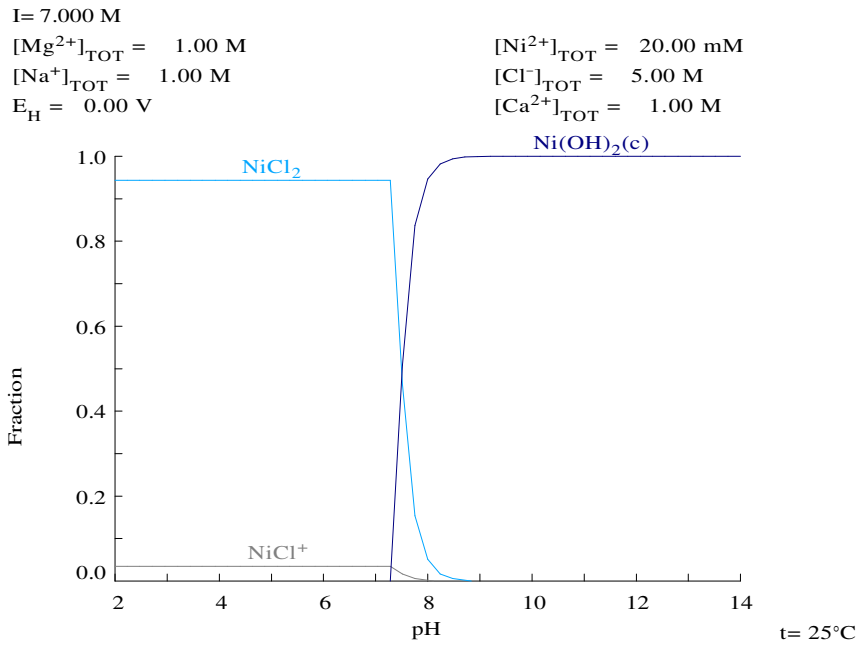pH = 7.00   [Na$^+$]$_{TOT}$ = 1.00 M

Figure A.16: A typical solubility vs. potential curve for PW III at pH 4 -10

A.3. Behaviour of nickel species in PW IV

I= 7.000 M
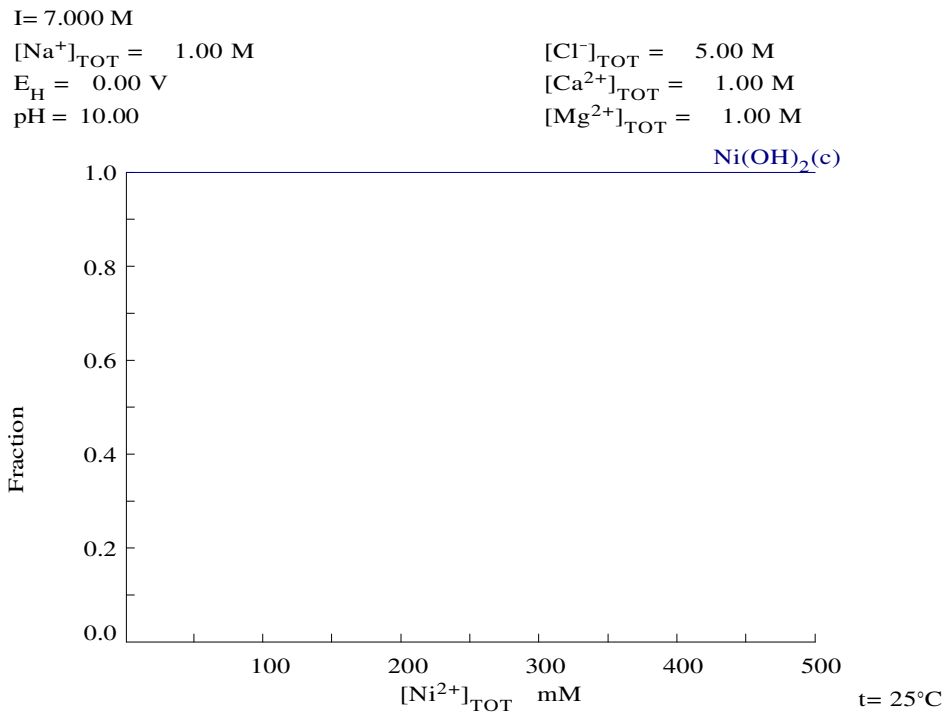[Mg^{2+}]$_{TOT}$ = 1.00 M   [Ni^{2+}]$_{TOT}$ = 20.00 mM
[Na$^+$]$_{TOT}$ = 1.00 M   [Cl$^-$]$_{TOT}$ = 5.00 M
E$_H$ = 0.50 V   [Ca^{2+}]$_{TOT}$ = 1.00 M

Figure A.17: Solubility of Ni in synthetic produced water PW IV

I= 7.000 M

[Mg^{2+}]$_{TOT}$ = 1.00 M   [Ni^{2+}]$_{TOT}$ = 20.00 mM

[Na$^+$]$_{TOT}$ = 1.00 M   [Cl$^-$]$_{TOT}$ = 5.00 M

E$_H$ = 0.00 V   [Ca^{2+}]$_{TOT}$ = 1.00 M

Figure A.18: Fraction of Ni species in PW IV at different pH

I= 7.000 M

[Na$^+$]$_{TOT}$ = 1.00 M   [Cl$^-$]$_{TOT}$ = 5.00 M

E$_H$ = 0.00 V   [Ca^{2+}]$_{TOT}$ = 1.00 M

pH = 7.00   [Mg^{2+}]$_{TOT}$ = 1.00 M
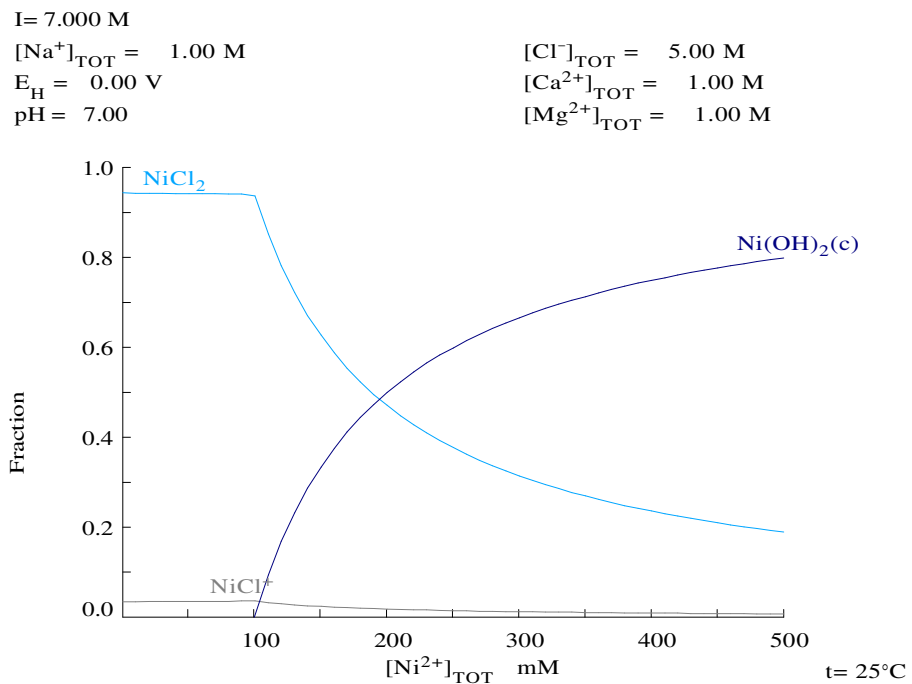
**Figure A.19: Fraction of Ni species in PW IV at pH 7 and different
concentrations**

277

I= 7.000 M

[Na$^+$]$_{TOT}$ =   1.00 M   [Cl$^-$]$_{TOT}$ =   5.00 M

E$_H$ =   0.00 V   [Ca^{2+}]$_{TOT}$ =   1.00 M

pH = 10.00   [Mg^{2+}]$_{TOT}$ =   1.00 M

Figure A.20: Fraction of Ni species in PW IV at pH 10 and different concentrations

I= 7.000 M

[Na$^+$]$_{TOT}$ =   1.00 M   [Cl$^-$]$_{TOT}$ =   5.00 M

E$_H$ =   0.00 V   [Ca^{2+}]$_{TOT}$ =   1.00 M

pH = 4.00   [Mg^{2+}]$_{TOT}$ =   1.00 M
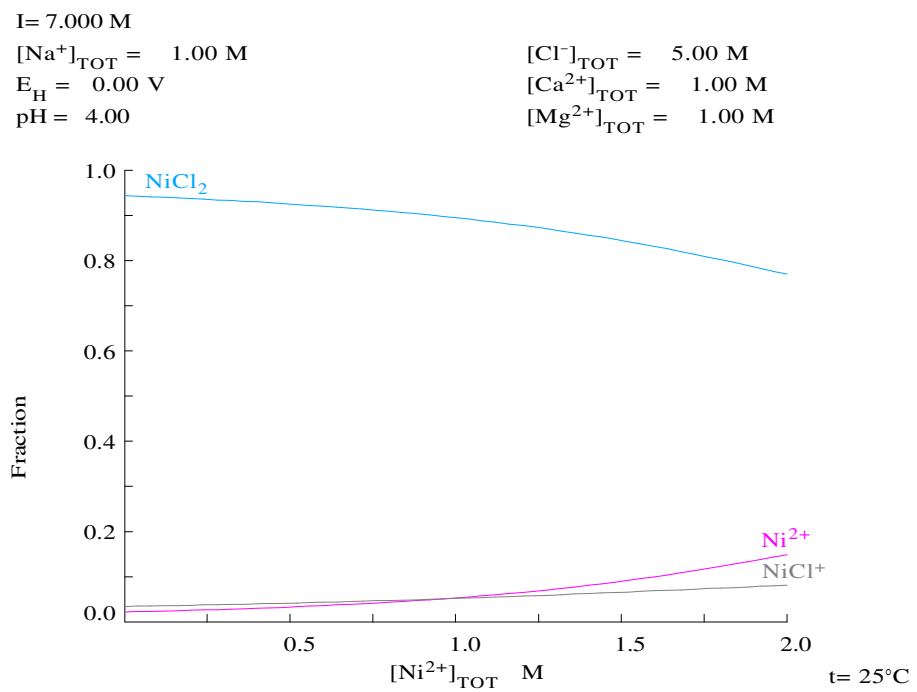
Figure A.21: Fraction of Ni species in PW IV at pH 4 and different

concentration

278

I= 7.000 M
[Mg^{2+}]$_{TOT}$ =   1.00 M   [Ni^{2+}]$_{TOT}$ =   20.00 mM
[Na$^+$]$_{TOT}$ =   1.00 M   [Cl$^-$]$_{TOT}$ =   5.00 M
pH = 10.00   [Ca^{2+}]$_{TOT}$ =   1.00 M
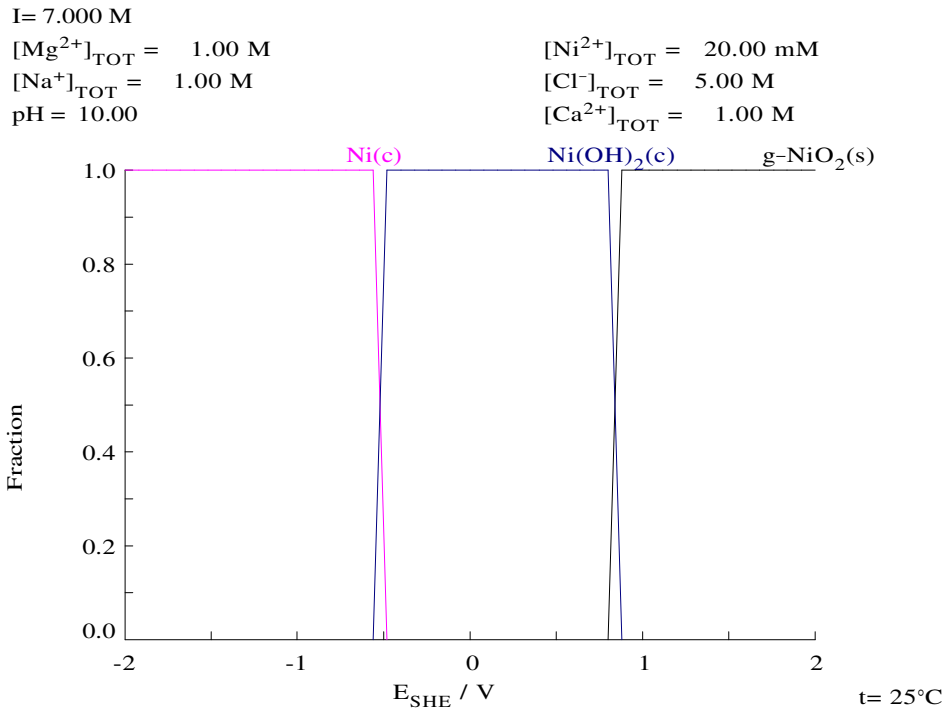
Figure A.22: Effect of applied potential on Ni species in PW IV at pH 10

I= 7.000 M
[Mg^{2+}]$_{TOT}$ =   1.00 M   [Ni^{2+}]$_{TOT}$ =   20.00 mM
[Na$^+$]$_{TOT}$ =   1.00 M   [Cl$^-$]$_{TOT}$ =   5.00 M
pH = 7.00   [Ca^{2+}]$_{TOT}$ =   1.00 M
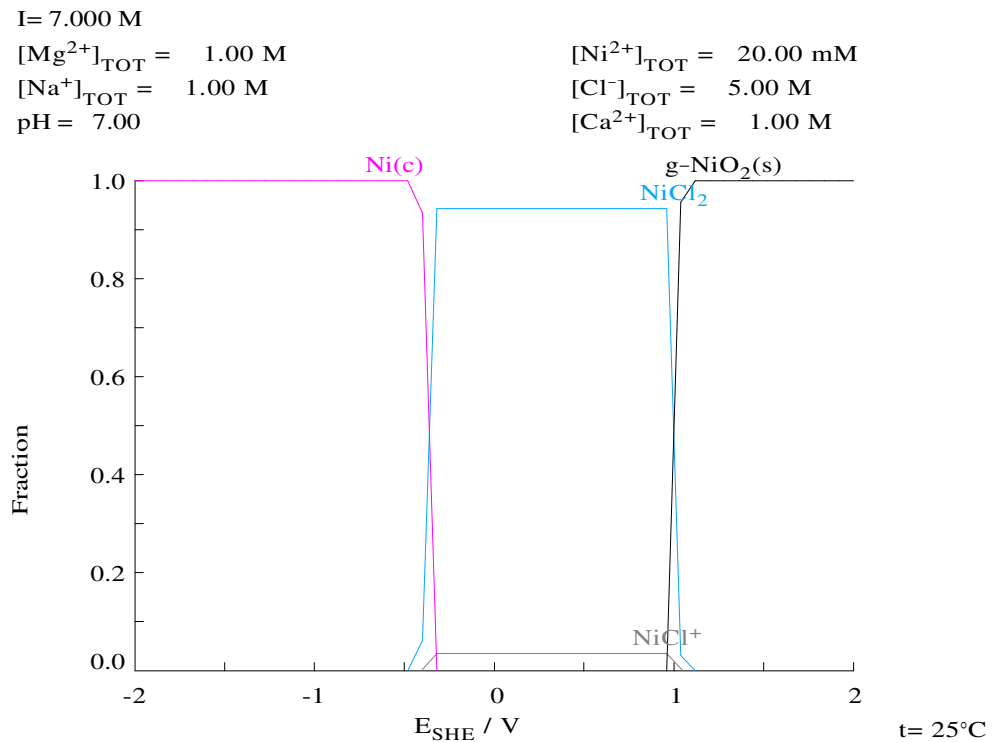
Figure A.23: Effect of applied potential on Ni species in PW IV at pH 7

I= 7.000 M

[Mg^{2+}]$_{TOT}$ = 1.00 M   [Ni^{2+}]$_{TOT}$ = 20.00 mM

[Na$^+$]$_{TOT}$ = 1.00 M   [Cl$^-$]$_{TOT}$ = 5.00 M

pH = 4.00   [Ca^{2+}]$_{TOT}$ = 1.00 M

g-NiO$_2$(s)
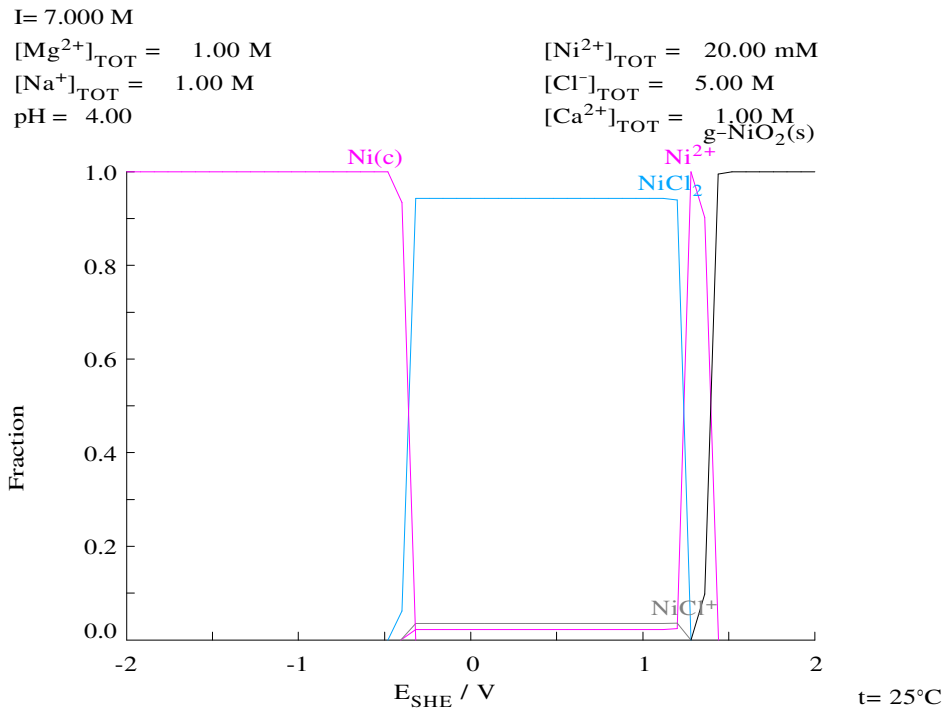
Figure A.24: Effect of applied potential on Ni species in PW IV at pH 4
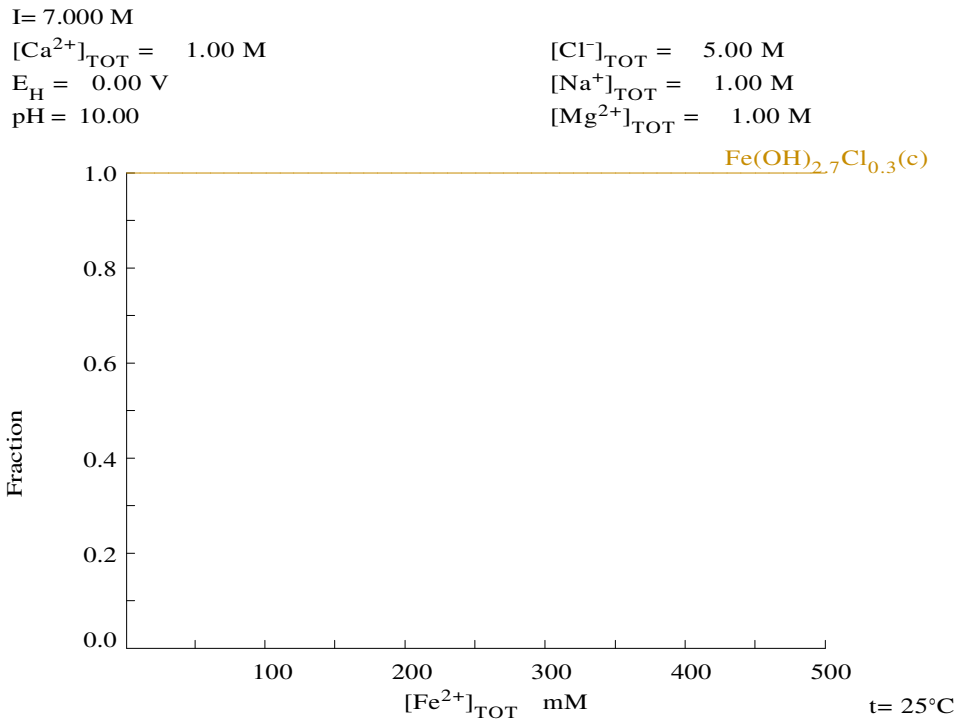
A.4.   Behaviour of iron species in PW V

I= 7.000 M

[Mg^{2+}]$_{TOT}$ = 1.00 M   [Cl$^-$]$_{TOT}$ = 5.00 M

[Ca^{2+}]$_{TOT}$ = 1.00 M   [Fe^{2+}]$_{TOT}$ = 20.00 mM

E$_H$ = 0.00 V   [Na$^+$]$_{TOT}$ = 1.00 M
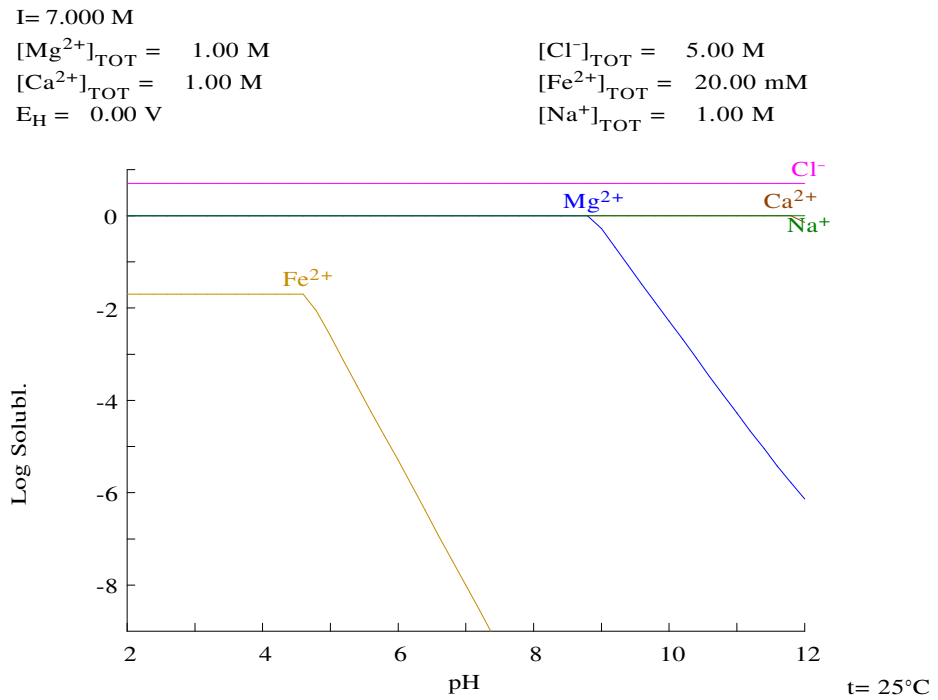
Figure A.25: Solubility of species in PW V

I= 7.000 M
$[Mg^{2+}]_{TOT}$ =   1.00 M $[Cl^-]_{TOT}$ =   5.00 M
$[Ca^{2+}]_{TOT}$ =   1.00 M $[Fe^{2+}]_{TOT}$ =   20.00 mM
E_H =   0.00 V $[Na^+]_{TOT}$ =   1.00 M

$Fe(OH)_{2.7}Cl_{0.3}(c)$ $MgFe_2O_4(c)$

Fe^{2+}
$FeCl^+$

Fraction

pH

t= 25°C
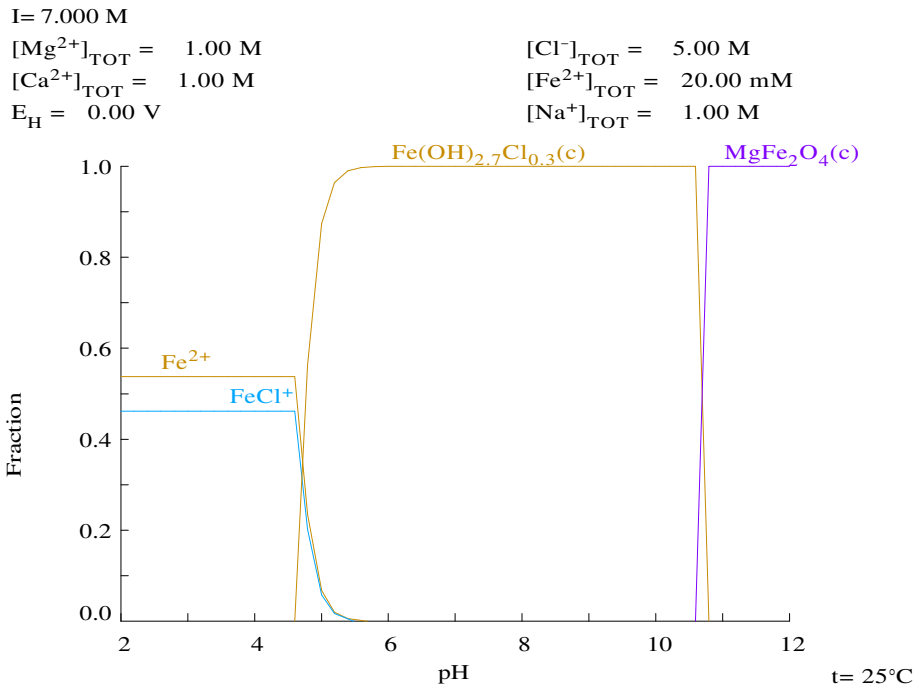
Figure A.26: Fraction of Fe in PW V

I= 7.000 M
$[Ca^{2+}]_{TOT}$ =   1.00 M $[Cl^-]_{TOT}$ =   5.00 M
E_H =   0.00 V $[Na^+]_{TOT}$ =   1.00 M
pH =   7.00 $[Mg^{2+}]_{TOT}$ =   1.00 M

$Fe(OH)_{2.7}Cl_{0.3}(c)$

Fraction

$[Fe^{2+}]_{TOT}$ mM

t= 25°C
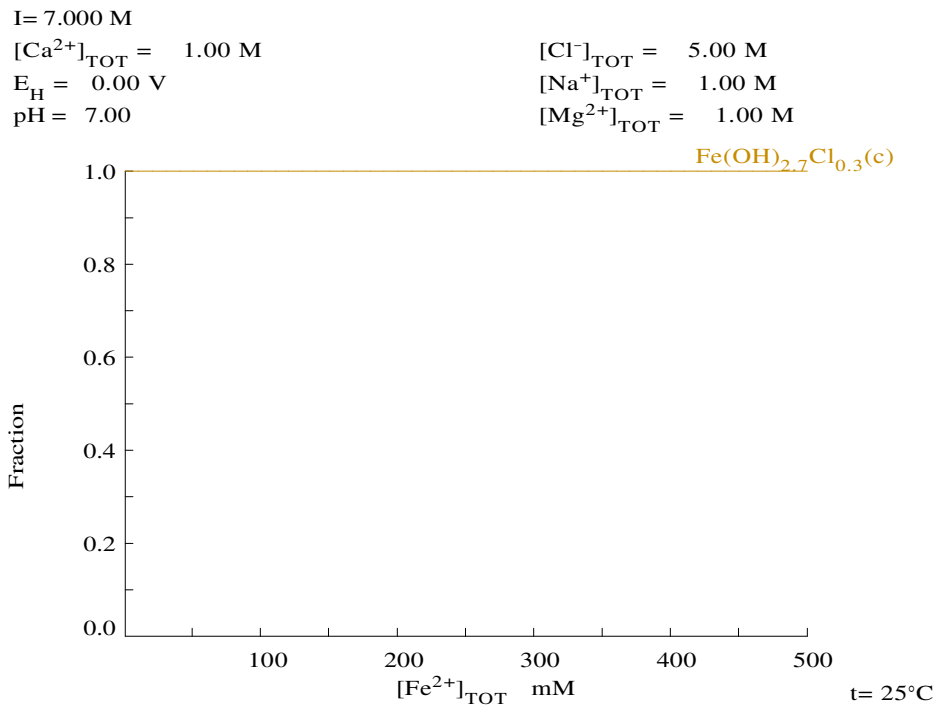
Figure A.27: Effect of concentration on Fe(II) fraction in PW V at pH 7

I= 7.000 M
$[Ca^{2+}]_{TOT} =$ 1.00 M $\qquad$ $[Cl^-]_{TOT} =$ 5.00 M
$E_H =$ 0.00 V $\qquad$ $[Na^+]_{TOT} =$ 1.00 M
pH = 10.00 $\qquad$ $[Mg^{2+}]_{TOT} =$ 1.00 M

$Fe(OH)_{2.7}Cl_{0.3}(c)$

Fraction

$[Fe^{2+}]_{TOT}$ mM

t= 25°C

Figure A.28: Effect of concentration on Fe(II) fraction in PW V at pH 10

I= 7.000 M
$[Ca^{2+}]_{TOT} =$ 1.00 M $\qquad$ $[Cl^-]_{TOT} =$ 5.00 M
$E_H =$ 0.00 V $\qquad$ $[Na^+]_{TOT} =$ 1.00 M
pH = 4.00 $\qquad$ $[Mg^{2+}]_{TOT} =$ 1.00 M

Fe^{2+}

$FeCl^+$

Fraction

$[Fe^{2+}]_{TOT}$ mM

t= 25°C
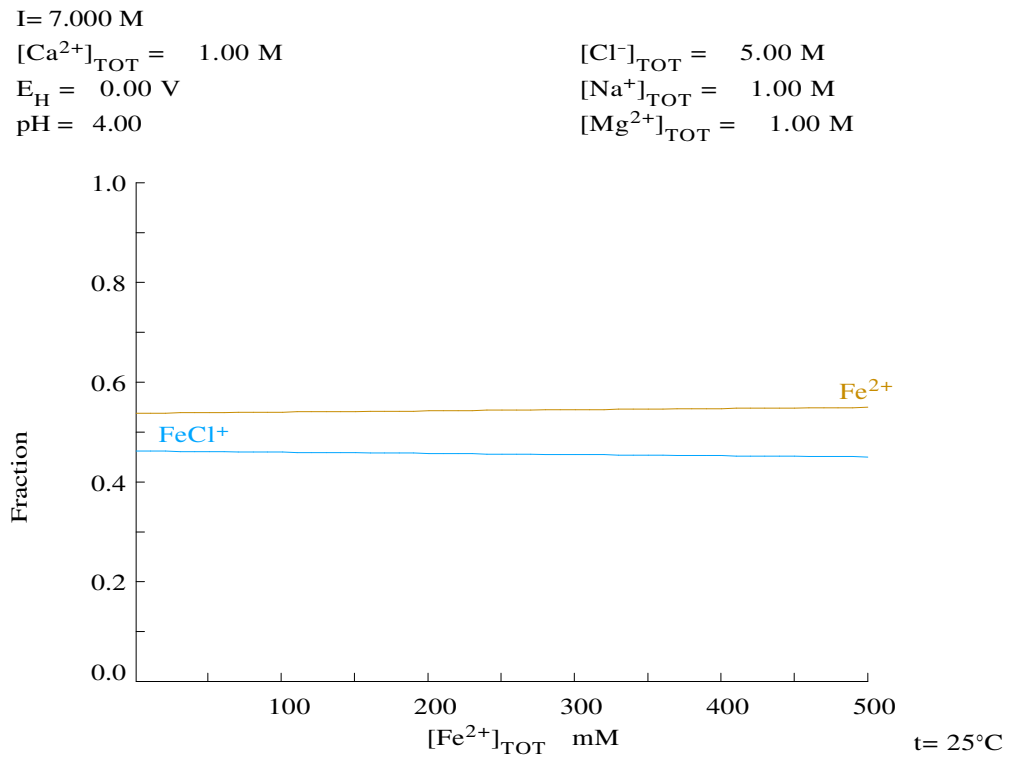
Figure A.29: Effect of concentration on Fe(II) fraction in PW V at pH 4

I= 7.000 M

[Mg^{2+}]$_{TOT}$ = 1.00 M   [Cl$^-$]$_{TOT}$ = 5.00 M

[Ca^{2+}]$_{TOT}$ = 1.00 M   [Fe^{2+}]$_{TOT}$ = 20.00 mM

pH = 7.00   [Na$^+$]$_{TOT}$ = 1.00 M

t= 25°C
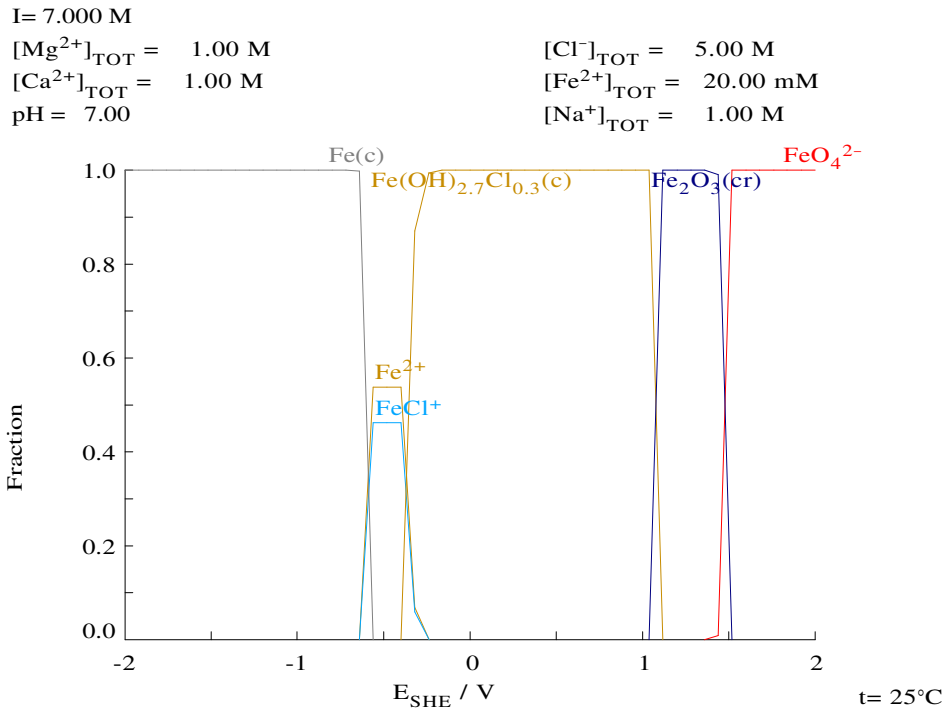
Figure A.30: Effect of applied potential on Fe species in PW V at pH 7

I= 7.000 M

[Mg^{2+}]$_{TOT}$ = 1.00 M   [Cl$^-$]$_{TOT}$ = 5.00 M

[Ca^{2+}]$_{TOT}$ = 1.00 M   [Fe^{2+}]$_{TOT}$ = 20.00 mM

pH = 10.00   [Na$^+$]$_{TOT}$ = 1.00 M

t= 25°C
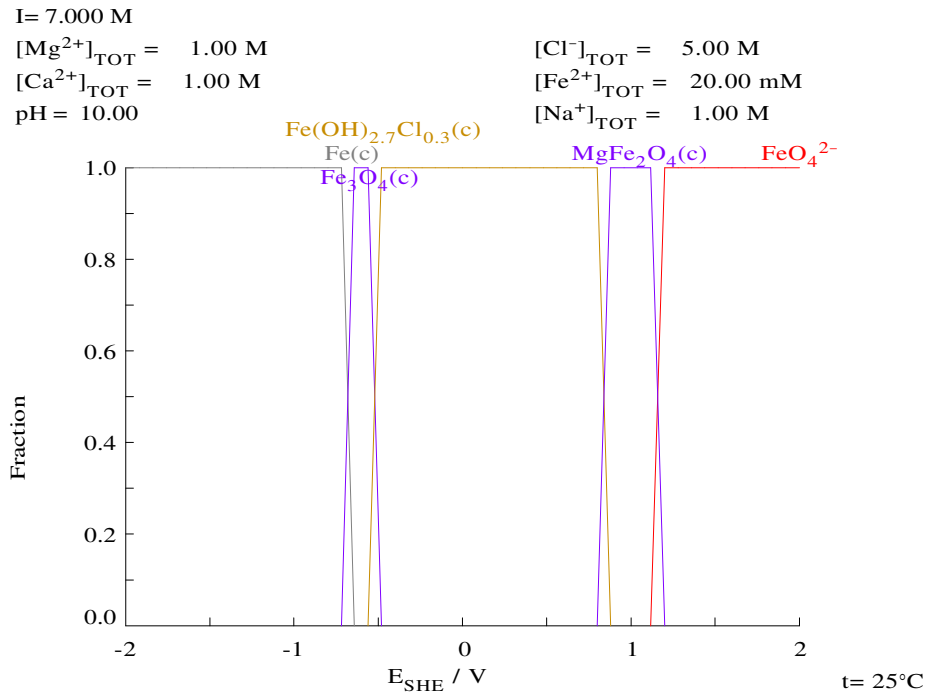
Figure A.31: Effect of applied potential on Fe species in PW V at pH 10

A.5.   Behaviour of multiple metal ions in PW VI

Computational analysis using MEDUSA software shows that PW VI (cf. Table 3.3) containing multiple metal ions is a complex mixture, containing possibly 10 soluble components, 86 soluble complexes and 44 solid complexes. MEDUSA cannot ordinarily handle such a complex solution. Therefore, solid complex species that do not contain lead, copper, nickel or iron were deactivated in the program in order to predict the behaviour of each heavy metal ions in PW VI. The solubility of metal ions as a function of pH, and the fractions of each heavy metal ions in solution and the effects of applied potential on the possible chemical species are estimated in this section

A.5.1. Solubility of heavy metal ions

$[Fe^{2+}]_{TOT} = 20.00$ mM $\qquad$ I= 7.160 M
$[Ca^{2+}]_{TOT} = 1.00$ M $\qquad$ $[Cl^-]_{TOT} = 5.00$ M
$[Na^+]_{TOT} = 1.00$ M $\qquad$ $[Pb^{2+}]_{TOT} = 20.00$ mM
$[Mg^{2+}]_{TOT} = 1.00$ M $\qquad$ $[Cu^{2+}]_{TOT} = 20.00$ mM
$E_H = 0.00$ V $\qquad$ $[Ni^{2+}]_{TOT} = 20.00$ mM

Figure A.32: Solubility of metal species in PW VI

A.5.2. Behaviour of copper species in PW VI

$[Fe^{2+}]_{TOT} = 20.00$ mM

$[Ca^{2+}]_{TOT} = 1.00$ M

$[Na^+]_{TOT} = 1.00$ M

$[Mg^{2+}]_{TOT} = 1.00$ M

$E_H = 0.00$ V

$I = 7.160$ M

$[Cl^-]_{TOT} = 5.00$ M

$[Pb^{2+}]_{TOT} = 20.00$ mM

$[Cu^{2+}]_{TOT} = 20.00$ mM

$[Ni^{2+}]_{TOT} = 20.00$ mM

Figure A.33: Distribution of Cu species in PW VI

$[Fe^{2+}]_{TOT} = 20.00$ mM

$[Ca^{2+}]_{TOT} = 1.00$ M

$[Na^+]_{TOT} = 1.00$ M

$[Mg^{2+}]_{TOT} = 1.00$ M

pH = 4.00

$I = 7.160$ M

$[Cl^-]_{TOT} = 5.00$ M

$[Pb^{2+}]_{TOT} = 20.00$ mM

$[Cu^{2+}]_{TOT} = 20.00$ mM

$[Ni^{2+}]_{TOT} = 20.00$ mM

Figure A.34: Effect of applied potential on Cu species in PW VI at pH 4

$[Fe^{2+}]_{TOT} = 20.00$ mM $\qquad$ I= 7.160 M
$[Ca^{2+}]_{TOT} = 1.00$ M $\qquad$ $[Cl^-]_{TOT} = 5.00$ M
$[Na^+]_{TOT} = 1.00$ M $\qquad$ $[Pb^{2+}]_{TOT} = 20.00$ mM
$[Mg^{2+}]_{TOT} = 1.00$ M $\qquad$ $[Cu^{2+}]_{TOT} = 20.00$ mM
pH = 7.00 $\qquad$ $[Ni^{2+}]_{TOT} = 20.00$ mM

Figure A.35: Effect of applied potential on Cu species in PW VI at pH 7

$[Fe^{2+}]_{TOT} = 20.00$ mM $\qquad$ I= 7.160 M
$[Ca^{2+}]_{TOT} = 1.00$ M $\qquad$ $[Cl^-]_{TOT} = 5.00$ M
$[Na^+]_{TOT} = 1.00$ M $\qquad$ $[Pb^{2+}]_{TOT} = 20.00$ mM
$[Mg^{2+}]_{TOT} = 1.00$ M $\qquad$ $[Cu^{2+}]_{TOT} = 20.00$ mM
pH = 10.00 $\qquad$ $[Ni^{2+}]_{TOT} = 20.00$ mM

Figure A.36: Effect of applied potential on Cu species in PW VI at pH 10

$[Ca^{2+}]_{TOT} = 1.00 M$ $I= 7.160 M$
$[Na^+]_{TOT} = 1.00 M$ $[Cl^-]_{TOT} = 5.00 M$
$[Mg^{2+}]_{TOT} = 1.00 M$ $[Pb^{2+}]_{TOT} = 20.00 mM$
$E_H = 0.00 V$ $[Ni^{2+}]_{TOT} = 20.00 mM$
$pH = 4.00$ $[Fe^{2+}]_{TOT} = 20.00 mM$
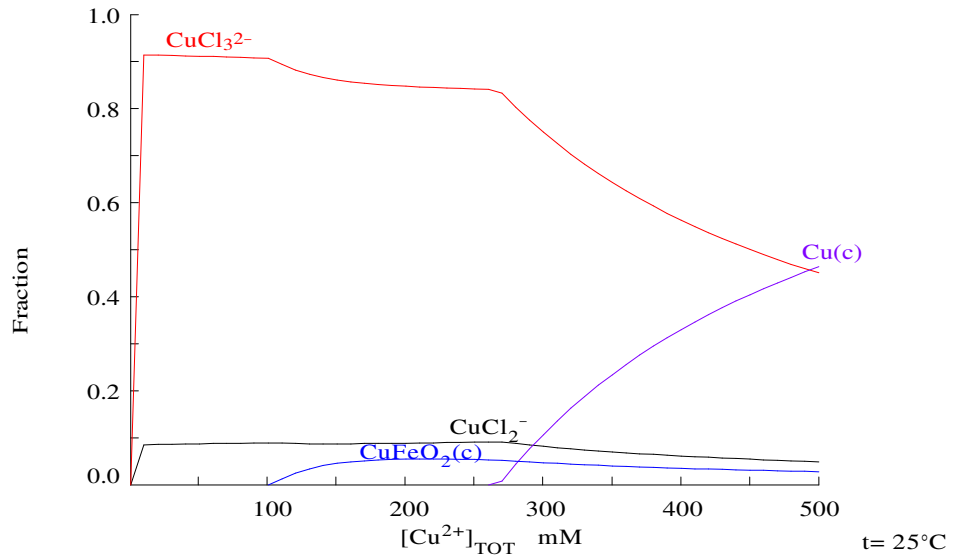
Figure A.37: Effect of concentration of Cu species in PW VI at pH 4

$[Ca^{2+}]_{TOT} = 1.00 M$ $I= 7.160 M$
$[Na^+]_{TOT} = 1.00 M$ $[Cl^-]_{TOT} = 5.00 M$
$[Mg^{2+}]_{TOT} = 1.00 M$ $[Pb^{2+}]_{TOT} = 20.00 mM$
$E_H = 0.00 V$ $[Ni^{2+}]_{TOT} = 20.00 mM$
$pH = 7.00$ $[Fe^{2+}]_{TOT} = 20.00 mM$
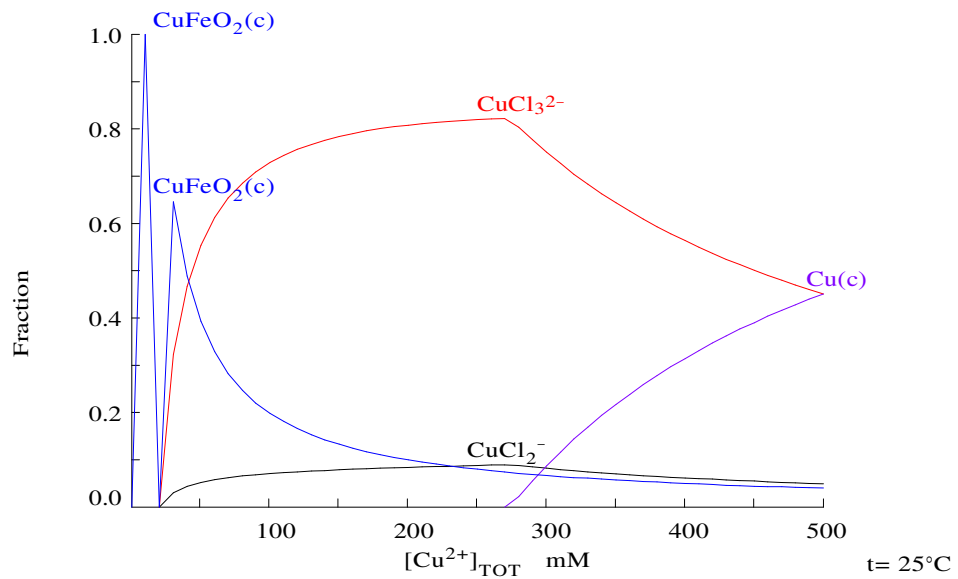
Figure A.38: Effect of concentration of Cu species in PW VI at pH 7

$[Ca^{2+}]_{TOT} = 1.00$ M

$[Na^+]_{TOT} = 1.00$ M

$[Mg^{2+}]_{TOT} = 1.00$ M

$E_H = 0.00$ V

pH = 10.00

I= 7.160 M

$[Cl^-]_{TOT} = 5.00$ M

$[Pb^{2+}]_{TOT} = 20.00$ mM

$[Ni^{2+}]_{TOT} = 20.00$ mM
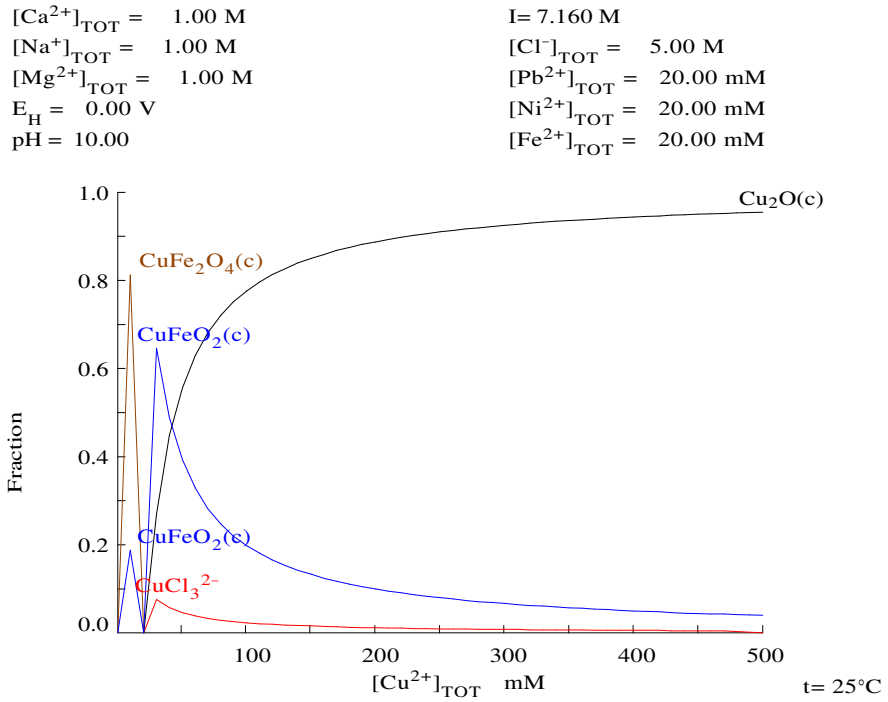
$[Fe^{2+}]_{TOT} = 20.00$ mM

Figure A.39: Effect of concentration of Cu species in PW VI at pH 7

A.5.3. Behaviour of lead species in PW VI

$[Ca^{2+}]_{TOT} = 1.00$ M

$[Na^+]_{TOT} = 1.00$ M

$[Mg^{2+}]_{TOT} = 1.00$ M

$E_H = 0.00$ V

pH = 7.00

I= 7.160 M

$[Cl^-]_{TOT} = 5.00$ M

$[Cu^{2+}]_{TOT} = 20.00$ mM

$[Ni^{2+}]_{TOT} = 20.00$ mM
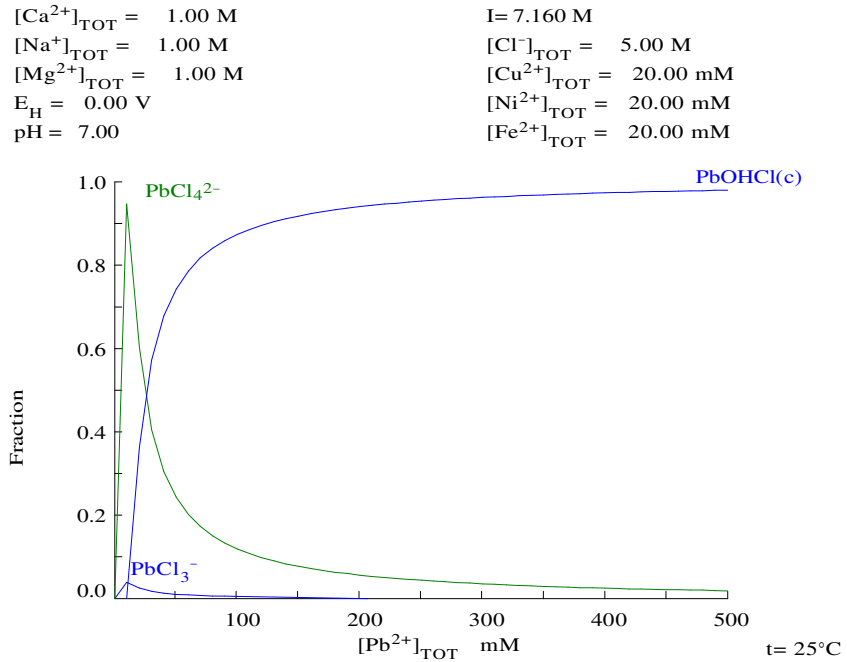
$[Fe^{2+}]_{TOT} = 20.00$ mM

Figure A.40: Effect of concentration on Pb species in PW VI at pH 7

A.5.4. Behaviour of nickel species in PW VI

$[Fe^{2+}]_{TOT} = 20.00$ mM $I = 7.160$ M
$[Ca^{2+}]_{TOT} = 1.00$ M $[Cl^-]_{TOT} = 5.00$ M
$[Na^+]_{TOT} = 1.00$ M $[Pb^{2+}]_{TOT} = 20.00$ mM
$[Mg^{2+}]_{TOT} = 1.00$ M $[Cu^{2+}]_{TOT} = 20.00$ mM
$E_H = 0.00$ V $[Ni^{2+}]_{TOT} = 20.00$ mM

t= 25°C

Figure A.41: Fraction of Ni species in PW VI at different pH values

A.5.5. Behaviour of iron species in PW VI

$[Fe^{2+}]_{TOT} = 20.00$ mM $I = 7.160$ M
$[Ca^{2+}]_{TOT} = 1.00$ M $[Cl^-]_{TOT} = 5.00$ M
$[Na^+]_{TOT} = 1.00$ M $[Pb^{2+}]_{TOT} = 20.00$ mM
$[Mg^{2+}]_{TOT} = 1.00$ M $[Cu^{2+}]_{TOT} = 20.00$ mM
$E_H = 0.00$ V $[Ni^{2+}]_{TOT} = 20.00$ mM

t= 25°C

Figure A.42: Fraction of Fe in PW VI

$[Ca^{2+}]_{TOT} =$ 1.00 M $I = 7.160$ M
$[Na^+]_{TOT} =$ 1.00 M $[Cl^-]_{TOT} =$ 5.00 M
$[Mg^{2+}]_{TOT} =$ 1.00 M $[Pb^{2+}]_{TOT} =$ 20.00 mM
$E_H =$ 0.00 V $[Cu^{2+}]_{TOT} =$ 20.00 mM
pH = 4.00 $[Ni^{2+}]_{TOT} =$ 20.00 mM

t= 25°C
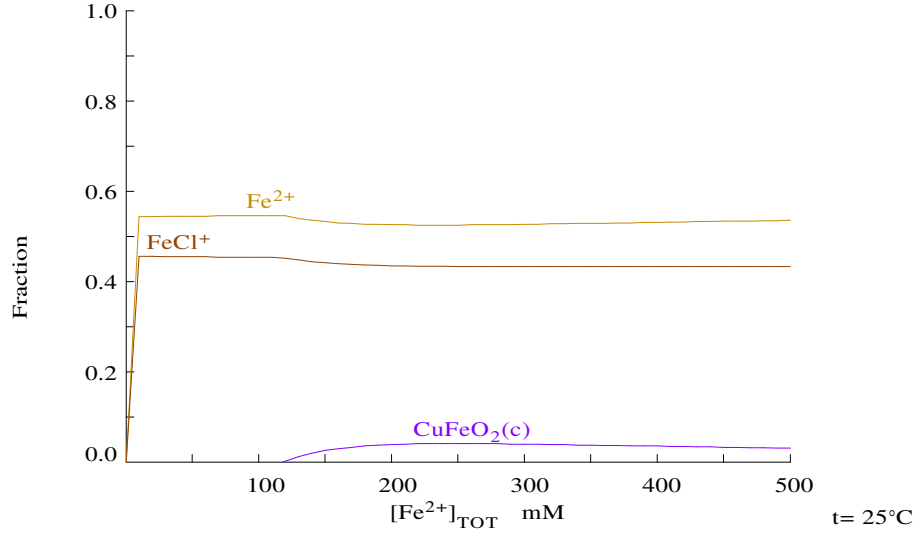
Figure A.43: Effect of concentration of Fe species in PW VI at pH 4

$[Ca^{2+}]_{TOT} =$ 1.00 M $I = 7.160$ M
$[Na^+]_{TOT} =$ 1.00 M $[Cl^-]_{TOT} =$ 5.00 M
$[Mg^{2+}]_{TOT} =$ 1.00 M $[Pb^{2+}]_{TOT} =$ 20.00 mM
$E_H =$ 0.00 V $[Cu^{2+}]_{TOT} =$ 20.00 mM
pH = 7.00 $[Ni^{2+}]_{TOT} =$ 20.00 mM

t= 25°C

Figure A.44: Effect of concentration of Fe species in PW VI at pH 4

$[Fe^{2+}]_{TOT} = 20.00$ mM

$[Ca^{2+}]_{TOT} = 1.00$ M

$[Na^+]_{TOT} = 1.00$ M

$[Mg^{2+}]_{TOT} = 1.00$ M

pH = 7.00

I= 7.160 M

$[Cl^-]_{TOT} = 5.00$ M

$[Pb^{2+}]_{TOT} = 20.00$ mM

$[Cu^{2+}]_{TOT} = 20.00$ mM

$[Ni^{2+}]_{TOT} = 20.00$ mM

t= 25°C
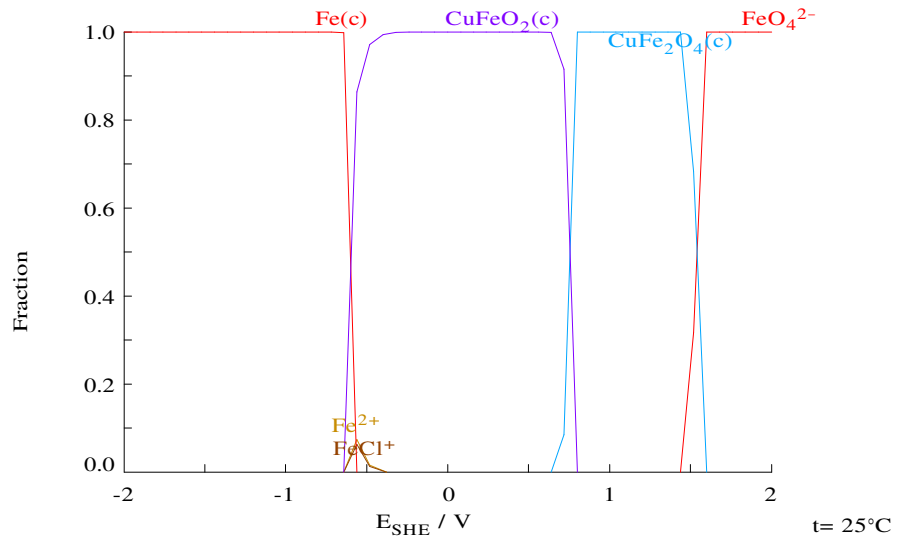
Figure A.45: Effect of applied potential on Fe species in PW VI at pH 7